UNIVERSITY OF WASHINGTON

COLLEGE OF ENGINEERING

SOIL ENGINEERING RESEARCH REPORT NO. 13

MICROZONATION BY AMPLIFICATION RATIO TECHNIQUE

BY

MEHMET A. SHERIF

ISAO ISHIBASHI

JAMES K. KEARNES

MAY, 1976

DEPARTMENT OF CIVIL ENGINEERING

UNIVERSITY OF WASHINGTON

SEATTLE, WASHINGTON 98195

Any opinions, findings, conclusions or recommendations expressed in this publication are those of the author(s) and do not necessarily reflect the views of the National Science Foundation.

ABSTRACT

In this report the authors investigate the seismic behavior of the Satsop nuclear reactor site by the ratio microzonation method (Refs. 5 and 6), which involves simultaneous observations of microseismic signals at two stations with identical recording seismometers and utilization of the ratio of power spectra to identify ground amplification and frequency distribution.

The study reveals that (1) microseismic power spectra are nonstationary within the time constraints of this study; however, (2) even though the amplification spectra are not stationary in the strict sense of the word, they do appear to be consistently more stationary than the corresponding power spectral ratio; and (3) there is a good correlation between the resonant site frequencies determined by microseismic amplification spectra and those calculated from field shear wave velocity measurements.

TABLE OF CONTENTS

LIST OF FIGURES

LIST OF TABLES

ACKNOWLEDGMENT

The authors gratefully acknowledge the financial assistance of the National Science Foundation which made this investigation possible.

1.0 INTRODUCTION

1.1 INTRODUCTION

It is generally held that, while the use of microseisms or microtremors for seismic zoning and design is a valid topic for scientific research, this type of analysis does not yet appear to be well enough developed for practical engineering applications. To date, one of the major difficulties has been the nonstationarity of microseismic motions. "Nonstationarity" refers to the time dependence of the frequency content of wave trains of finite length.

It is common for the frequency content of microseismic wave trains to be presented as Fourier power spectra. In this study, microseismic amplification spectra are calculated from Fourier power spectra and used as indicators of site specific seizure behavior. Results are then critically examined.

1.2 BACKGROUND

Although passive and not serving as an energy source, the response of a site's soil and subsurface to seismic excitation is a primary determinant of the resultant effect of a seismic event on man-made structures. As early as 1908, Wood (ref. 26)

demonstrated a relationship between ground conditions and damage caused by the 1906 California earthquake. Resonance effects are to be expected in a bounded, layered medium and it has become empirically evident that structures sited on bedrock are, in general, less prone to earthquake damage than those located on a layered sedimentary section.

In 1934, Inouye (ref. 11) suggested that there exists a "dominant frequency" at the ground surface which is related to the dominant seismic excitation at bedrock. Later, in 1945, Carder and Gilmore (ref. 8) noticed the same phenomena when monitoring "ground vibrations." They proposed that one or more of the natural (resonant) frequencies of the ground might be determined by the observation of microseisms.

Beginning in 1954, Kanai and others (ref. 12,13,14) published a number of pioneering papers on microseismic motions which he called microtremors. Kanai defined microtremors as seismic motions which are continuously present, have amplitudes of about 0.1 to 1.0 micron, and periods between 0.05 and 2 seconds. In most cases, Kanai feels that such motions may be attributed to artificial disturbances such as traffic and industrial machines.

Kanai's recordings of microtremors (see fig. 1.2-1) were made with pendulum/transducer-type velocity seismometers

FIGURE 1.2-1 (after Kanai)

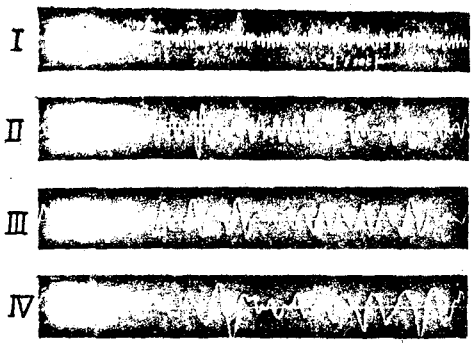

Representative records of microtremors observed at the various kinds of ground. The symbols of I, II, III and IV represent the kinds of ground used in the Building Code of Japan.

FIGURE 1.2-2 (after Kanai)

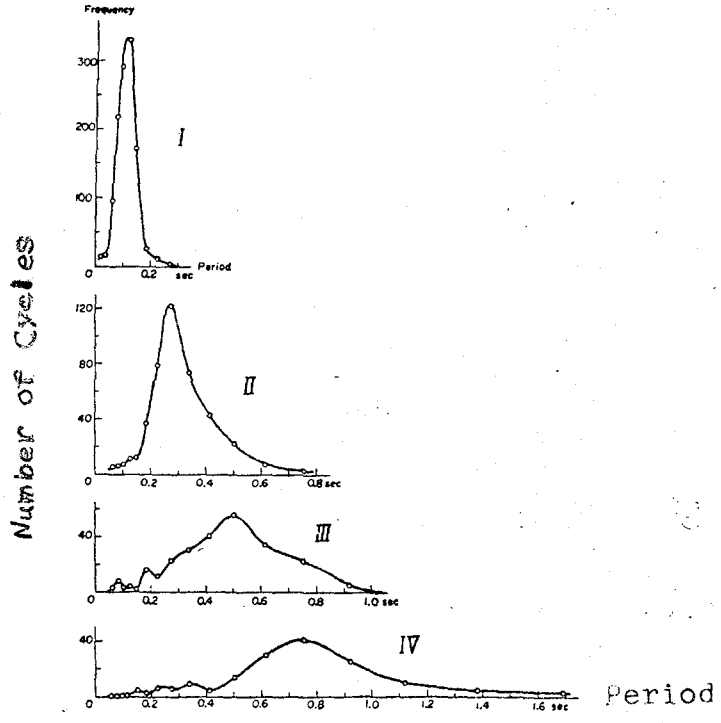

Representative period distribution curves of microtremors at the various kinds of ground.

recording on smoked drums. He characterized the frequency content of the recorded signals by means of a "period distribution function" which was calculated in the following manner.

A section of record (typically two minutes) was selected for analysis. Then the time intervals between zero-crossings were measured. Twice the time interval between a pair of zero-crossings was considered to be equal to the period of one cycle of microseismic motion. (Because Kanai's seismometers measured velocity, the time between zero-crossings corresponds to the time between maximum displacements.) A period distribution function (sometimes called a "frequency-period curve") was then constructed by plotting period on the abscissa and the number of cycles of each period on the ordinate. (See fig. 1.2-2.)

After analysis of many recordings of Japanese microtremors Kanai concluded that: 1) the period distribution functions of microtremors show a definite form for particular types of subsoil (see fig. 1.2-2); 2) because of resonance, the amplitude of microtremors at the earth surface becomes greater as the period of the microtremor approaches the natural period of the geologic column; and 3) "considerable similarity" exists between the period distribution functions of microtremors and earthquakes recorded at the same location.

In 1961, Akamatu (ref. 1) performed a study which used power spectra to characterize the frequency content of microseisms in the 1 to 200 hz. frequency range. Although his method of analysis was not strictly comparable, Akamatu's study seemed to confirm Kanai's observation that there exist period distributions or "dominant frequencies" which are characteristic of their recording location. Akamatu concluded that there exists a dominant frequency of short-period microseisms which is particular to its recording site. He further concluded that, based on data from the six Japanese sites at which his study was conducted, sites may be classified into two general types on the basis of their microseismic power spectra: 1) sites where the dominant frequency appears as a remarkably sharp spectral peak; or 2) sites where the microseismic power spectra are composed of minor peaks but are generally flat. In retrospect, it seems that Kanai" frequency-period curves exhibit an analogous trend. (see fig. 1.2-2)

Also in 1961, Spieker (ref. 21), after prolonged observation of microseisms in the United States, concluded that, in general, microseisms are not stationary for periods longer than one hour. In other words, over time periods in excess of one hour, the frequency content of microseismic wave trains is not constant.

Bostrom and Sherif (ref. 5) have proposed a method whereby it may be possible to normalize for the effects of variable excitation by observing the ratio between the power spectra of microseisms recorded simultaneously by two identical seismometer stations. The application of this proposed method of site response determination is depenent upon the assumption that the geologic column behaves as a linear system in transmitting the seismic signal and that the same excitation function is active at both seismometer stations. If these conditions are met they suggest that the power spectral ratio will, in fact, represent the power transfer function active between the two stations. (The derivation of this function is discussed in more detail in Section 3.2 of this paper.) If the location of one station is fixed and designated the "base station", transfer functions relative to it may be calculated for a number of locations of the other "portable station." Any differences in the power transfer functions characterizing the various portable station locations could then be attributed solely to differences in the site response of those locations.

1.3 OBJECTIVE

It is the purpose of this study to investigate the seismic behavior of a site by means of a method very closely akin to that proposed by Bostrom and Sherif (ref. 5) and to critically examine the results of this investigation. This study will

confine itself to examining seismic signals within the frequency band 0 to 10 hz. as it has been shown that man-made structures are most susceptible to damage by low-frequency seismic motions.

2.0 THE STUDY AREA

2.1 LOCATION

The area in which this study was conducted lies in the Chehalis Lowland of Washington state and consists of a portion of the alluvial terraces and adjacent hills which comprise the south wall of the Chehalis River valley near the town of Satsop, Washington. Field data were recorded at four locations (one "base station" and three "portable station" locations), all of which are within an area of land totalling approximately 1.5 square miles and lying south and southwest of the Chehalis River at the point at which the Satsop River enters the Chehalis (see fig. 2.1-1). This area will be henceforth referred to as the study site. That area lying within 10 miles of the site will be referred to as the site locality, and that area within 200 miles of the site as the site region.

2.2 PHYSIOGRAPHY

The site locality can be divided into three local physiographic domains: 1) hills which are part of two larger regional physiographic provinces known as the Montesano and Willapa Hills; 2) stream terraces; and 3) river flood plains.

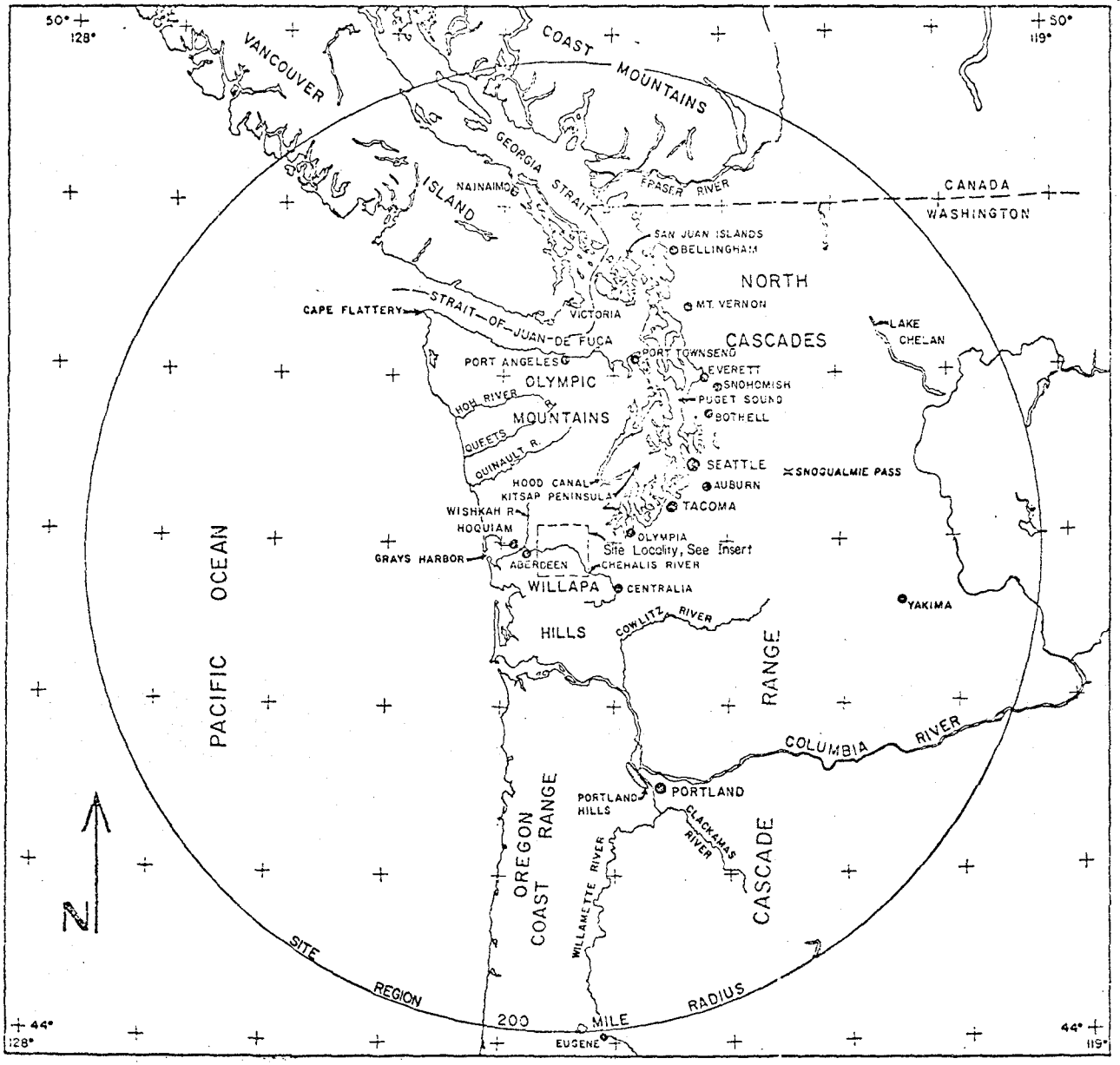

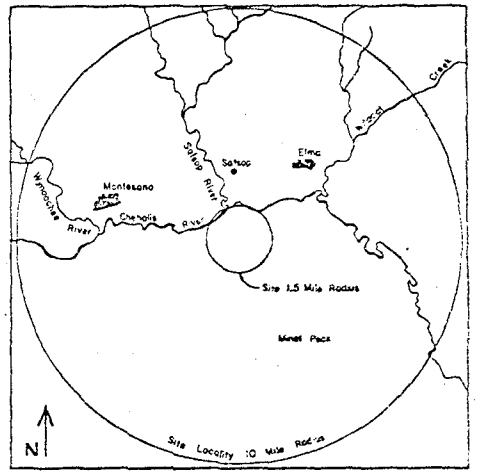

Insert, Site Locality

0 25 50 100 mi

FIGURE 2.1-1 (after WPPSS)

LOCATION MAP

The flood plain of the Chehalis River lies at a general elevation of 25 feet and is approximately 1.5 miles wide, while the adjacent Satsop River flood plain ranges in elevation from about 30 to 80 feet and is approximately 0.5 miles wide. Flanking both rivers is a series of three major sets of stream terraces. The lowest set, at a general elevation of 50 feet, is the Fraser terraces. The intermediate set, at about elevation 130, is the Salmon Springs terraces. The highest set, at 320 feet general elevation, is know as the Helm Creek terraces.

Drainage patterns in the site locality are mostly modified dendritic, and exhibit some structural control from regional folding and faulting. They do not, however, appear to be fault controlled.

Slopes at and adjacent to the study site are generally moderate, but range from nearly horizontal to nearly vertical. Low slopes are found on the Chehalis River flood plain (1%), and on the undissected surfaces of the Salmon Springs and Helm Creek terraces (1% and 2%). Steep slopes, ranging from 30% to 70%, occur on hillsides near the base station location and on the dissected portions of the terraces. (See fig. 2.2-1)

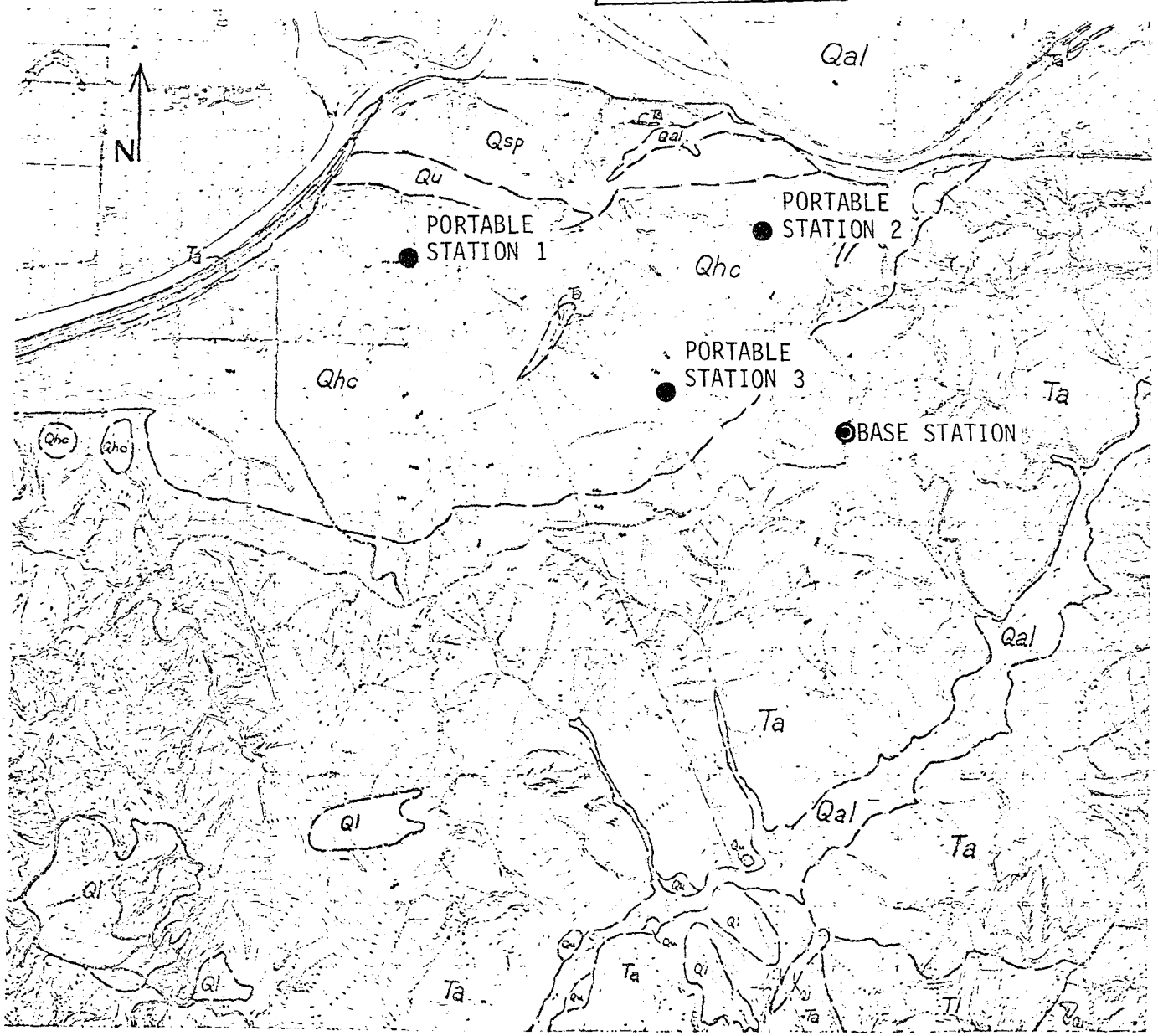

LEGEND

- Qal — Alluvium: Unconsolidated alluvial silts and sands.
- Ql — Landslides: Slumped masses of bedrock
- Qsp — Salmon Springs Deposit: Poorly graded glaciofluvial sands, and silty sands
- Qhc — Helm Creek Deposit: Poorly graded glaciofluvial sands, silty sands and clayey silts
- Qu — Undifferentiated Glaciofluvial Deposits

Unconformity

- Ta — Astoria Formation: Dark gray to brown, moderately sorted, poorly cemented marine sandstone and sandy marine siltstone composed of quartz, feldspar, mica and volcanic rock fragments. Tuff beds (e.g., Tuff Bed 1) are present locally. The diorite is massive but locally well bedded with abundant carbonaceous material which forms laminae. Concretions are common, megafossils and plant remains are rare. When weathered, the sandstone is yellowish to reddish-brown.

Unconformity

- Tl — Lincoln Creek Formation: Light olive-gray to dark greenish-gray tuffaceous marine siltstone and silty very fine to fine marine sandstone. Some glauconitic sandstone and siltstone

Contact
Contact, dashed where approximately located, queried where indefinite

Fault
Fault, showing angle of dip, dashed where approximately located, dotted where concealed. U, upthrown side, D, down thrown side.

Anticline / Syncline
Folds, approximately located, showing trace of axial plane and direction of plunge. Dotted where concealed.

- Strike and dip of beds
- Horizontal beds
- Strike and dip of local scour and fill features
- Strike and dip of joints
- Closed depression or pipe
- Location of outcrop, Ta
- Approximate location of Tuff Bed 1
- Discontinuous outcrops along creek bed
- Spring

Fossil Location
M Megafossil
P Plant

Based on Rau 1967, Sower and Pease 1965, Pease and Hoover 1957 and Carson 1970

0 500 1000 2000 3000 ft

FIGURE 2.2-1 (after WPPSS)

SITE,
GEOLOGY AND OUTCROP MAP

2.3 SITE STRATIGRAPHY AND SURFICIAL GEOLOGY

The stratigraphy of the study locality and adjacent area is summarized in figure 2.3-1. Formations present at the study site are marked with an asterisk (*).

At the study site, the Astoria formation of Tertiary age is the oldest unit known to be present. It is estimated to be approximately 3500 feet thick and for purposes of the present study, may be considered as "bedrock". It is on the weathered surface of the Astoria formation that the base station for this study was located. (See fig. 2.2-1) This formation is composed of friable to moderately hard, coarse to fine grained and generally moderately sorted sandstone. The sandstone grains are loosely cemented by silt and clay fines when fresh or weathered and by iron oxide near the base of the weathered zone. The finer sandstone tends to be better cemented due to its higher content of fines. Thin discontinuous beds of conglomeritic sandstone, conglomerate, and siltstone and thin carbonaceous beds are known to occur locally. When encountered, the gravel in conglomeritic layers is commonly composed of fine-grained, dark-colored, volcanic rocks and is poorly cemented. Siltstones are generally hard and highly cemented. In addition, five separate tuff beds are known to occur within the Astoria formation at the site. (Ref. 25) Generally, bedding in the sandstone is poorly-defined and massive. In

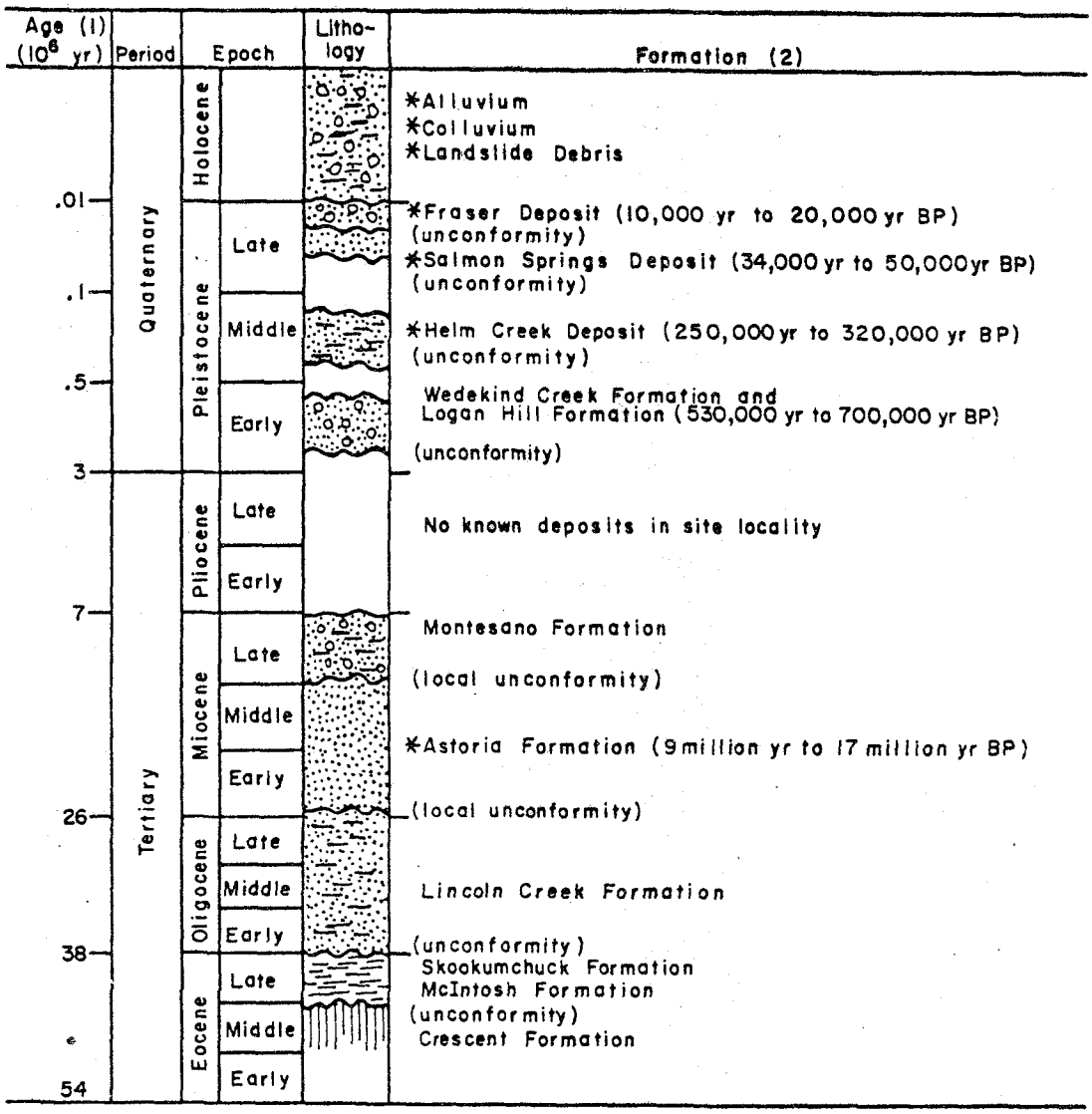

*Formations present within 1.5 mi of plant location

(1) Age based on Van Eysinga 1972

(2) Formations and ages based on Carson 1970 ; Snavely et al 1973 ; Pease and Hoover, USGS, 1957 ; Rau 1967 ; Fowler 1965 ; Eddy 1966; Birkeland et al 1971 ; Easterbrook et al 1967; Easterbrook 1969.

FIGURE 2.3-1 (after WPPSS)

LOCAL STRATIGRAPHIC COLUMN

outcrop, the sandstone of the Astoria formation dips 4 to 19 degrees to the north.

Glaciofluvial deposits overlie the Astoria formation to the northwest of the base station location. (See fig. 2.2-1) These deposits consist of alluvial sands, silts, and gravels which were deposited at three different elevations representing different ages of deposition: 1) the Helm Creek deposit at approximately 320 feet elevation; 2) the Salmon Springs deposit at approximately 130 feet elevation; and 3) the Fraser deposit which is present below the alluvium of the Chehalis River. Other undifferentiated glaciofluvial deposits are also present.

All three portable station locations are on erosional remnants of the Helm Creek deposit. (See fig. 2.2-1) Based on radiometric dates of more than 40,000 years BP and on field relationships with the Salmon Springs deposit, it has been shown that the Helm Creek deposit is of pre-Salmon Springs age. It has been tentatively correlated with the Stuck glaciation of the Puget Lowland (320,000 to 250,000 years BP). At the study site, the Helm Creek deposit consists principally of discontinuous layers of sand, silty sand, and silt with occasional coarser clasts. Figures 2.3-2, 3, and 4 present the detailed stratigraphy of the Helm Creek and other deposits present at each portable station location. These figures are based on logs of exploration borings made by the Washington Public

FIGURE 2.3-2 SUMMARY BORING LOG OF WPPSS BORING A-30 LOCATED AT PORTABLE STATION LOCATION 1

Ground Surface Elevation 292.5 ft.

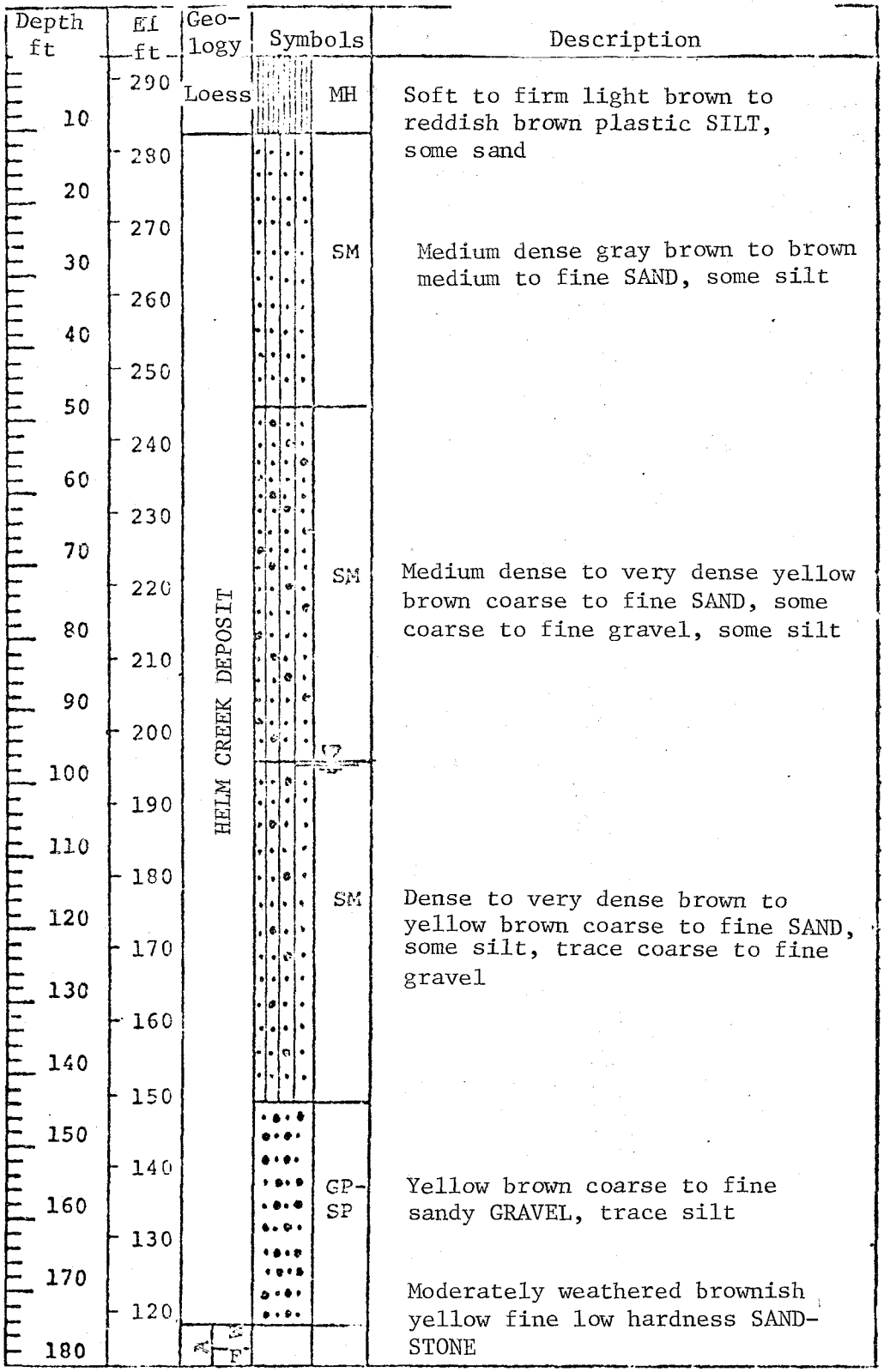

FIG. 2.3-2 (continued)

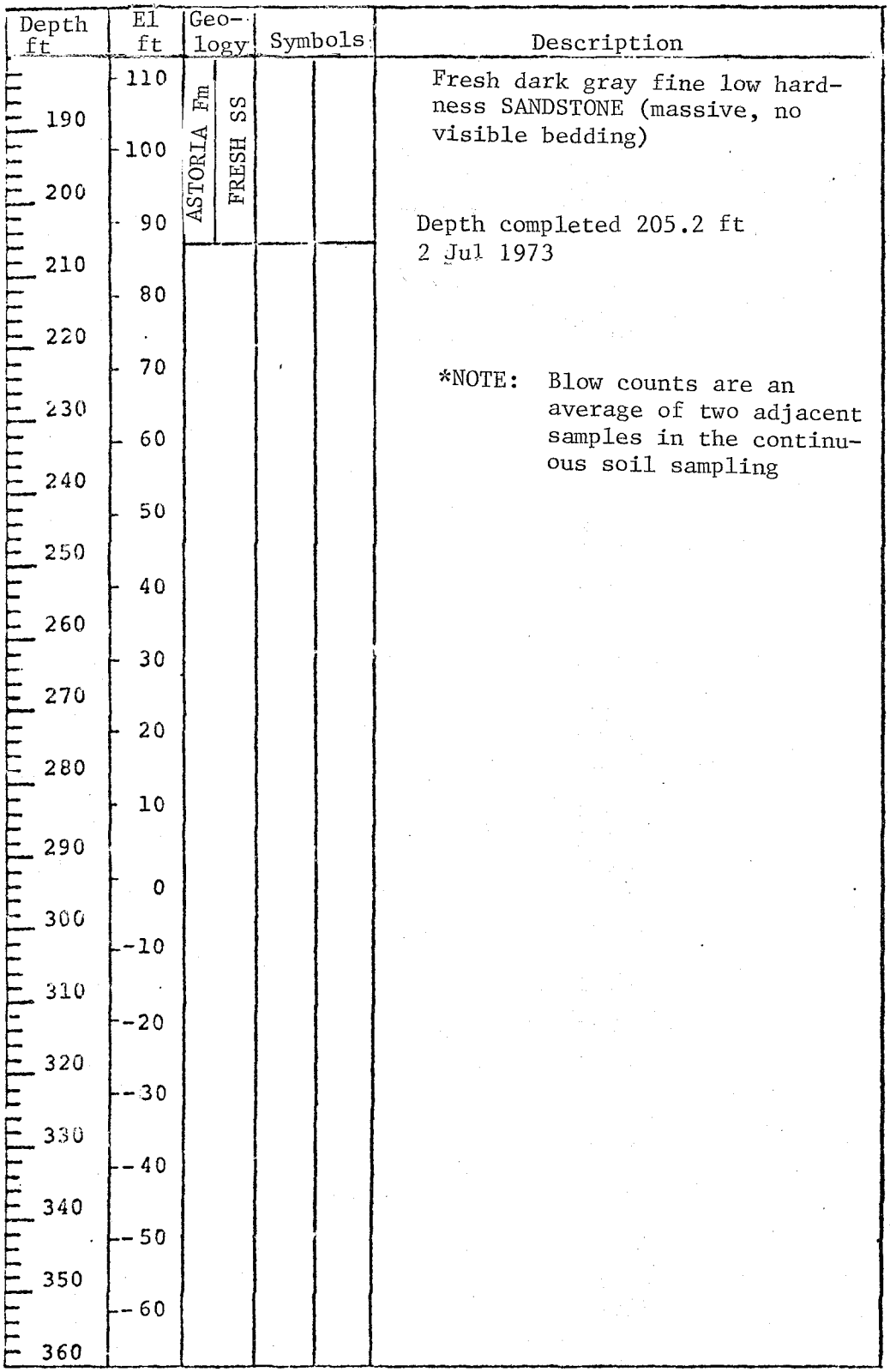

FIGURE 2.3-3 SUMMARY BORING LOG OF WPPSS BORING A-13 LOCATED AT PORTABLE STATION LOCATION 2

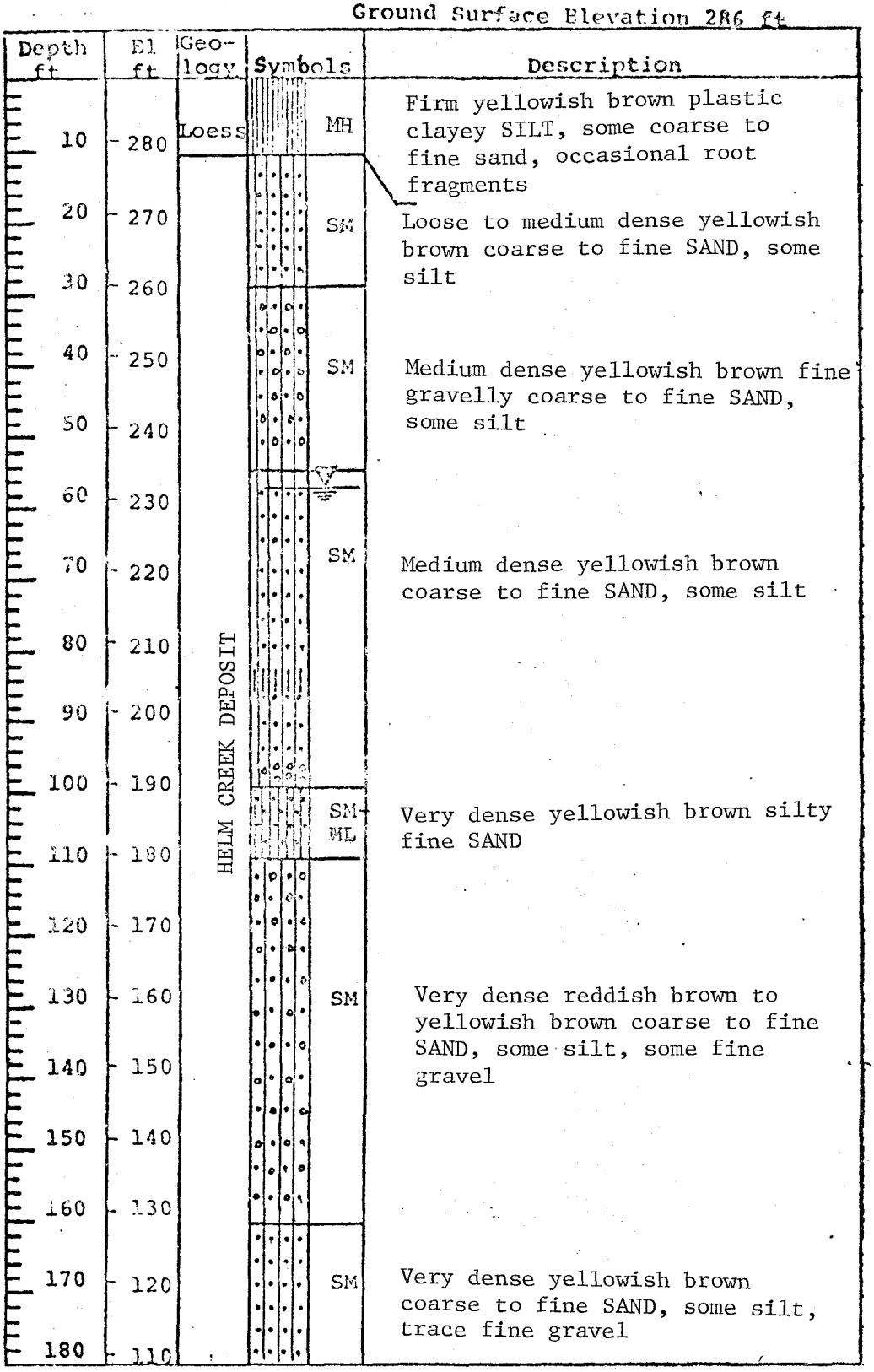

FIG. 2.3-3 (continued)

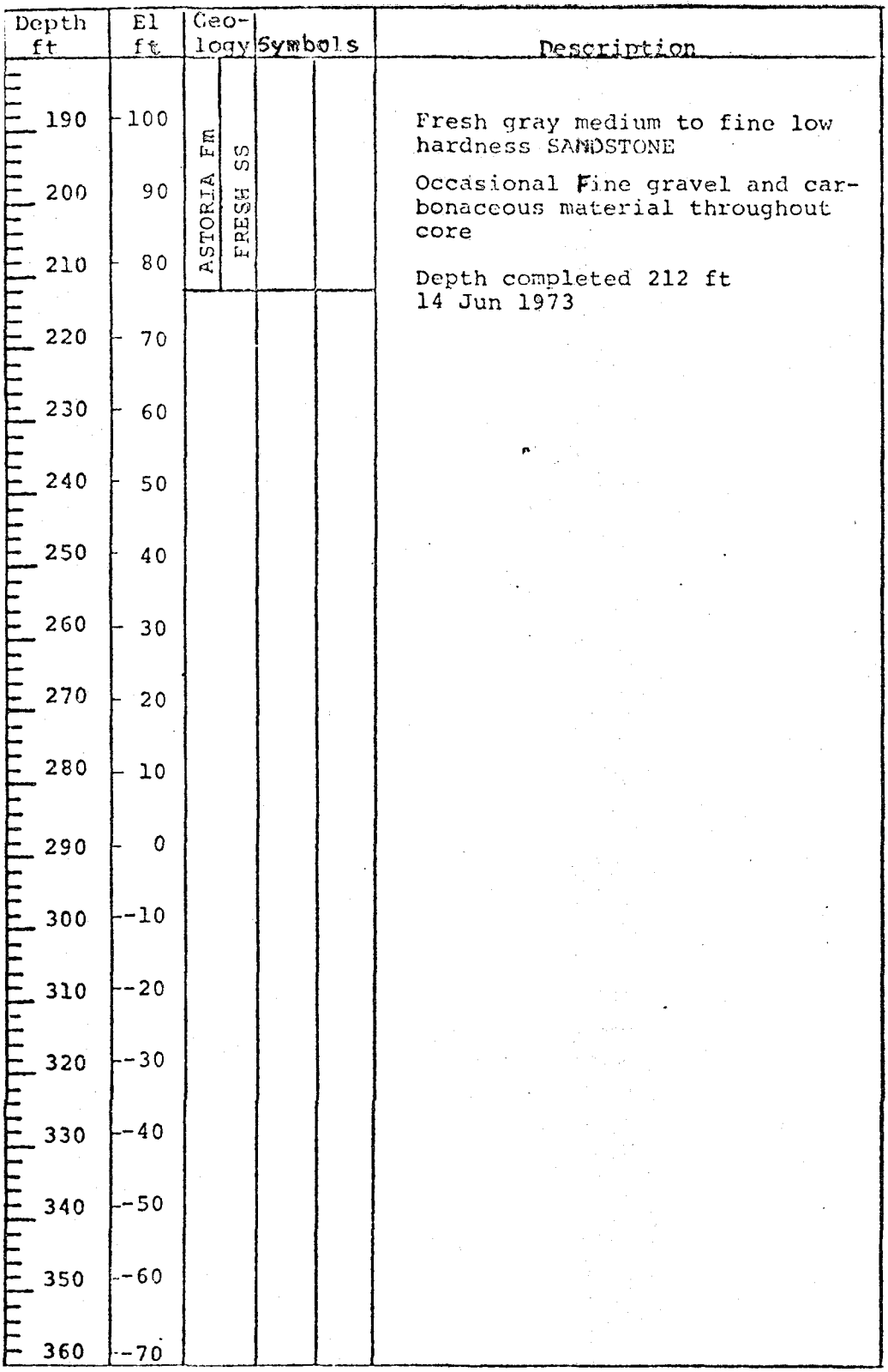

FIGURE 2.3-4 SUMMARY BORING LOG OF WPPSS BORING A-19 LOCATED AT PORTABLE STATION LOCATION 3

Ground Surface Elevation 333 ft

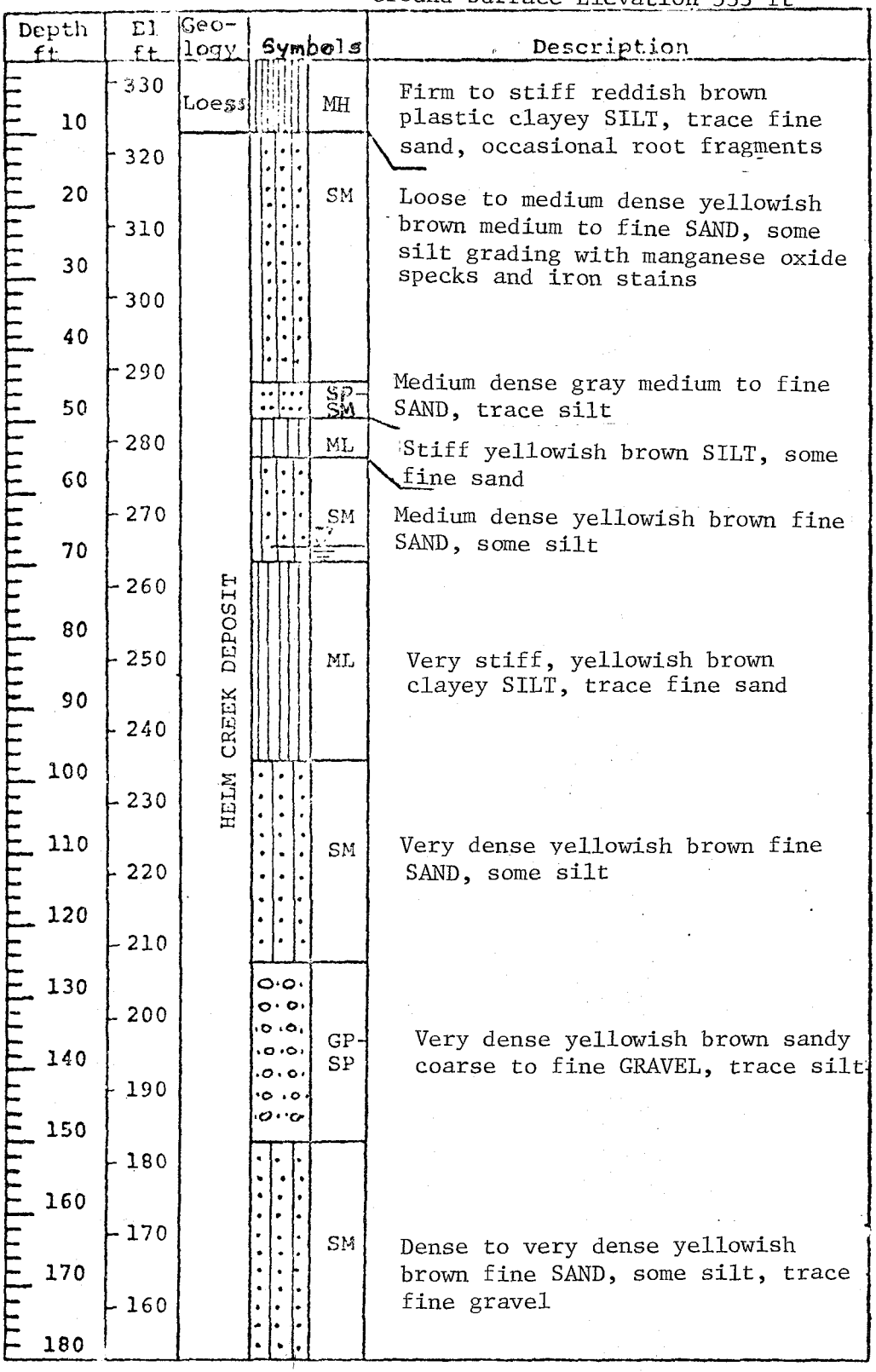

FIG. 2.3-4 (continued)

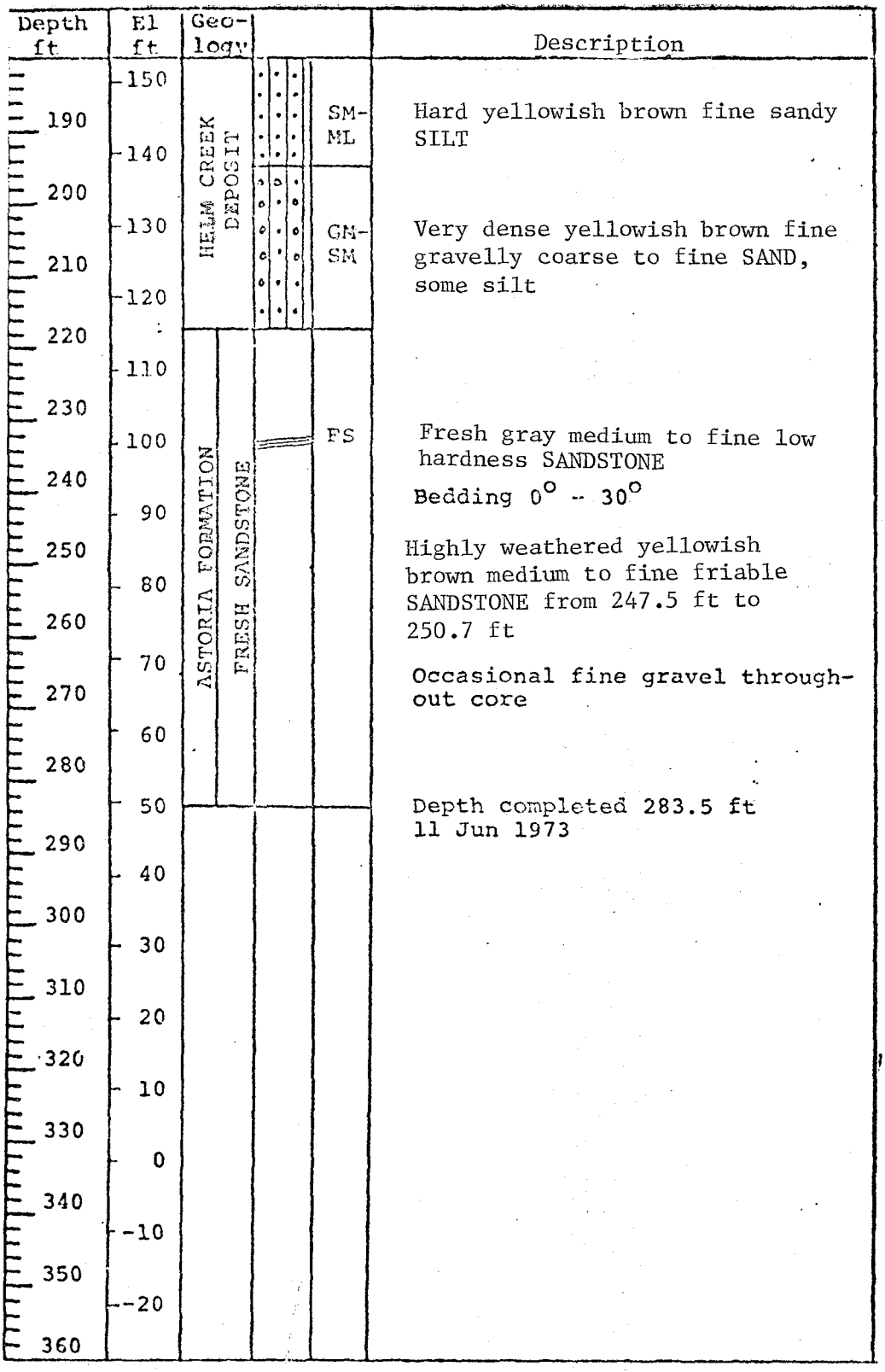

Power Supply System (WPPSS).

Topographically lower and younger than the Helm Creek deposit is the remnant of the Salmon Springs deposit. It lies to the north of and adjacent to the Helm Creek deposit. (See fig. 2.2-1) The Salmon Springs deposit has been correlated to the middle and early Salmon Springs glaciation (50,000 to 34,000 years BP). It overlies the Astoria formation and consists of 30 to 60 feet of silty sand and clayey silt.

The youngest glaciofluvial deposit in the area is the Fraser deposit. This deposit (20 to 120 feet thick) underlies the alluvium of the Chehalis River valley and consists mainly of sandy gravel with layers of clayey silt. It is correlated to the Fraser glaciation (20,000 to 10,000 years BP).

At the study site, loess (5 to 15 feet thick) overlies both the Astoria formation and glaciofluvial deposits. Colluvium is present downslope from the base station and elsewhere in the study area. This colluvium results from the downslope movement (slide and creep) of weathered sandstone and loess and is generally thickest at the base of slopes. Alluvium occurs along the Chehalis River, Workman Creek, and other small streams in the study area. In the Chehalis valley, the alluvium is composed of 3 to 20 feet of sand and silt.

2.4 STRUCTURAL GEOLOGY

Broad, poorly-defined anticlines and steeper, more clearly-defined synclines generally trend north-south in the site locality. (See fig. 2.4-1) At the site, the Astoria sandstone beds dip 5 to 15 degrees north toward the Chehalis River reflecting these gentle folds.

Several faults are known in the region immediately surrounding the study area. (See fig. 2.4-2 and tables 2.4-1,2, and 3) These faults are of high angle, reverse, and normal type, and generally trend northwest-southeast and east-west. They are related to compressional forces that produced folding and faulting during late Tertiary time. (See section 2.5) These faults do not offset or control drainage. There is no evidence of Quaternary movement of the faults.

Joints are present in only a few of the outcrops of the Astoria formation at the site. Out of some 80 outcrops of sandstone, previous investigators (ref. 25) found joint sets in only six exposures. Two dominant orientations of joints were found; one striking northwest and one northeast.

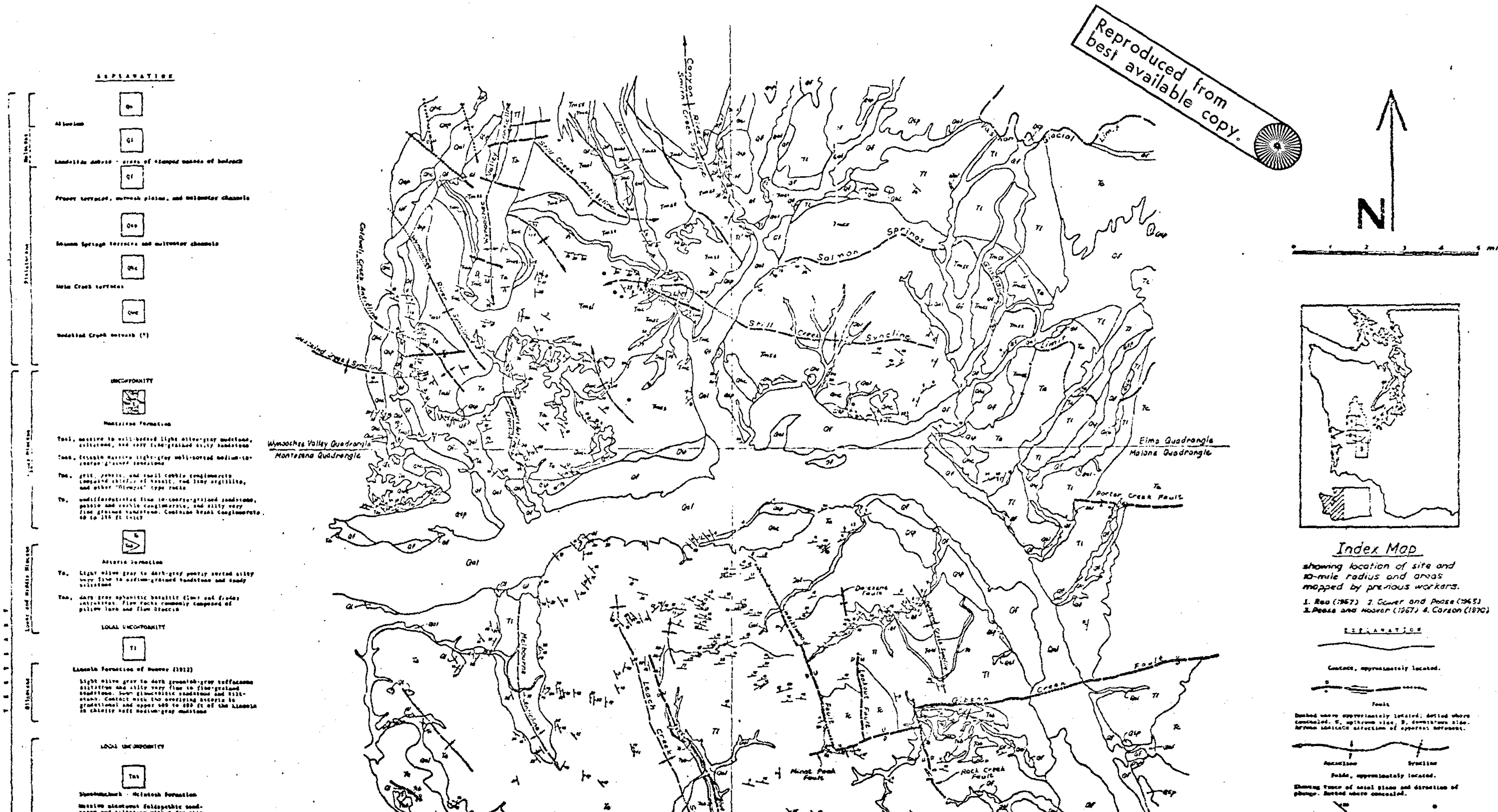

FIGURE 2.4-1 (after WPPSS)

SITE LOCALITY
GEOLOGY AND STRUCTURE MAP

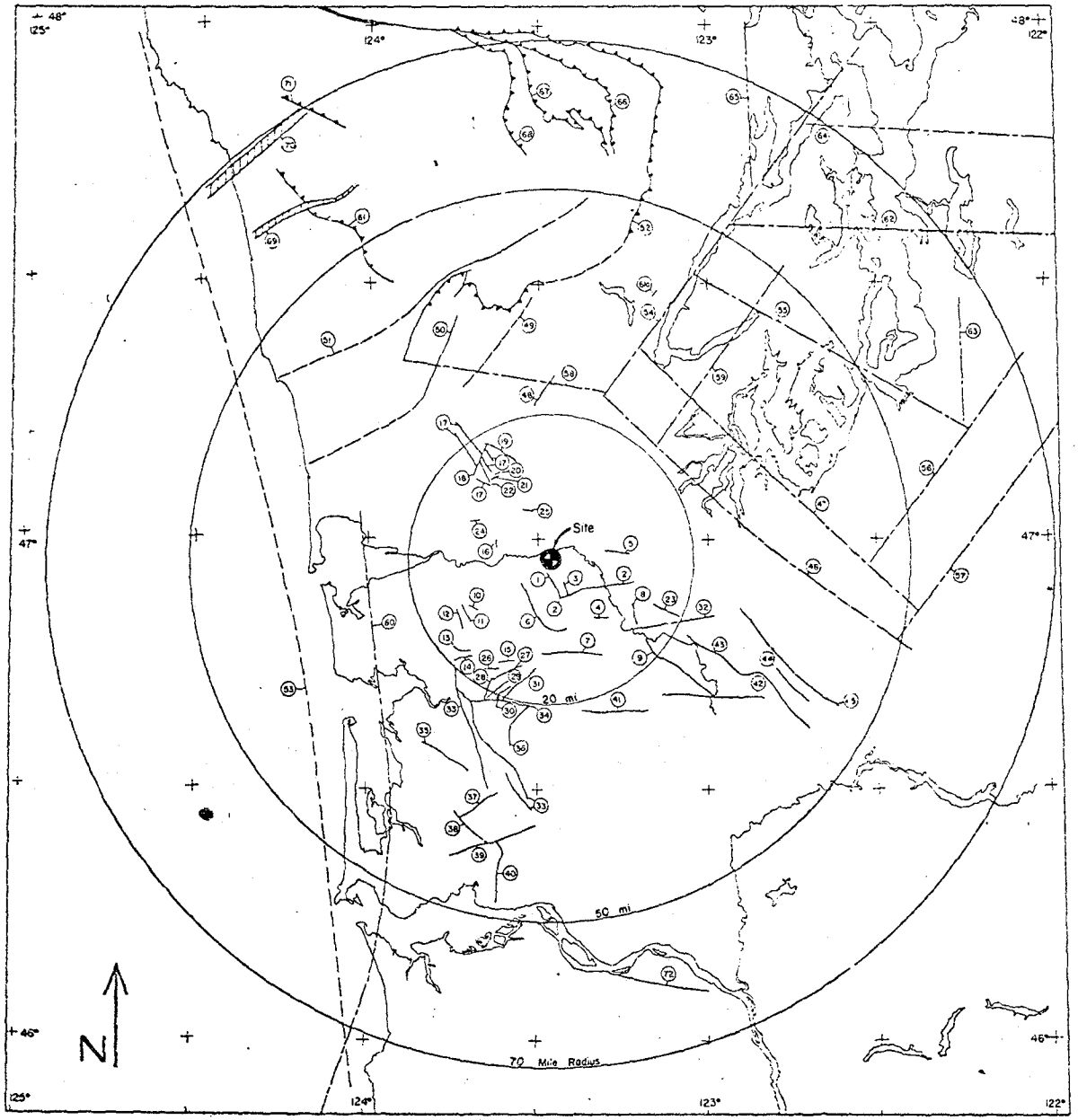

LEGEND

Known Faults

- High Angle
- Thrust (barbs on upper plate)
- Major Shear Zone

Lineaments

- Based Mainly on Geophysical and Physiographic Evidence

Postulated Faults

- Based on Minimal Evidence

(45) Numbers refer to faults and lineaments on Tables 2.4-1, 2.4-2, & 2.4-3.

Based on Bromery 1962, Cady et al 1972a and 1972b, Danes et al 1965, Gower and Pease 1965, Hamlin 1962, Harvey 1956, Hunting et al 1961, King 1969, Pease and Hoover 1957, Rau 1966 and 1967, Rogers 1970, Snavely et al 1968, Stewart 1970, Tabor et al 1972, Wagner 1967a and 1967b, Wells and Peck 1961, Wolfe and McKee 1968, Zietz et al 1971, Tabor and Crowder 1969, Walker and King 1969, Brown 1966, Gower 1960, Brown et al 1960, Meyers 1971, Pevani 1966, Schlicker et al 1972, Wilkinson et al 1946, Lindquist 1961, Sceva, V. 1957, Waldron 1967, 1961, 1962, Waldron et al 1962, Mullineaux 1965a, 1965b, 1965c, Vine 1969, Gard 1968, Roberts 1958, Livingston 1966, Carson 1973

0 10 20 40 mi

FIGURE 2.4-2 (after WPPSS)

SIGNIFICANT FAULTS AND LINEAMENTS WITHIN 70 MI OF SITE

TABLE 2.4-1 FAULTS AND LINEAMENTS LONGER THAN ONE MILE WITHIN TWENTY MILES OF THE SITE (after WPPSS)

Map No.	Name	Minimum Distance from Site (Miles)	Sense of Motion	Length (Miles) (Measured on Map)	Last Movement/ Activity	Displacement
1	Weikswood Fault	1.5	Reverse (5)	4	Miocene or later (cuts Astoria Fm)	1500 ft (1)
2	Gibson Creek-Minot Peak Faults	5.5	High Angle	12	Miocene or later (cuts Astoria Fm)	?
3	Lookout Fault	2	Reverse	2.5	Miocene or later (cuts Lincoln Creek Fm)	?
4	Williams Creek Fault	10	High Angle	2.5	Oligocene or later (cuts Lincoln Creek Fm)	?
5	Porter Creek Fault	7.5	High Angle	3	Miocene or later (cuts Lincoln Creek Fm)	?
6	Blue Mountain Fault	4.5	Reverse	10.5	Miocene or later (cuts Astoria Fm)	3000 ft (1)
7	Redfield Creek Fault	13	High Angle	7.5	Miocene or later (cuts Astoria Fm)	1500 ft (2)
8	Oakville Fault	13	High Angle	3	Miocene or later (cuts Lincoln Creek Fm)	?
9	Scammon Creek Fault	18	Reverse (5)	13	Pliocene or earlier (5)	1000 ft (3)
10	Scar Hill North Fault	12	High Angle	1	Miocene or later (cuts Astoria Fm)	?
11	Scar Hill West Fault	13	High Angle	1.5	Miocene or later (cuts Lincoln Creek Fm)	?
12	Joe Creek Fault	14	High Angle	2.5	Miocene or later (cuts Lincoln Creek Fm)	?
13	Elkhorn Creek Fault	16.5	High Angle	2.5	Miocene (cuts Astoria Fm)	?
14	Smith Creek North Fault	17	High Angle	2.5	Miocene or later (cuts Astoria Fm)	?
15	Smith Creek East Fault	14.5	High Angle	2.5	Miocene or later (cuts Astoria Fm)	?
16	Silver Creek Fault	7	High Angle	1	Miocene or later (cuts Astoria Fm)	?
17	Wishkah River Fault Zone	12.5	Reverse	10 (2-3 wide)	Miocene (pre-Montesano Fm)	9000 ft (2)
18	East Fork Fault	14.5	Strike Slip	4.5	Miocene (pre-Montesano Fm)	1 mile (4)
19	Carter Creek Fault	14	Normal	5	Post Miocene (cuts Montesano Fm)	1000 ft (1)
20	Wynoochee Anticline #1 Fault	12	High Angle	1	Post Miocene (cuts Montesano Fm)	?
21	Wynoochee Anticline #2 Fault	12	High Angle	2	Post Miocene (cuts Montesano Fm)	?
22	Wynoochee Anticline #3 Fault	11	High Angle	1.5	Post Miocene (cuts Montesano Fm)	?
23	Cedar Creek Fault	16	High Angle	4	Eocene or later (cuts McIntosh Fm)	?
24	Caldwell Creek Fault	9.5	High Angle	2	Post Miocene (cuts Montesano Fm)	?
25	Confluence Fault	5.5	High Angle	1.5	Post Miocene (cuts Montesano Fm)	?
26	Smith Creek South Fault	17	High Angle	2	Miocene or later (cuts Astoria Fm)	?
27	Pack Sack Lookout Fault	16	High Angle	5	Post Miocene (cuts Montesano Fm)	?
28	Ward Creek Fault	17	High Angle	3.5	Miocene or later (cuts Astoria Fm)	?
29	North Fork Fault	18	High Angle	4	Miocene or later (cuts Astoria Fm)	?
30	Fairchild Creek Fault	18	High Angle	2	Miocene or later (cuts Astoria Fm)	?
31	Fall Creek Fault	14	High Angle	7	Post Miocene (cuts Montesano Fm)	?
32	Rochester Lineament (6)	16	High Angle	10	?	?

Footnotes
(1) Scaled from cross section
(2) Estimated from stratigraphic hiatus
(3) Snavely et al 1958
(4) Rau 1967
(5) Field studies
(6) Based on geophysical evidence

TABLE 2.4-2 FAULTS AND LINEAMENTS LONGER THAN 5 MILES AND 20 TO 50 MILES FROM THE SITE (after WPPSS)

Map No.	Name	Minimum Distance from Site (Miles)	Sense of Motion	Length (Miles) (Measured on Map)	Last Movement/ Activity	Displacement
33	Willapa River Fault Zone	20	High Angle or Strike Slip	25 (1-5 wide)	Miocene or later (cuts Lincoln Creek Fm)	3000 ft+ (1) (a) if high angle; 10 miles if strike slip
34	Wilson Creek Fault	21	High Angle	10	Miocene or later (cuts Astoria Fm)	?
35	South Fork Fault	30	High Angle	7.5	Eocene or later (cuts Crescent Fm)	?
36	Firdale Fault	21	High Angle	6.5	Miocene or later (cuts Astoria Fm)	?
37	Alder Creek Fault	34	High Angle	6 (1-2 wide)	Eocene or later (cuts "Unit B")	2000 ft (1)
38	Naselle River Fault	37	High Angle	7.5+	Eocene or later (cuts "Unit B")	3000 ft (2)
39	Salmon Creek Fault	38	High Angle	13+	Miocene or later (cuts Astoria Fm)	5000 ft (1)
40	Crooked Creek Fault	40	High Angle	9.5	Post Miocene (cuts post Astoria strata)	3000 ft (1)
41	Doty Fault	21	Normal (3) Reverse (4)	19	Pre-Miocene (overlapped by Astoria Fm)	4000 ft (3) 400 ft (4)
42	Salzer Creek Fault	25	Normal	14	Post Eocene (cuts Skookumchuck Fm)	1500 ft (4)
43	Kopiah Fault	22	Reverse	23	Post Eocene (cuts Skookumchuck Fm)	500 ft (4)
44	Newaukum Fault	35	Reverse	11	Miocene or later (cuts Lincoln Creek Fm)	700 ft (1)
45	Coal Creek Fault	28	Reverse	19	Post Eocene (cuts Skookumchuck Fm)	400 ft (4)
46	Olympia Lineament (12)	22	Normal (?)	55	Holocene(?) (10)	1+ km(?) (9)
47	Nisqually Lineament (12)	30	Normal (?)	50	Holocene(?) (10)	1+ km(?) (9)
48	Canyon River Fault	20	Strike Slip	5	Miocene(cuts Astoria Fm, overlapped by Montesano Fm)	2000 ft (5)
49	Weatherwax Fault (13)	26	High Angle(?)	15	Post Eocene (cuts Crescent Fm)	?
50	Humptulips Fault	28	High Angle	15 (7) 32 (8)	Post Eocene (cuts Crescent Fm)	?
51	Quinault Shear Zone	40	High Angle	28	Holocene(?)	?
52	Hurricane Ridge Fault	37	High Angle/ Thrust	65	Post Eocene(cuts late Eocene strata)	?
53	Postulated Offshore Fault (13)	35	High Angle(?)	500	?	?
54	Hood Canal Lineament (12)	28	High Angle(?)	35-60 (11) 90 (8)	Holocene (10)	4 km (9)
55	Tacoma-Gig Harbor Lineament (12)	43	High Angle	45	Holocene (11) (cuts late Pleistocene)	3-4 km (9)
56	Summer Lineament (12)	45	?	35	Holocene(?) (10)	?
57	Buckley Lineament (12)	49	?	55+	Holocene(?) (10)	?
58	South Olympic Mountains Lineament	25	?	30	?	?
59	Shelton Lineament	22	High Angle	30	Holocene(?) (10)	?
60	Coastal Magnetic Lineament	26	Normal (?)	250+	?	?
61	Salmon River Shear Zone	44	Thrust	18	?	?
61a	Saddle Mountain Fault	40	Reverse	1	Active	6-20 ft

Footnotes

(1) From cross section
(2) Estimated from stratigraphic hiatus
(3) Pease and Hoover 1957, cross section
(4) Snavely et al 1958
(5) Scaled from map
(6) Fronts on prominent scarp
(7) Harvey 1959
(8) King 1969
(9) Danes et al 1965
(10) Area is seismically active
(11) Rogers 1970
(12) Existence largely based on geophysical evidence
(13) Existence speculative; little supporting evidence

*Faults less than 5 miles long are not considered

TABLE 2.4-3 FAULTS AND LINEAMENTS LONGER THAN 10 MILES AND 50 TO 70 MILES FROM THE SITE (after WPPSS)

Map No.	Name	Minimum Distance from Site (Miles)	Sense of Motion	Length (Miles) (Measured on Map)	Last Movement/ Activity	Displacement
62	Seattle-Bremerton (1) Lineament	52	Normal (?)	50	Active	10 km
63	Duwamish-Puyallup (1) Valley Lineament	61	High Angle	18	Inactive	5000 ft (?)
64	Kingston-Bothell (1) Lineament	69	High Angle	42	Active	Large
65	Leland Lake-Snow Creek Lineament	58	High Angle(?)	24	?	?
66	Gray Wolf Ridge Fault	55	Thrust	32	Inactive	?
67	Lost Pass Fault	55	Thrust	30	Inactive	?
68	Mount Carrie Fault	54	Thrust	24	Inactive	?
69	Clearwater River Shear Zone	56	Strike Slip	20	?	?
70	Hoh River Shear Zone	69	Strike Slip	13	?	?
71	Heulsdonk Shear Zone	65	Thrust	10	?	?
72	Beaver Creek Fault	58	High Angle(?)	13	?	?

Footnote

(1) Existence largely based on geophysical evidence

2.5 GEOLOGIC HISTORY

In order to better understand the deposits present at the site, some understanding of the processes that made the deposits is helpful. The early to middle Tertiary history in the site locality is recorded by the deposition of submarine basalts and elastic sediment in a periodically subsiding and uplifting geosynclinal basin. The record began with the deposition of Eocene basalts, but these deposits are not known to be present at the study site. The oldest rocks underlying the site were formed during the middle Miocene (approx. 17 to 9 million BP) as sediments deposited in a subsiding geosynclinal basin. At the site, these sediments of coarse elastics, sand and gravel were laid down on older tilted and eroded strata and compose the Astoria formation. Deposition was into a shallow water marine basin and included feldspathic, basaltic, and quartz sands. Concurrently, intermittent volcanic activity occured. This resulted in the deposition of two extensive pillow basalts early in Astoria time and tuffaceous deposits in middle and late Astoria time.

The depositional environment during late Astoria time was such that deltaic or alluvial plain deposits were submerged at the site, at least periodically, allowing the growth of clams and snails. Carbonaceous material was carried into this environment by rivers that drained adjacent lands to the east.

Continental volcanoes errupted ash, adding tuffaceous material to the basin.

During late middle Miocene time, the site underwent deformation which folded the rocks along northwest-southeast axes. This deformation folded, faulted, and uplifted the Astoria formation and underlying older rocks. During late Miocene time, and possibly through late Pliocene time, the area continued to be uplifted and eroded, and the drainage systems present today were formed. It is largely the erosional surface resulting from this period of uplift which exsists today as the upper surface of the Astoria formation. (See fig. 2.5-1)

Throughout the Quaternary the site was subjected to continuing stream erosion, and hence, the major younger deposits are alluvial deposits of the Chehalis and ancestral Chehalis Rivers. But Tertiary erosional surfaces were deeply weathered prior to this later alluvial dissection. The depth of oxidation of the sandstones and siltstones of the uppermost Astoria formation is generally greater than 100 feet and locally may be greater than 200 feet.

The Quaternary alluvial deposits present at the site reflect a complicated sequence of stream erosion and deposition during several periods of glacial outwash. This outwash came from the Puget Lobe of the continental glacier that terminated

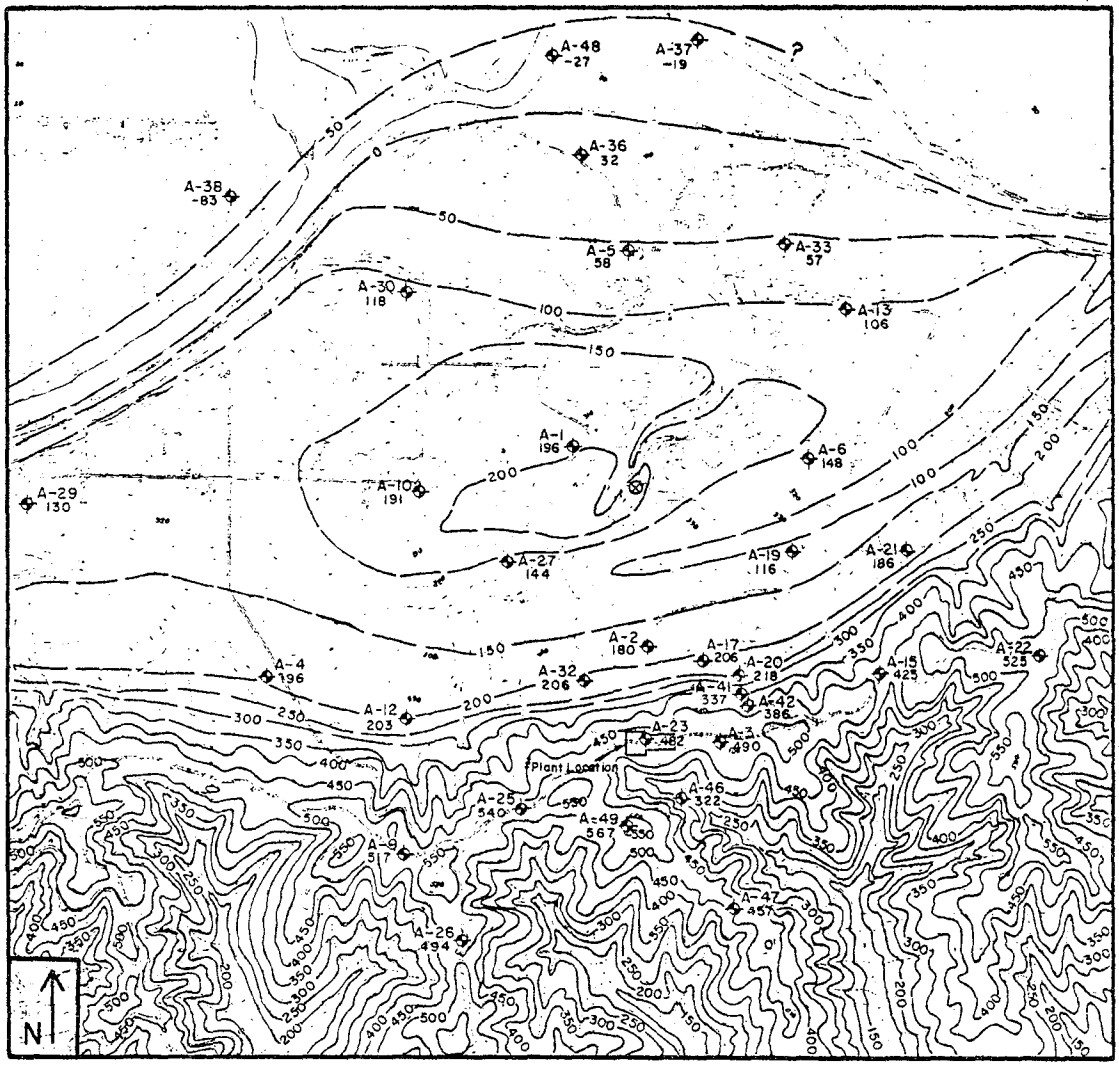

Legend

400 — Contour, elevation erosional surface of Astoria formation

150 — Contour, elevation Astoria formation concealed by glaciofluvial deposits

A-32 206 — Boring location showing elevation of top of Astoria formation, ft

⊗ Outcrop

Note: This map based on interpretation of presently available geologic data and applicant field investigations.

0 500 1000 2000 3000

Contour Interval: 50ft

FIGURE 2.5-1 (after WPPSS)

SITE, CONTOUR MAP OF EROSIONAL SURFACE OF ASTORIA FORMATION

near Olympia, Washington, and discharged meltwater down the Chehalis and Satsop Rivers to the Pacific. The Pleistocene discharge of this river system was many times greater than at present because the Chehalis River was the only drainage path available for meltwater from the Puget Lobe and nearby alpine glaciers. The result is that the Chehalis River is plainly underfit at present. The contrast in discharge is shown in the present meander pattern of the Chehalis River, which is considerably smaller than one would expect from the width of the Chehalis River Valley.

In Quaternary time, glacial outwash streams, coupled with raising and lowering of sea level, created conditions which were ideal for valley cutting and filling by the Chehalis River and its tributaries. The terraced topography at the site as well as the deep alluvial accumulation in the Chehalis River valley reflects this sequence of events. Furthermore, the present position of the Chehalis River, along the south side of its valley, appears to be caused by a greater influx of coarse alluvial material from the Satsop and Wynoochee Rivers on the north than the Chehalis River can now remove. The Satsop and Wynoochee Rivers have consideralby steeper gradients than the Chehalis River, hence, these rivers can carry coarse debris into the Chehalis River valley which continually accumulates and forces the Chehalis to erode southward. Thus, the Chehalis River is actively eroding the Astoria sandstone

along its southern bank.

2.6 SEISMOLOGY

It is generally held that the study site is located in a region of moderately high seismic activity. Maximum seismic intensities recorded within the site region are shown in figure 2.6-1. Historic earthquake activity in southwestern Washington state is also presented in fugure 2.6-2. From this plot of the historic record, seismic trends near the site may be observed.

The area within 20 miles of the site includes one Intensity V shock located about 19 miles north of the site. This shock may be associated with either the Olympia fault or the Hood Canal fault (lineaments numbers 46 and 54 on fig. 2.4-2) since it lies approximately at the intersection of the fault traces. There are a number of historic earthquakes located within 20 to 50 miles of the site. These range up to Intensity VII but are all overshadowed by the magnitude 7.0 to 7.1 Olympia earthquake of April 13, 1949. This earthquake is estimated to have caused an intensity of MM VII at the site, with acceleration peakes greater than 0.1 g lasting approximately 20 seconds. (ref. 25)

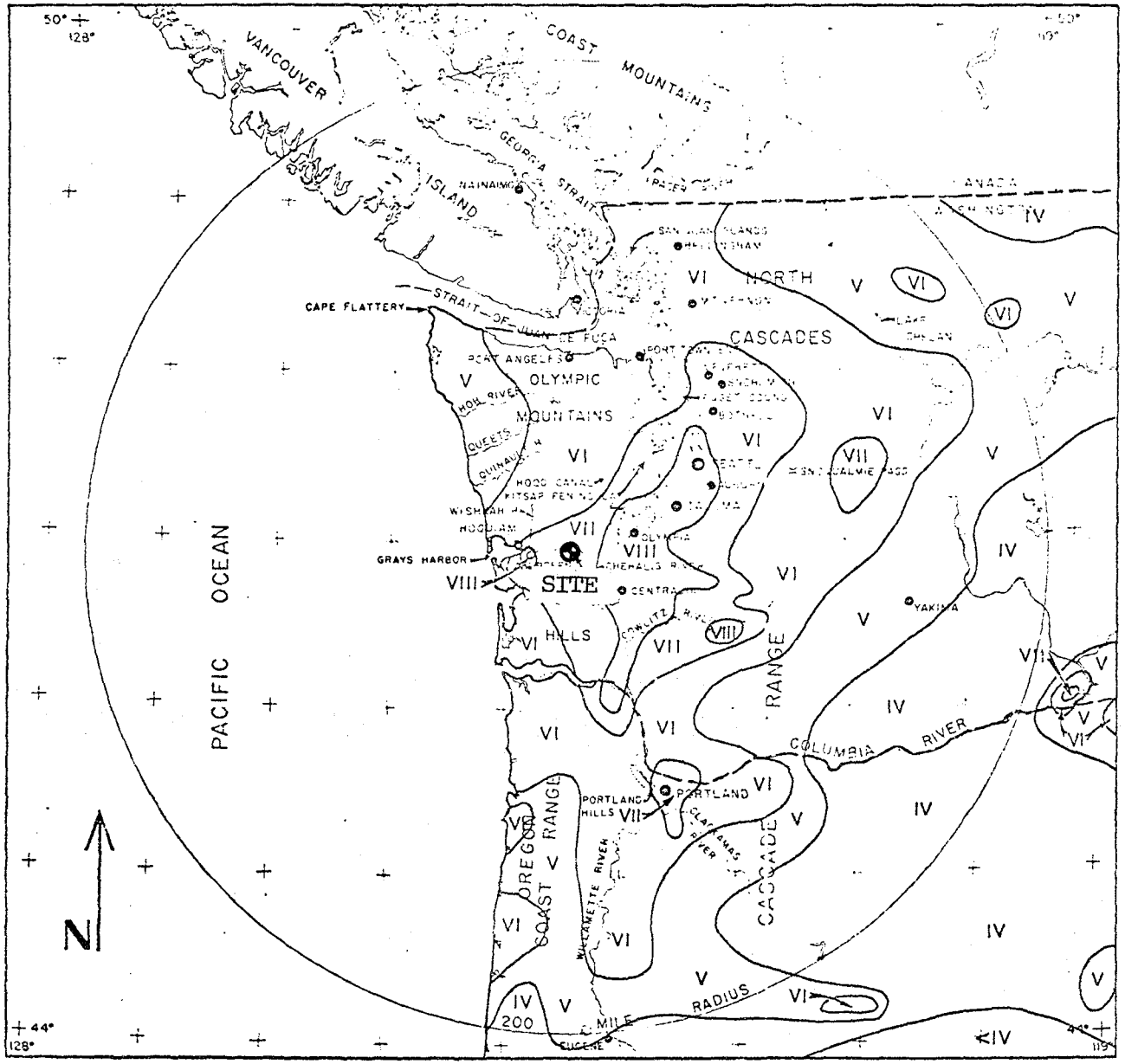

LEGEND

VII MODIFIED MERCALLI INTENSITY

Note: This map does not include data from 1872 North Cascades or 1904 Olympic Mountains earthquakes.

Based on Algermissen et al 1969

0 25 50 100 mi

FIGURE 2.6-1 (after WPPSS)

MAXIMUM HISTORICAL MODIFIED MERCALLI INTENSITY, MAP OF WASHINGTON AND NORTHERN OREGON

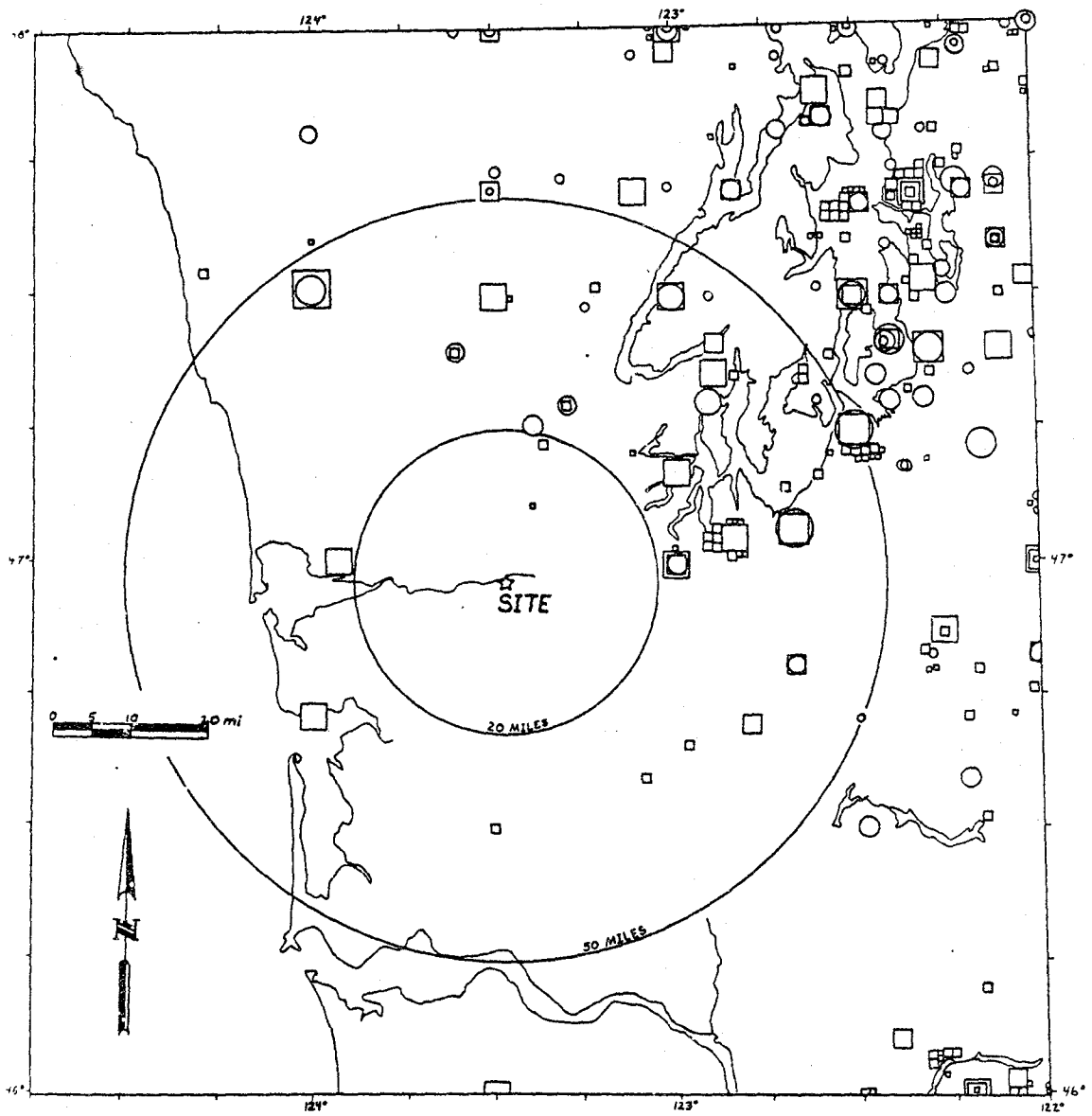

LEGEND:

	IX-XI	VIII	VI-VII	V	III-IV	Felt
Intensity	□	□	□	□	▫	▫
Magnitude	○	○	○	○	○	
	6-7	5-6	4-5	3-4	1-3	

FIGURE 2.6-2 EARTHQUAKE ACTIVITY 1840-1972 (after WPPSS)

Thus, it seems that the site is located in a region of moderately high seismicity. However, there is no indication of significant earthquake activity within 20 miles of the site. A two-month microearthquake survey of the area lying within approximately 30 miles of the site was conducted by the Washington Public Power Supply System during the summer of 1973. (Ref. 27) This survey indicates that the study area is in a region of current relatively low seismicity with an equivalent of 14 earthquakes greater than Richter magnitude 1 per 1000 km^2 per year. The distribution of microearthquakes did not indicate aligment of activity along any known faults.

3.0 DATA COLLECTION AND PROCESSING

The data collection and processing sequence used in this study is summarized in figure 3.0-1.

3.1 INSTRUMENTATION AND DATA COLLECTION

During the summer of 1975, field recordings of microseisms were made simultaneously at two triaxial seismometer sations at the study site. One of these was designated the "base station" and was located on an outcrop of weathered sandstone of the Astoria formation. (See figure 2.2-1) At the study site, this formation may be considered to be bedrock. The second seismometer station was designated the "portable station" and was operated at three different locations on the Helm Creek deposit. (See figure 2.2-1)

At each seismometer station, the recording equipment and accompanying power supply consisted of the following pieces of equipment:

3 each	Critically damped Ranger seismometers
3 each	Newport 60 differential amplifiers with adjustable gain and low-pass filter
1 each	Ampex PR-500 FM analog tape recorder

FIGURE 3.0-1 SUMMARY OF DATA PROCESSING SEQUENCE

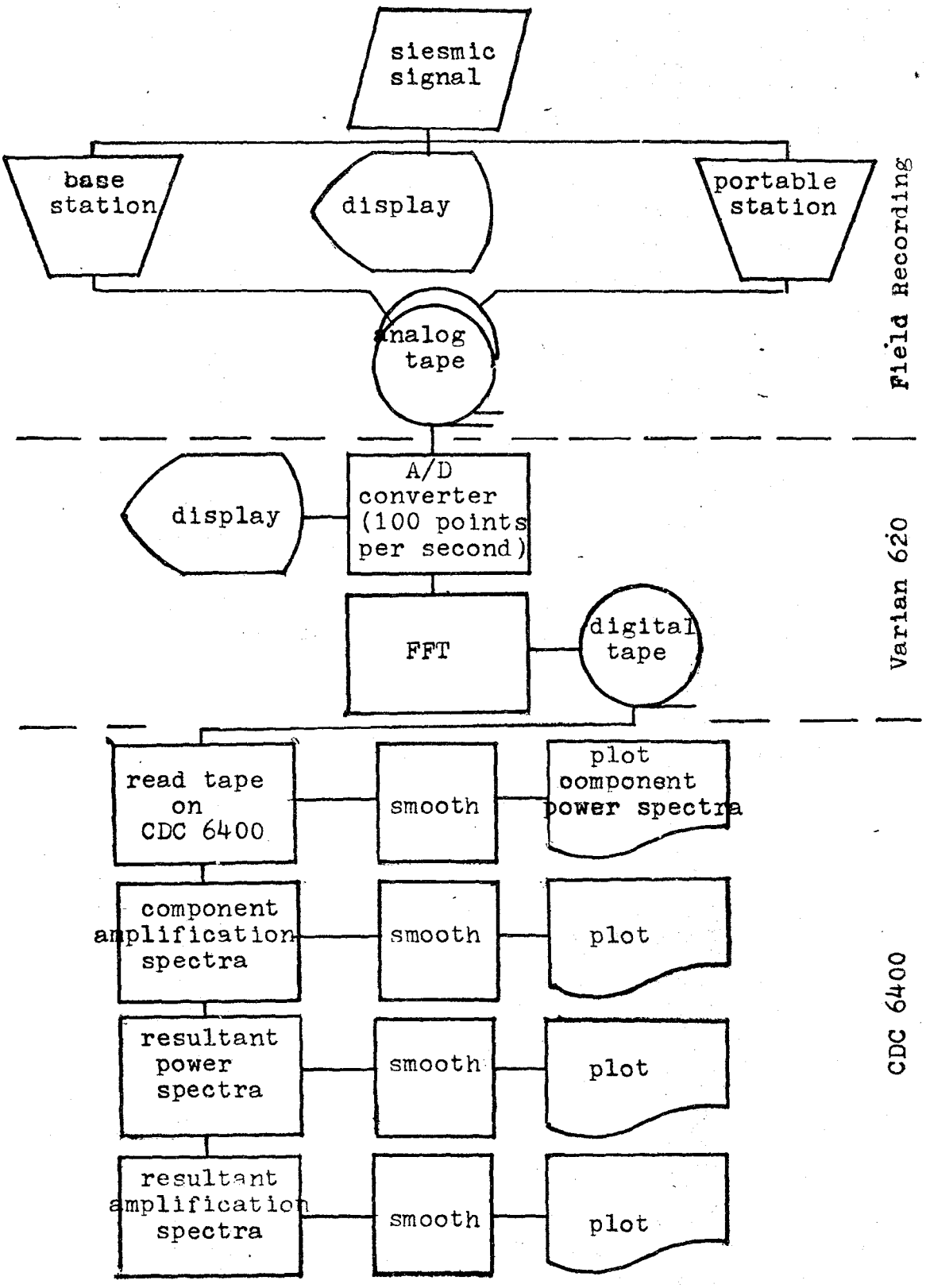

1 each Topaz 24v DC to 110v AC static inverter

4 each Automobile-type batteries

In addition, an oscilloscope was available at the portable station to visually monitor incoming signals. Figures 3.1-1 and 3.1-2 show the recording equipment as used at the base and portable stations respectively and figure 3.1-3 shows the generalized equipment layout of the portable station in block diagram form.

When recording, a gain of 2000 and a 30 hz low-pass filter were used at both field stations. This recording gain allowed the range of the recorded signal to be matched as nearly as posible to the dynamic range of the recording system. The use of the 30 hz low-pass filter during recording (and again during playback) allowed the signal lying within the predetermined frequency band of interest (0 to 10 hz) to remain essentially unchanged while removing undesirable higher frequency signal components. Figure 3.1-4 shows the frequency response of the filter system used in this study.

From 10 to 12 recordings were made at each portable station location. Simultaneous recordings were made at the base station while base and portable station operations were synchronized by means of verbal radio communication. Of 33 pairs of field recordings made in this manner, 15 pairs were

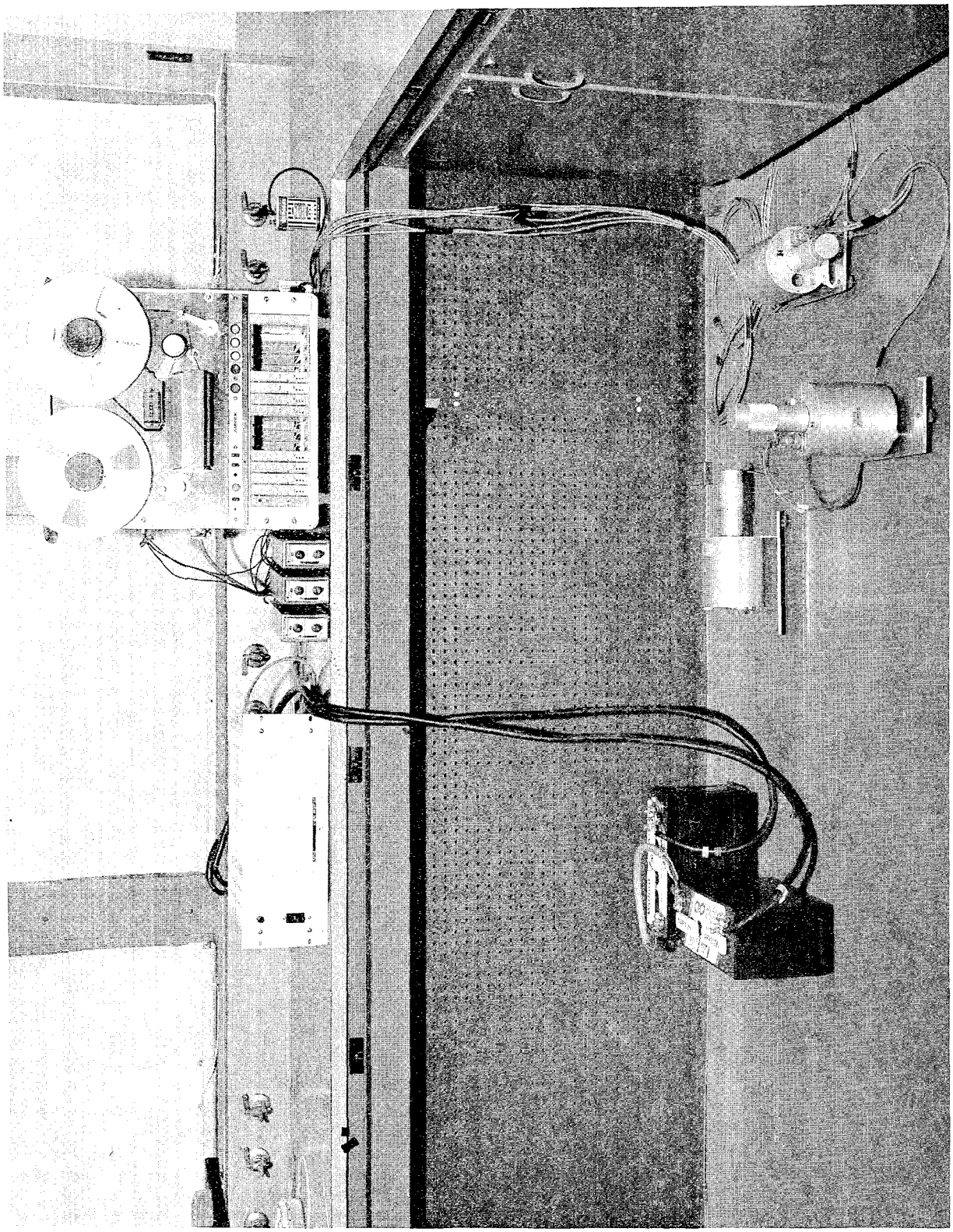

FIGURE 3.1-1 BASE STATION EQUIPMENT

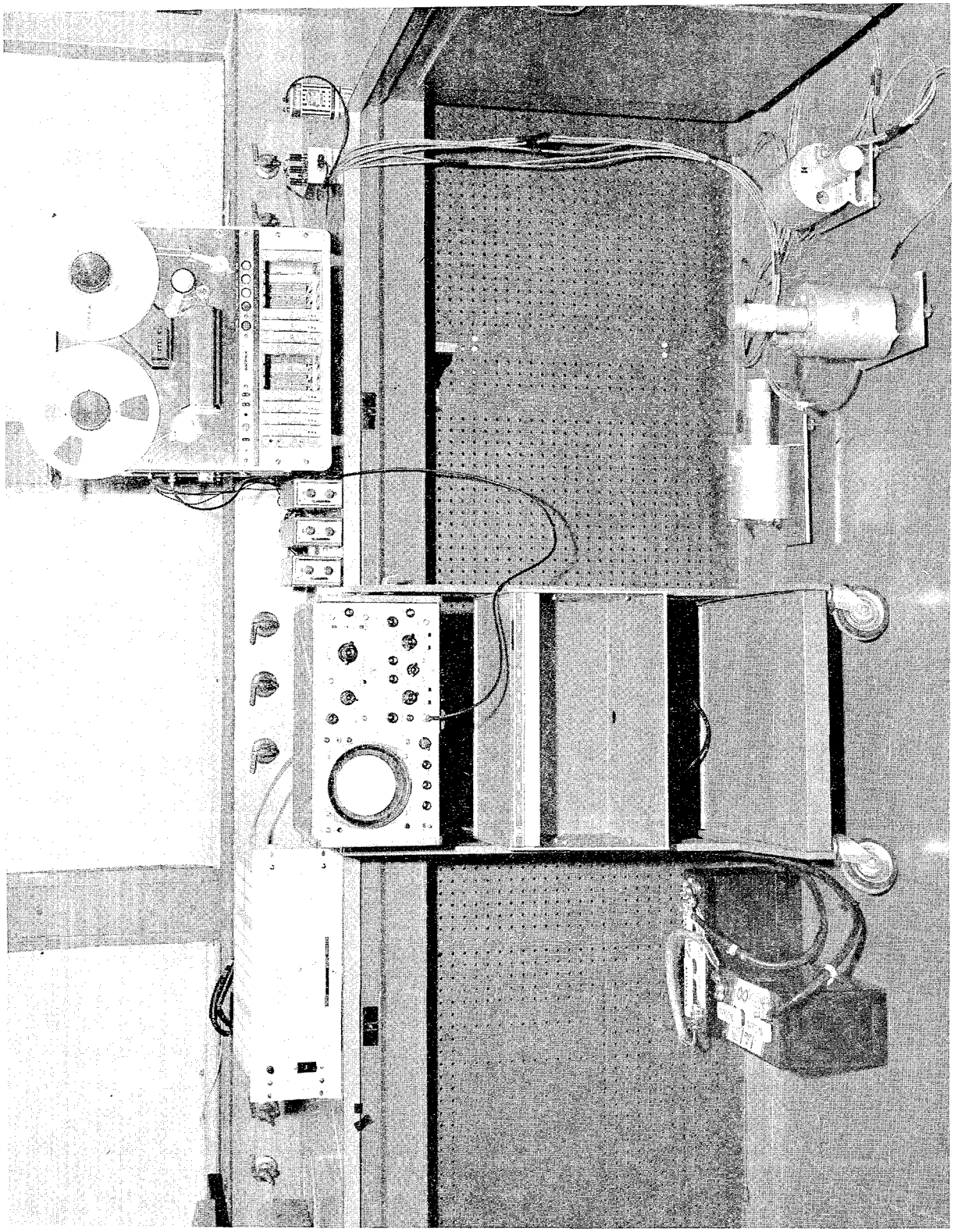

FIGURE 3.1-2 PORTABLE STATION EQUIPMENT

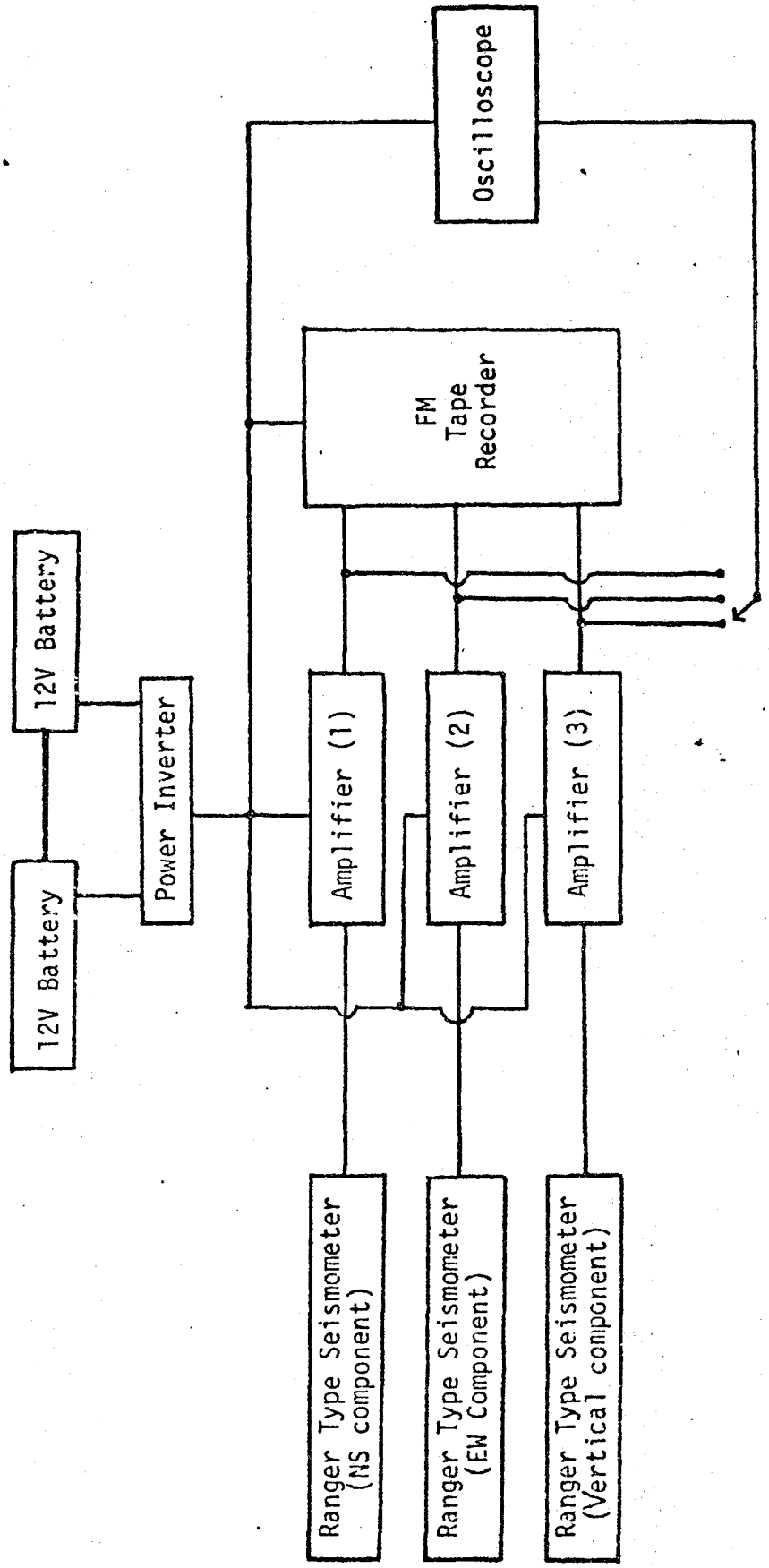

FIGURE 3.1-3 BLOCK DIAGRAM OF EQUIPMENT AS USED AT PORTABLE STATION

FIGURE 3.1-4 FREQUENCY RESPONSE OF RECORDING EQUIPMENT (DOUBLE PASS THROUGH 30 HZ LOW-PASS FILTER)

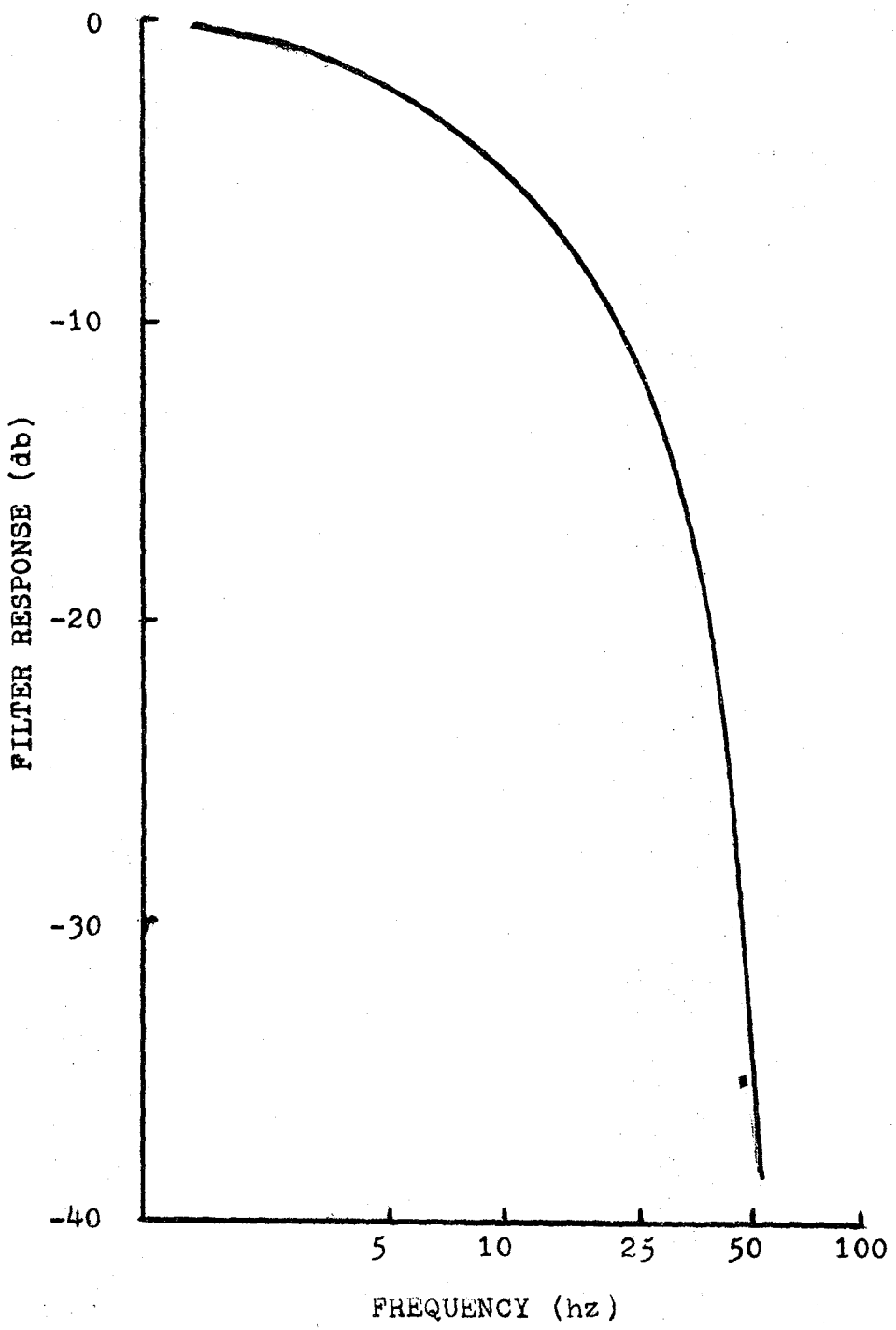

later selected for further analysis.

In addition to normal traffic on nearby roads, there was some logging taking place on land adjacent to the study site during the period of field data collection. All possible care was taken to record only during periods of minimum disturbance from these and other sources of undesirable seismic noise.

3.2 DATA PROCESSING

3.2.1 Analog to Digital Conversion

Upon returning from the field, all recordings were visually reviewed on an oscilloscope. Any record which showed obvious evidence of equipment malfunction, excessive noise, or undesirable signal was discarded at that time. Concurrently, "good" pairs of data were selected for further analysis. These were again played back through the amplifiers and 30 hz low-pass filters and reviewed on the oscilloscope. Analog playback gains were then selected so as to give each record a dynamic range less than but as nearly as possible equal to 10 volts peak-to-peak (the dynamic range of the digitizer to be used).

The frequency response of the record/playback system is shown in figure 3.1-4. The signal is down nearly 38 db

(the dynamic range of the recording equipment) at 50 hz. Therefore, a digital sampling rate of 100 samples per second was judged adequate to avoid aliasing of data processed in the manner described above.

Aliasing is the phenomena whereby upon conversion from analog to digital form, high frequency signal components may impersonate low frequency ones. (See figure 3.2-1.) Whether or not aliasing takes place is dependent upon the rate of digital sampling and upon the frequency content of the sampled waveform. Aliasing will take place if frequency components higher than what is called the Nyquist or "folding" frequency are present. The Nyquist frequency (f_n) may be defined as being equal to half the reciprocal of the sampling interval (T_s) or to half the sampling frequency (f_s). Thus,

$$f_n = \tfrac{1}{2} f_s = 1/(2T_s) \qquad (3.2.1)$$

In the present case, 50 hz is the highest frequency component present in the analog signal as it is played back. (See figure 3.1-4.) Therefore, we must sample in such a manner that the Nyquist frequency will be equal to or greater that 50 hz in order to avoid aliasing. Thus,

$$f_n = \tfrac{1}{2} f_s = 50 \text{ hz} \qquad (3.2.2)$$

$$f_s = 100 \text{ hz} \qquad (3.2.3)$$

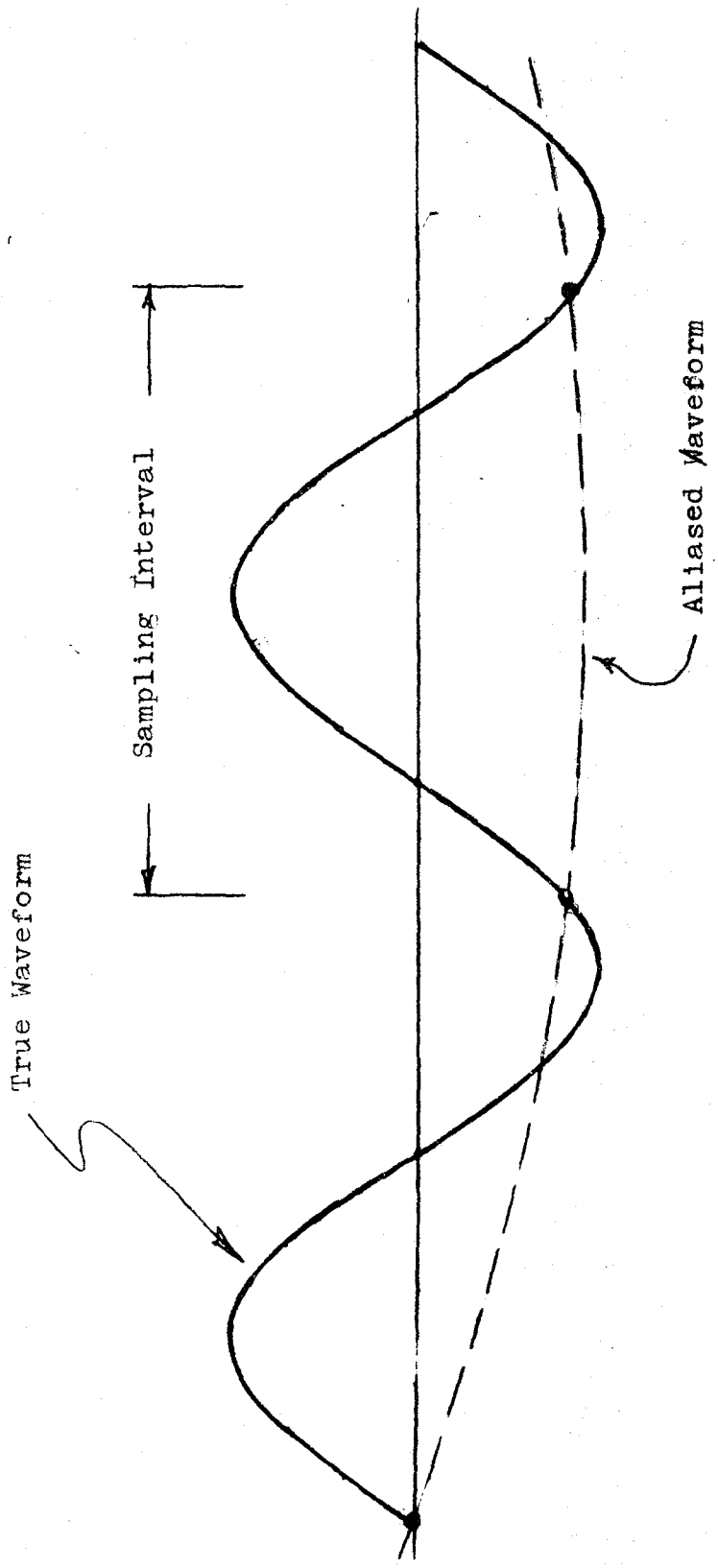

FIGURE 3.2-1 ALIASING

By this argument, 100 samples per second was chosen as an appropriate sampling rate and the analog data was digitized on a Varian 620 computer with Analog/Digital Converter at the University of Washington Geophysics Data Processing Center.

3.2.2 Transformation to the Frequency Domain.

Digitized data was transformed to the frequency domain on the Varian 620 by means of a Cooley-Tukey-type fast Fourier transform. The Fourier transform has long been used to characterize linear systems and to identify the frequency components which go to make up a continuous waveform. The transform is founded on the Fourier theorem which states that any waveform may be represented as the sum of a series of sinusoidal waves. The transform provides a means of mathematically decomposing a waveform into its component sinusoids and calculating their amplitude. This calculation has traditionally been a very tedious and time consuming operation. Also, the very large amounts of data calculation required tended to reduce the precision of the operation. The relatively recent development of an effecient computing algorithm now allows the numerical calculation of the Fourier transform with relative ease.

When dealing with a sampled waveform, the finite or discrete form of the Fourier transform (the discrete Fourier transform or DFT) must be used. The fast Fourier transform (FFT) is simply an efficient means of computing the DFT.

The Fourier transform pair for a continuous signal may be written in the form

$$x(t) = \int_{-\infty}^{\infty} X(f) e^{i2\pi ft} df \qquad (3.2.4)$$

$$X(f) = \int_{-\infty}^{\infty} x(t) e^{-i2\pi ft} dt \qquad (3.2.5)$$

for $-\infty < x < \infty$, $-\infty < f < \infty$, and $i = \sqrt{-1}$. The lower-case $x(t)$ represents the time-domain function and the upper-case $X(f)$ represents the corresponding frequency-domain function. It should be noted that the transform is symmetrical and reversible.

The analogous discrete Fourier transform pair which applies to periodically sampled versions of the functions $x(t)$ and $X(f)$ may be written in the form

$$x(j\Delta t) = x(j) = \sum_{k=0}^{N-1} X(k) e^{i2\pi jk/N} \qquad (3.2.6)$$

$$X(k\Delta f) = X(k) = \frac{1}{N} \sum_{j=0}^{N-1} x(j) e^{-i2\pi jk/N} \qquad (3.2.7)$$

for $j = 0, 1, \ldots, N-1$; and $k = 0, 1, \ldots, N-1$ where N is the number of sample points. A complete derivation of the discrete Fourier transform may be found in references (4) and (7).

When the expression $e^{-2\pi i/N}$ in equations 3.2.6 and 3.2.7 is replaced by the term W_n, the DFT pair takes the form

$$x(j) = \sum_{k=0}^{N-1} X(k) W_n^{-jk} \qquad (3.2.8)$$

$$X(k) = \frac{1}{N} \sum_{k=0}^{N-1} x(j) W_n^{jk} \qquad (3.2.9)$$

Let us now look at the derivation of the Cooley-Tukey FFT algorithm for the evaluation of equation 3.2.9 in the case where N = 8. When N = 8, it is convenient to represent both j and k as binary numbers; that is, for

$$j = 0, 1, \ldots, 7 \quad \text{and} \quad k = 0, 1, \ldots, 7$$

we can write

$$J = j_2 4 + j_1 2 = j_0 \quad \text{and} \quad k = k_2 4 + k_1 2 * k_0 \qquad (3.2.10)$$

where j_0, j_1, j_2, k_0, k_1, and k_2 can take on the values 0 and 1 only. Using this representation and remembering that in this case N = 8, equation 3.2.9 becomes

$$X(k_2,k_1,k_0) = \frac{1}{8} \sum_{j_2=0}^{1} \sum_{j_1=0}^{1} \sum_{j_0=0}^{1} x(j_2,j_1,j_0) W^{(j_2 4+j_1 2+j_0)(k_2 4+k_1 2+k_0)} \qquad (3.2.11)$$

where $W = \exp(-2\pi i/8)$.

Noting that $W^{m+n} = W^m + W^n$, we have

$$W^{(j_2 4+k_1 2+j0)(k_2 4+k_1 2+k_0)} = W^{(k_2 4+k_1 2+k_0) j_2 4} \; W^{(k_2 4+k_1 2+k_0) j_1 2} \; W^{(k_2 4+k_1 2+k_0) j_0} \qquad (3.2.12)$$

If we look at these terms individually, we see that they may be written in the form

$$W^{(k_2 4+k_1 2+k_0)j_2 4} = [W^{8(k_2+k_1)j_2}]W^{k_0 j_2 4} \qquad (3.2.13)$$

$$W^{(k_2 4+k_1 2+k_0)j_1 2} = [W^{8k_2 j_1}]W^{(k_1 2+k_0)j_2} \qquad (3.2.14)$$

$$W^{(k_2 4+k_1 2+k_0)} = W^{(k_2 4+k_1 2+k0)j_0} \qquad (3.2.15)$$

Note however that

$$W^8 = (e^{-2\pi i/8})^8 = e^{-2\pi i} = 1 \qquad (3.2.16)$$

Therefcre, the bracketed portions of equations 3.2.13 and 3.2.14 may be replaced by a one. This means that equation 3.2.11 may be written in the form

$$X(k_2,k_1,k_0) = \frac{1}{8}\sum_{j_2=0}^{1}\sum_{j_1=0}^{1}\sum_{j_0=0}^{1} x(j_2,j_1,j_0)W^{k_0 j_2 4}W^{(k_2+k_0)j_1 2}W^{(k_2 4+k_1 2+k_0)j_0} \qquad (3.2.17)$$

In this form it is convenient to perform each of the summations separately and to label the results. Note that each set consists of only eight terms and that only the latest set need be saved. Thus, the equations can be written in the form

$$x_1(k_0,j_1,j_0) = \sum_{j_2=0}^{1} x(j_2,j_1,j_0)W^{k_0 j_2 4} \qquad (3.2.18)$$

$$x_2(k_0,k_1,j_0) = \sum_{j_1=0}^{1} x_1(k_0,j_1,j_0)W^{(k_1 2+k_0)j_1 2} \qquad (3.2.19)$$

$$x_3(k_0,k_1,k_2) = \sum_{j_0=0}^{1} x_2(k_0,k_1,j_0)W^{(k_2 4+k_1 2+k_0)j_0} \qquad (3.2.20)$$

Then,

$$X(k_2,k_1,k_0) = \frac{1}{8}\, x_3(k_0,k_1,k_2) \qquad (3.2.21)$$

Although the direct evaluation of equation 3.2.7 for N = 8 would require nearly 64 complex multiply-and-add operations, the FFT equations show only 48 operations. By noting that the first multiplication of each summation is actually a multiplication by +1, the number of multiplications may be reduced to 24. By further noting that $W^0 = -W^4$, $W^1 = -W^5$, etc., the number of multiplications may be reduced to 12. These reductions carry on to the general case of $N = 2^m$ where m is an integer reducing the computation of nearly N^2 operations to $(N/2)\log_2 N$ complex multiplications, $(N/2)\log_2 N$ complex additions, and $(N/2)\log_2 N$ subtractions. (See figure 3.2-2 for comparison of FFT and DFT)

By using the Varian 620 and the Cooley-Tukey FFT, it was possible to transform 2048 data points or about 20.5 seconds of record for each data set. The specific transfrom program used yields a Fourier power spectrum which consists of the squares of the Fourier transform amplitudes. By using this algorithm, a computational reduction of slightly over 180 to 1 was realized over direct computation. Transform arrays from the Varian 620 were output to magnetic tape for later analysis by the CDC 6400. The tapes were read at the University of Washington Computer center and converted to a format compatible with the CDC 6400 at that facility.

FIGURE 3.2-2 COMPARISON OF FFT AND DFT

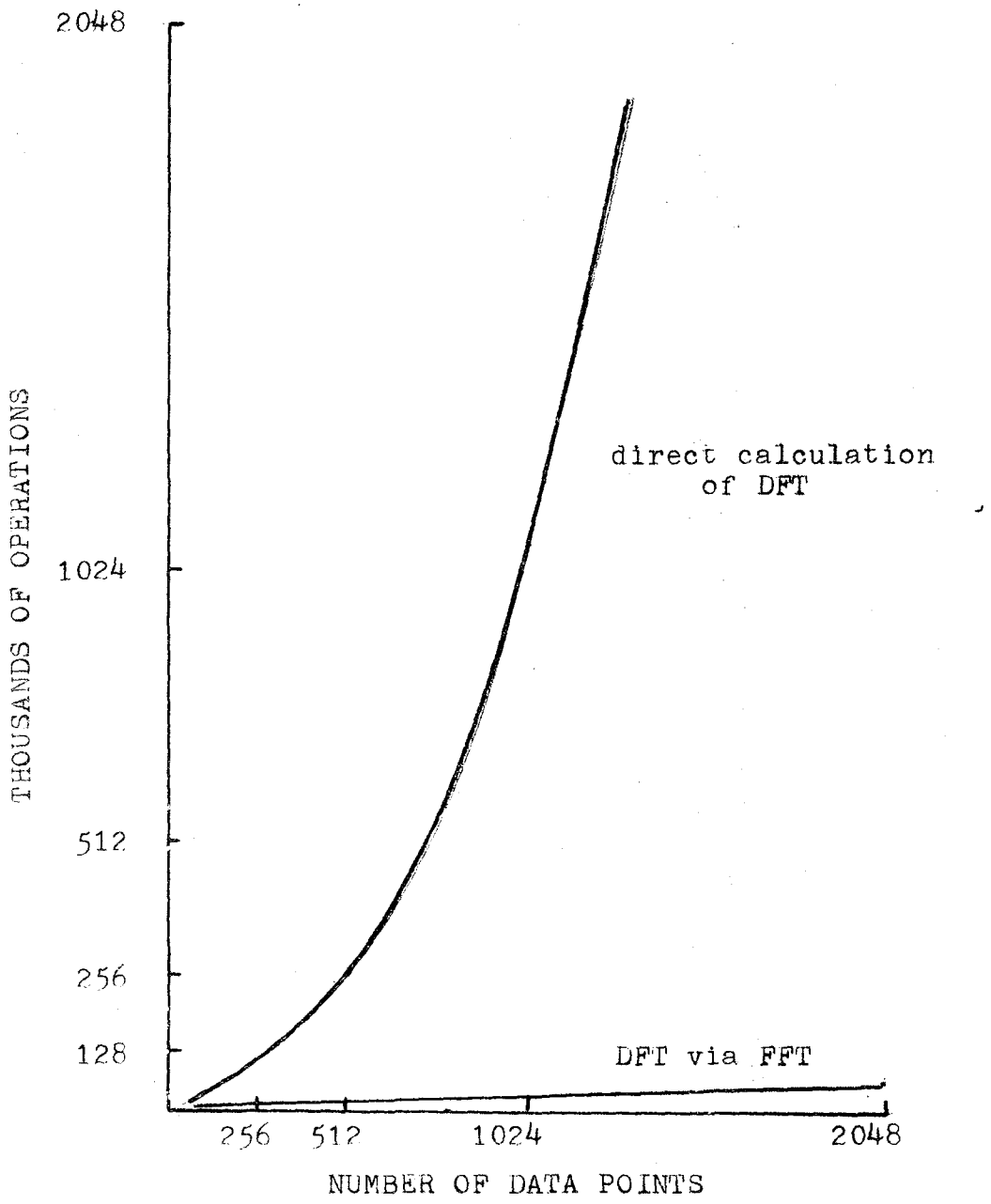

3.2.3 Component Power Spectra

Transform arrays from the Varian 620 were read into the CDC 6400 and a CalComp plotter was used to plot all transform points in the range 0 to 10 hz. For each data set (triaxial base station record and simultaneous triaxial portable station record) the Fourier power spectra of the three base and three portable station components were plotted. (See figure 3.2-3)

3.2.4 Component Amplification Spectra

Amplification spectra are derived in the following manner. The site soil and subsurface are assumed to act upon seismic signals as a filter with linear characteristics. Then, the system through which seismic signals pass may be modeled as shown in figure 3.2-4 where the symbols s(t), f(t), i(t), and r(t) denote time-domain functions. If all system components are assumed to possess linear characteristics, linear operator theory tells us that the response of the system, r(t), will be defined by

$$r(t) = s(t) * f(t) * i(t) \qquad (3.2.22)$$

where the symbol "*" denotes the mathematical process of convolution.

Also, if S(f), F(f), I(f), and R(f) are taken to represent

FIGURE 3.2-3 EXAMPLE OF BASE STATION COMPONENT POWER SPECTRA

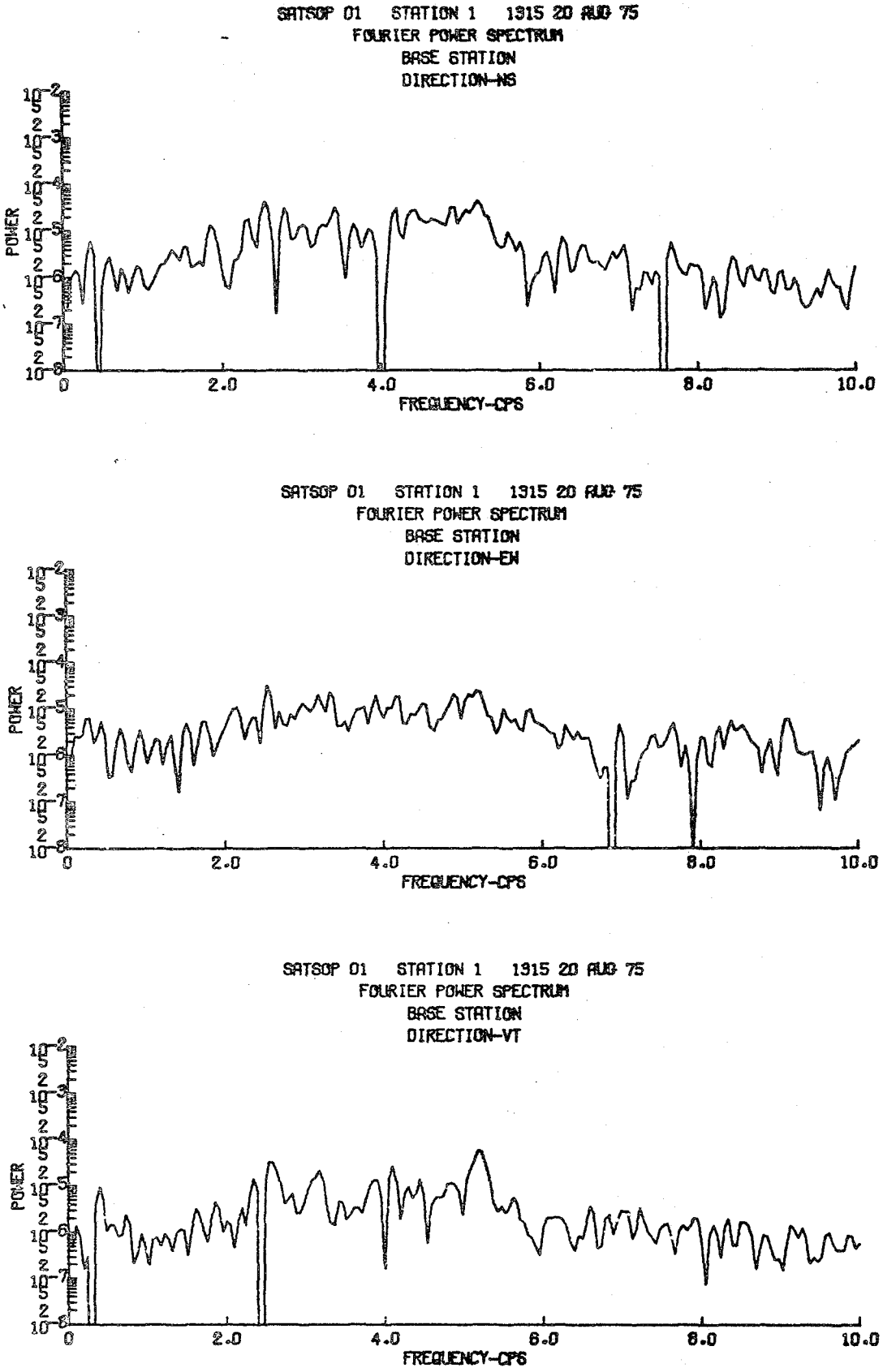

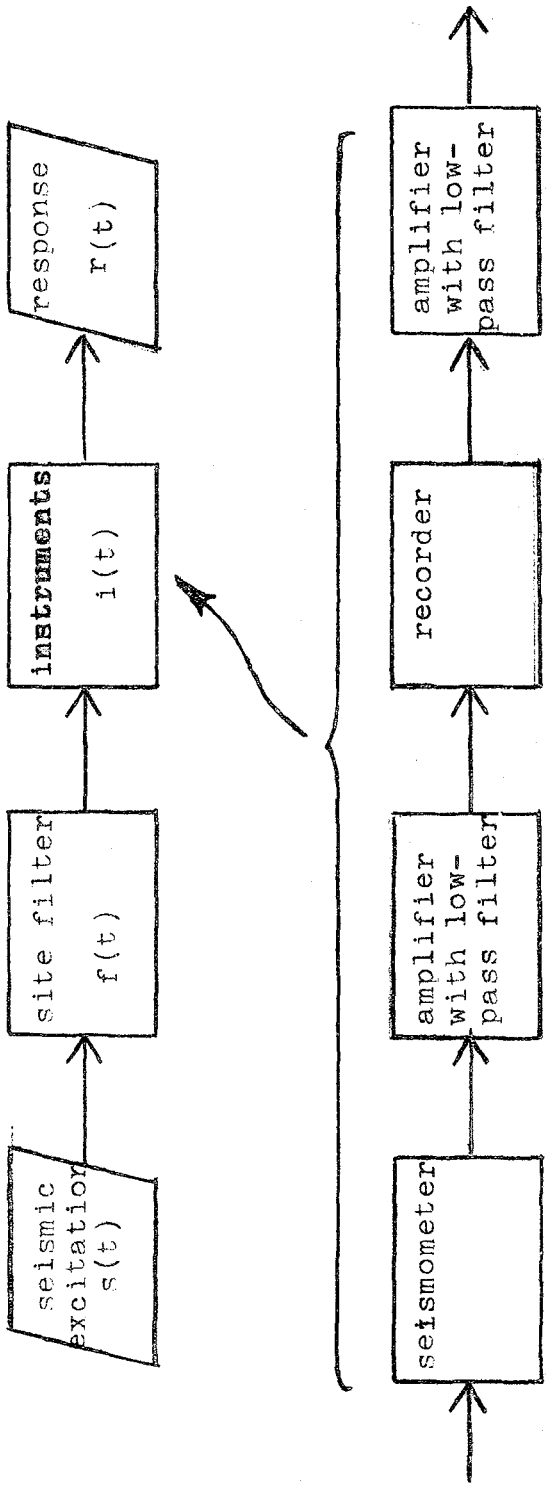

FIGURE 3.2-4 LINEAR SYSTEM DIAGRAM

frequency-domain functions corresponding to those time-domain functions shown in figure 3.2-4 (i.e. s(t) and S(f) are a Fourier transform pair), then the frequency-domain response, R(f), of the system will be defined by

$$R(f) = S(f) \times F(f) \times I(f) \qquad (3.2.23)$$

where "x" denotes multiplication. In this study, the Fourier power spectrum is equated with R(f).

Therefore, the ratio of the power spectrum of the portable station to that of the base station will be

$$\frac{R_p(f)}{R_b(f)} = \frac{S_p(f) \times F_p(f) \times I_p(f)}{S_b(f) \times F_b(f) \times I_b(f)} \qquad (3.2.24)$$

Now, if it is assumed that $S_p(f) = S_b(f)$ because the data from both stations was recorded simultaneously, and that $I_p(f) = I_b(f)$ because the instruments at both stations are identical, then equation 3.2.24 reduces to

$$\frac{R_p(f)}{R_b(f)} = \frac{F_p(f)}{F_b(f)} \qquad (3.2.25)$$

Thus, the power spectral ratio yields a function which reflects solely the relative effect of the site filter on the system response.

It must be noted that Fourier power spectra which are used

in this study as measures of frequency-domain functions are by definition composed of the squares of Fourier amplitudes. Thus,

$$\frac{R_p(f)}{R_b(f)} = \frac{(X_p(f))^2}{(X_b(f))^2} \qquad (3.2.26)$$

where $X_p(f)$ and $X_b(f)$ are analogous to $X(f)$ in equation 3.2.5. We therefore see that the square root of the power spectral ratio will yield a function which is a measure of the amplification as a function of frequency of signals measured at the portable station relative to those measured at the base station. This function is called the amplification spectra and is defined by

$$\text{AMPLIFICATION SPECTRA} = \sqrt{\frac{R_p(f)}{R_b(f)}} = \sqrt{\frac{X_p(f)^2}{X_b(f)^2}} = \frac{X_p(f)}{X_b(f)} \qquad (3.2.27)$$

Amplification for all individual triaxial portable station components relative to the corresponding base station components were calculated and plotted. (See figure 3.2-5)

3.2.5 Resultant Power Spectra

The resultant power spectra of the triaxial components of each data set were calculated by the equation

$$\text{RESULTANT} = (C_{ns}^2 + C_{ew}^2 + C_{vt}^2)^{\frac{1}{2}} \qquad (3.2.26)$$

FIGURE 3.2-5 EXAMPLE OF COMPONENT AMPLIFICATION SPECTRA

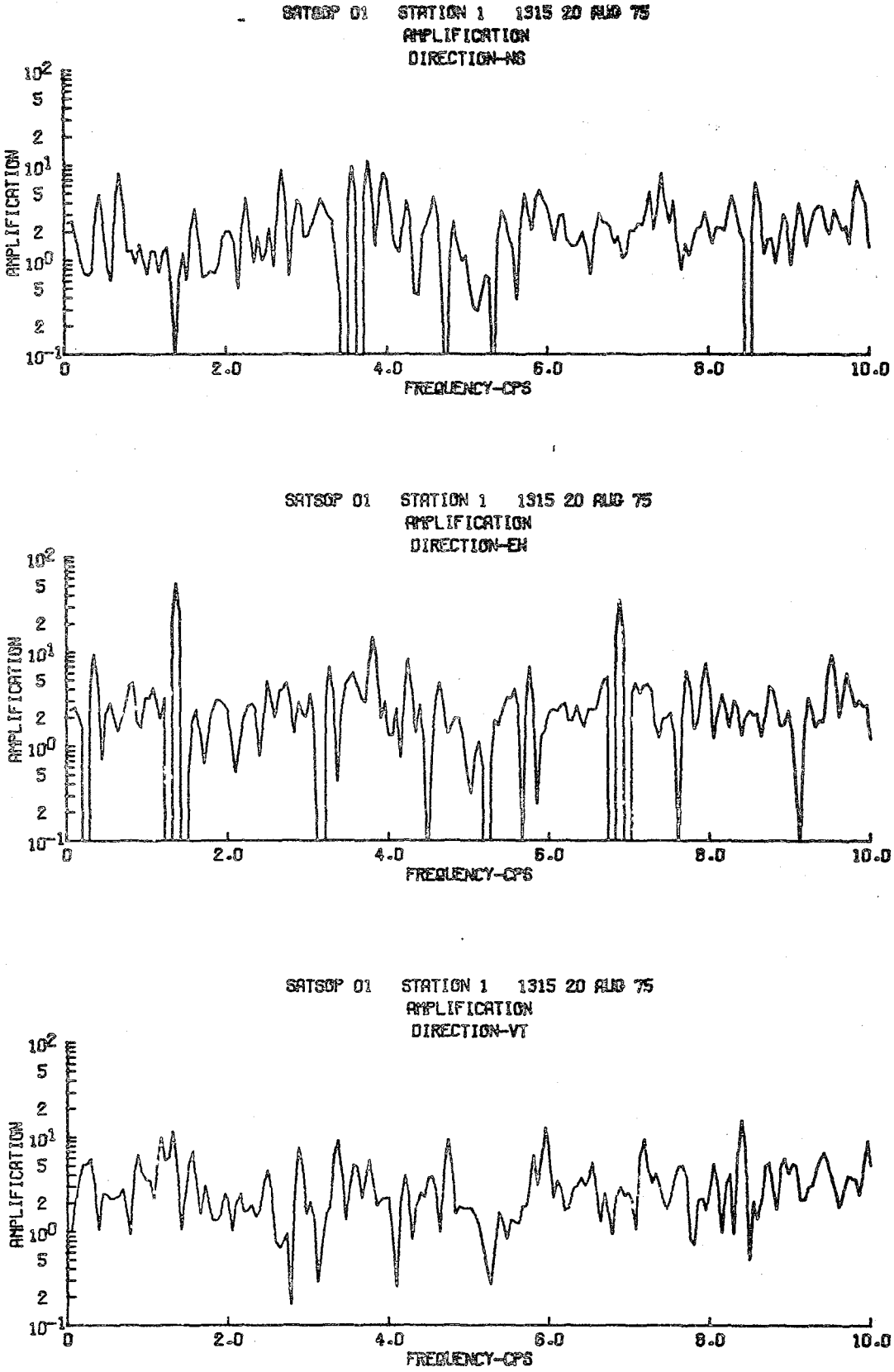

where C_{ns}, C_{ew}, and C_{vt} are the power spectral amplitudes of the north-south, east-west, and vertical triaxial components respectively. The resultant power spectra of each station was plotted as shown in figure 3.2.6.

3.2.6 Resultant Amplification Spectra

For each data set, the amplification spectrum of the portable station resultant relative to the base station resultant was calculated and plotted in the same manner as for individual component amplification spectra. (See figure 3.2-7)

3.2.7 Plotted Presentation of Processed Data

All computer generated plots described above were smoothed with a (1, -18, 63, 164, 63, -18, 1) moving average filter immediately prior to plotting. All such plots are presented in Appendix A.

FIGURE 3.2-6 EXAMPLE OF RESULTANT POWER SPECTRA

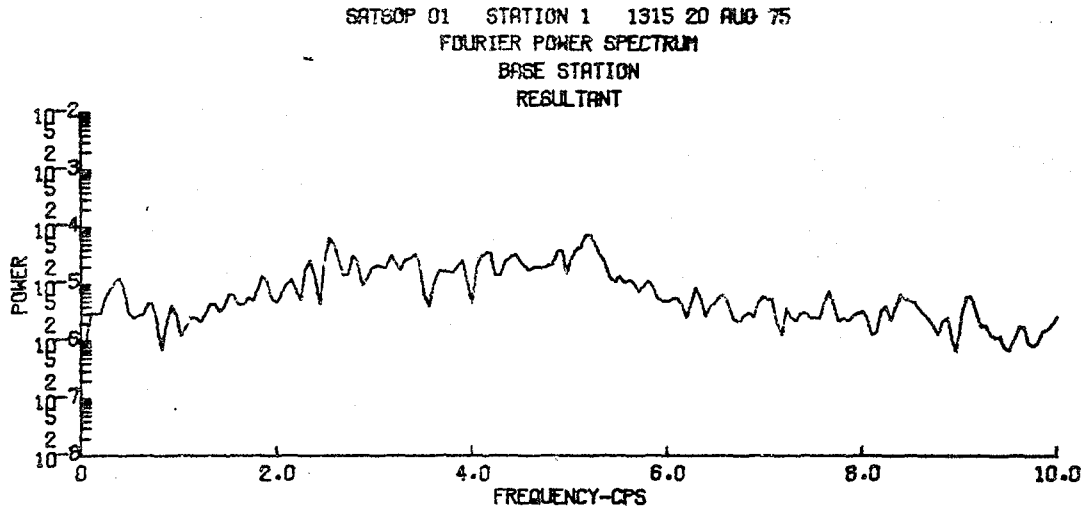

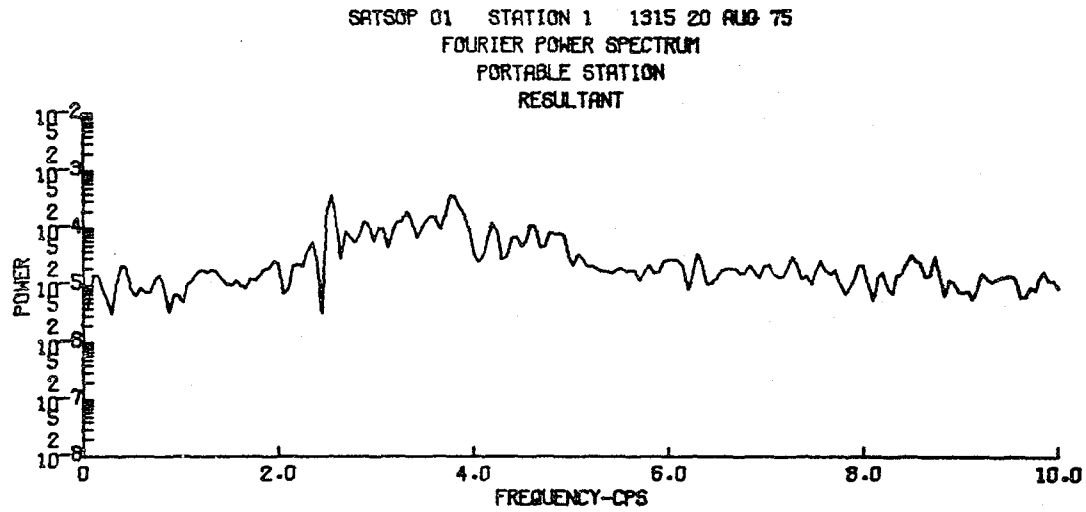

FIGURE 3.2-7 EXAMPLE OF RESULTANT AMPLIFICATION SPECTRA

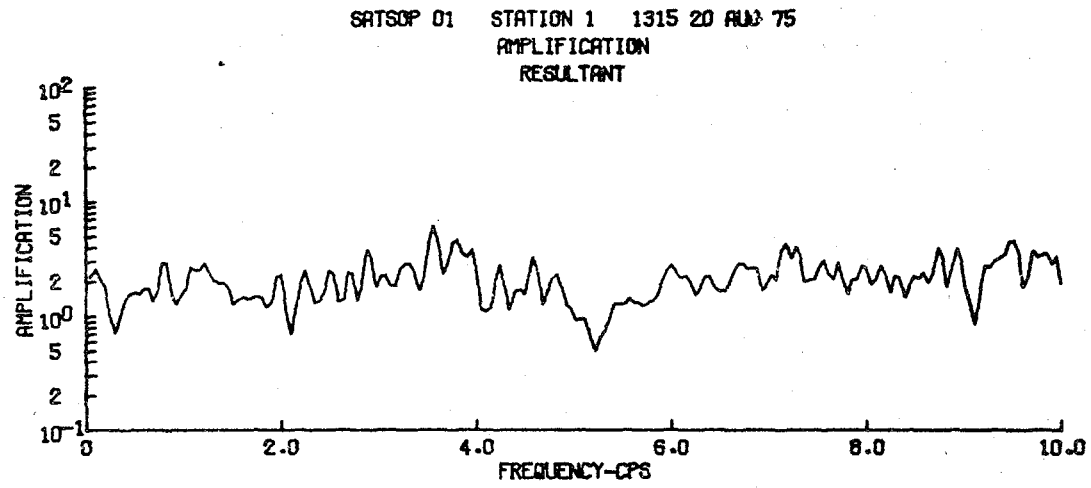

4.0 DISCUSSION AND ANALYSIS OF PROCESSED DATA

4.1 POWER SPECTRA

Inspection of the power spectra of individual triaxial components reveals the fact that these spectra often exhibit sharp peaks or narrow bands of very low power while resultant power spectra do not. (See fig. 4.1-1a and 4.1-1b) This suggests a frequency dependant polarization of the incoming wave train. Also, a cursory examination of resultant power spectra of recordings made at the same Location at different times shows these power spectra to be nonstationary. In other words, the power distribution changes with time. (See fig. 4.1-2) This fact is in agreement with Spiekers' findings that microseismic power spectra are not stationary over time periods in excess of one hour.

4.2 RESULTANT AMPLIFICATION SPECTRA

An examination of resultant amplification spectra calculated for data recorded at the same location at different times indicates that, like the resultant power spectra, they are nonstationary. However, the amplification spectra appear to retain certain general trends through time. (See fig. 4.2-1) Perhaps then, the resultant amplification spectra may be termed "semi-stationary." The fact that these amplification

FIGURE 4.1-1a EXAMPLE OF INDIVIDUAL TRIAXIAL COMPONENT POWER SPECTRA

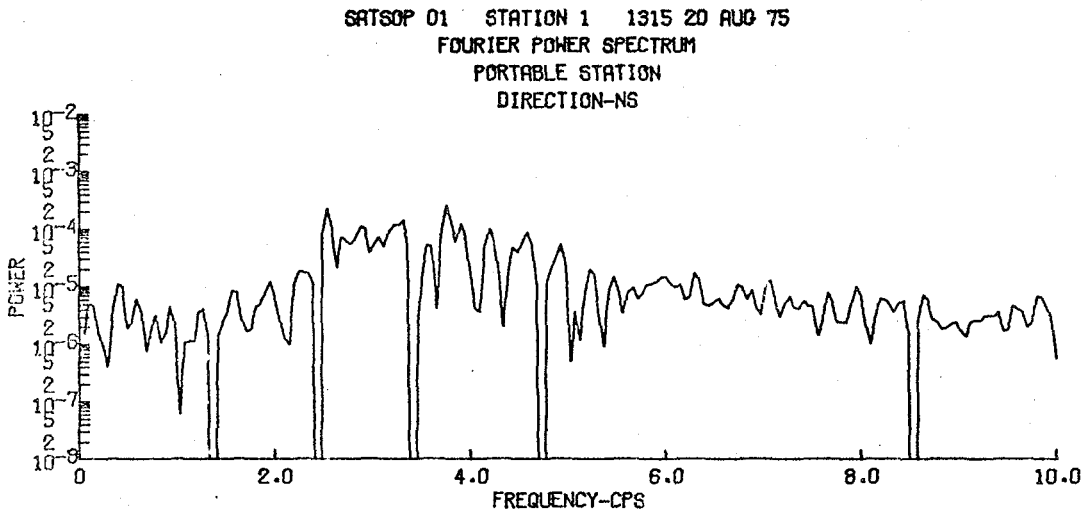

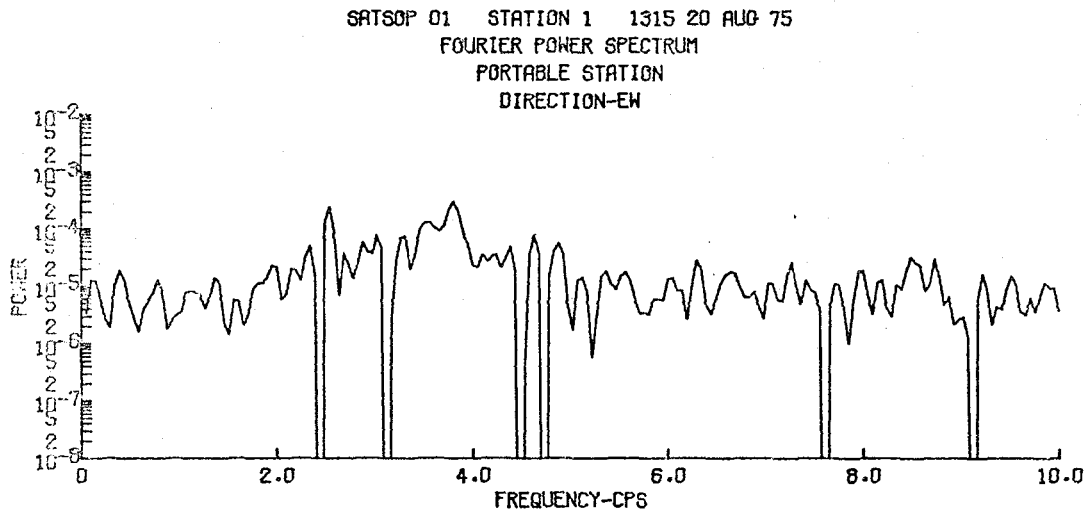

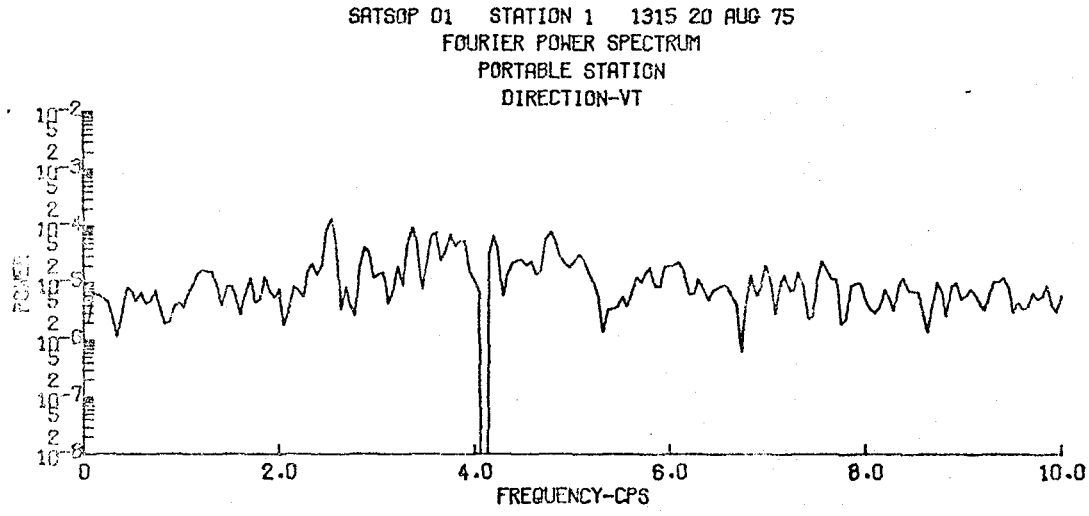

FIGURE 4.1-1b EXAMPLE OF RESULTANT POWER SPECTRA

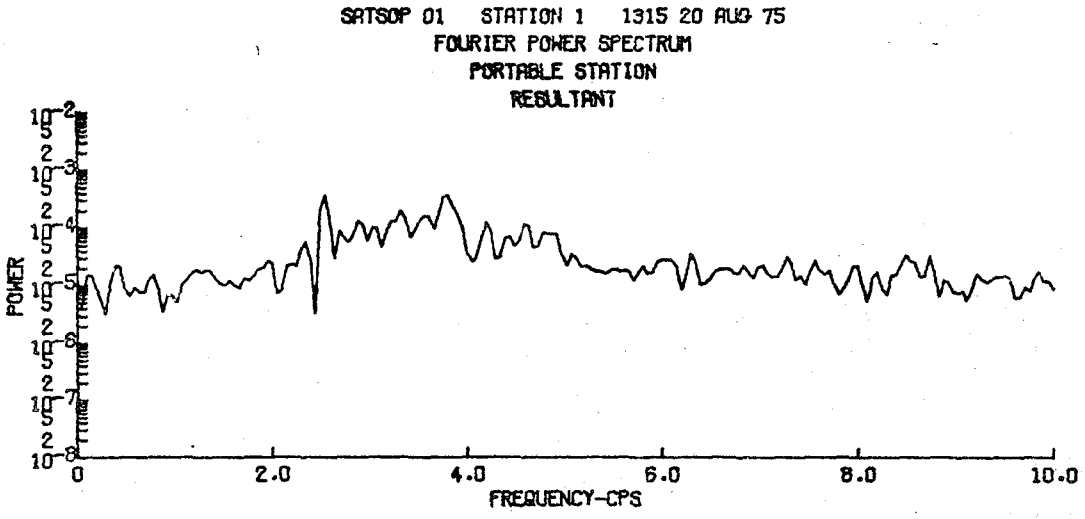

FIGURE 4.1-2 COMPARISON OF RESULTANT POWER SPECTRA

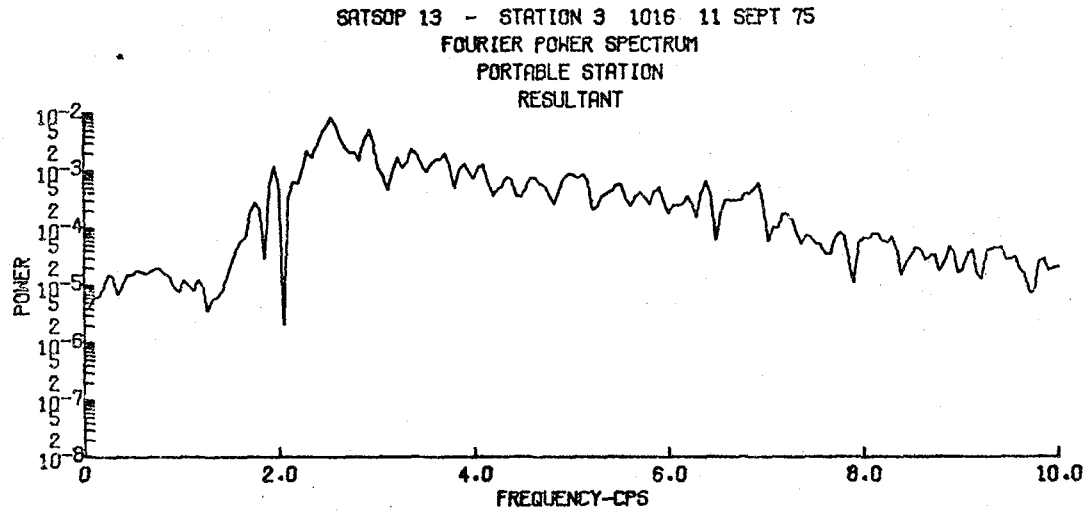

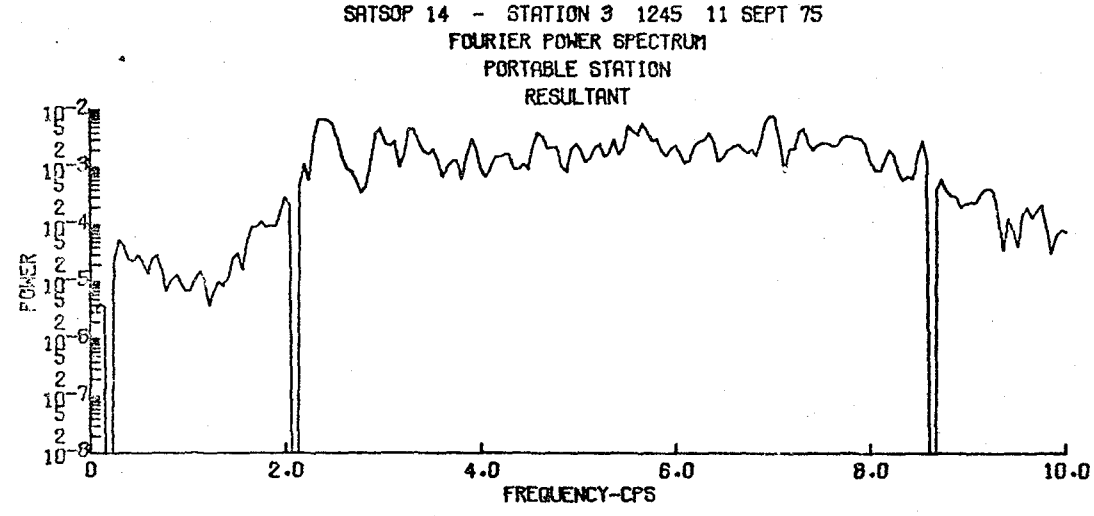

FIGURE 4.2-1 COMPARSION OF RESULTANT AMPLIFICATION SPECTRA

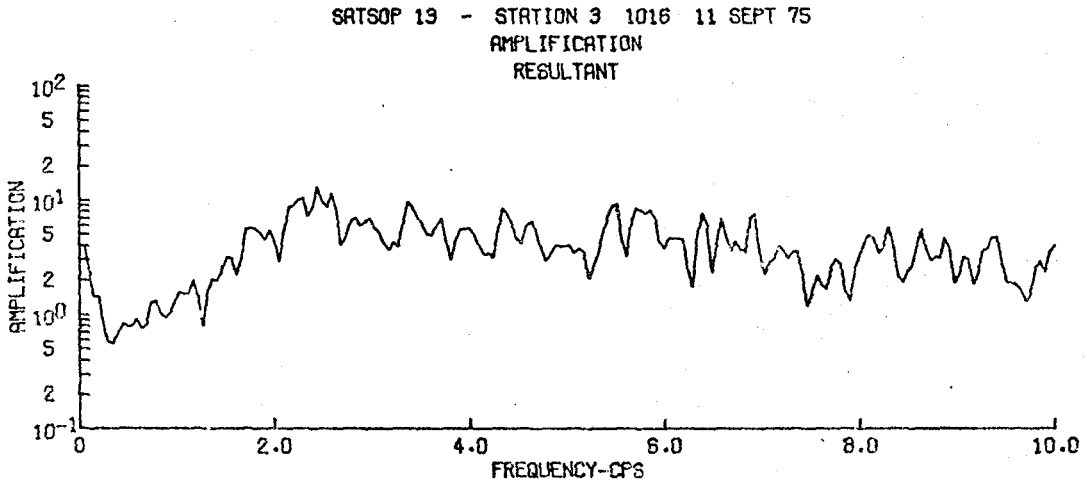

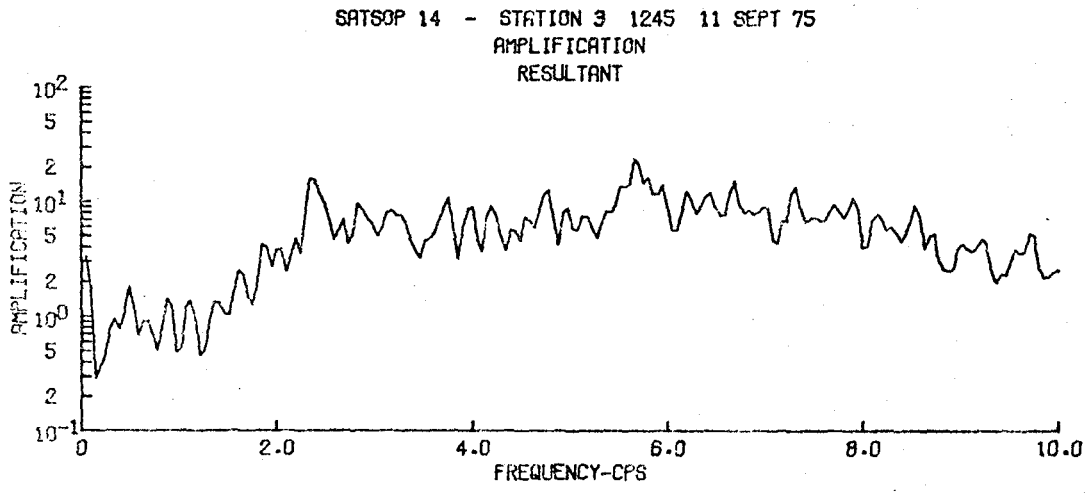

spectra do not exhibit a greater degree of stationarity may be attributable to one of two things: Either 1) the response of the site filter is nonstationary in time, or 2) the site response is stationary but other factors make it appear to be nonstationary. Intuitively it would seem that the behavior of the site filter should be stationary, at least within the time frame and strain range of this study. Therefore, let us consider what other factors might make it appear to be nonstationary.

Assuming that the response of all site and equipment components of the system shown in figure 3.2-4 is linear within the range of strains experienced in this study, nonstationary amplification spectra must be attributable to nonidentity of the excitation functions acting at the two recording stations at the time of recording. In other words, referring back to Section 3.2 of this paper, equation 3.2.25 is not valid if $S_p(f) \neq S_b(f)$. This nonidentity of excitation functions may be the result of either temporal identity of excitation functions and inadequate synchronization of recording stations or of actual nonidentity of excitation functions. True nonidentity of excitation functions might be caused by either dispersion of the wave train between recording stations or by the presence of sources of local excitation which are active at one recording station but not at the other. Both of these conditions are believed to have contributed to the nonstation-

arity of amplification spectra in this study. However, it is believed that the effects of undesirable excitation of local origin were the primary causes of the observed nonstationarity of amplification spectra.

In future studies, a greater degree of stationarity might be obtained by the use of a more sophisticated and efficient means of synchronizing operations at the two recording stations and by the use of a different source of seismic excitation. Artificial or stronger natural excitation may be more appropriate energy sources than microseisms. The use of microseisms is attractive because they are everpresent, nondestructive, and very economical. However, the point of origin of microseisms is indeterminate. Moreover, they are commonly of mixed origin, it being extremely difficult to distinguish motions of local origin from those of more remote origin. If the microseismic excitation is partly of local origin, excitation at the base and portable recording stations will likely be nonidentical unless the distance between recording stations is very small.

Therefore, if the distance between recording stations is to be other than very small, it is suggested that future work be conducted using a unique excitation source readily distinguishable from the microseismic background and originating at a point sufficiently remote from the two recording stations that the distance between the stations is of relative insignificance.

The use of natural earthquakes as an excitation source is limited by practical considerations. Thus, artificial means of excitation such as impact, explosive charges, and vibration generators would seem to be appropriate. For the investigation of sites of practical size, the distance which the energy source must be removed from the site and the need to maintain a signal of minimum strength would seem to favor the use of explosive energy sources. Cherry (ref. 9) has used offshore underwater explosions to mimic earthquake signals with favorable results.

In order to mitigate the effect of nonstationarity of amplification spectra in the present study, spectra derived from recordings made at the same locations at different times were averaged. Figures 4.2-2, 3, and 4 each show the mean and extreme values of a set of five amplification spectra for a given portable station location. It should be noted that the mean values are skewed well toward the upper limit of the range of values in each case. Therefore, the mean resultant amplification spectra should be reasonable indicators of the maximum amplification probable at a given frequency.

Furthermore, it should be noted that the mean resultant amplification spectra are characterized by many peaks but not by any one or two "dominant frequencies." (See fig. 4.2-2,3, and 4) This implies that the ground at the study site is not highly tuned. Presumably, this may be attributed to a low level of

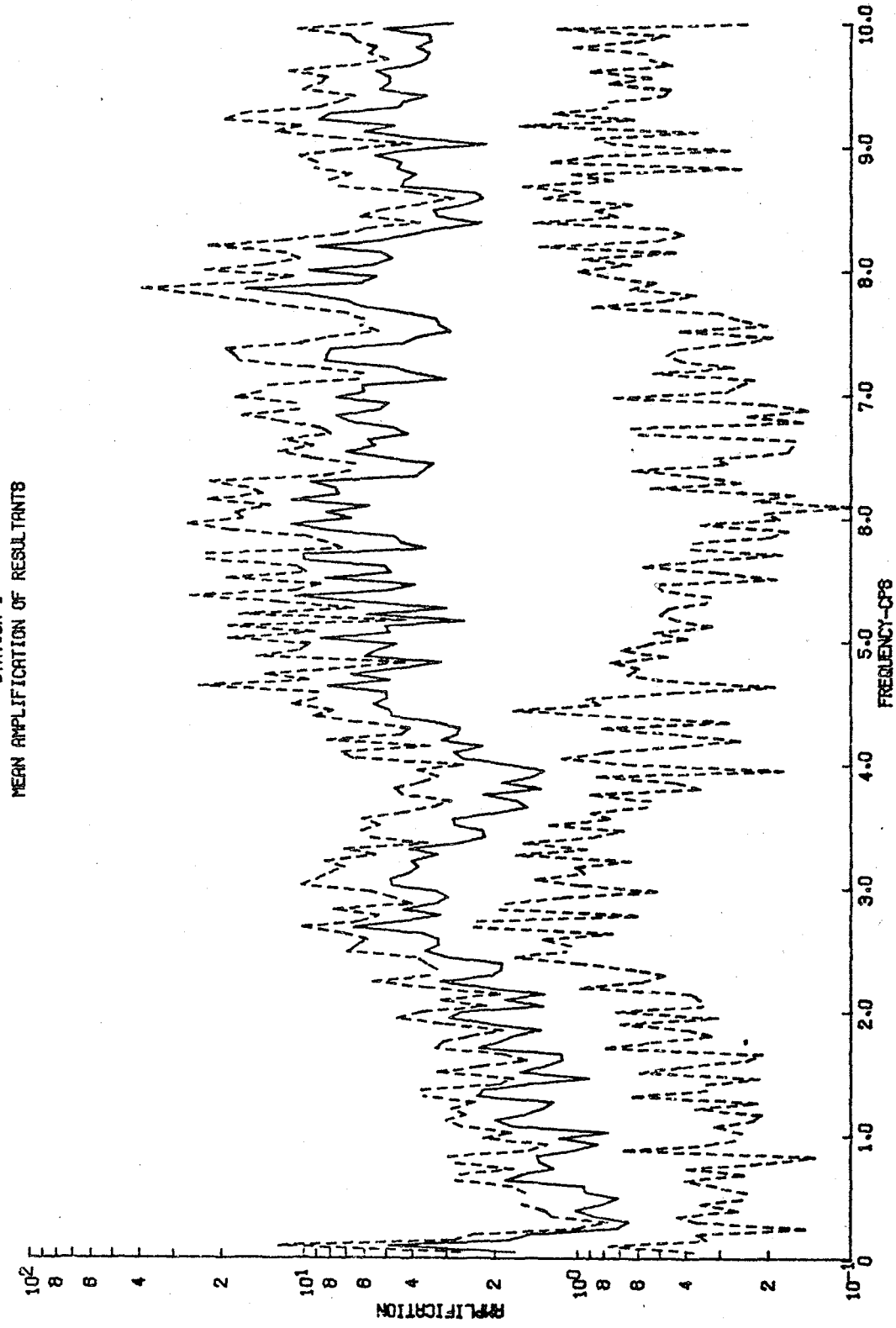

FIGURE 4.2-2 MEAN RESULTANT AMPLIFICATION - STATION 1

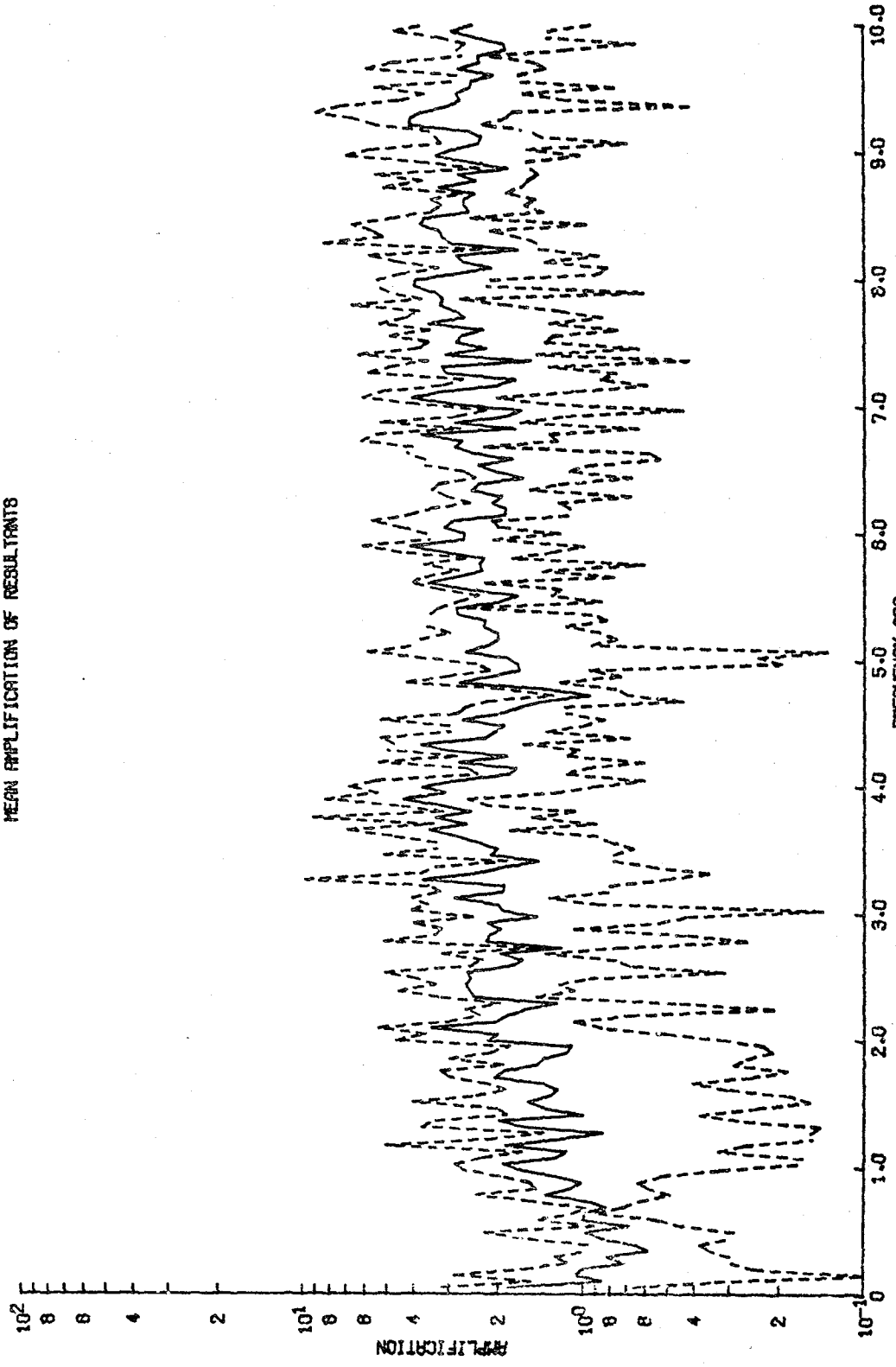

FIGURE 4.2-3 MEAN RESULTANT AMPLIFICATION - STATION 2

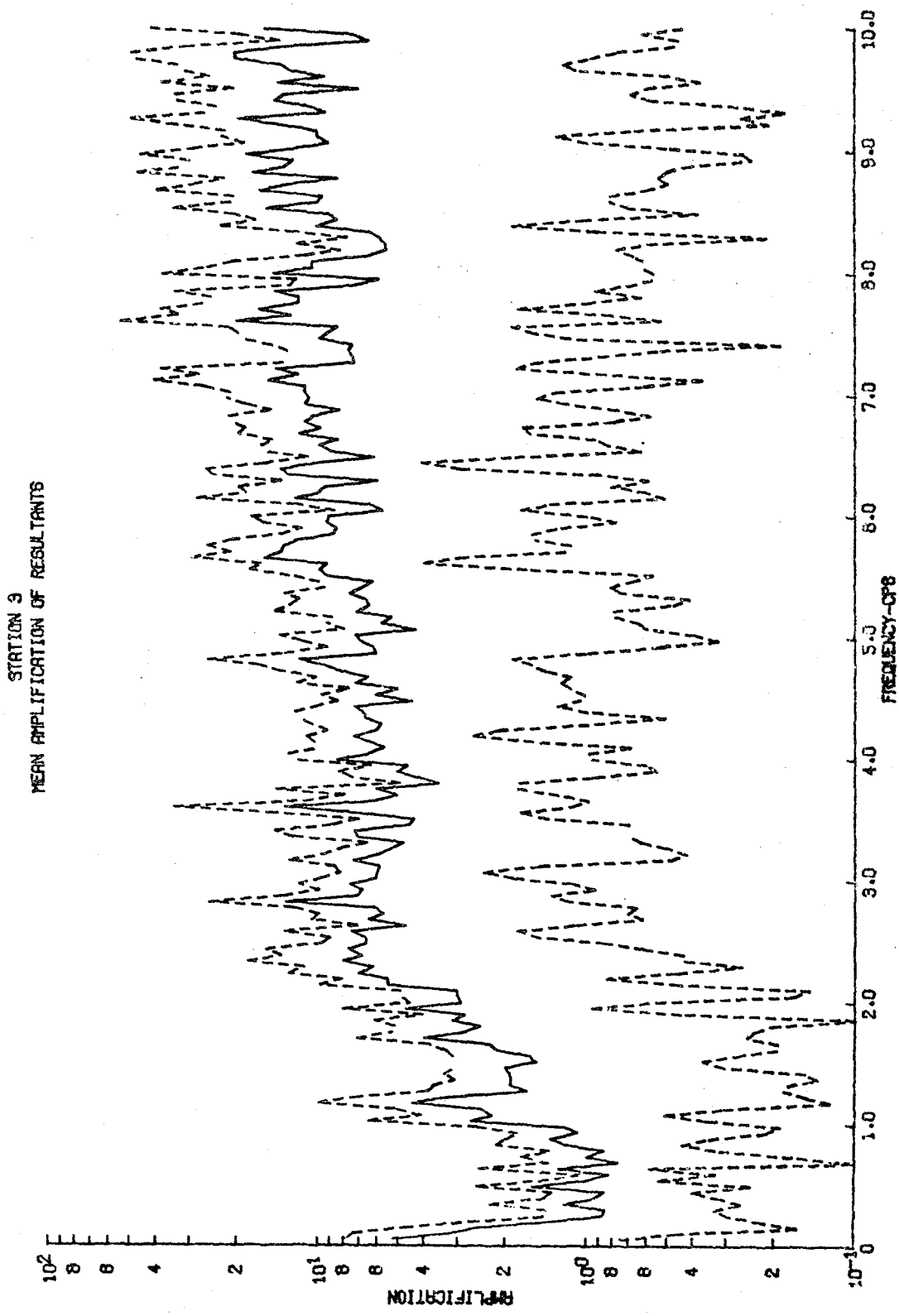

FIGURE 4.2-4 MEAN RESULTANT AMPLIFICATION - STATION 3

resonance or to the destructive interference of multiplly reflected waves within the soil column.

4.3 COMPARISON OF RESULTS WITH OTHER THEORETICAL CALCULATIONS

Comparison of spectral amplification peaks with other measures of resonance frequency necessitates the use of a much broader spectral window than that used in the determination of power and amplification spectra in this study. Therefore, mean amplification spectral values were averaged over intervals of approximately 0.25 hz. and plotted as shown in figures 4.3-1, 2, and 3. These figures represent smoothed forms of the mean values shown in figures 4.2-2, 3, and 4.

During the preliminary design phase of the proposed Satsop Nuclear Power Plant, seismic velocities of the major geologic units present in the area were determined by cross-hole velocity measurements. (ref. 25 & 27) Both compressional and shear wave velocities (here designated V_c and V_s respectively) were determined. First, a range of velocity values was determined for each geologic unit by actual field measurement. Then, design values were selected in such a manner as to be most nearly characteristic of each geologic unit. Measured and design values for geologic units found at the study site are listed in tables 4.3-1 and 2.

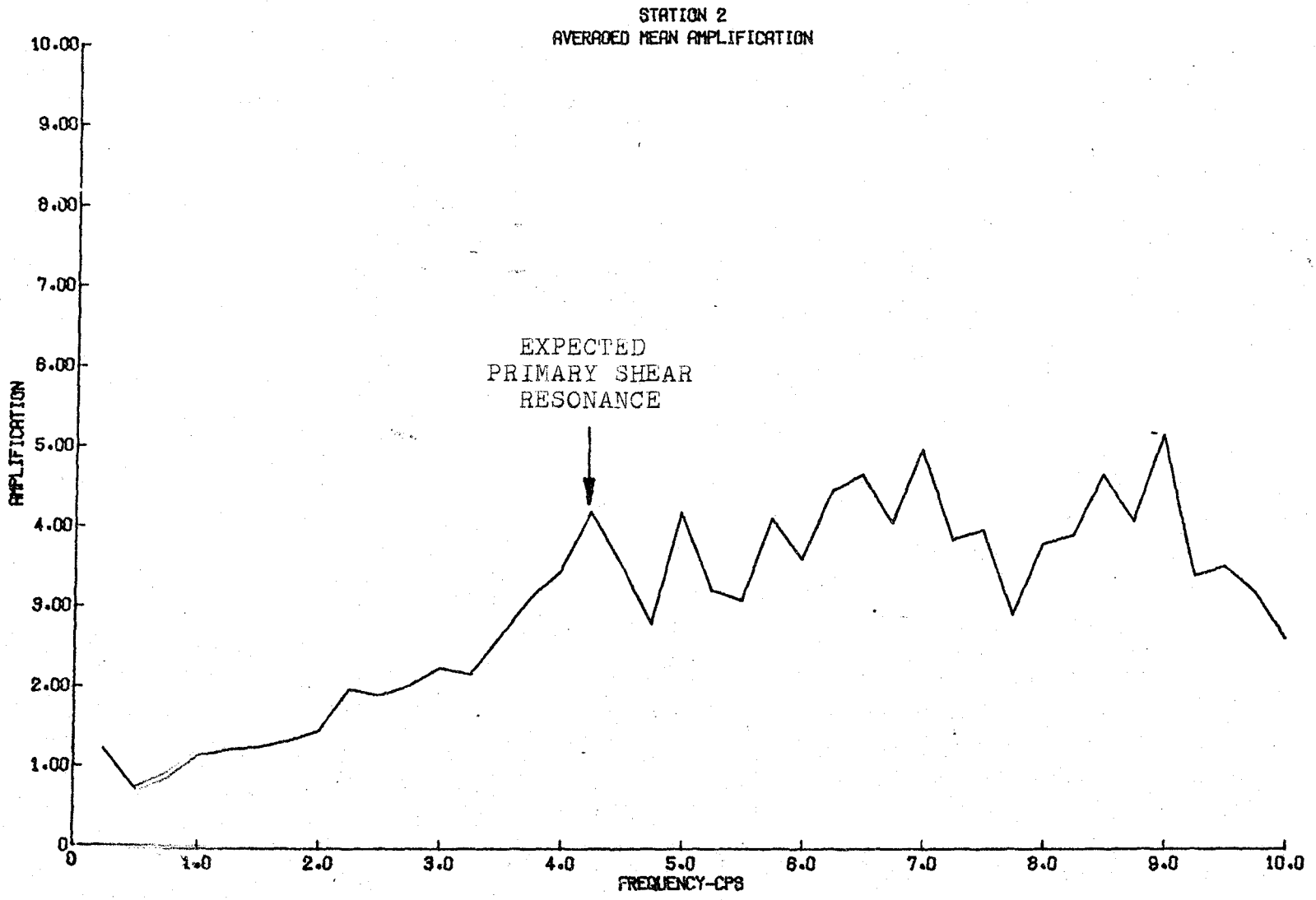

FIGURE 4.3-2 AVERAGED MEAN RESULTANT AMPLIFICATION - STATION 2

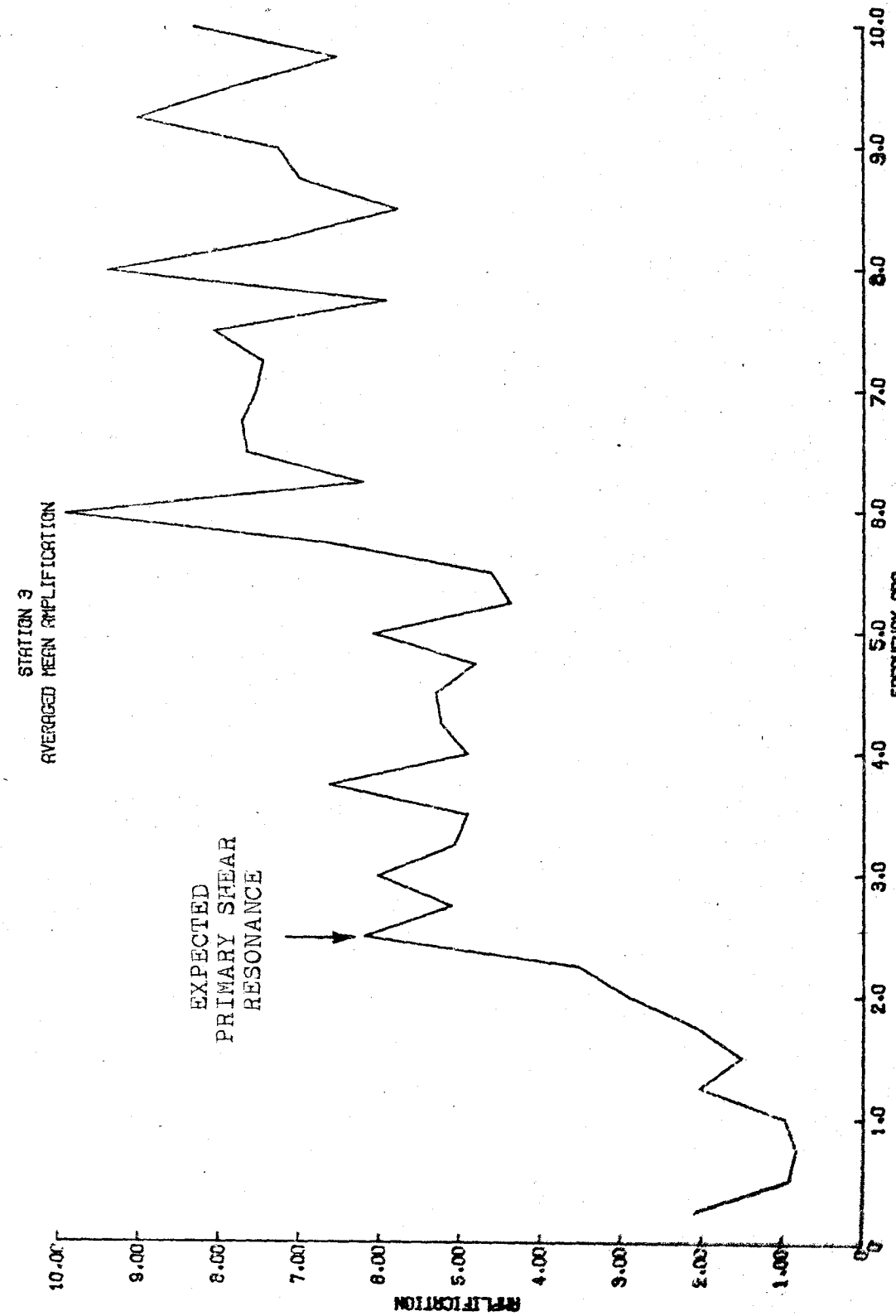

FIGURE 4.3-3 AVERAGED MEAN RESULTANT AMPLIFICATION - STATION 3

TABLE 4.3-1 COMPRESSIONAL WAVE VELOCITIES (ft/sec)

	Loess	Residual Soil & Weathered Sandstone	
		above water table	below water table
V_c (measured)	650-1000	1300-3500	5000
V_c (design)	900	2200	5000

TABLE 4.3-2 SHEAR WAVE VELOCITIES (ft/sec)

	Loess	Residual Soil	Weathered Sandstone
V_s (measured)	1100	1100-2000	2300-4100
V_s (design)	1100	1100	3200

From such seismic velocities and geologic unit thicknesses it is possible to calculate an expected resonance frequency for a given set of subsurface conditions. First, it is assumed that resonance will take place vertically within the soil column. This assumption is supported by Snell's Law which defines the refracted path of waves in a layered medium. Snell's Law states that,

$$\frac{\sin i}{\sin r} = \frac{V_i}{V_r} \qquad (4.3.1)$$

where "i" and "r" are the angles of incidence and refraction and "V_i" and "V_r" are the wave velocities in the incident and refracting medium. (See figure 4.3-4.) In a multilayered medium where V_i is consistently greater than V_r (as in the case of a seismic wave rising through a typical soil column) sin r will approach zero and the wave path become more nearly vertical at each velocity interface. If resonance is assumed to take place vertically, it may be expected that the longest resonant period of the soil column will be equal to the two-way travel time of a seismic signal passing vertically through the entire column. In other words, the lowest expected resonant frequency will be defined by,

$$f_r = \frac{1}{\sum (H/V)} \qquad (4.3.2)$$

where "f_r" is the expected resonant frequency, and "H" and "V" are the thickness and design seismic velocity for all geologic

FIGURE 4.3-4 SNELL'S LAW

$$\frac{\sin i}{\sin r} = \frac{V_i}{V_r}$$

Where, V_i = incident velocity

V_r = refracted velocity

i = angle of incidence

r = angle of refraction

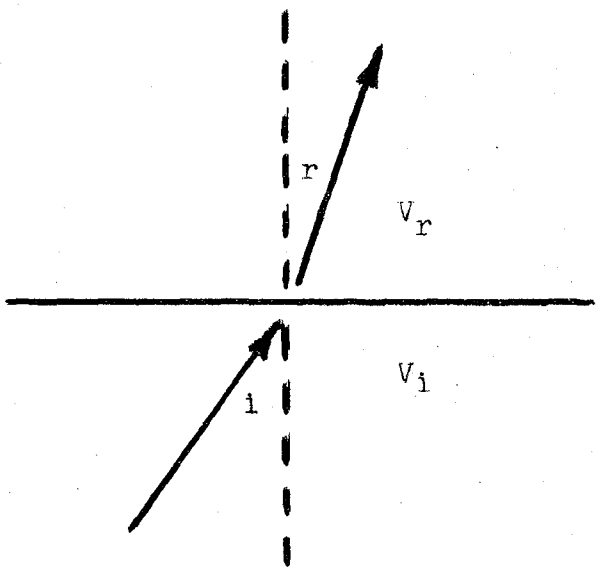

units overlying bedrock.

In order to provide a reference with which to compare resultant amplification spectra, the expected resonance frequency at each portable station location was calculated according to equation 4.3.2.using design seismic velocities from tables 4.3-1 and 2 and geologic unit thicknesses from boring logs (figures 2.3-2, 3, and 4). Tables 4.3-3 and 4 summarize the data used to make these calculations and the results obtained in the compressional and shear modes respectively. It should be noted that expected resonant frequencies derived in this manner represent only expected resonances of the entire column of soil overlying bedrock. Higher frequency resonances originating within individual soil and geologic units are to be expected also.

Comparison of calculated expected resonance frequencies (see tables 4.3-3 and 4) with averaged mean amplification spectra (see figures 4.3-1, 2, and 3) shows excellent correlation of expected resonance frequencies and spectral amplification peaks in the shear mode. Correlation in the compressional mode is poor or indeterminate. It is believed that this poor correlation in the compressional mode is due to the masking effect of higher frequency shear resonances involving one or more geologic units but not the entire column.

TABLE 4.3-3 SUMMARY OF EXPECTED RESONANCE CALCULATIONS (COMPRESSIONAL MODE)

	Loess	Soil & Weathered Sandstone		EXPECTED RESONANCE FREQUENCY
		above water table	below water table	
V_c (ft/sec)	900	2200	5000	
Thickness (ft)				
Station 1	12	84	84	7.3 hz
Station 2	10	48	124	8.7 hz
Station 3	10	58	150	7.4 hz

TABLE 4.3-4 SUMMARY OF EXPECTED RESONANCE CALCULATIONS (SHEAR MODE)

	Loess	Residual Soil	Weathered Sandstone	EXPECTED RESONANCE FREQUENCY
V_s (ft/sec)	1100	1100	3200	
Thickness (ft/sec)				
Station 1	12	163	5	3.1 hz
Station 2	10	172	0	4.2 hz
Station	10	208	0	2.5 hz

It is significant that, at all test locations, the lowest frequency amplification peak of significant size corresponds to the resonance frequency predicted by calculation from two-way travel time of shear waves through the soil column. (See figures 4.3-1, 2, and 3.) This is particularly pertinent in view of the fact that most earthquake damage to buildings is generally attributed to shear waves. Therefore, it is concluded that, even though much refinement of the method is needed, the investigation of site seismic characteristics by the method of amplification spectra yields results compatible with other more conventioal methods of analysis. Finally, it is suggested that the method of amplification spectra may be developed so as to make possible the determination of site seismic characteristics more economically and in greater detail than by other metods in current use.

5.0 CONCLUSIONS

1. Microseismic power spectra are nonstationary within the time constraints of this study. Comparison of triaxial component and resultant Fourier power spectra indicates that incoming waves are polarized in a frequency dependent manner.

2. Amplification spectra are not stationary in the strict sense of the word. But, they appear to be consistently more stationary than the corresponding power spectra. In light of the fact that such natural site conditions as soil density, water table elevation, and internal stress may be expected to vary with time, statistical averaging of five or more amplification will give a reasonable measure of the site response at a given location. In addition, the stationarity of amplification spectra may be improved if measures are taken to insure identity of excitation functions at the time of data collection.

3. Correlation of site resonances predicted by microseismic amplification spectra with those predicted from shear wave velocities and geologic unit thicknesses is good.

4. With future development and refinement, the method of

amplification spectra may provide an accurate, economic, and practical means of determining the seismic response of a specified site.

BIBLIOGRAPHY

1. Akamatu, K., "On Microseisms in Frequency Range from 1 c/s to 200 c/s," Bull. Earthquake Res. Inst., vol. 39, Tokyo, 1961, pp. 23-75.

2. Aki, K., "Space and Time Spectra of Stationary Stochastic Waves with Special Reference to Microseisms," Bull. Earthquake Res. Inst., vol. 35, Tokyo, 1957, pp. 415-456.

3. Bergland, G. D., "A Guided Tour of the Fast Fourier Transform," IEEE Spectrum, July 1969, pp. 41-52.

4. Blackman, R. B. and Tukey, J. W., The Measurement of Power Spectra, Dover Pub., New York, 1959.

5. Bostrom, R. C. and Sherif, M. A., "A Microzonation Technique Employing a Base Station," Proc. 1st Internat. Conf. Internat. Assoc. Eng. Geology, Paris, 1970.

6. Bostrom, R. C. and Sherif, M. A., "United States Microzonation Procedures," Proc. Internat. Conf. on Microzonation, Seattle, 1972, pp. 183-212.

7. Brigham, O., The Fast Fourier Transform, McGraw-Hill, New York, 1970.

8. Carder, D. S. and Gilmore, M. H., "Ground Vibrations," Bull. Seis. Soc. Am., vol. 35, no. 1, 1945, pp. 13-26.

9. Cherry, S., "A Field Investigation of the Influence of Site Conditions on Ground and Structural Response," Proc. 4th Wld. Conf. on Earthquake Engr., Santiago , 1969.

10. Housner, G. W. and Jennings, P. C., "Problems in Seismic Zoning," Proc. 5th Wld. Conf. on Earthquake Engr., Rome, 1973.

11. Inouye, U., "Comparison of Earth Shaking Above-Ground and Under-Ground," Bull. Earthquake Res. Inst., vol. 12, Tokyo, 1934, pp. 712-741. (in Japanese)

12. Kanai, K., Tanaka, T., and Osada, K., "Measurement of the Micro-Tremor. I.", Bull. Earthquake Res. Inst., vol. 32, Tokyo, 1954, pp. 199-210.

13. Kanai, K., "The Requisite Conditions for the Predominant Vibration of the Ground," Bull. Earthquake Res. Inst., vol. 35, Tokyo, 1957, pp. 457-472.

14. Kanai, K., and Tanaka, T., "On Microtremors. VIII.," Bull. Earthquake Res. Inst., vol 39, Tokyo, 1961, pp. 97-111.

15. Kolsky, H., Stress Waves in Solids, Dover Pub., New York, 1963.

16. McKee, B., Cascadia: the Geologic Evolution of the Pacific Northwest, McGraw-Hill, New York, 1972.

17. Ohsaki, Y., "Japanese Microzonation Methods," Proc. Internat. Conf. on Microzonation., Seattle, 1972, pp. 61-86.

18. Richter, C. F., Elementary Seismology, Freeman ndd Co., San Francisco, 1958.

19. Seed, H. B. and Schnabel, P. B., "Soil and Geologic Effects on Site Response During Earthquakes", Proc. Internat. Conf. on Microzonation, Seattle, 1972, pp. 61-86.

20. Sherif, M. A., "Microzonation of Thessaloniki Using the Sherif-Bostrom (USA) Method," UNDP/UNESCO Survey of the Seismicity of the Balkan Region, 1973.

21. Spieker, L. J.,(Project Manager), "Seismometer Array and Data Processing System: Final Report, Phase 1, Contract AF-33(600) 41840," Texas Instruments, Dallas, 1961.

22. Tien, Y. B., "An Introduction to Power Spectral Analysis Regarking a Microseismic Motion Stuey Involving the Use of the Fast Fourier Transform," (Unpublished), 1970.

23. Tien, Y. B., "Site Response and Seismicity in the Seattle Area," PhD. Thesis, University of Washington, Seattle, 1970.

24. Toksoz, M. N., "Microseisms and an Attempted Application to Exploration," Geophysics, vol. 29, no. 2, April 1964, pp. 152- 177.

25. Washington Public Power Supply System, Preliminary Safty Analysis Report: WPPSS Nuclear Project No. 3, vol. 3, WPPSS, 1973.

26. Wood, H. O., "Distribution of Apparent Intensity in San Francisco," The California Earthquake of April 18, 1906, Report of the State Earthquake Investigation Committee, Carnegie Insti of Washington, Washington D.C., 1908, pp. 220-245.

27. Woodward-Lundgren Assoc., "Preliminary Evaluation of Baserock Acceleration at the Satsop Site for the WPPSS Nuclaar Power Project No. 3;" Technical Report 1, Project 8-12805," Woodward-Lundgren, Oakland, 1973.

28. Woodward-Lundgren Assoc., "WPPSS Nuclear Project No. 3: PSAR Submittal 3," Woodward-Lundgren, 1973.

APPENDIX A

PROCESSED DATA

INDEX OF PROCESSED DATA

SATSOP 01 STATION 1 1315 20 AUG 75
FOURIER POWER SPECTRUM
BASE STATION
DIRECTION-NS

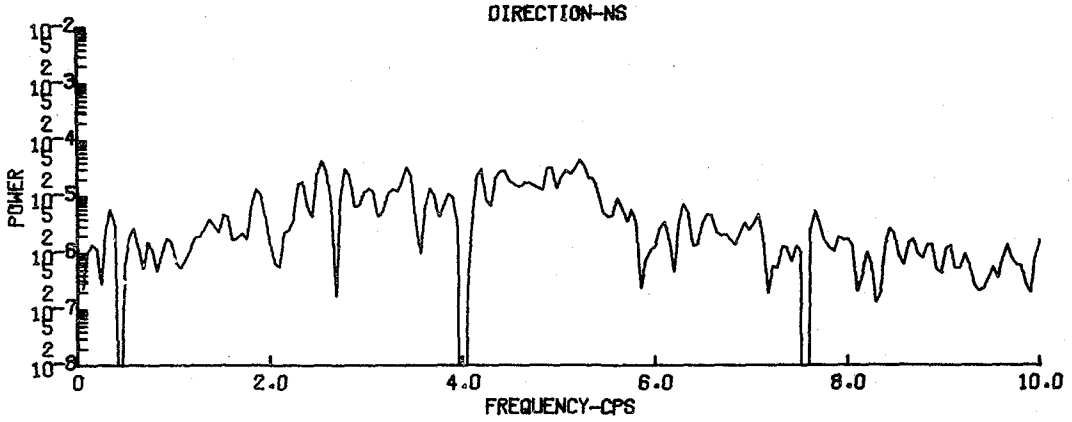

SATSOP 01 STATION 1 1315 20 AUG 75
FOURIER POWER SPECTRUM
BASE STATION
DIRECTION-EW

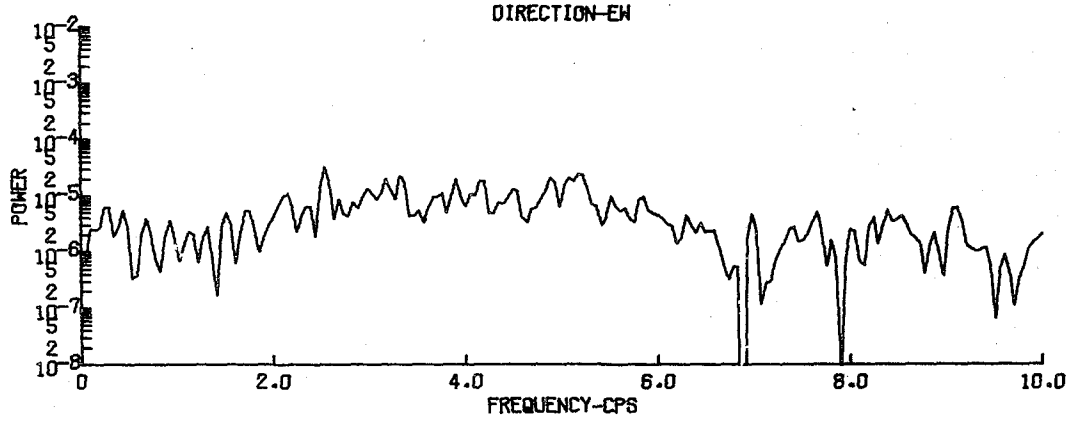

SATSOP 01 STATION 1 1315 20 AUG 75
FOURIER POWER SPECTRUM
BASE STATION
DIRECTION-VT

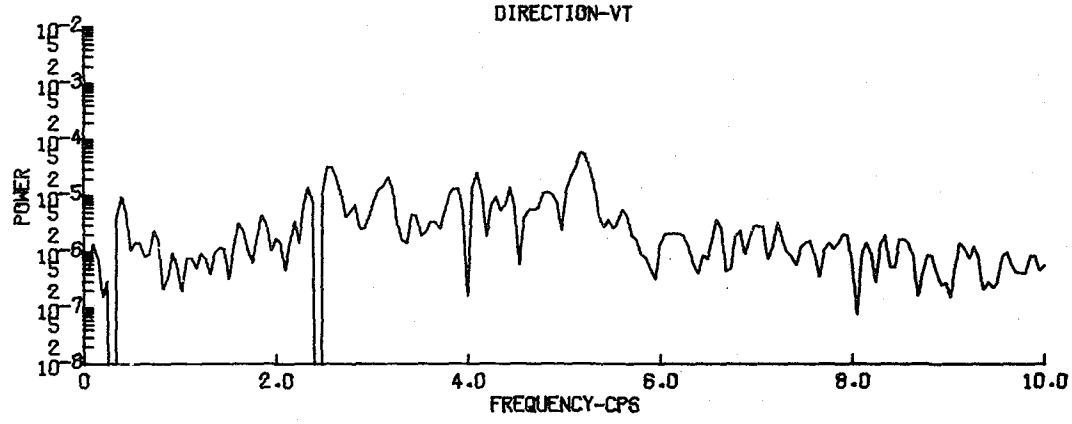

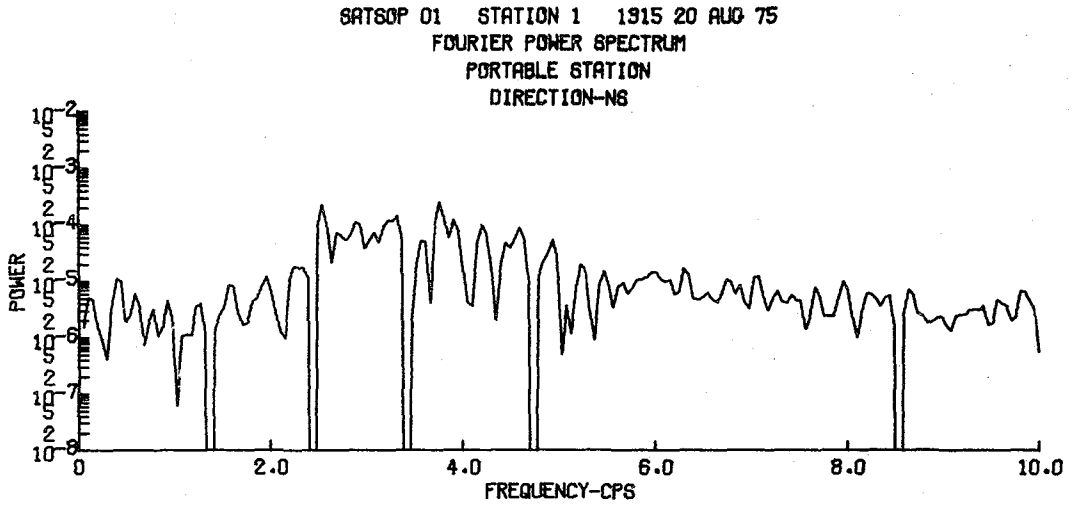
SATSOP 01 STATION 1 1315 20 AUG 75
FOURIER POWER SPECTRUM
PORTABLE STATION
DIRECTION-NS
POWER
FREQUENCY-CPS
0
2.0
4.0
6.0
8.0
10.0

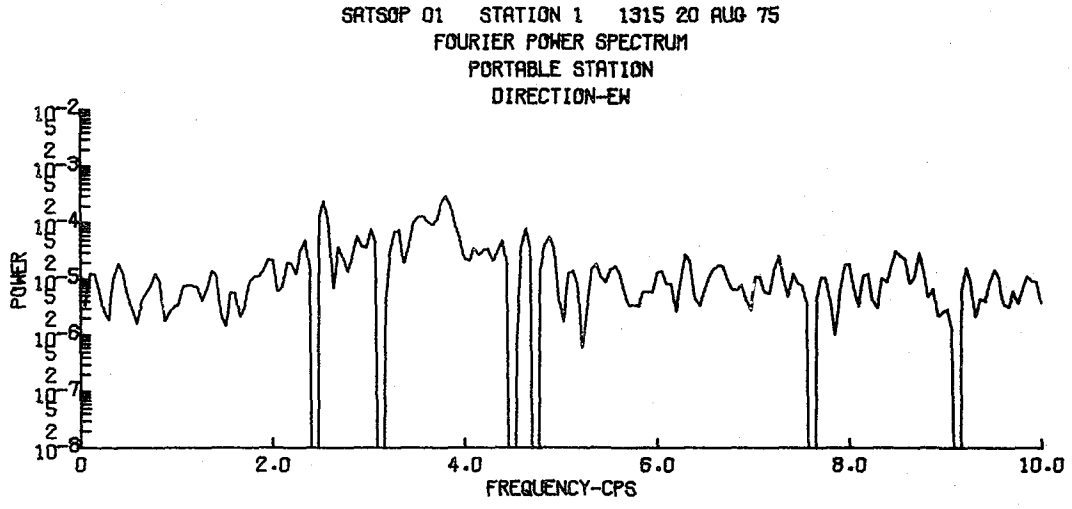
SATSOP 01 STATION 1 1315 20 AUG 75
FOURIER POWER SPECTRUM
PORTABLE STATION
DIRECTION-EW
POWER
FREQUENCY-CPS
0
2.0
4.0
6.0
8.0
10.0

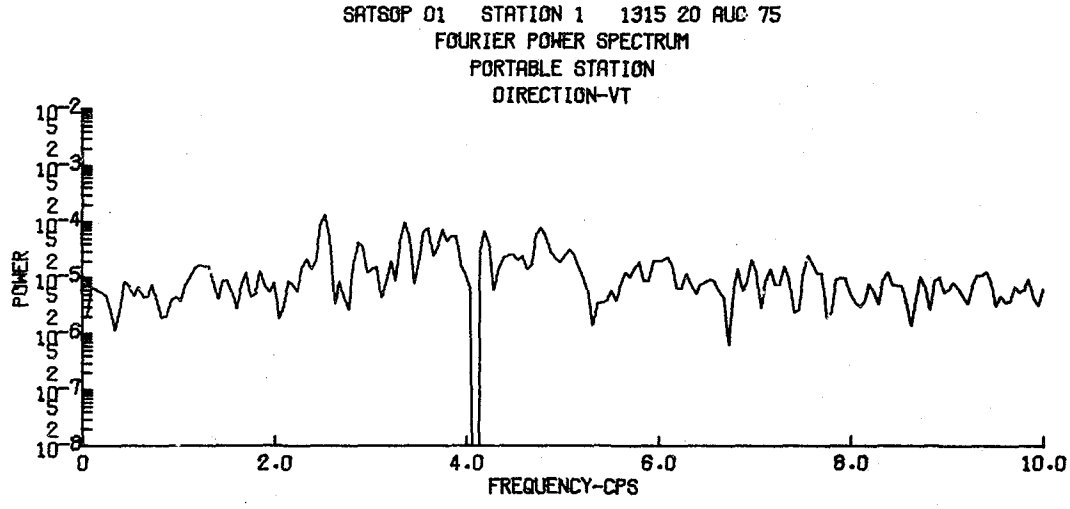
SATSOP 01 STATION 1 1315 20 AUG 75
FOURIER POWER SPECTRUM
PORTABLE STATION
DIRECTION-VT
POWER
FREQUENCY-CPS
0
2.0
4.0
6.0
8.0
10.0

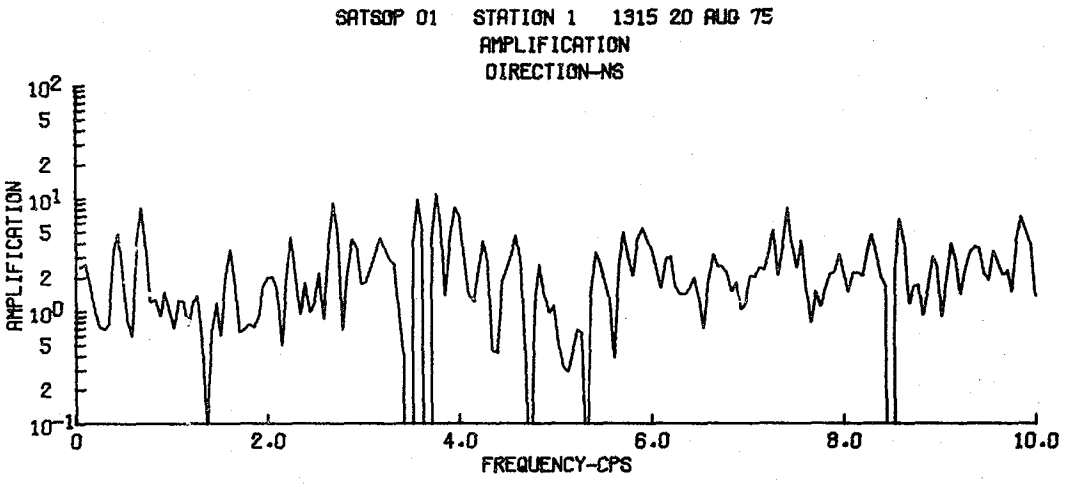
SATSOP 01 STATION 1 1315 20 AUG 75
AMPLIFICATION
DIRECTION-NS
AMPLIFICATION
FREQUENCY-CPS

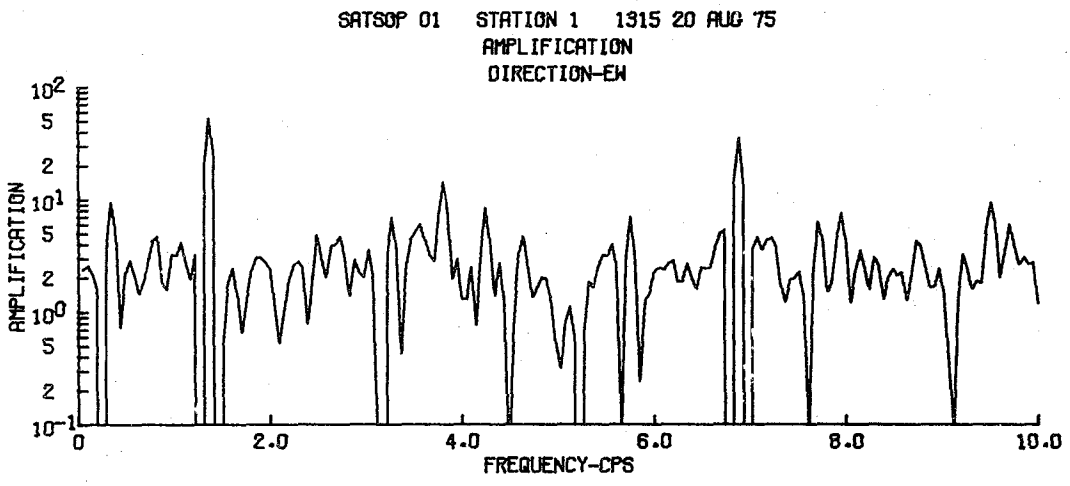
SATSOP 01 STATION 1 1315 20 AUG 75
AMPLIFICATION
DIRECTION-EW
AMPLIFICATION
FREQUENCY-CPS

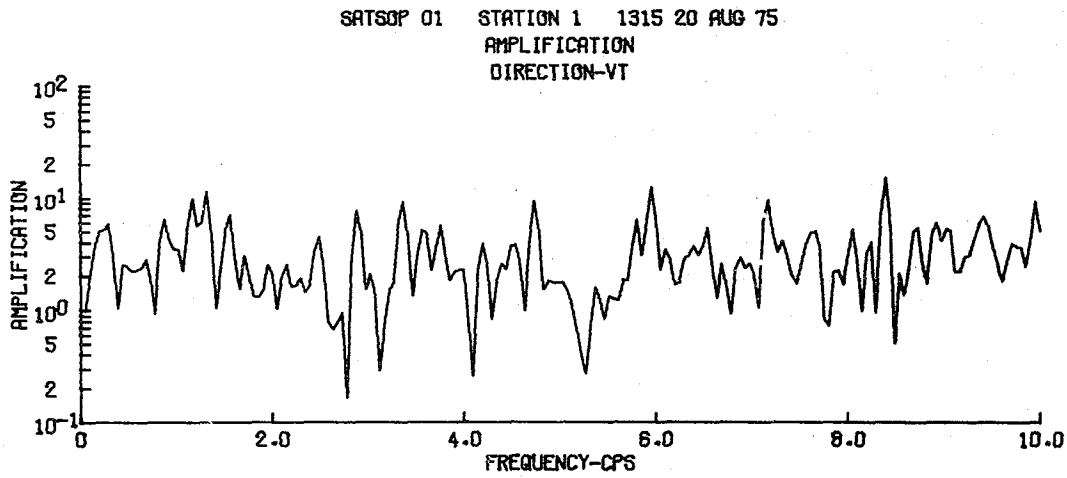
SATSOP 01 STATION 1 1315 20 AUG 75
AMPLIFICATION
DIRECTION-VT
AMPLIFICATION
FREQUENCY-CPS

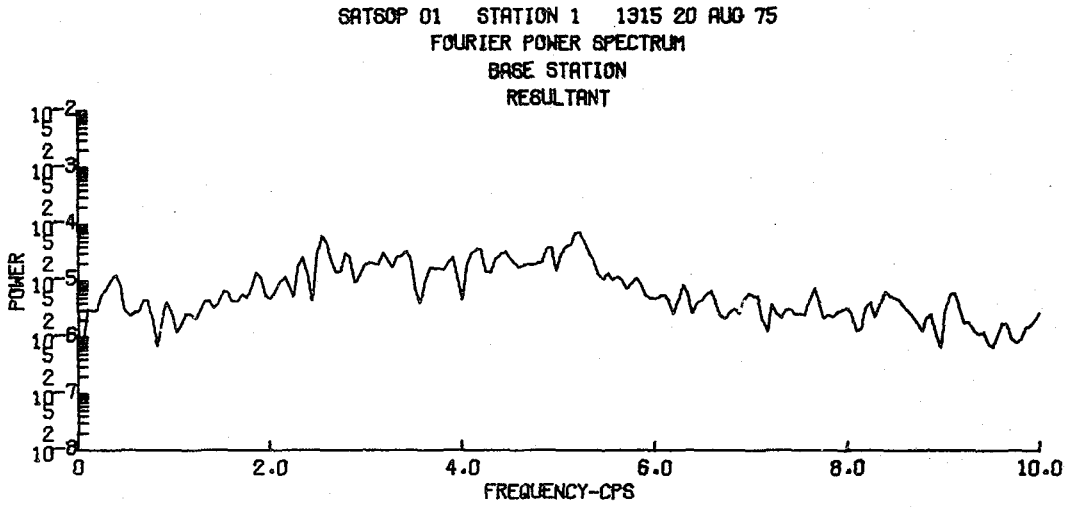
SATSOP 01 STATION 1 1315 20 AUG 75
FOURIER POWER SPECTRUM
BASE STATION
RESULTANT
POWER
FREQUENCY-CPS
0
2.0
4.0
6.0
8.0
10.0

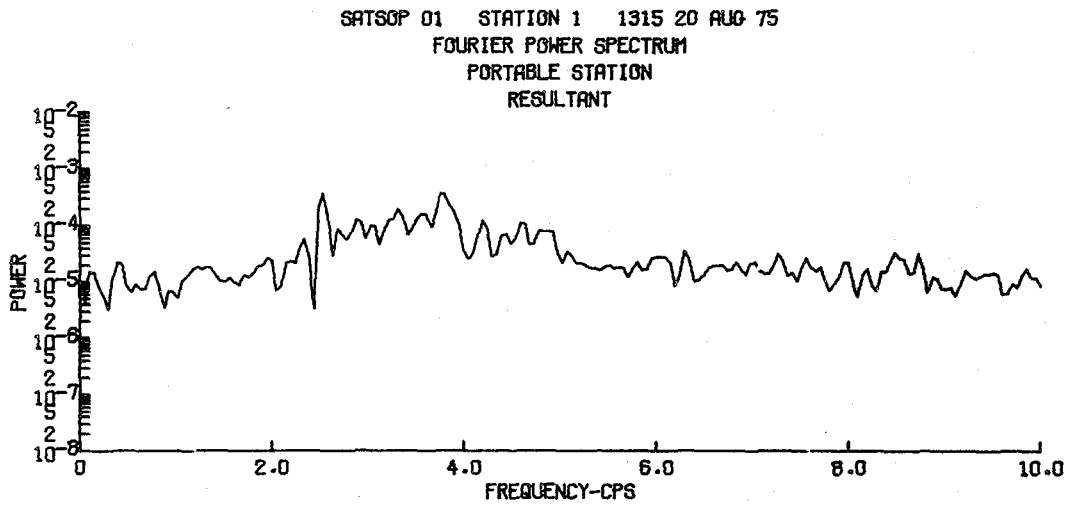
SATSOP 01 STATION 1 1315 20 AUG 75
FOURIER POWER SPECTRUM
PORTABLE STATION
RESULTANT
POWER
FREQUENCY-CPS
0
2.0
4.0
6.0
8.0
10.0

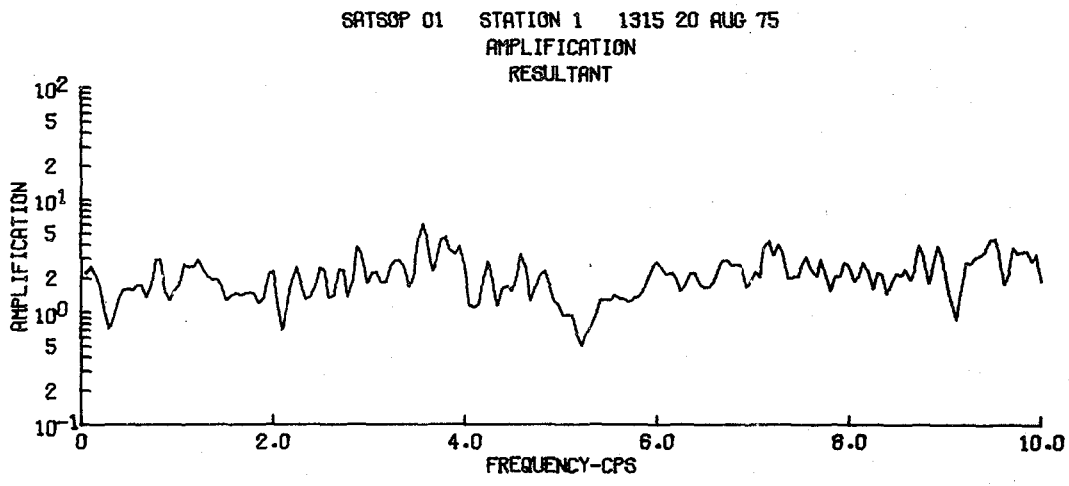
SATSOP 01 STATION 1 1315 20 AUG 75
AMPLIFICATION
RESULTANT
AMPLIFICATION
FREQUENCY-CPS
0
2.0
4.0
6.0
8.0
10.0

SATSOP 02 - STATION 1 1450 20 AUG 75
FOURIER POWER SPECTRUM
BASE STATION
DIRECTION-NS

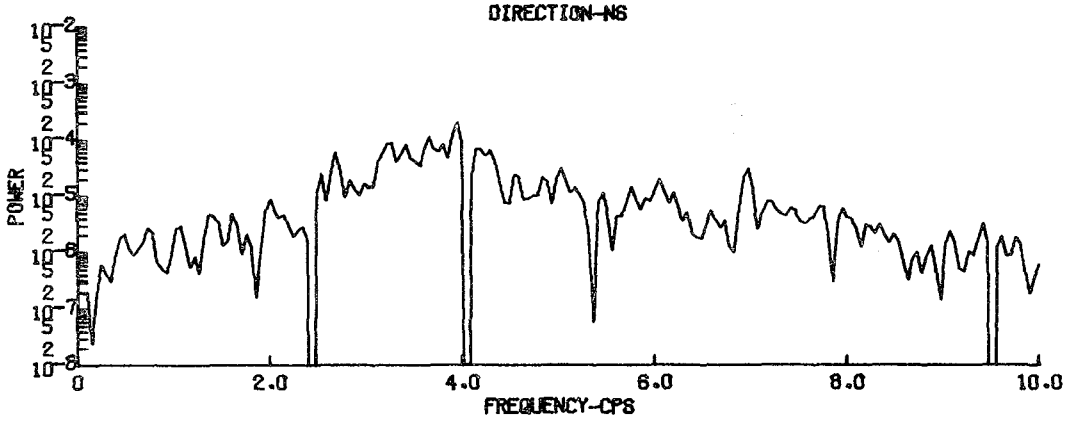

SATSOP 02 - STATION 1 1450 20 AUG 75
FOURIER POWER SPECTRUM
BASE STATION
DIRECTION-EW

SATSOP 02 - STATION 1 1450 20 AUG 75
FOURIER POWER SPECTRUM
BASE STATION
DIRECTION-VT

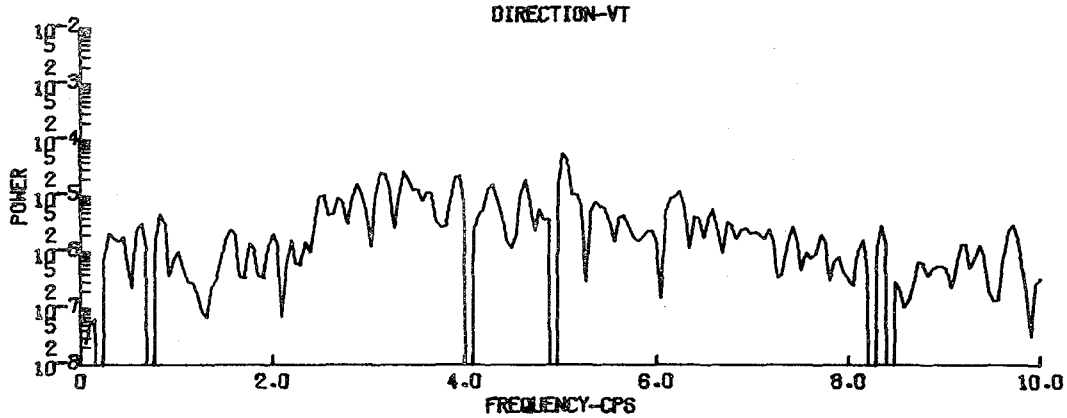

SATSOP 02 - STATION 1 1450 20 AUG 75
FOURIER POWER SPECTRUM
PORTABLE STATION
DIRECTION-NS

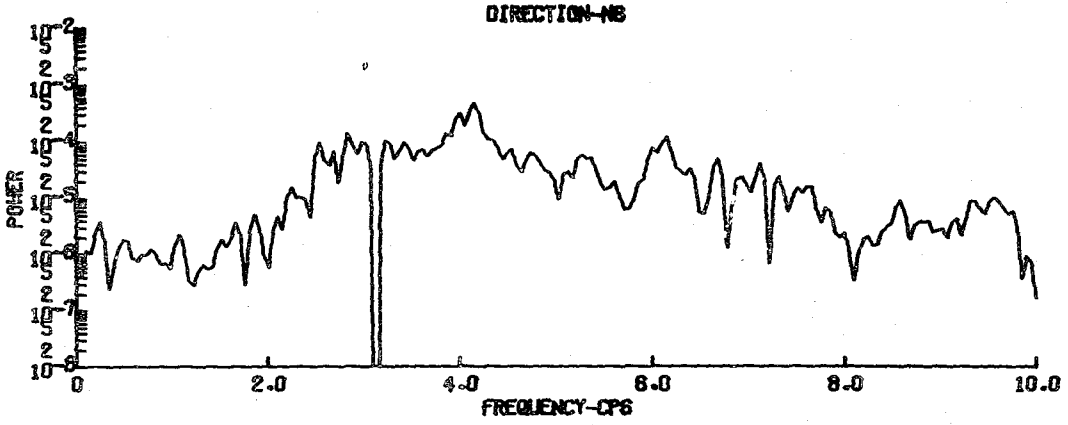

SATSOP 02 - STATION 1 1450 20 AUG 75
FOURIER POWER SPECTRUM
PORTABLE STATION
DIRECTION-EW

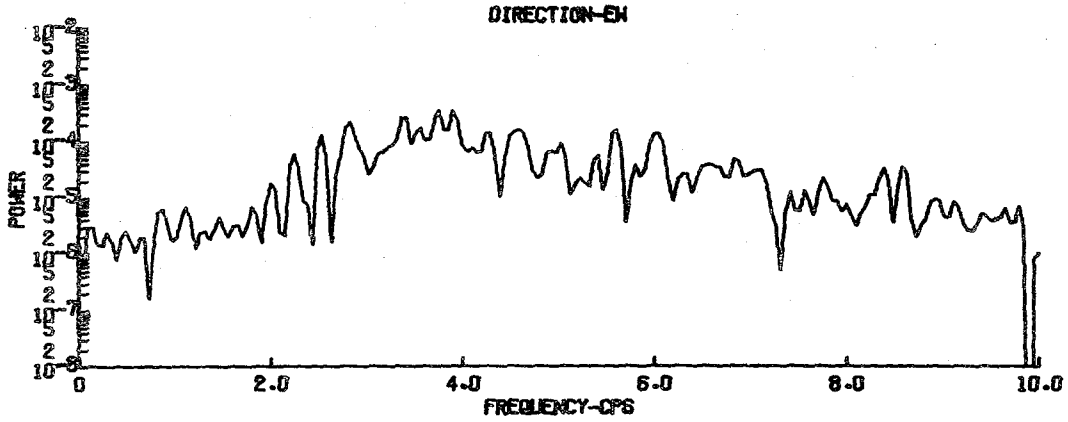

SATSOP 02 - STATION 1 1450 20 AUG 75
FOURIER POWER SPECTRUM
PORTABLE STATION
DIRECTION-VT

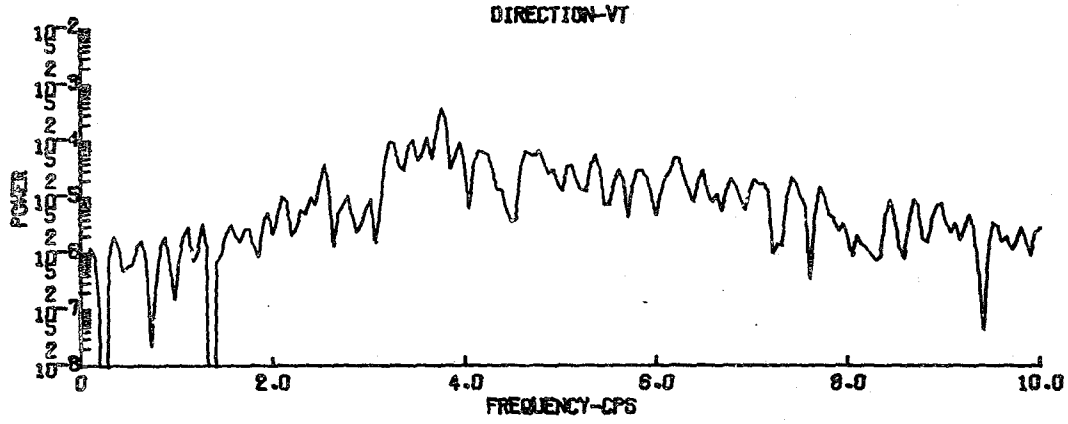

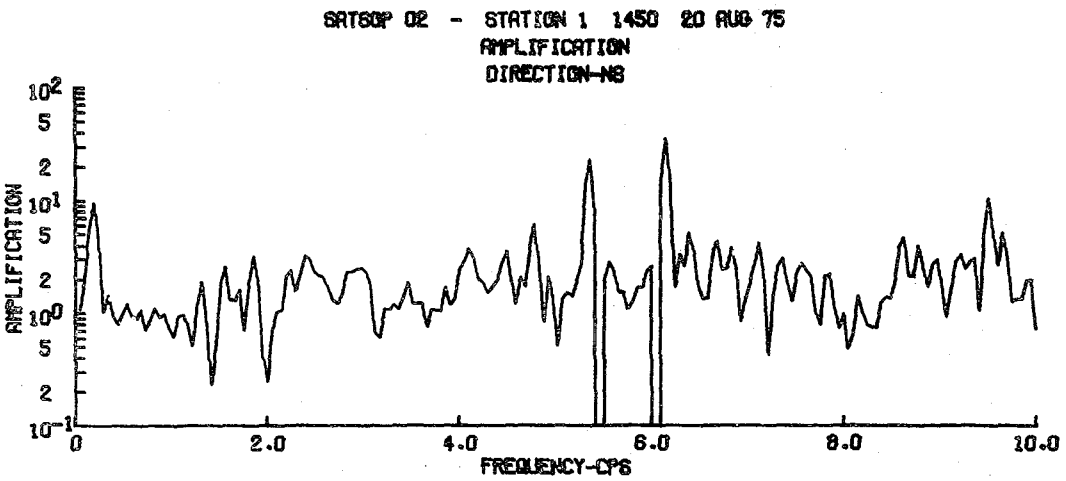
SATSOP 02 - STATION 1 1450 20 AUG 75
AMPLIFICATION
DIRECTION-NS
AMPLIFICATION
FREQUENCY-CPS

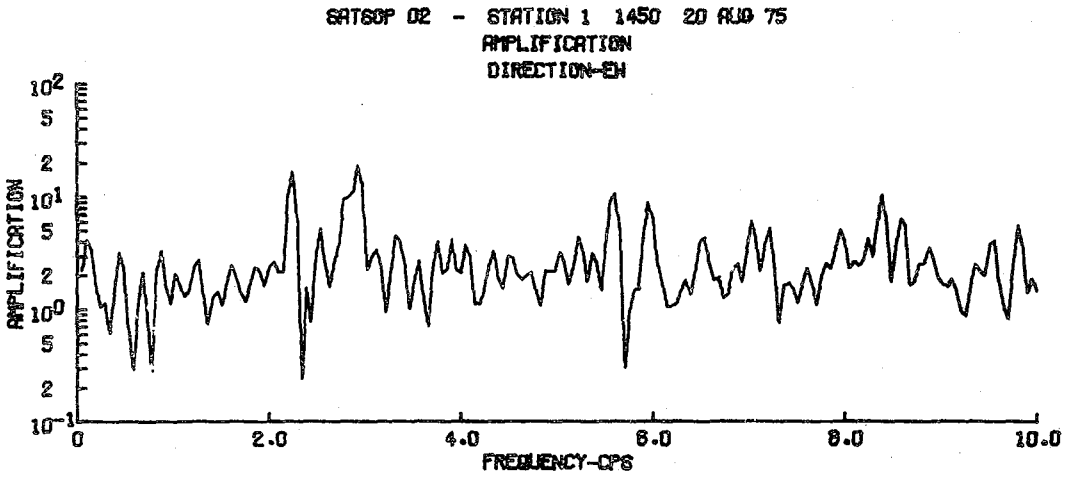
SATSOP 02 - STATION 1 1450 20 AUG 75
AMPLIFICATION
DIRECTION-EW
AMPLIFICATION
FREQUENCY-CPS

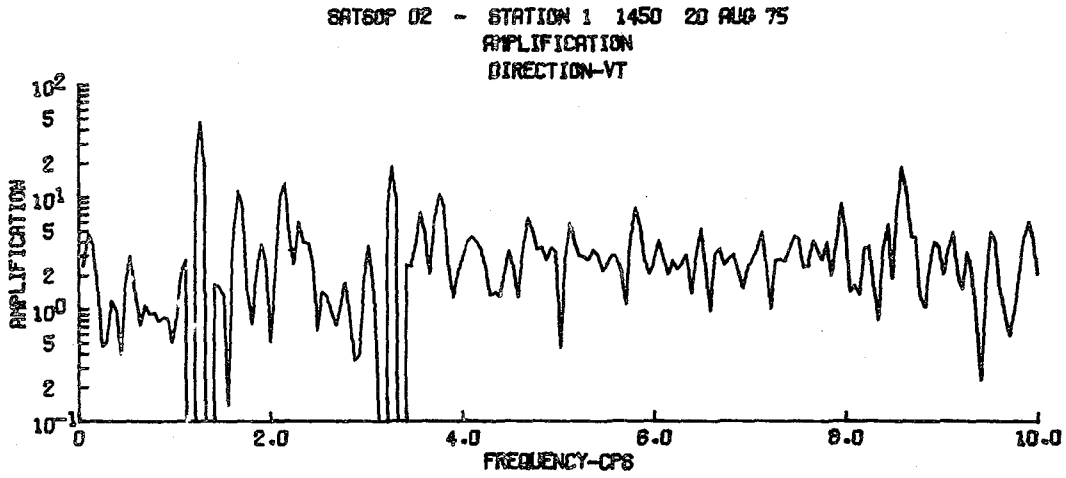
SATSOP 02 - STATION 1 1450 20 AUG 75
AMPLIFICATION
DIRECTION-VT
AMPLIFICATION
FREQUENCY-CPS

SATSOP 02 - STATION 1 1450 20 AUG 75
FOURIER POWER SPECTRUM
BASE STATION
RESULTANT

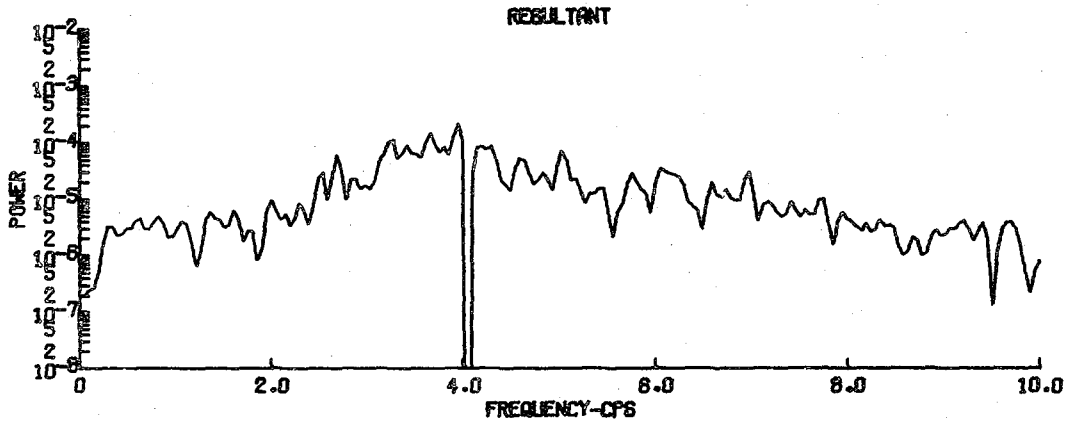

SATSOP 02 - STATION 1 1450 20 AUG 75
FOURIER POWER SPECTRUM
PORTABLE STATION
RESULTANT

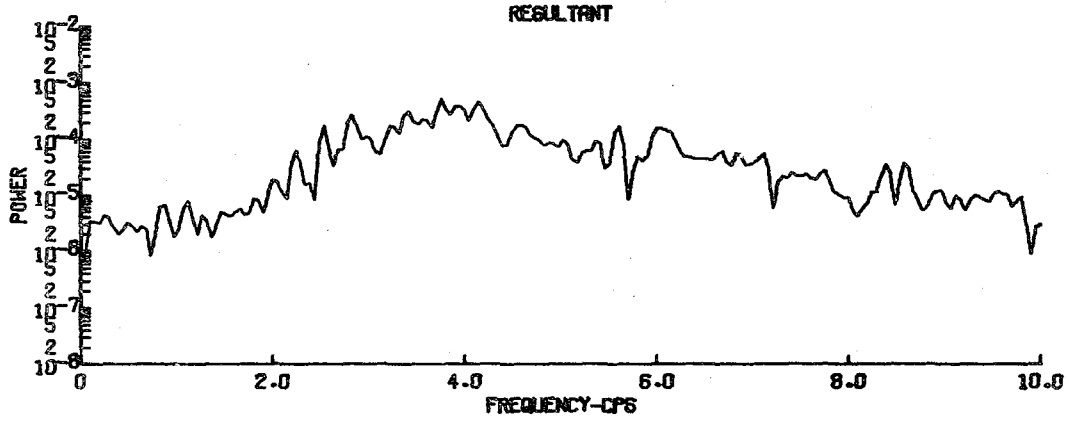

SATSOP 02 - STATION 1 1450 20 AUG 75
AMPLIFICATION
RESULTANT

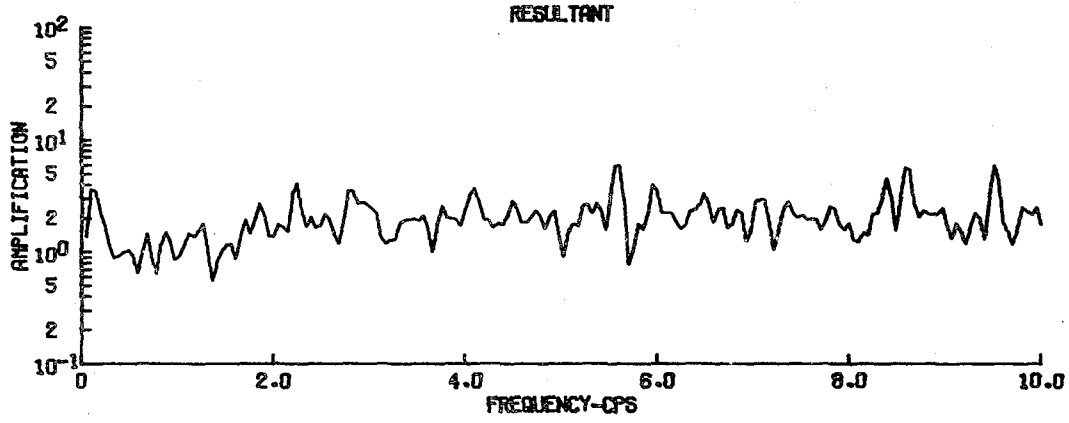

SATSOP 03 - STATION 1 1125 21 AUG 75
FOURIER POWER SPECTRUM
BASE STATION
DIRECTION-NS

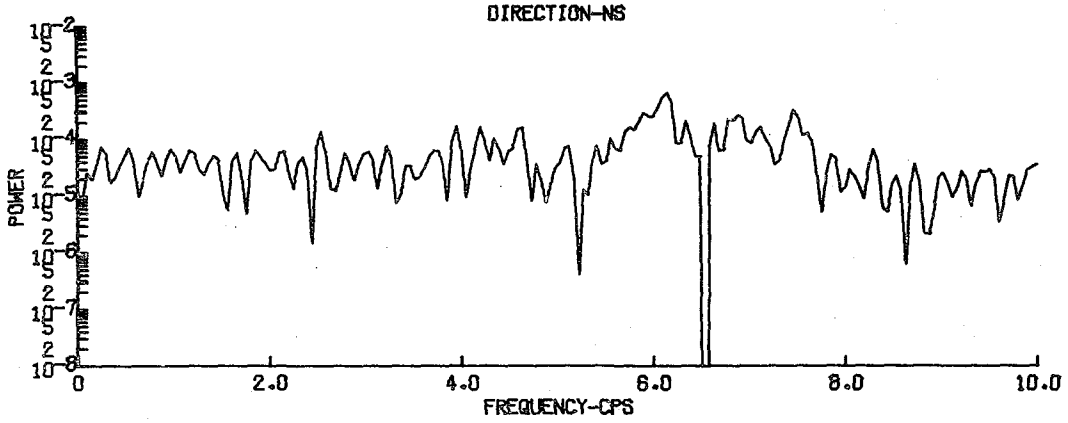

SATSOP 03 - STATION 1 1125 21 AUG 75
FOURIER POWER SPECTRUM
BASE STATION
DIRECTION-EW

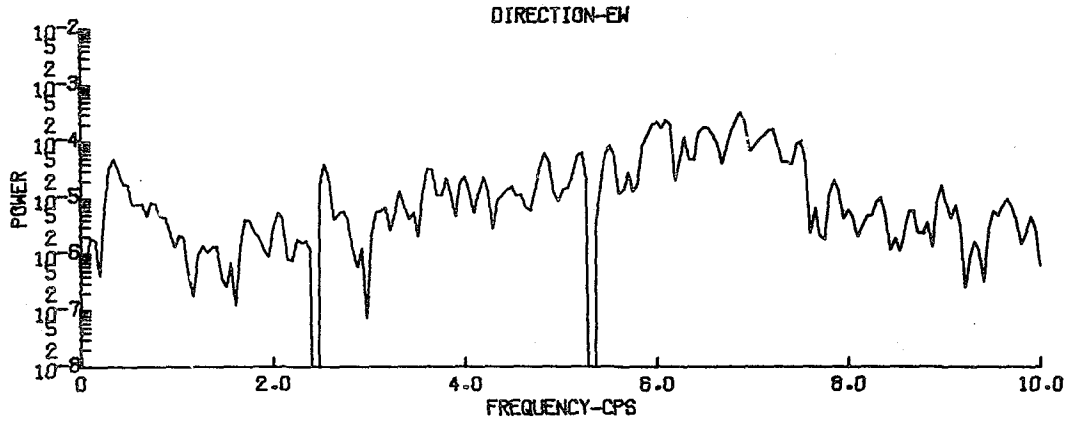

SATSOP 03 - STATION 1 1125 21 AUG 75
FOURIER POWER SPECTRUM
BASE STATION
DIRECTION-VT

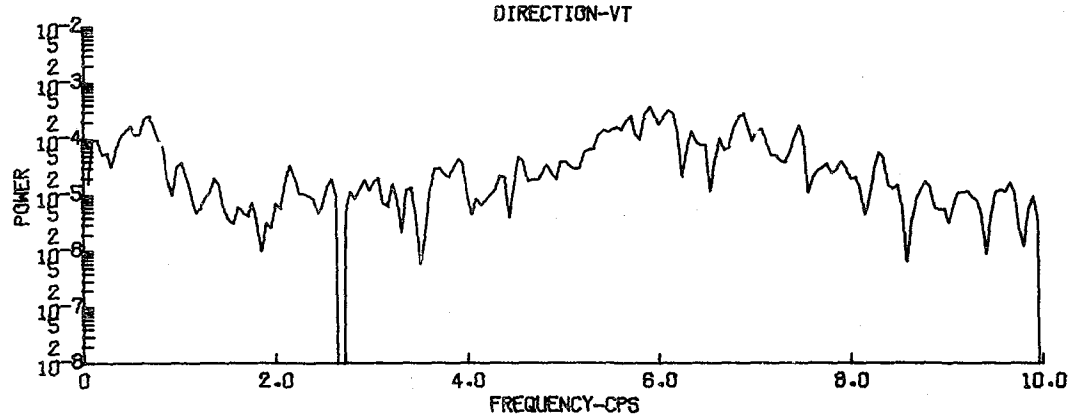

SATSOP 03 - STATION 1 1125 21 AUG 75
FOURIER POWER SPECTRUM
PORTABLE STATION
DIRECTION-NS

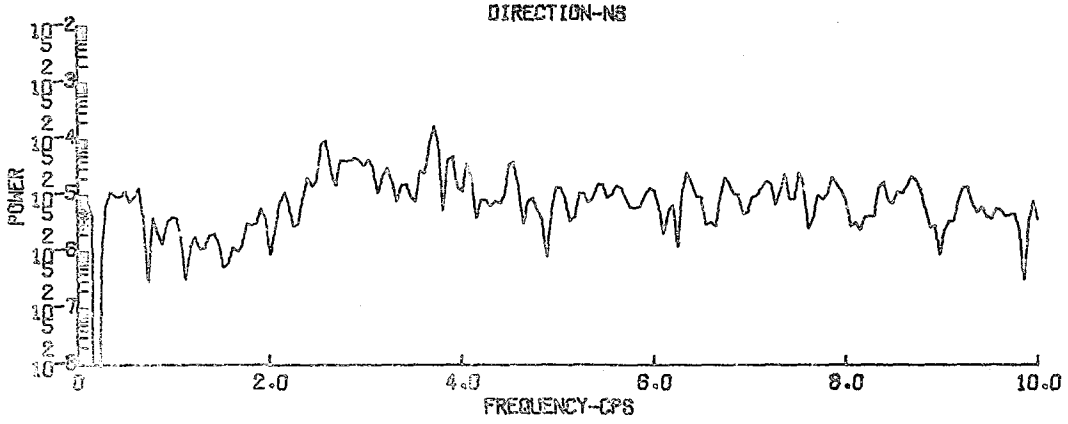

SATSOP 03 - STATION 1 1125 21 AUG 75
FOURIER POWER SPECTRUM
PORTABLE STATION
DIRECTION-EW

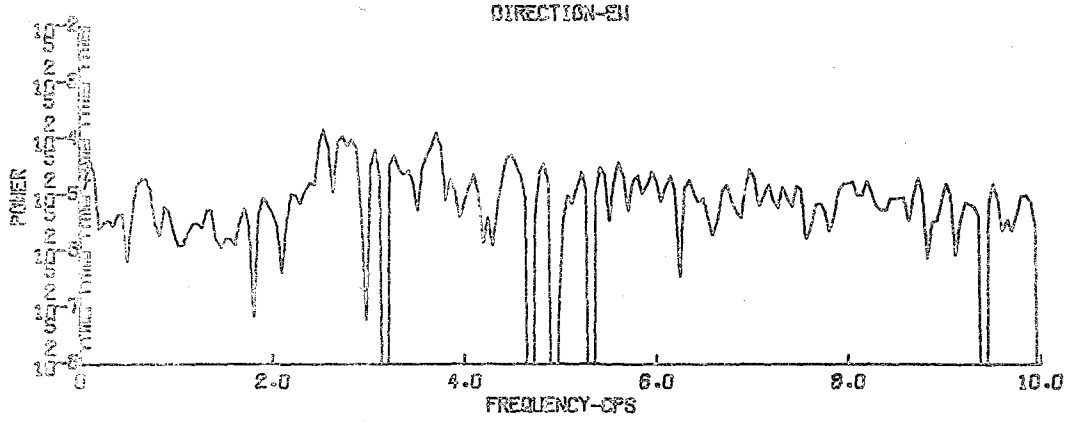

SATSOP 03 - STATION 1 1125 21 AUG 75
FOURIER POWER SPECTRUM
PORTABLE STATION
DIRECTION-VT

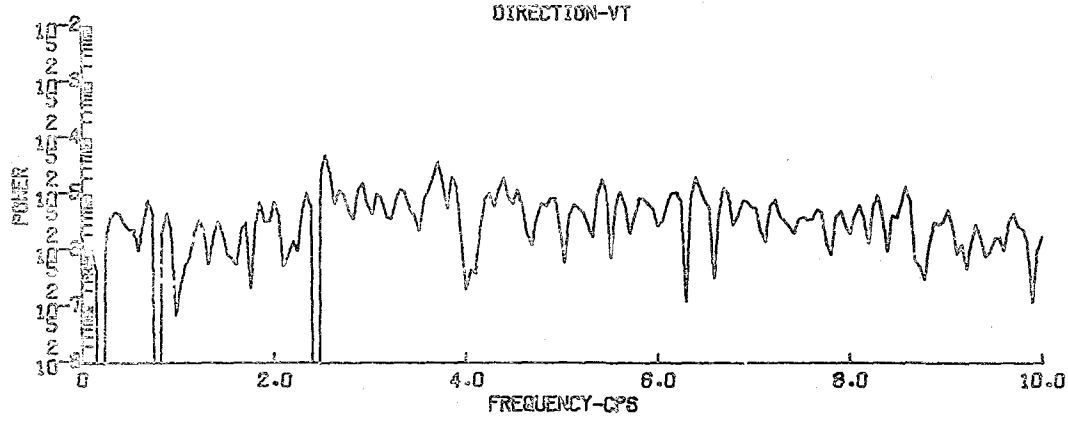

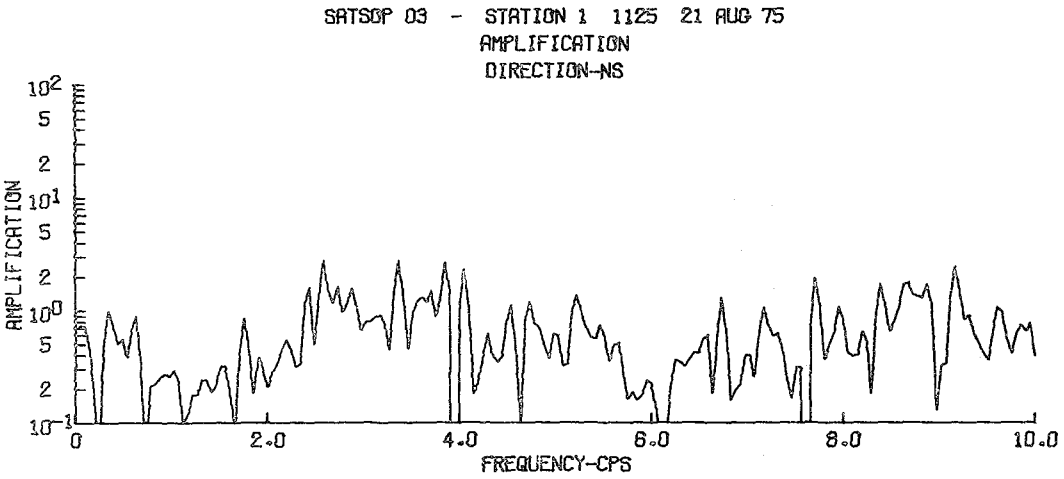
SATSOP 03 - STATION 1 1125 21 AUG 75
AMPLIFICATION
DIRECTION-NS
AMPLIFICATION
FREQUENCY-CPS
0
2.0
4.0
6.0
8.0
10.0

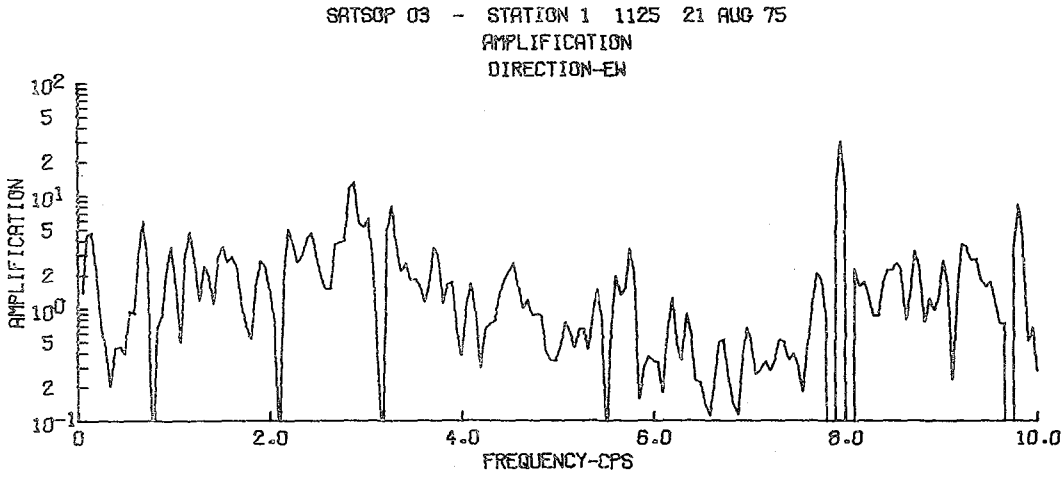
SATSOP 03 - STATION 1 1125 21 AUG 75
AMPLIFICATION
DIRECTION-EW
AMPLIFICATION
FREQUENCY-CPS
0
2.0
4.0
6.0
8.0
10.0

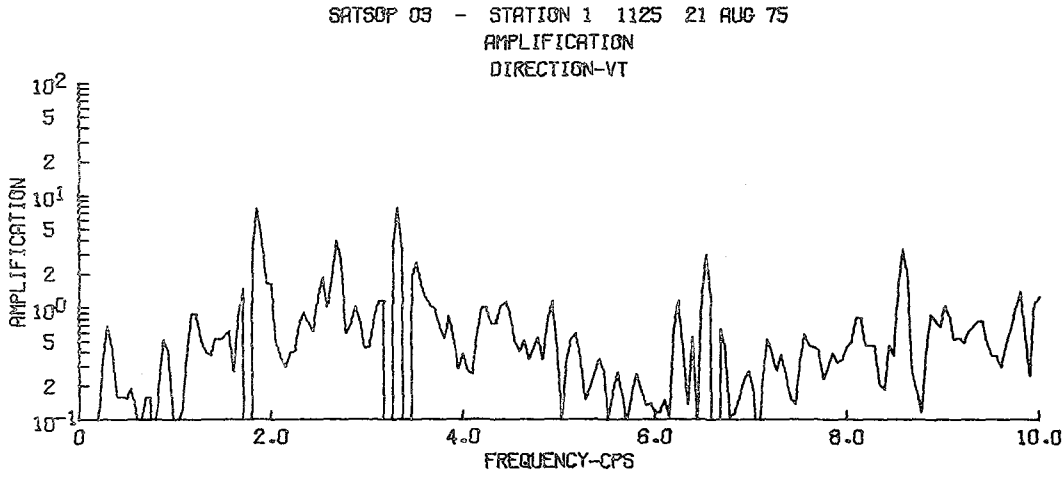
SATSOP 03 - STATION 1 1125 21 AUG 75
AMPLIFICATION
DIRECTION-VT
AMPLIFICATION
FREQUENCY-CPS
0
2.0
4.0
6.0
8.0
10.0

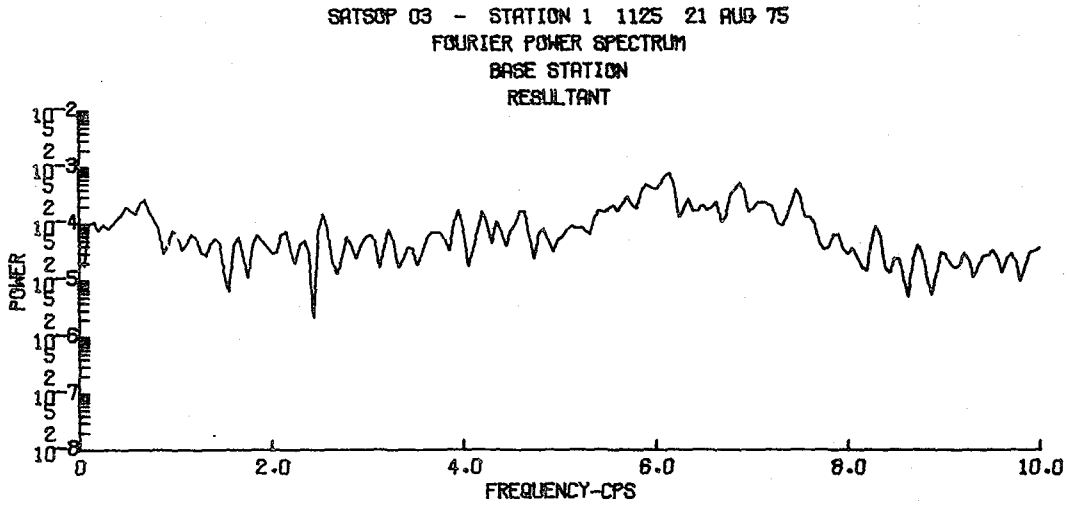
SATSOP 03 - STATION 1 1125 21 AUG 75
FOURIER POWER SPECTRUM
BASE STATION
RESULTANT
POWER
FREQUENCY-CPS
0
2.0
4.0
6.0
8.0
10.0

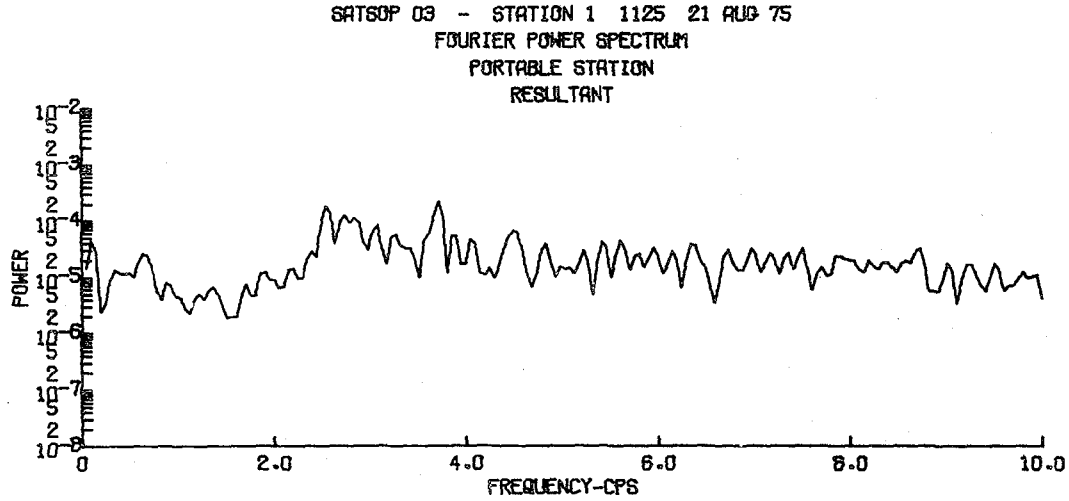
SATSOP 03 - STATION 1 1125 21 AUG 75
FOURIER POWER SPECTRUM
PORTABLE STATION
RESULTANT
POWER
FREQUENCY-CPS
0
2.0
4.0
6.0
8.0
10.0

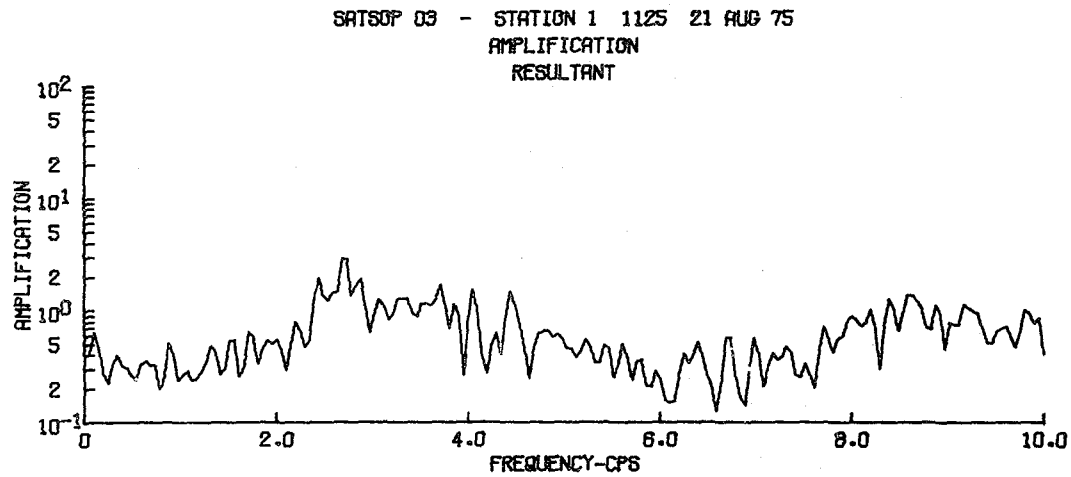
SATSOP 03 - STATION 1 1125 21 AUG 75
AMPLIFICATION
RESULTANT
AMPLIFICATION
FREQUENCY-CPS
0
2.0
4.0
6.0
8.0
10.0

SATSOP 04 - STATION 1 1006 12 SEPT 75
FOURIER POWER SPECTRUM
BASE STATION
DIRECTION-NS

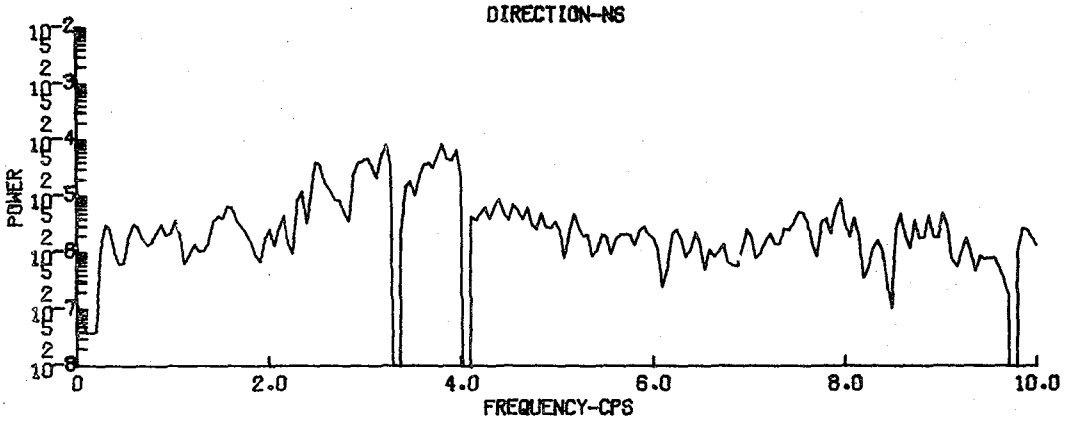

SATSOP 04 - STATION 1 1006 12 SEPT 75
FOURIER POWER SPECTRUM
BASE STATION
DIRECTION-EW

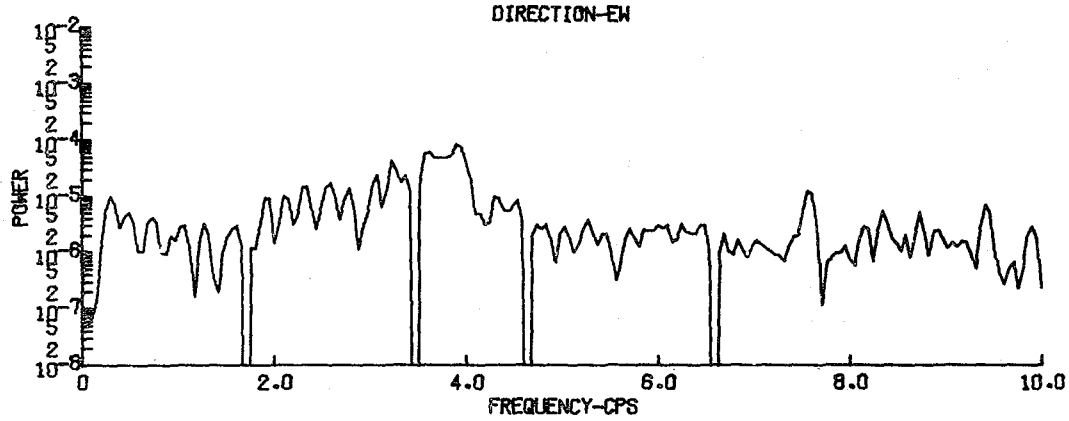

SATSOP 04 - STATION 1 1006 12 SEPT 75
FOURIER POWER SPECTRUM
BASE STATION
DIRECTION-VT

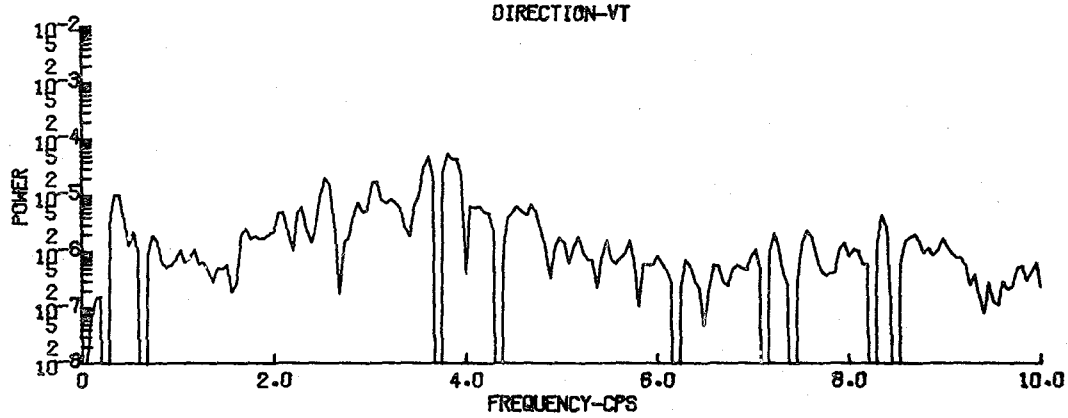

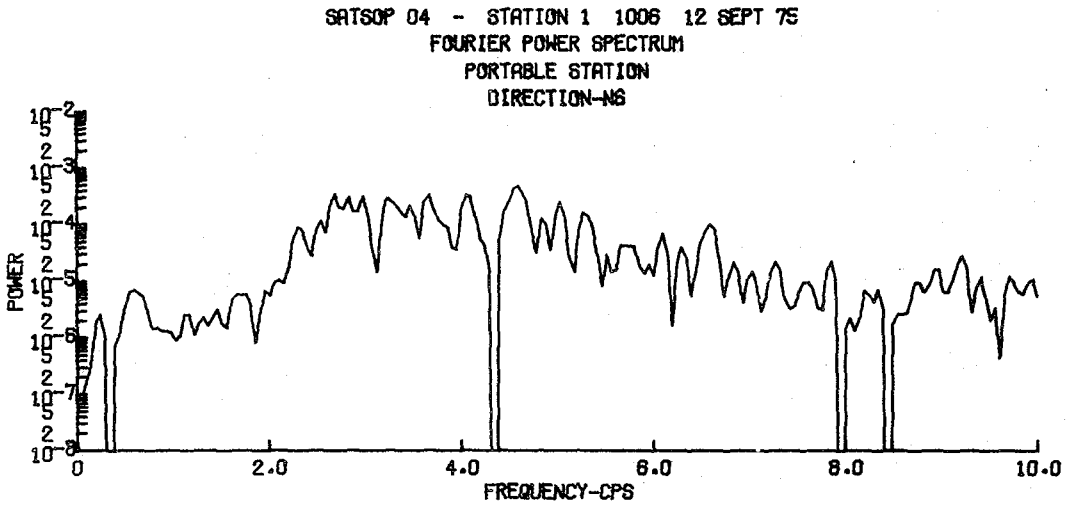
SATSOP 04 - STATION 1 1006 12 SEPT 75
FOURIER POWER SPECTRUM
PORTABLE STATION
DIRECTION-NS
POWER
FREQUENCY-CPS
0
2.0
4.0
6.0
8.0
10.0

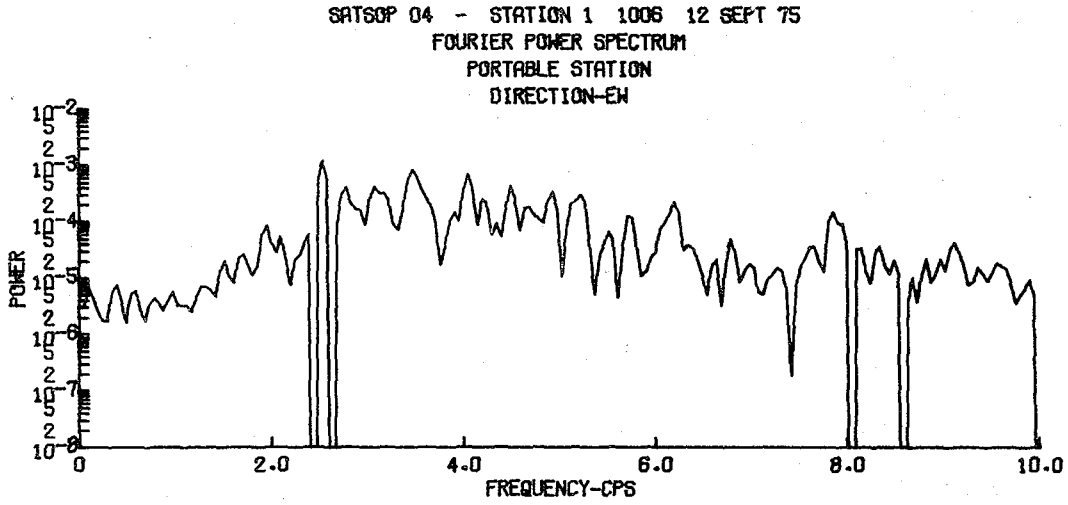
SATSOP 04 - STATION 1 1006 12 SEPT 75
FOURIER POWER SPECTRUM
PORTABLE STATION
DIRECTION-EW
POWER
FREQUENCY-CPS
0
2.0
4.0
6.0
8.0
10.0

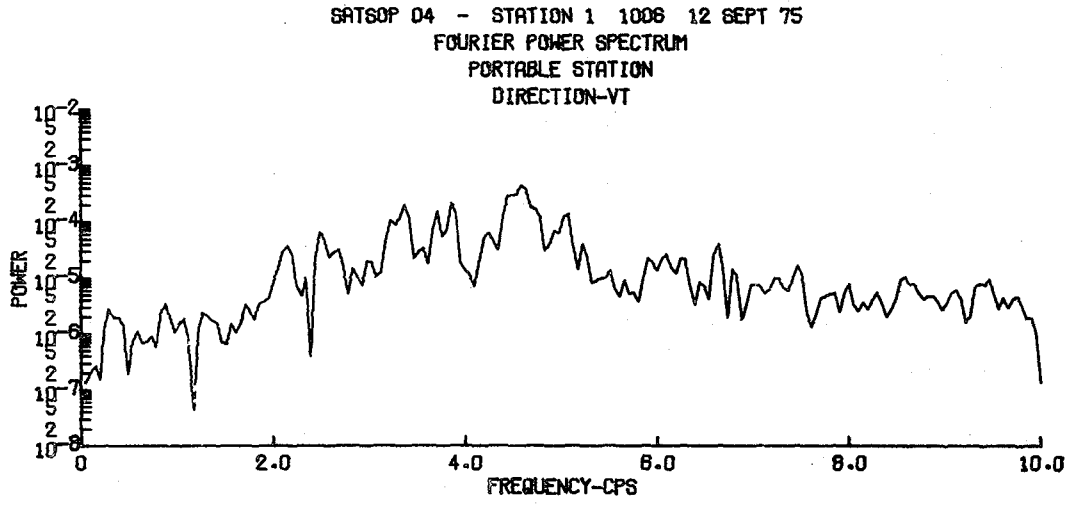
SATSOP 04 - STATION 1 1006 12 SEPT 75
FOURIER POWER SPECTRUM
PORTABLE STATION
DIRECTION-VT
POWER
FREQUENCY-CPS
0
2.0
4.0
6.0
8.0
10.0

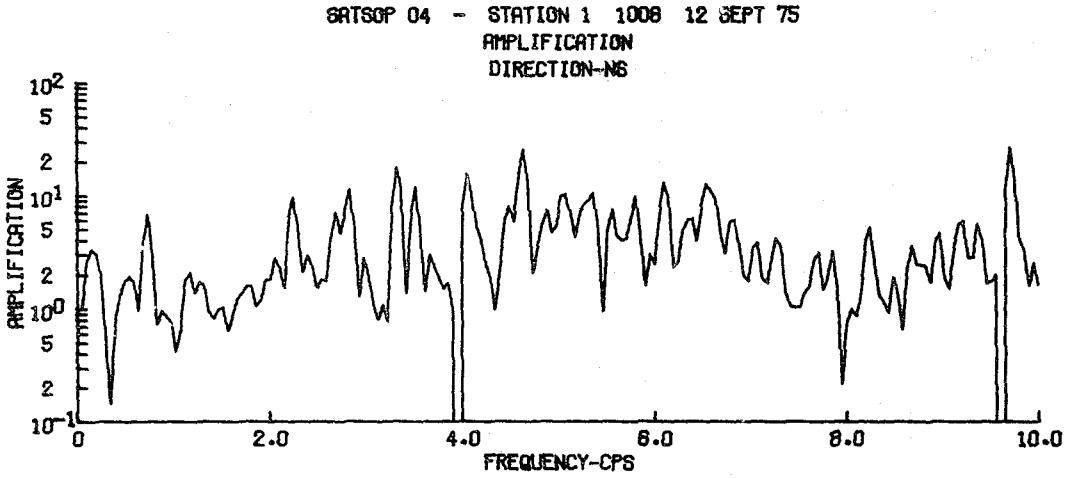
SATSOP 04 - STATION 1 1006 12 SEPT 75
AMPLIFICATION
DIRECTION-NS
AMPLIFICATION
FREQUENCY-CPS
0
2.0
4.0
6.0
8.0
10.0

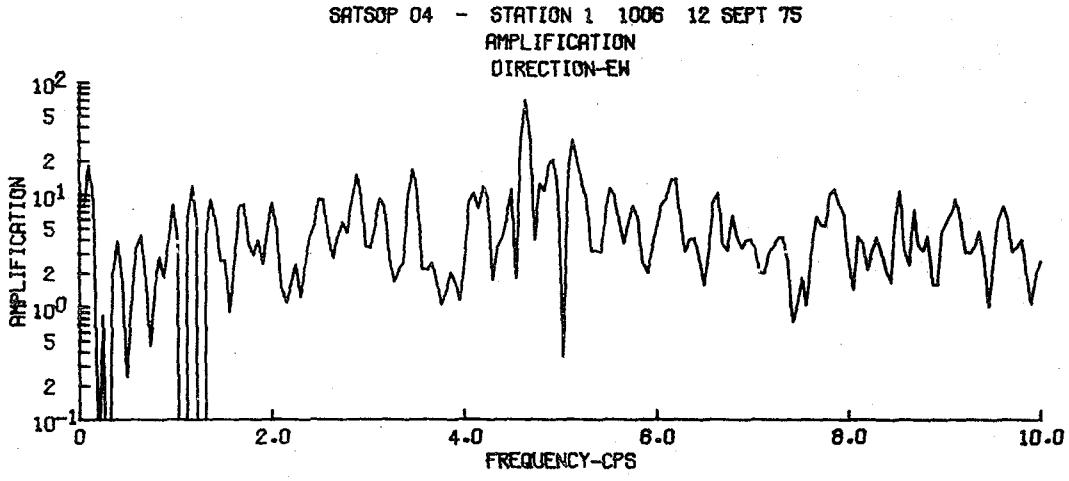
SATSOP 04 - STATION 1 1006 12 SEPT 75
AMPLIFICATION
DIRECTION-EW
AMPLIFICATION
FREQUENCY-CPS
0
2.0
4.0
6.0
8.0
10.0

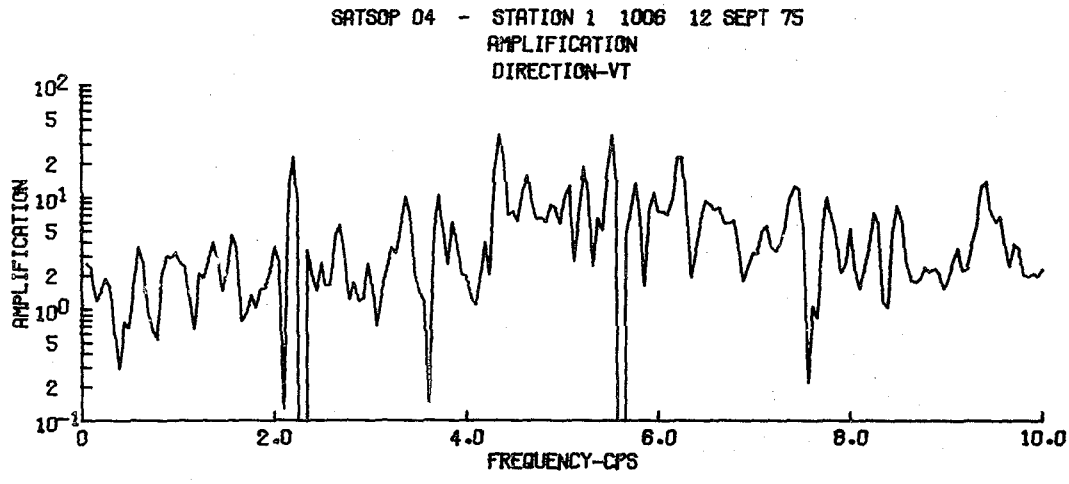
SATSOP 04 - STATION 1 1006 12 SEPT 75
AMPLIFICATION
DIRECTION-VT
AMPLIFICATION
FREQUENCY-CPS
0
2.0
4.0
6.0
8.0
10.0

SATSOP 04 - STATION 1 1006 12 SEPT 75
FOURIER POWER SPECTRUM
BASE STATION
RESULTANT

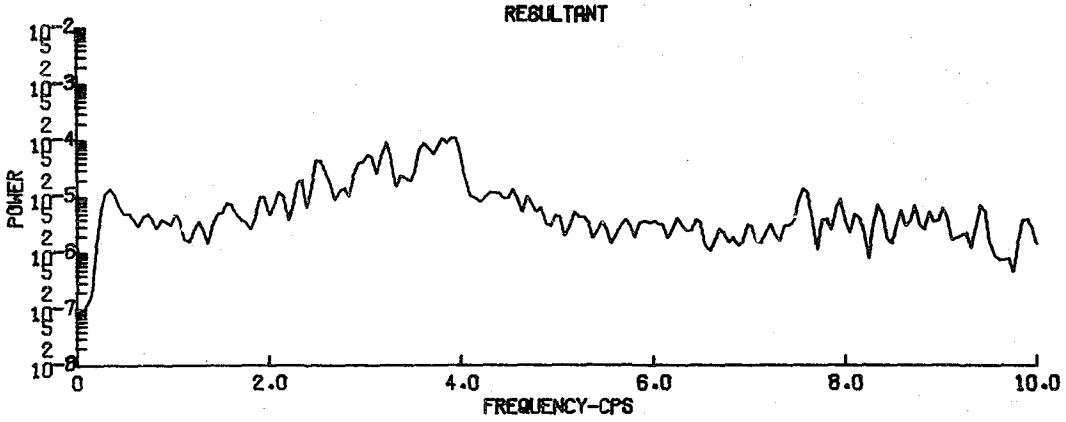

SATSOP 04 - STATION 1 1006 12 SEPT 75
FOURIER POWER SPECTRUM
PORTABLE STATION
RESULTANT

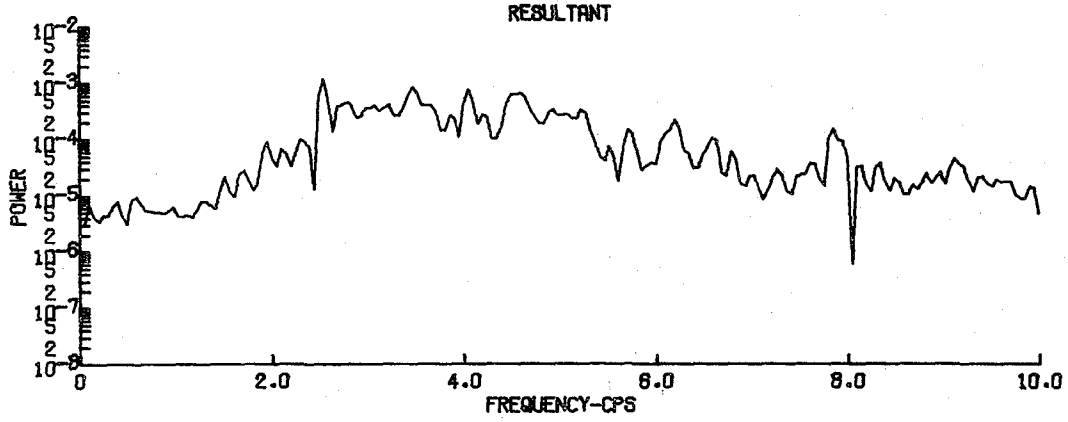

SATSOP 04 - STATION 1 1006 12 SEPT 75
AMPLIFICATION
RESULTANT

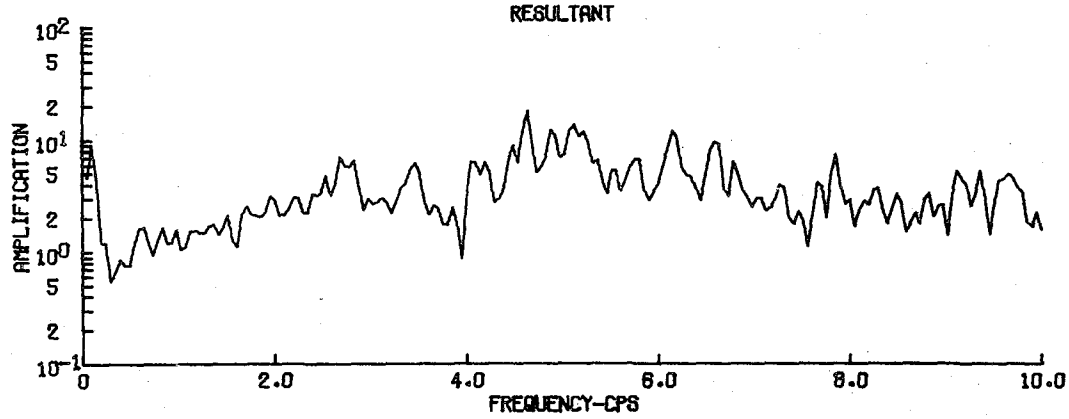

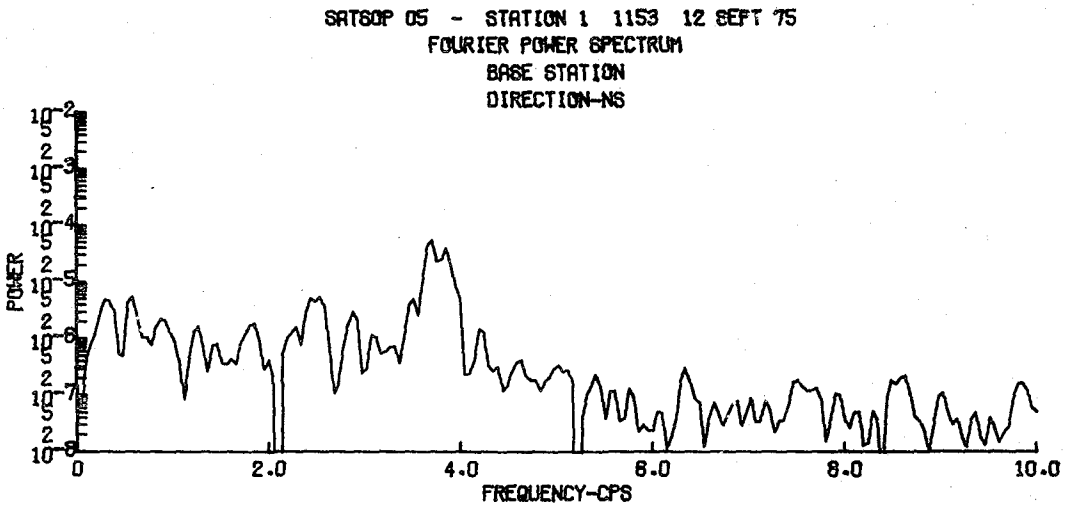
SATSOP 05 - STATION 1 1153 12 SEPT 75
FOURIER POWER SPECTRUM
BASE STATION
DIRECTION-NS
POWER
FREQUENCY-CPS
0
2.0
4.0
6.0
8.0
10.0

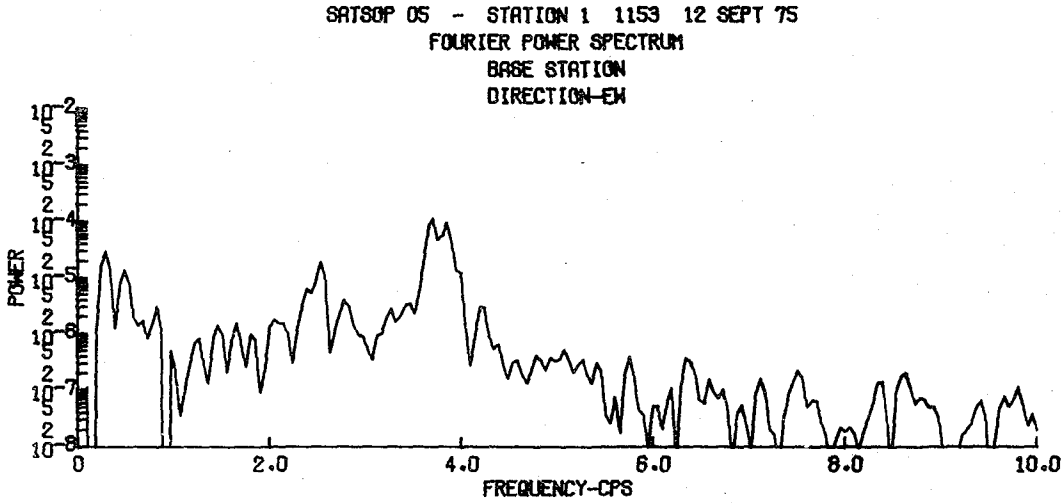
SATSOP 05 - STATION 1 1153 12 SEPT 75
FOURIER POWER SPECTRUM
BASE STATION
DIRECTION-EW
POWER
FREQUENCY-CPS
0
2.0
4.0
6.0
8.0
10.0

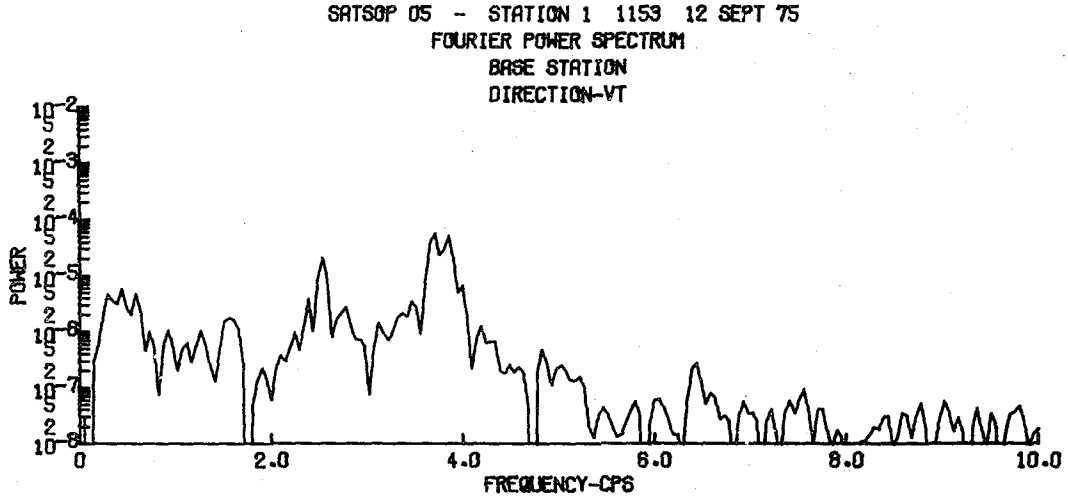
SATSOP 05 - STATION 1 1153 12 SEPT 75
FOURIER POWER SPECTRUM
BASE STATION
DIRECTION-VT
POWER
FREQUENCY-CPS
0
2.0
4.0
6.0
8.0
10.0

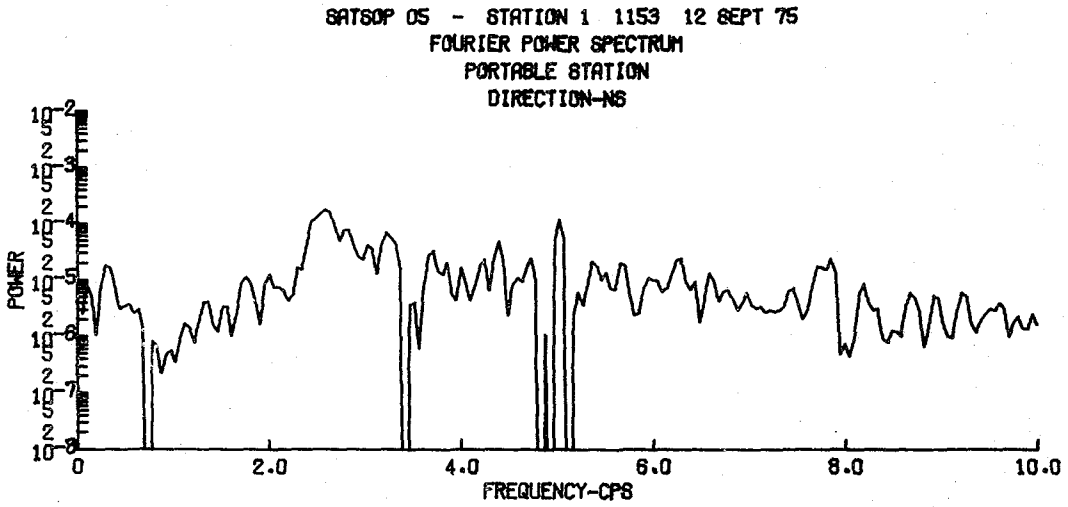
SATSOP 05 - STATION 1 1153 12 SEPT 75
FOURIER POWER SPECTRUM
PORTABLE STATION
DIRECTION-NS
POWER
FREQUENCY-CPS
0
2.0
4.0
6.0
8.0
10.0

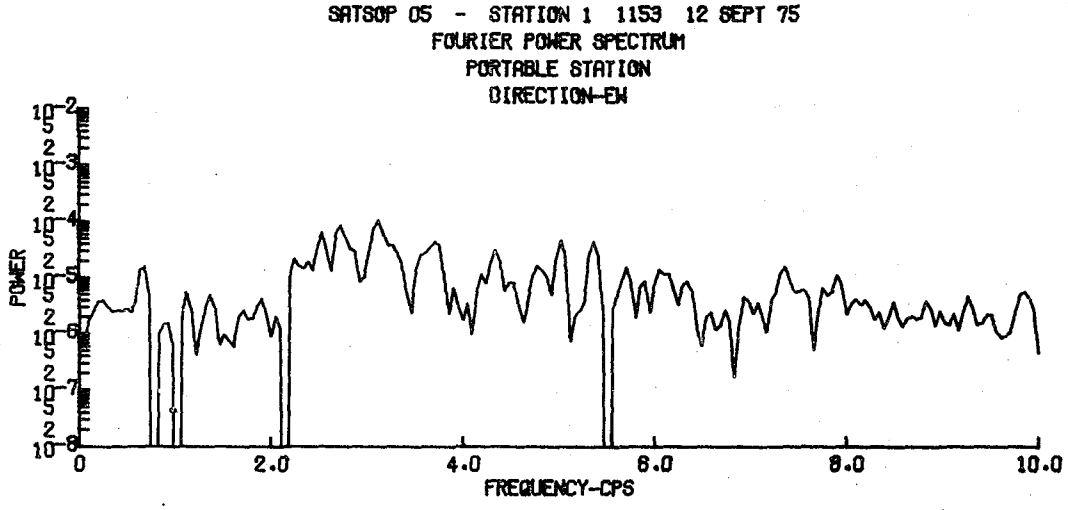
SATSOP 05 - STATION 1 1153 12 SEPT 75
FOURIER POWER SPECTRUM
PORTABLE STATION
DIRECTION-EW
POWER
FREQUENCY-CPS
0
2.0
4.0
6.0
8.0
10.0

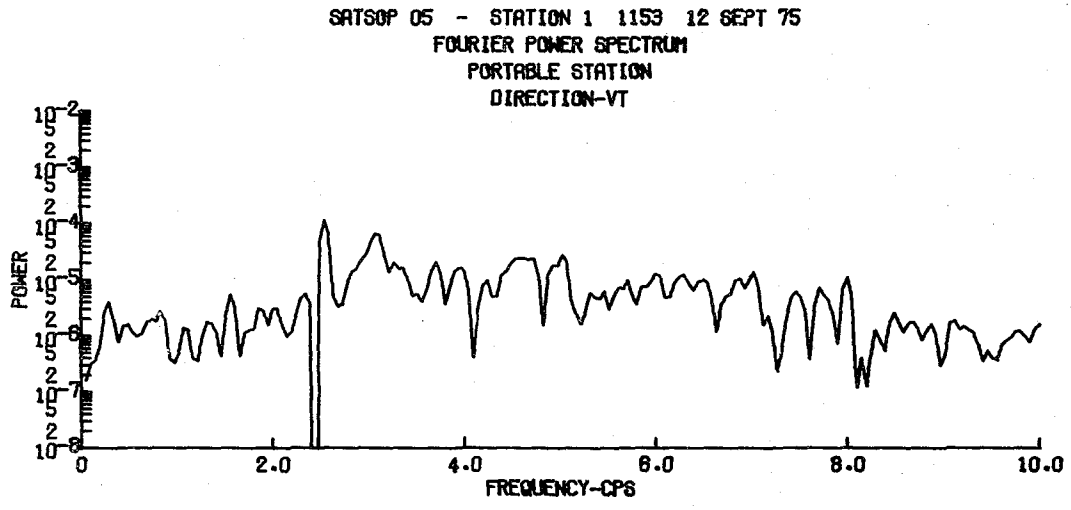
SATSOP 05 - STATION 1 1153 12 SEPT 75
FOURIER POWER SPECTRUM
PORTABLE STATION
DIRECTION-VT
POWER
FREQUENCY-CPS
0
2.0
4.0
6.0
8.0
10.0

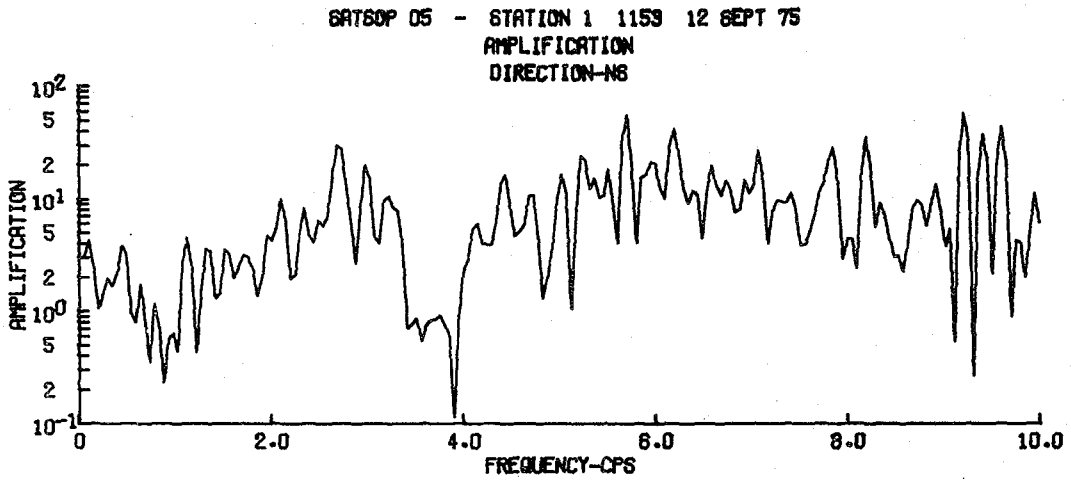
SATSOP 05 - STATION 1 1153 12 SEPT 75
AMPLIFICATION
DIRECTION-NS
AMPLIFICATION
FREQUENCY-CPS

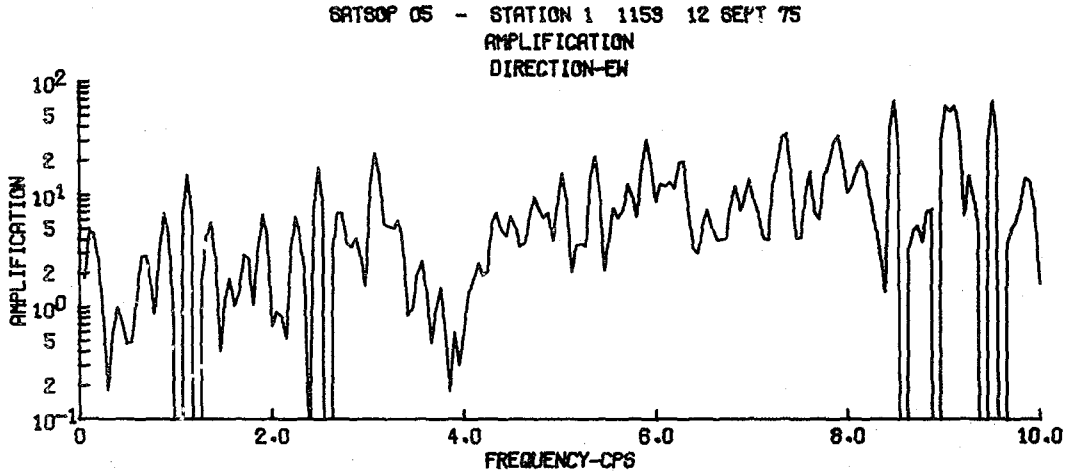
SATSOP 05 - STATION 1 1153 12 SEPT 75
AMPLIFICATION
DIRECTION-EW
AMPLIFICATION
FREQUENCY-CPS

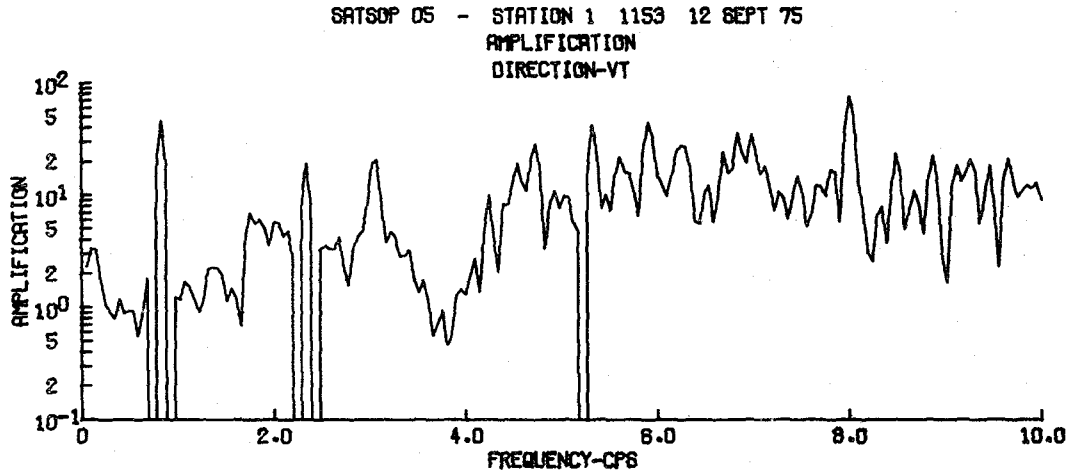
SATSOP 05 - STATION 1 1153 12 SEPT 75
AMPLIFICATION
DIRECTION-VT
AMPLIFICATION
FREQUENCY-CPS

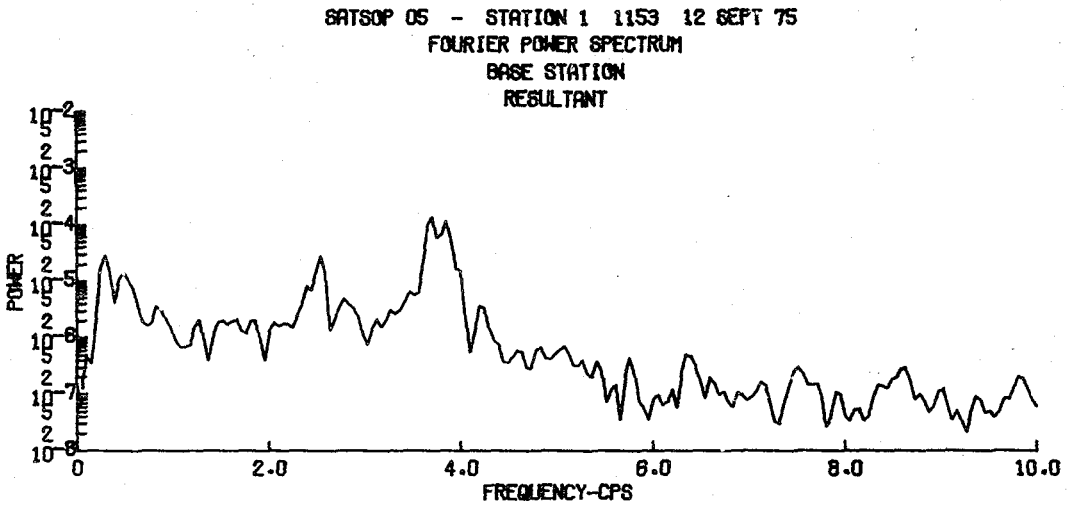
SATSOP 05 - STATION 1 1153 12 SEPT 75
FOURIER POWER SPECTRUM
BASE STATION
RESULTANT
POWER
FREQUENCY-CPS
0
2.0
4.0
6.0
8.0
10.0

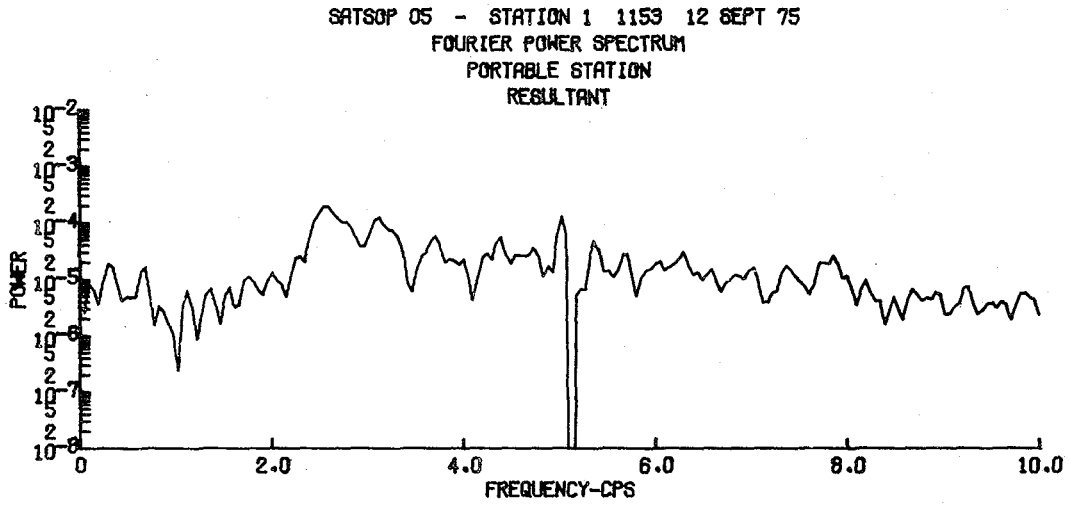
SATSOP 05 - STATION 1 1153 12 SEPT 75
FOURIER POWER SPECTRUM
PORTABLE STATION
RESULTANT
POWER
FREQUENCY-CPS
0
2.0
4.0
6.0
8.0
10.0

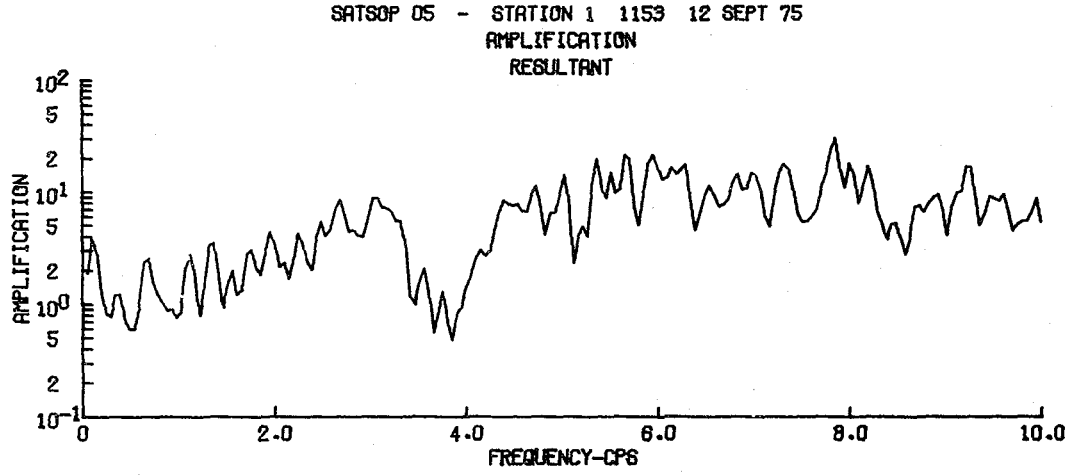
SATSOP 05 - STATION 1 1153 12 SEPT 75
AMPLIFICATION
RESULTANT
AMPLIFICATION
FREQUENCY-CPS
0
2.0
4.0
6.0
8.0
10.0

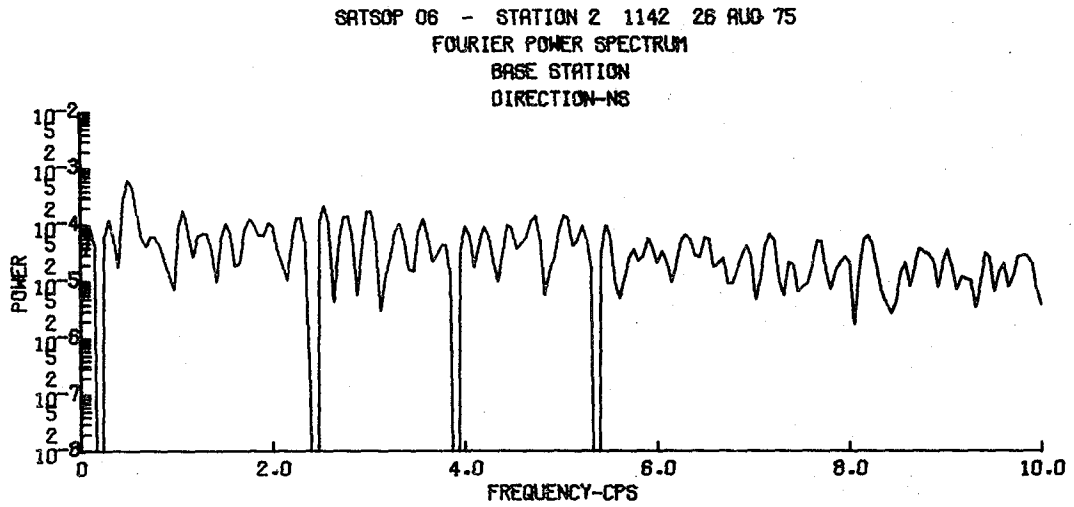
SATSOP 06 - STATION 2 1142 26 AUG 75
FOURIER POWER SPECTRUM
BASE STATION
DIRECTION-NS
POWER
FREQUENCY-CPS
0
2.0
4.0
6.0
8.0
10.0

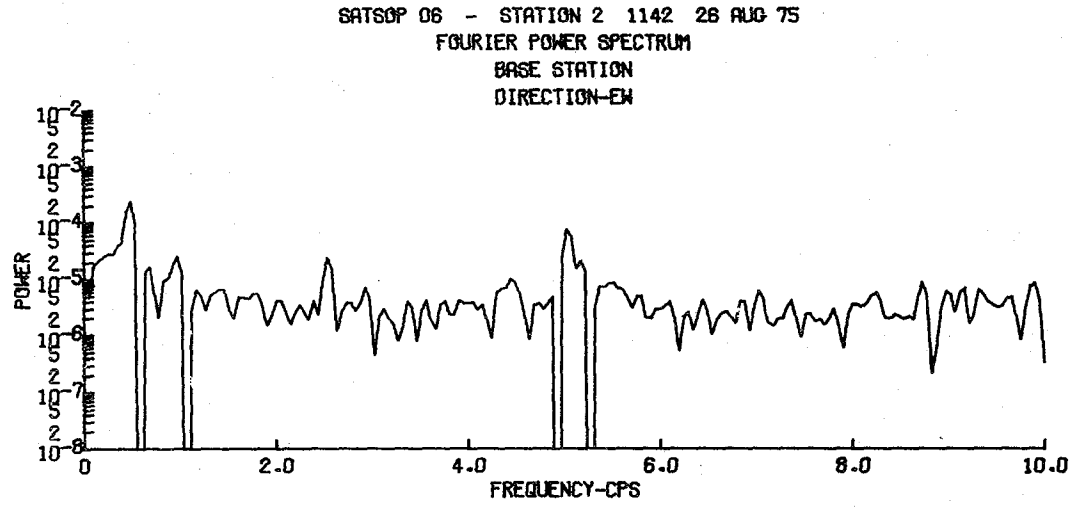
SATSOP 06 - STATION 2 1142 26 AUG 75
FOURIER POWER SPECTRUM
BASE STATION
DIRECTION-EW
POWER
FREQUENCY-CPS
0
2.0
4.0
6.0
8.0
10.0

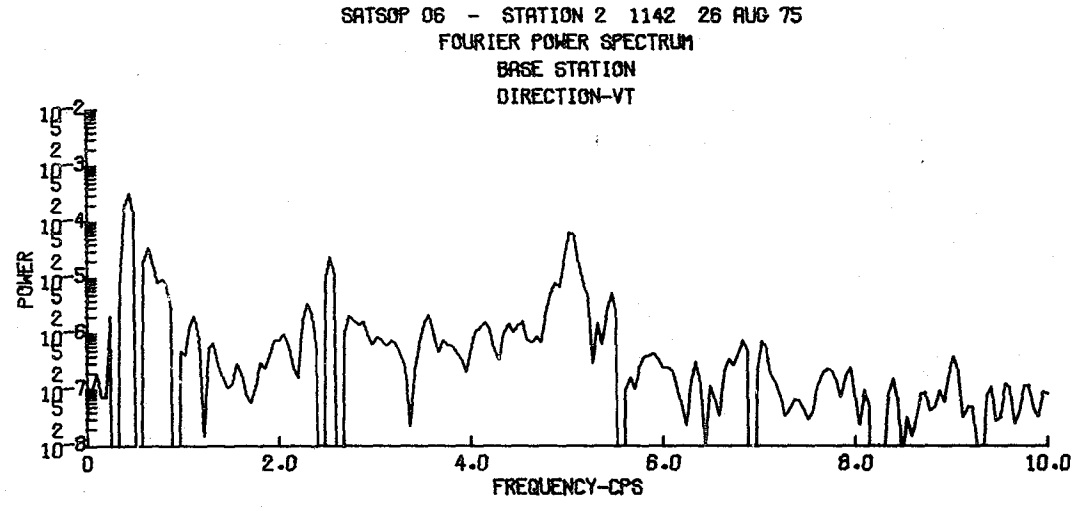
SATSOP 06 - STATION 2 1142 26 AUG 75
FOURIER POWER SPECTRUM
BASE STATION
DIRECTION-VT
POWER
FREQUENCY-CPS
0
2.0
4.0
6.0
8.0
10.0

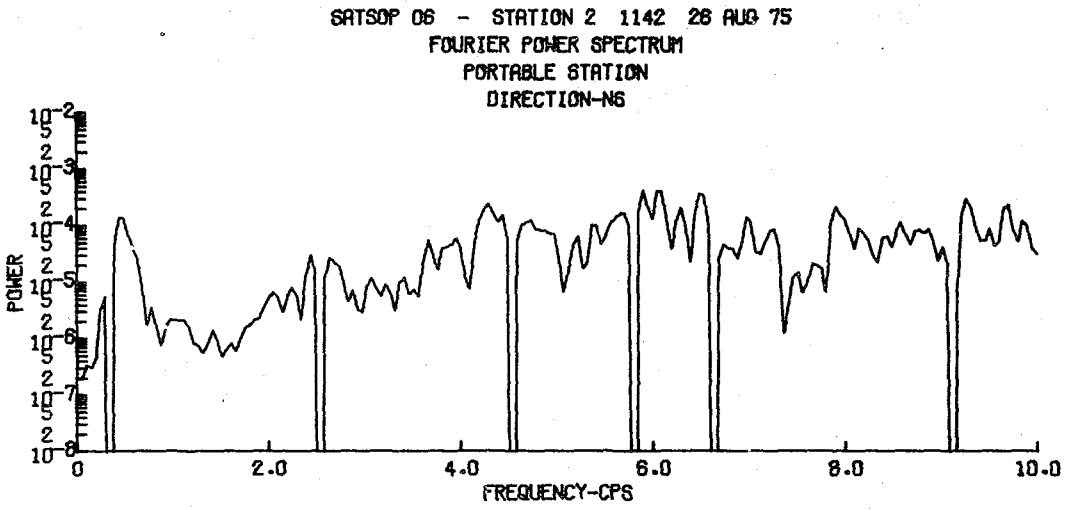
SATSOP 06 - STATION 2 1142 26 AUG 75
FOURIER POWER SPECTRUM
PORTABLE STATION
DIRECTION-NS
POWER
FREQUENCY-CPS
0
2.0
4.0
6.0
8.0
10.0

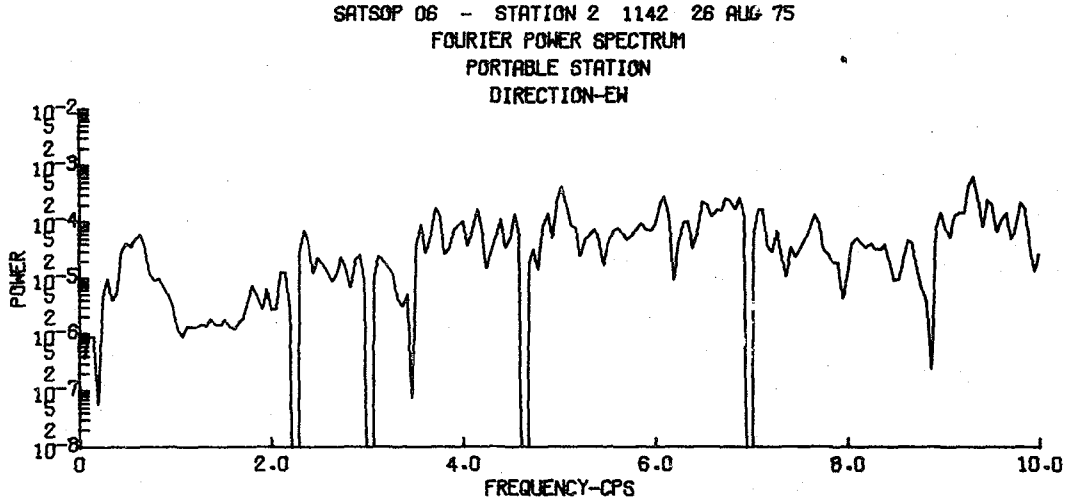
SATSOP 06 - STATION 2 1142 26 AUG 75
FOURIER POWER SPECTRUM
PORTABLE STATION
DIRECTION-EW
POWER
FREQUENCY-CPS
0
2.0
4.0
6.0
8.0
10.0

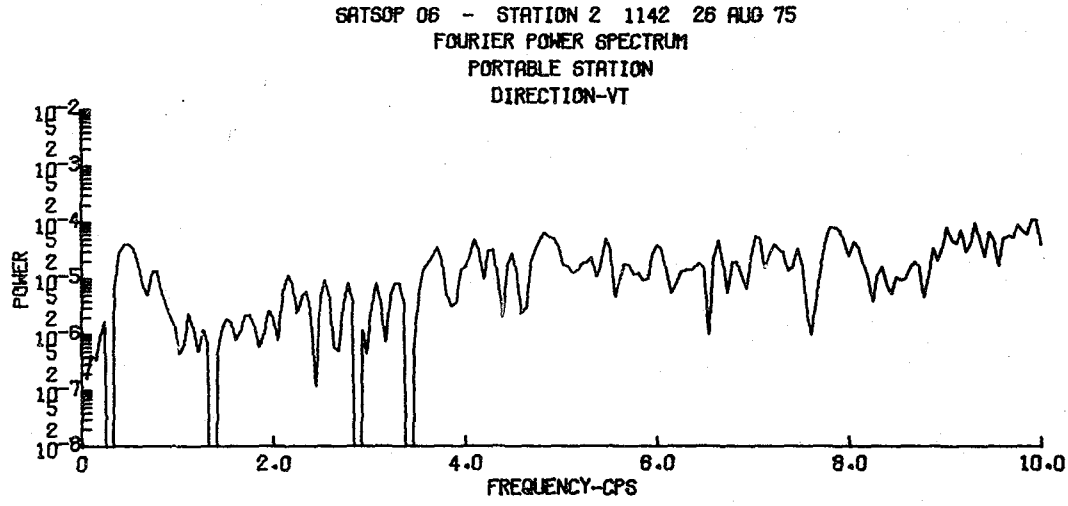
SATSOP 06 - STATION 2 1142 26 AUG 75
FOURIER POWER SPECTRUM
PORTABLE STATION
DIRECTION-VT
POWER
FREQUENCY-CPS
0
2.0
4.0
6.0
8.0
10.0

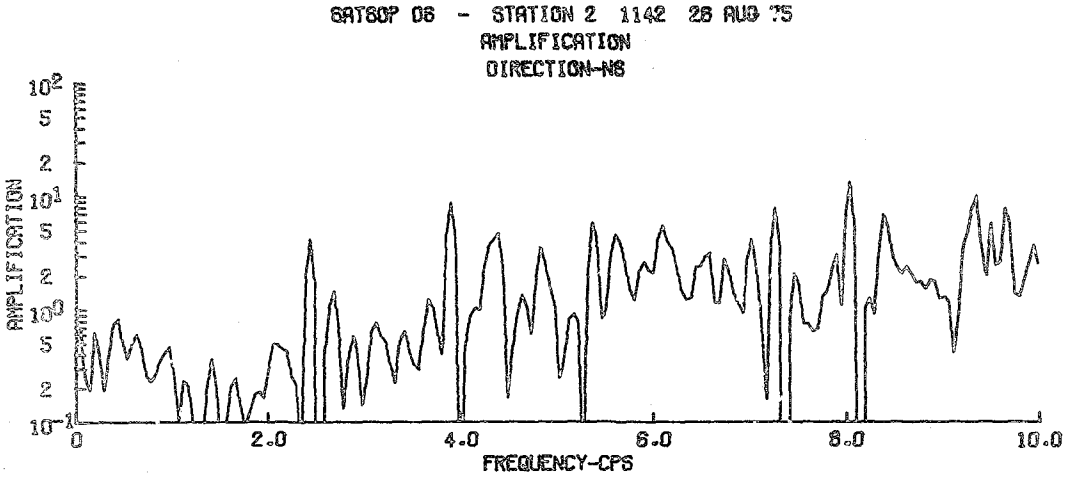
SATSOP 06 - STATION 2 1142 26 AUG 75
AMPLIFICATION
DIRECTION-NS
AMPLIFICATION
FREQUENCY-CPS
0
2.0
4.0
6.0
8.0
10.0

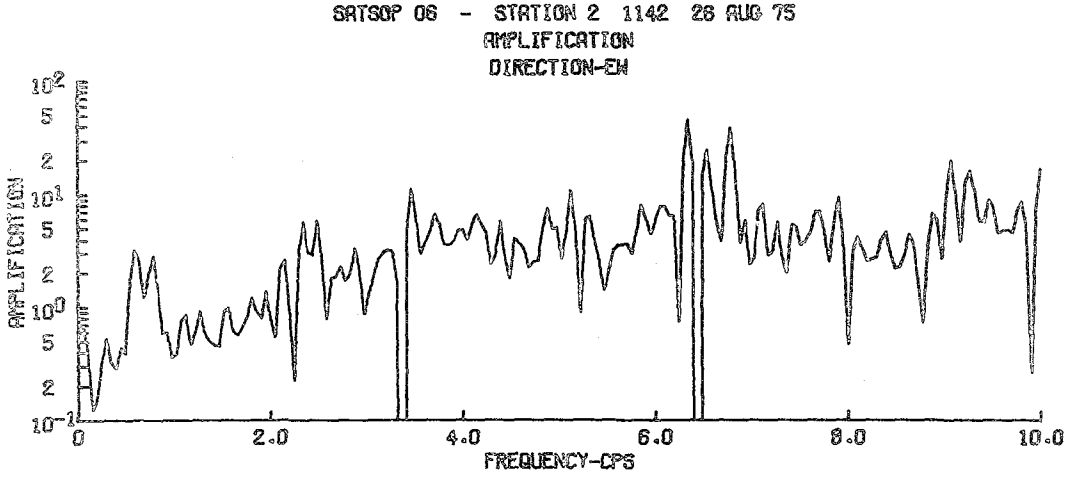
SATSOP 06 - STATION 2 1142 26 AUG 75
AMPLIFICATION
DIRECTION-EW
AMPLIFICATION
FREQUENCY-CPS
0
2.0
4.0
6.0
8.0
10.0

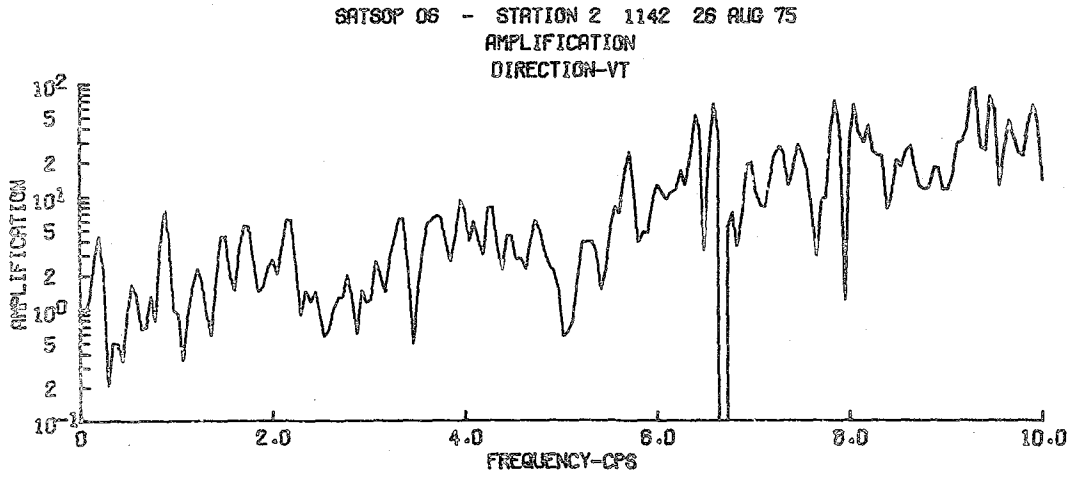
SATSOP 06 - STATION 2 1142 26 AUG 75
AMPLIFICATION
DIRECTION-VT
AMPLIFICATION
FREQUENCY-CPS
0
2.0
4.0
6.0
8.0
10.0

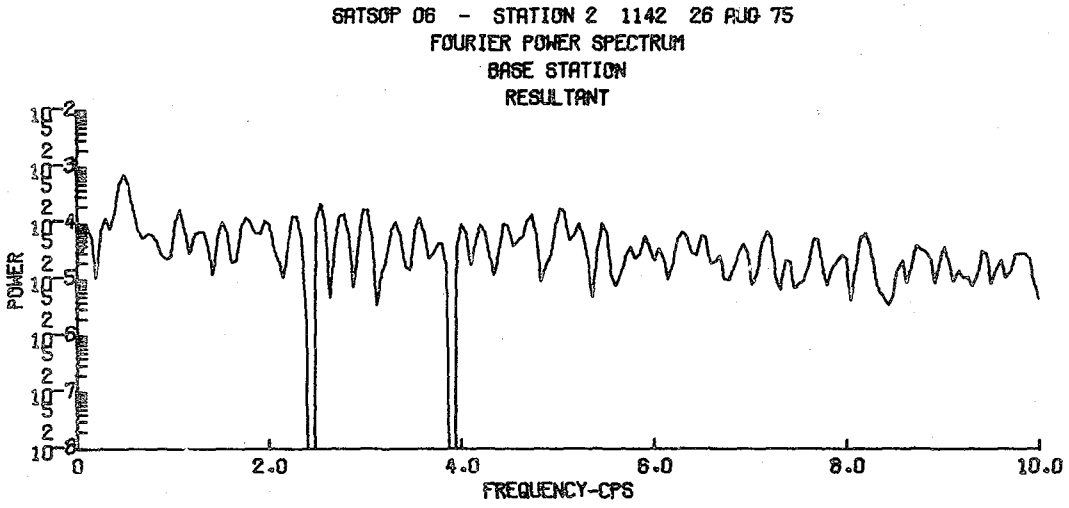
SATSOP 06 - STATION 2 1142 26 AUG 75
FOURIER POWER SPECTRUM
BASE STATION
RESULTANT
POWER
FREQUENCY-CPS
0
2.0
4.0
6.0
8.0
10.0

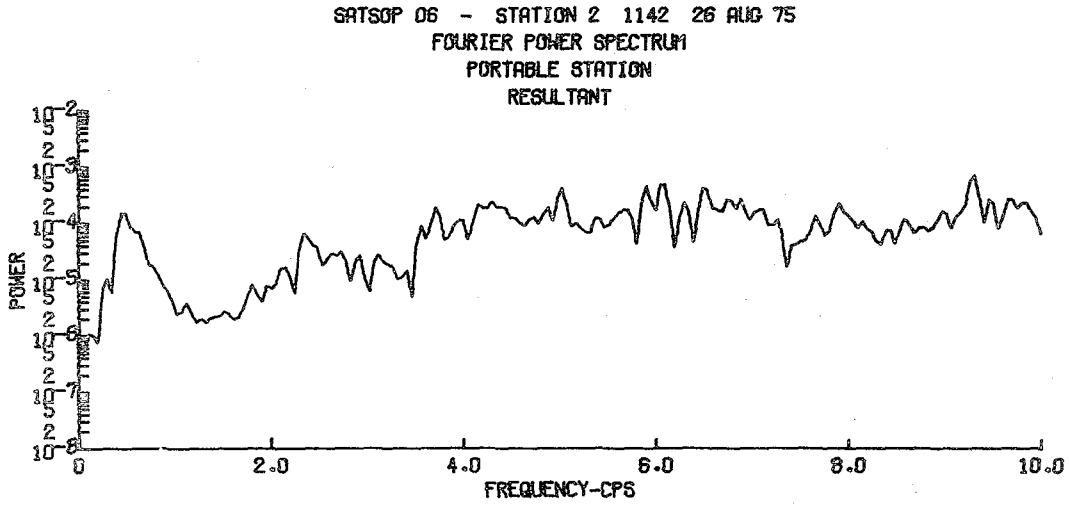
SATSOP 06 - STATION 2 1142 26 AUG 75
FOURIER POWER SPECTRUM
PORTABLE STATION
RESULTANT
POWER
FREQUENCY-CPS
0
2.0
4.0
6.0
8.0
10.0

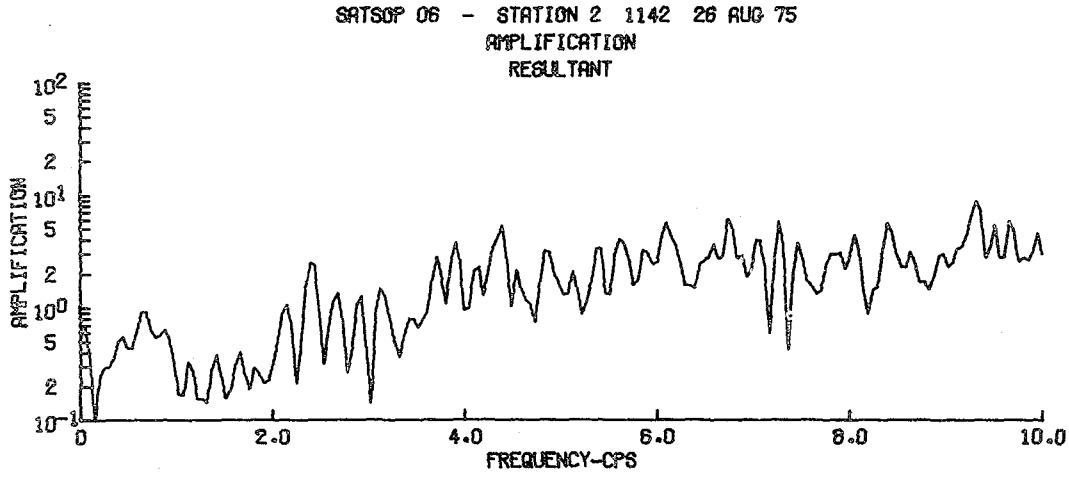
SATSOP 06 - STATION 2 1142 26 AUG 75
AMPLIFICATION
RESULTANT
AMPLIFICATION
FREQUENCY-CPS
0
2.0
4.0
6.0
8.0
10.0

SATSOP 07 - STATION 2 1506 26 AUG 75
FOURIER POWER SPECTRUM
BASE STATION
DIRECTION-NS

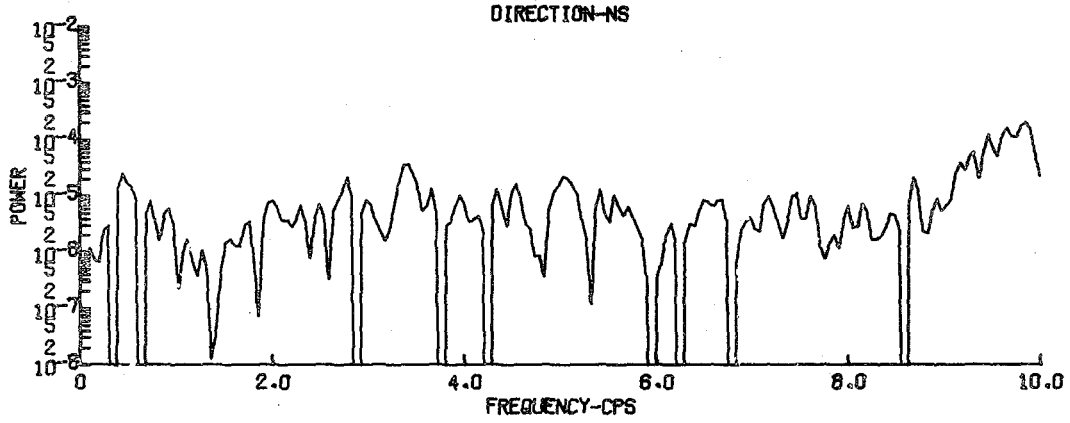

SATSOP 07 - STATION 2 1506 26 AUG 75
FOURIER POWER SPECTRUM
BASE STATION
DIRECTION-EW

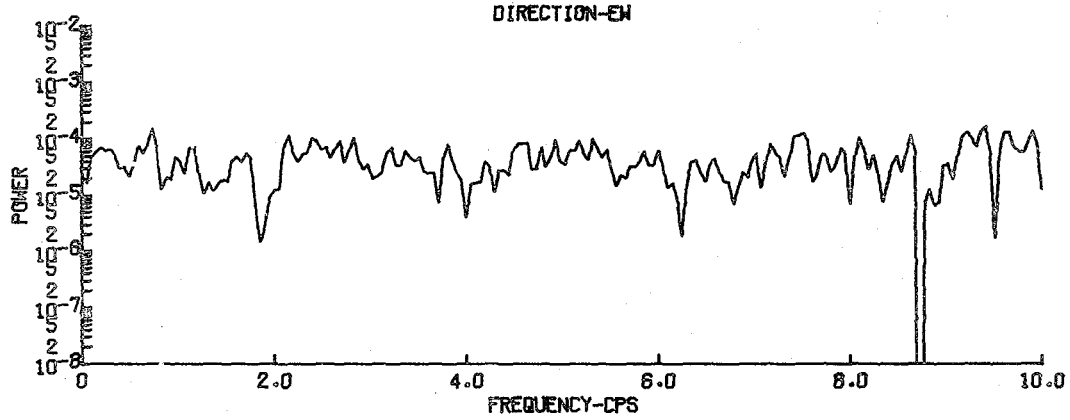

SATSOP 07 - STATION 2 1506 26 AUG 75
FOURIER POWER SPECTRUM
BASE STATION
DIRECTION-VT

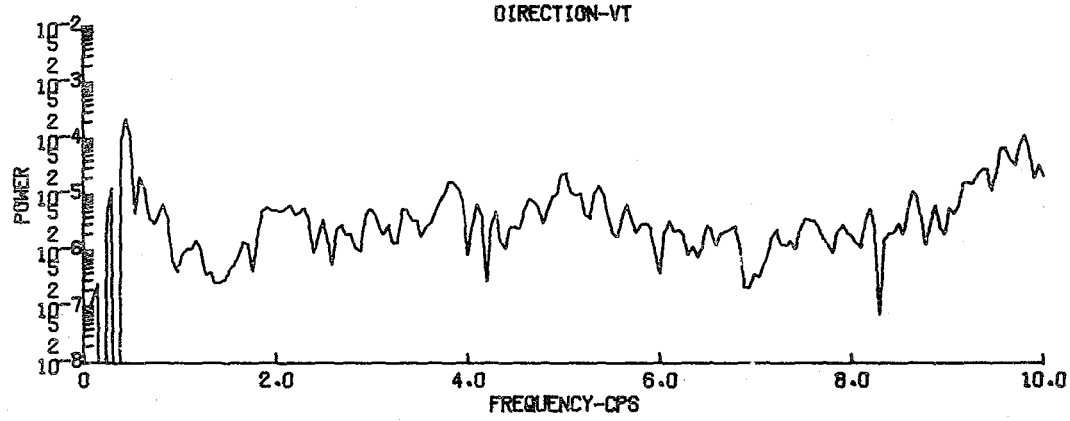

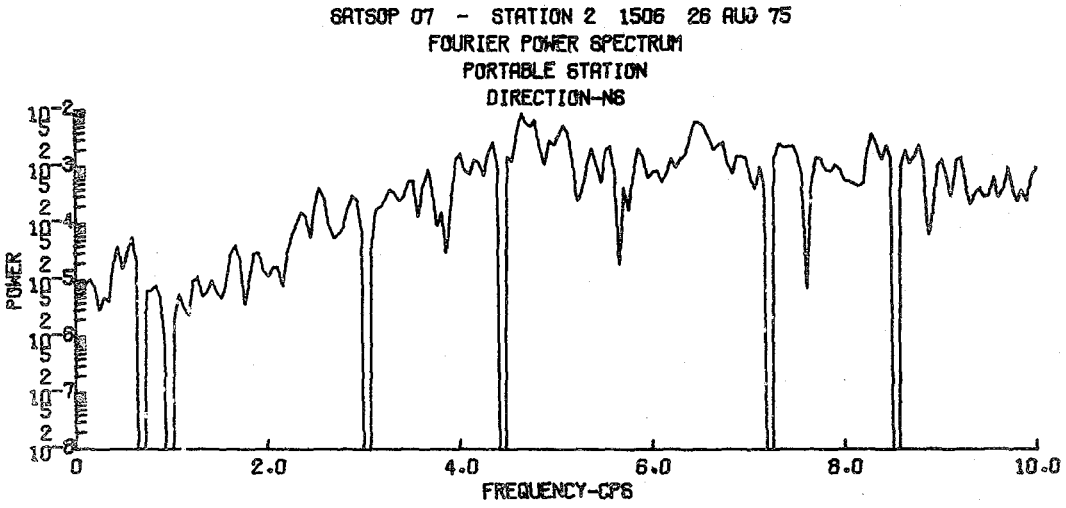
SATSOP 07 - STATION 2 1506 26 AUG 75
FOURIER POWER SPECTRUM
PORTABLE STATION
DIRECTION-NS
POWER
FREQUENCY-CPS
0
2.0
4.0
6.0
8.0
10.0

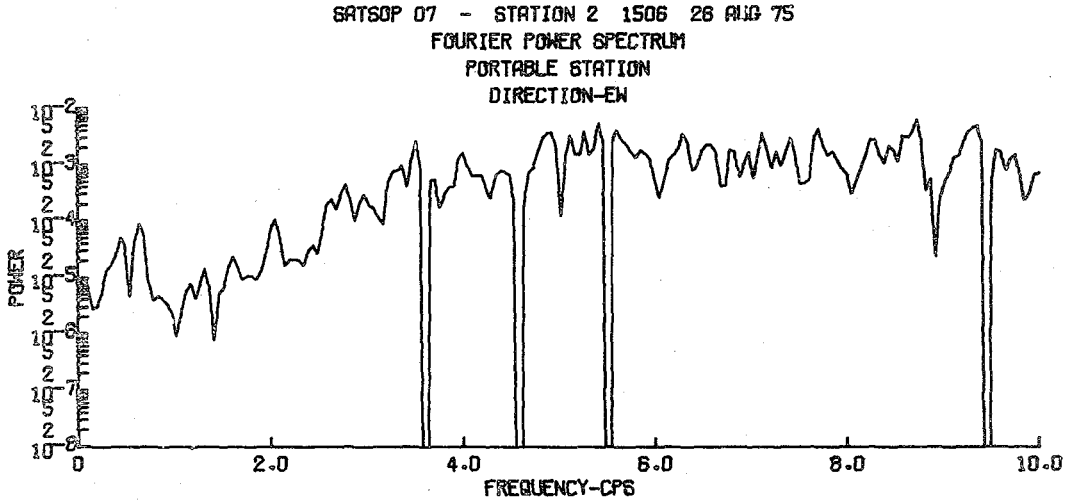
SATSOP 07 - STATION 2 1506 26 AUG 75
FOURIER POWER SPECTRUM
PORTABLE STATION
DIRECTION-EW
POWER
FREQUENCY-CPS
0
2.0
4.0
6.0
8.0
10.0

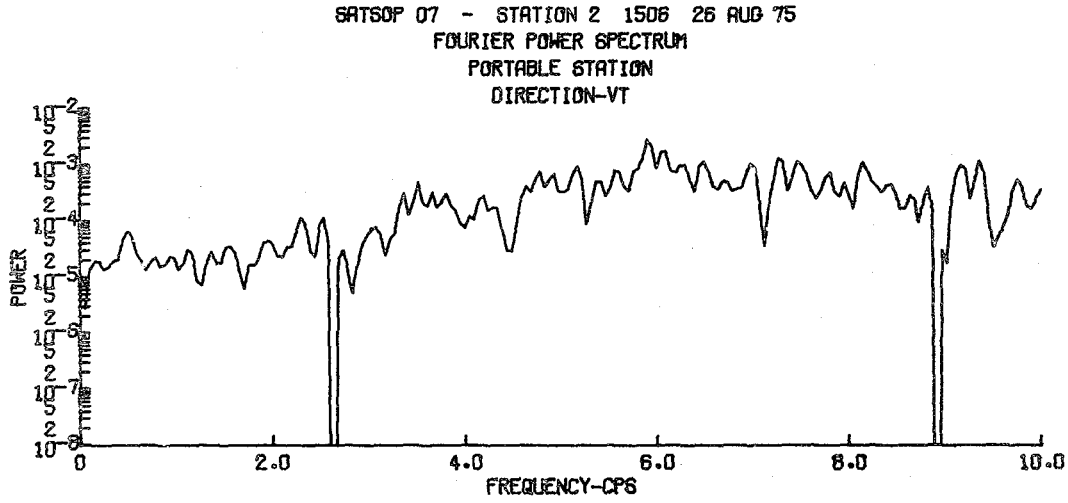
SATSOP 07 - STATION 2 1506 26 AUG 75
FOURIER POWER SPECTRUM
PORTABLE STATION
DIRECTION-VT
POWER
FREQUENCY-CPS
0
2.0
4.0
6.0
8.0
10.0

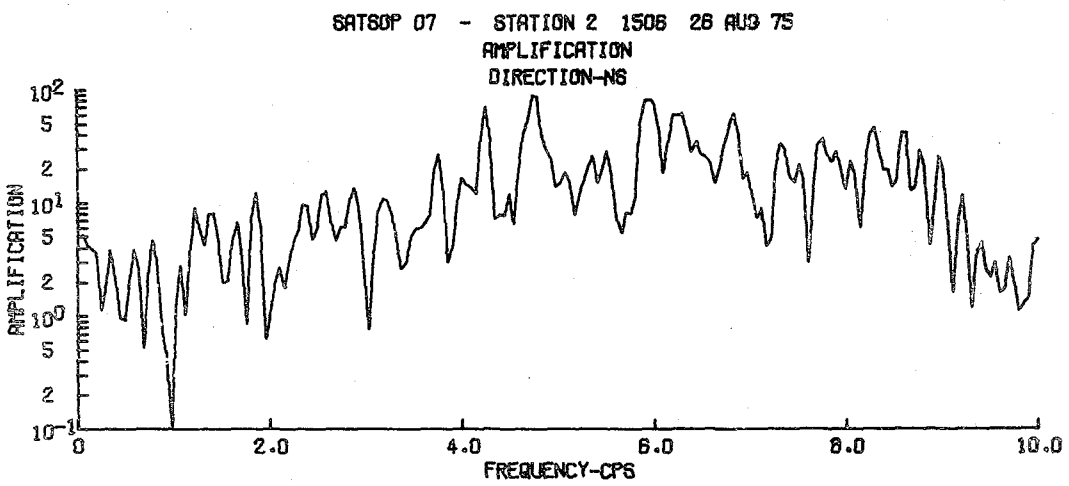
SATSOP 07 - STATION 2 1506 26 AUG 75
AMPLIFICATION
DIRECTION-NS
AMPLIFICATION
FREQUENCY-CPS

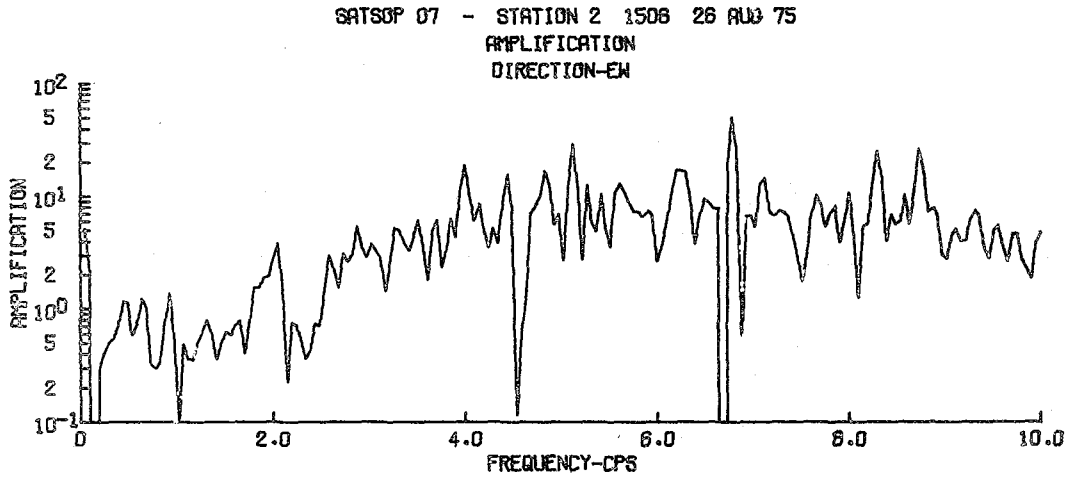
SATSOP 07 - STATION 2 1506 26 AUG 75
AMPLIFICATION
DIRECTION-EW
AMPLIFICATION
FREQUENCY-CPS

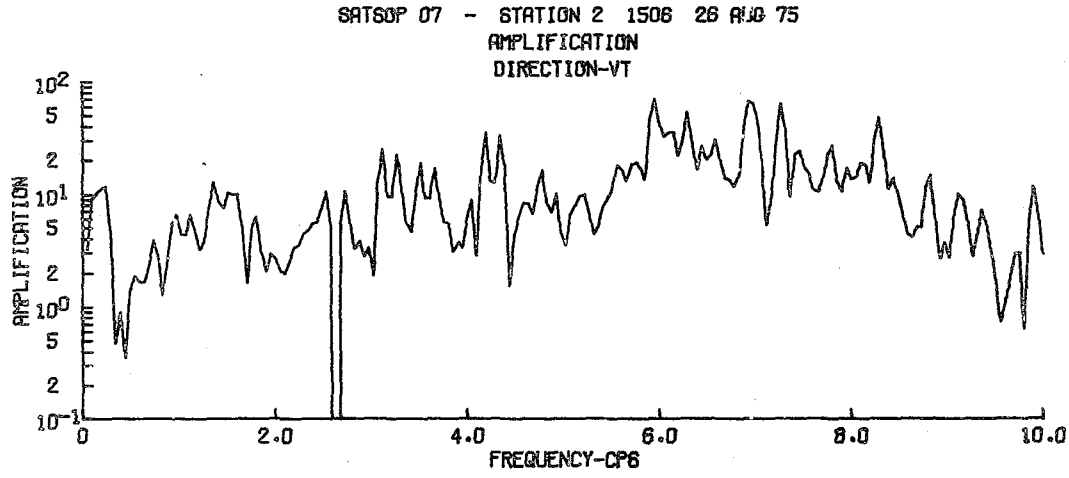
SATSOP 07 - STATION 2 1506 26 AUG 75
AMPLIFICATION
DIRECTION-VT
AMPLIFICATION
FREQUENCY-CPS

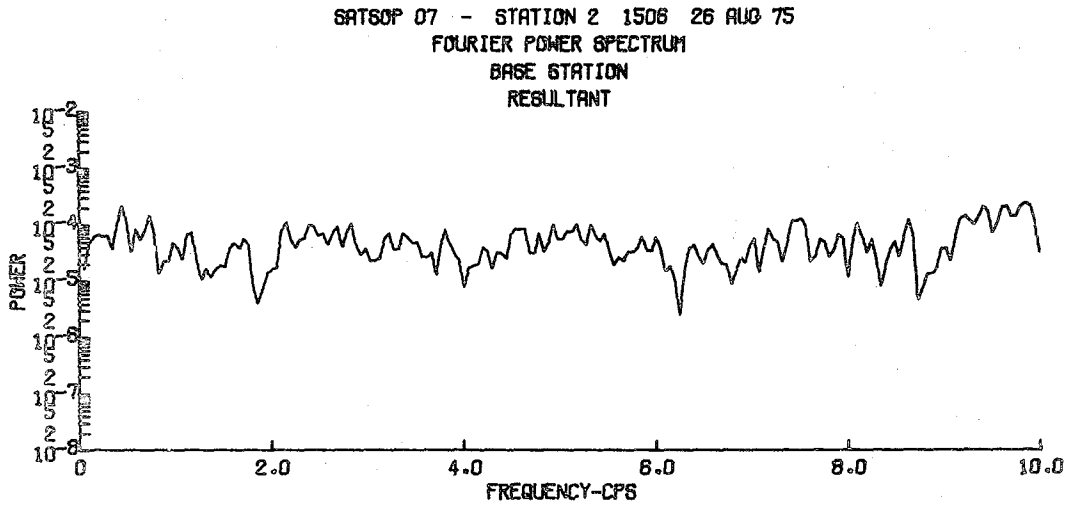
SATSOP 07 - STATION 2 1506 26 AUG 75
FOURIER POWER SPECTRUM
BASE STATION
RESULTANT
POWER
FREQUENCY-CPS
0
2.0
4.0
6.0
8.0
10.0

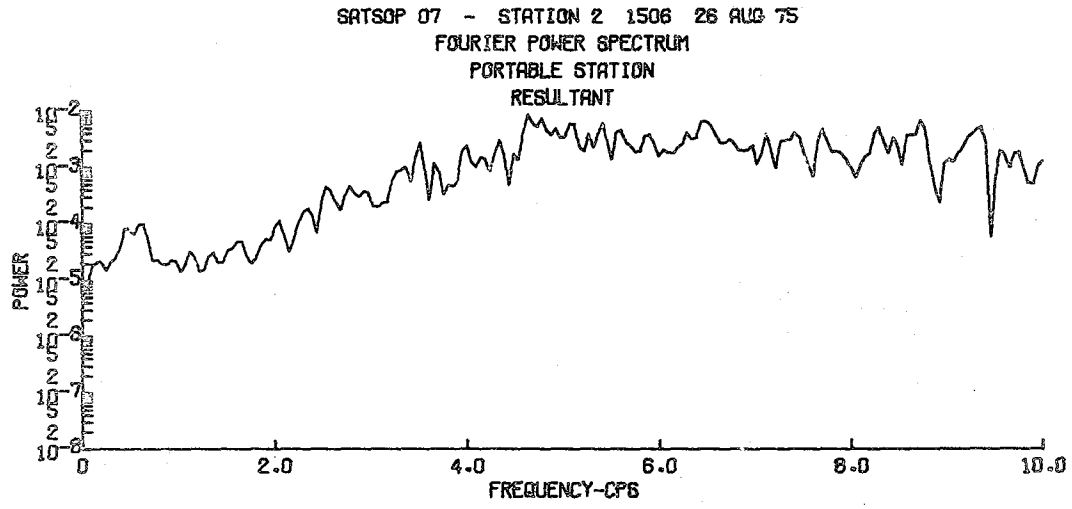
SATSOP 07 - STATION 2 1506 26 AUG 75
FOURIER POWER SPECTRUM
PORTABLE STATION
RESULTANT
POWER
FREQUENCY-CPS
0
2.0
4.0
6.0
8.0
10.0

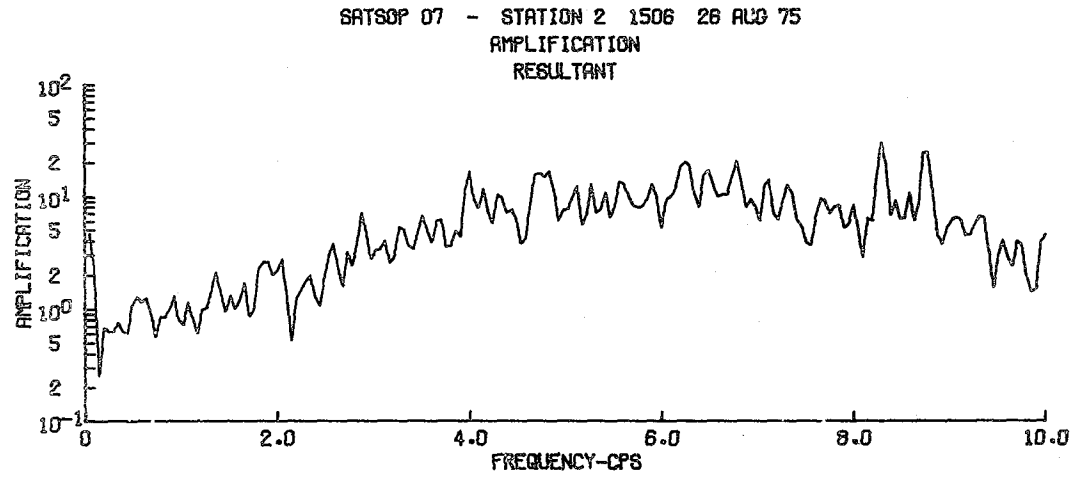
SATSOP 07 - STATION 2 1506 26 AUG 75
AMPLIFICATION
RESULTANT
AMPLIFICATION
FREQUENCY-CPS
0
2.0
4.0
6.0
8.0
10.0

SATSOP 08 - STATION 2 1630 26 AUG 75
FOURIER POWER SPECTRUM
BASE STATION
DIRECTION-NS

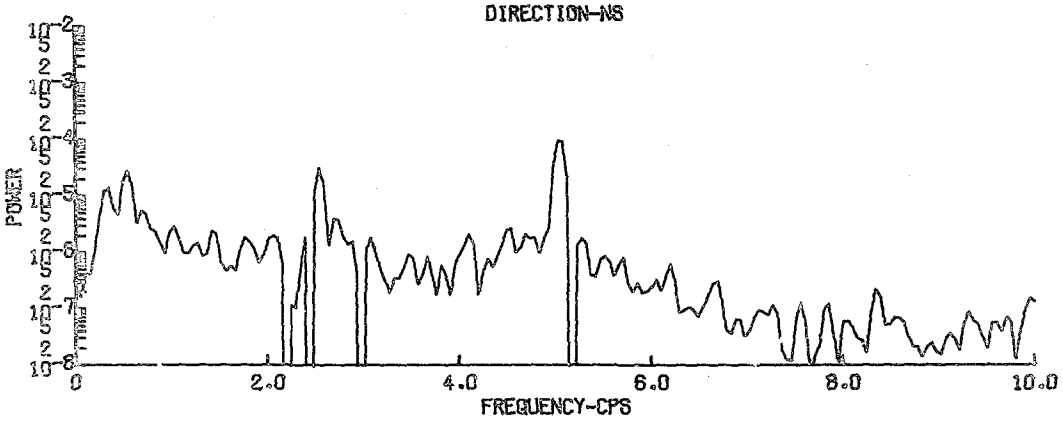

SATSOP 08 - STATION 2 1630 26 AUG 75
FOURIER POWER SPECTRUM
BASE STATION
DIRECTION-EW

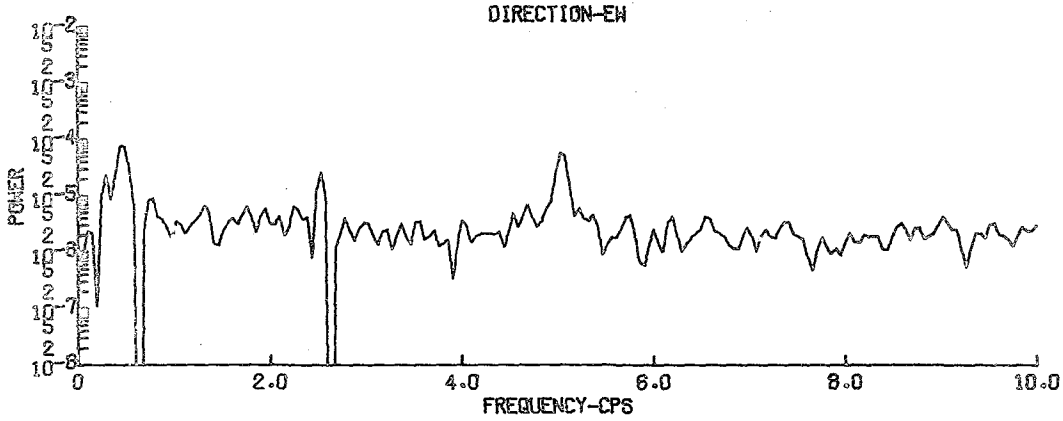

SATSOP 08 - STATION 2 1630 26 AUG 75
FOURIER POWER SPECTRUM
BASE STATION
DIRECTION-VT

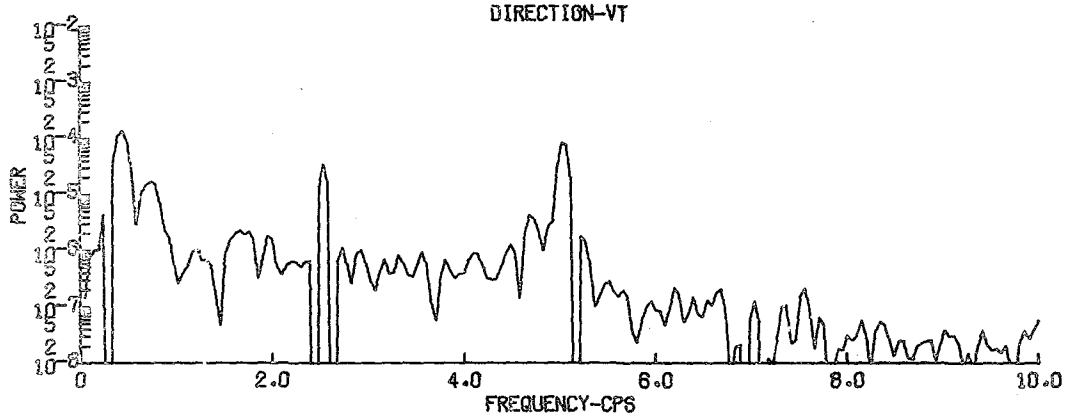

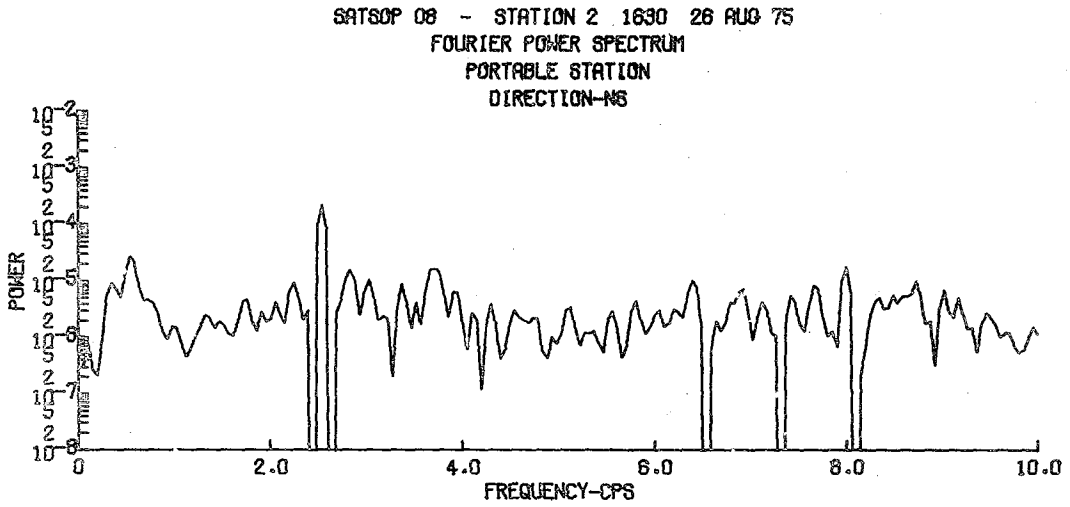
SATSOP 08 - STATION 2 1630 26 AUG 75
FOURIER POWER SPECTRUM
PORTABLE STATION
DIRECTION-NS
POWER
FREQUENCY-CPS
0
2.0
4.0
6.0
8.0
10.0

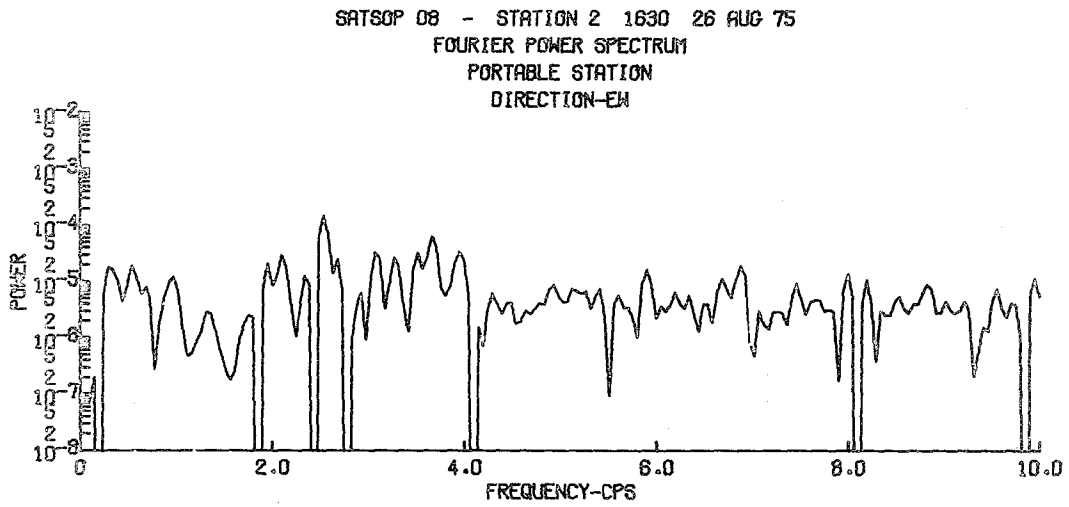
SATSOP 08 - STATION 2 1630 26 AUG 75
FOURIER POWER SPECTRUM
PORTABLE STATION
DIRECTION-EW
POWER
FREQUENCY-CPS
0
2.0
4.0
6.0
8.0
10.0

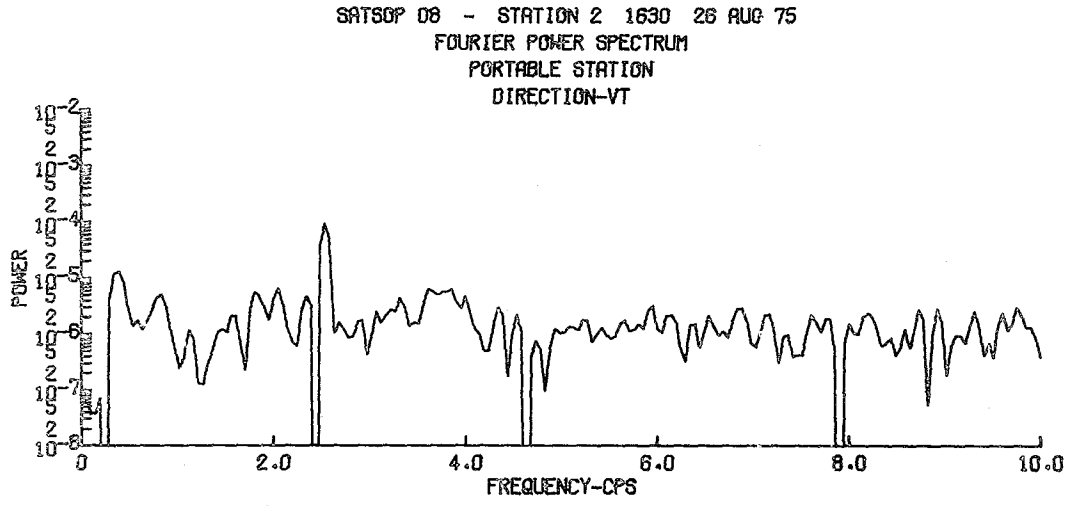
SATSOP 08 - STATION 2 1630 26 AUG 75
FOURIER POWER SPECTRUM
PORTABLE STATION
DIRECTION-VT
POWER
FREQUENCY-CPS
0
2.0
4.0
6.0
8.0
10.0

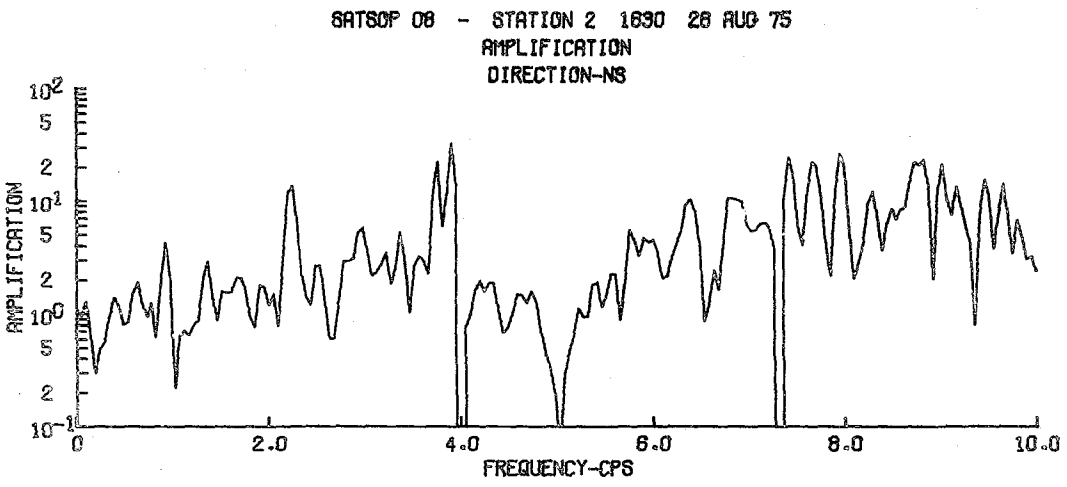
SATSOP 08 - STATION 2 1630 26 AUG 75
AMPLIFICATION
DIRECTION-NS
AMPLIFICATION
FREQUENCY-CPS

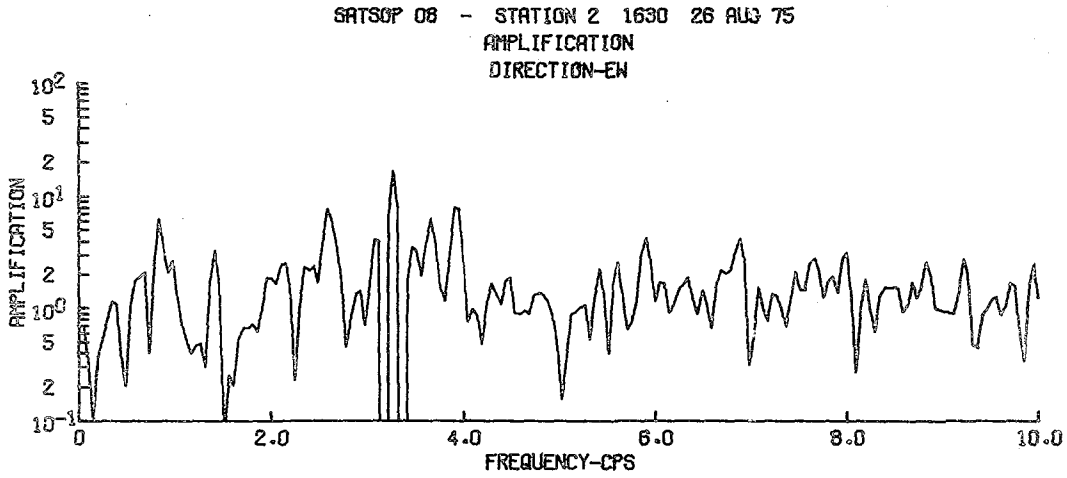
SATSOP 08 - STATION 2 1630 26 AUG 75
AMPLIFICATION
DIRECTION-EW
AMPLIFICATION
FREQUENCY-CPS

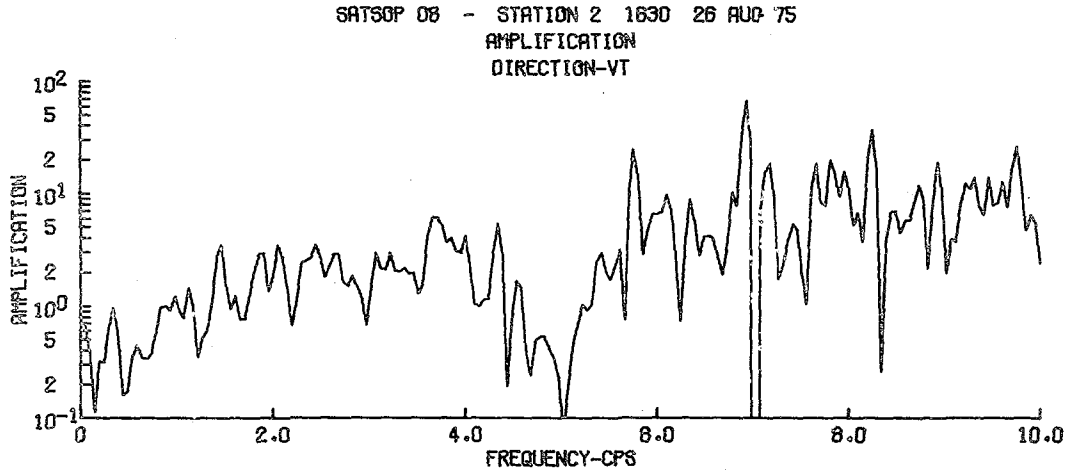
SATSOP 08 - STATION 2 1630 26 AUG 75
AMPLIFICATION
DIRECTION-VT
AMPLIFICATION
FREQUENCY-CPS

SATSOP 08 - STATION 2 1630 26 AUG 75
FOURIER POWER SPECTRUM
BASE STATION
RESULTANT

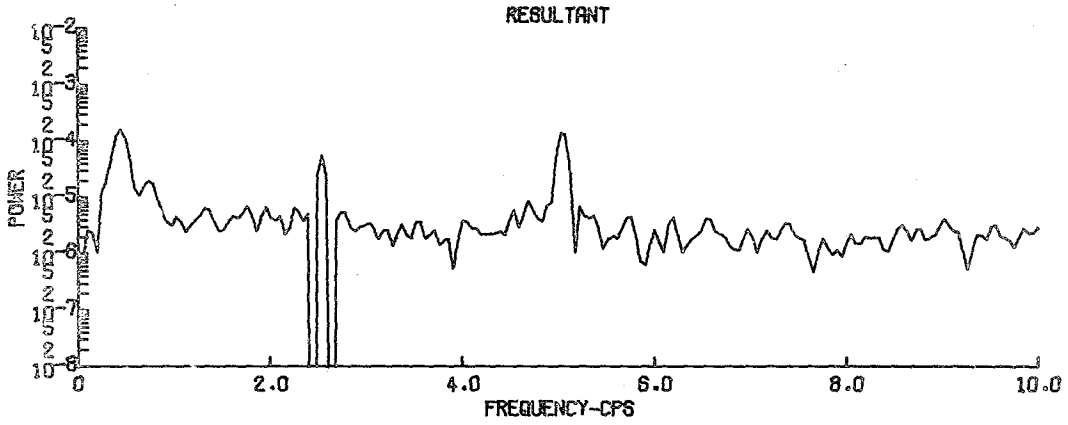

SATSOP 08 - STATION 2 1630 26 AUG 75
FOURIER POWER SPECTRUM
PORTABLE STATION
RESULTANT

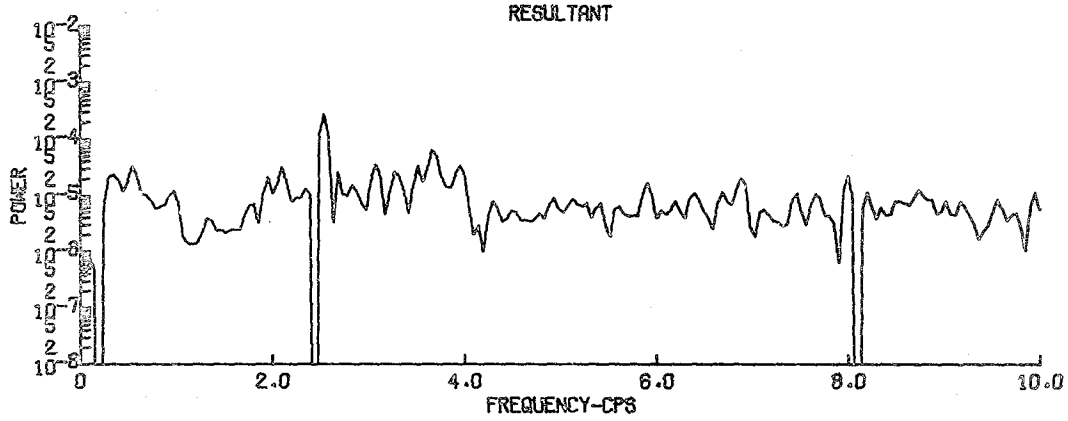

SATSOP 08 - STATION 2 1630 26 AUG 75
AMPLIFICATION
RESULTANT

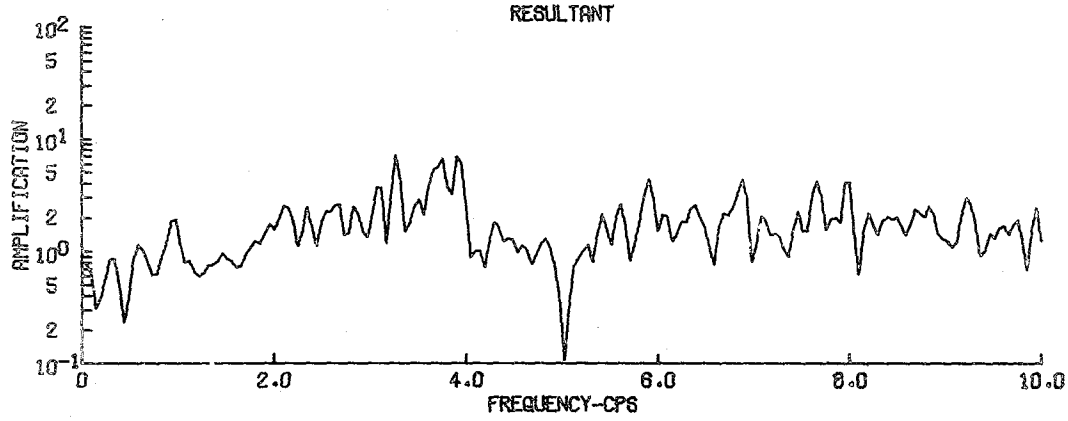

SATSOP 09 - STATION 2 1032 10 SEPT 75
FOURIER POWER SPECTRUM
BASE STATION
DIRECTION-NS

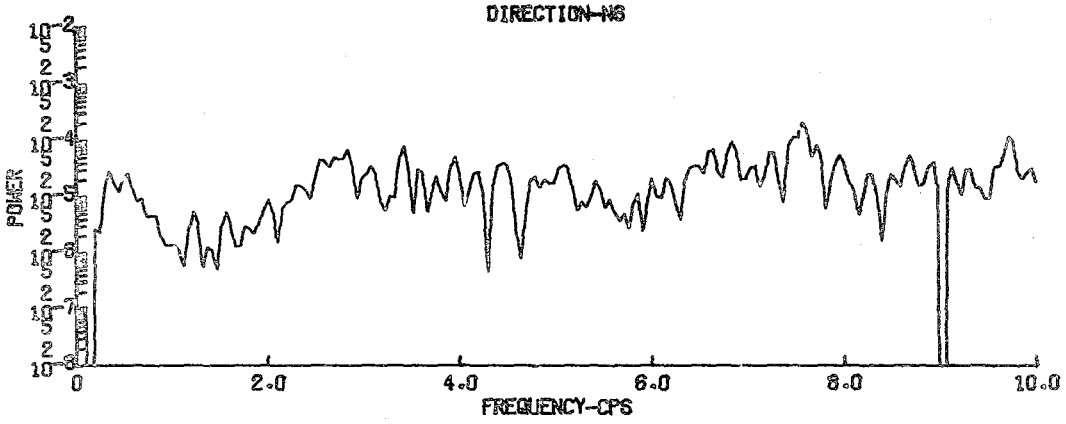

SATSOP 09 - STATION 2 1032 10 SEPT 75
FOURIER POWER SPECTRUM
BASE STATION
DIRECTION-EW

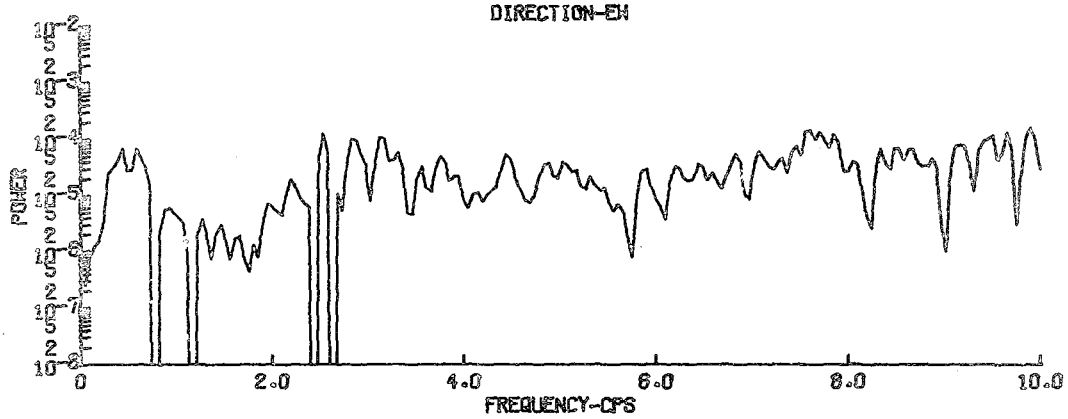

SATSOP 09 - STATION 2 1032 10 SEPT 75
FOURIER POWER SPECTRUM
BASE STATION
DIRECTION-VT

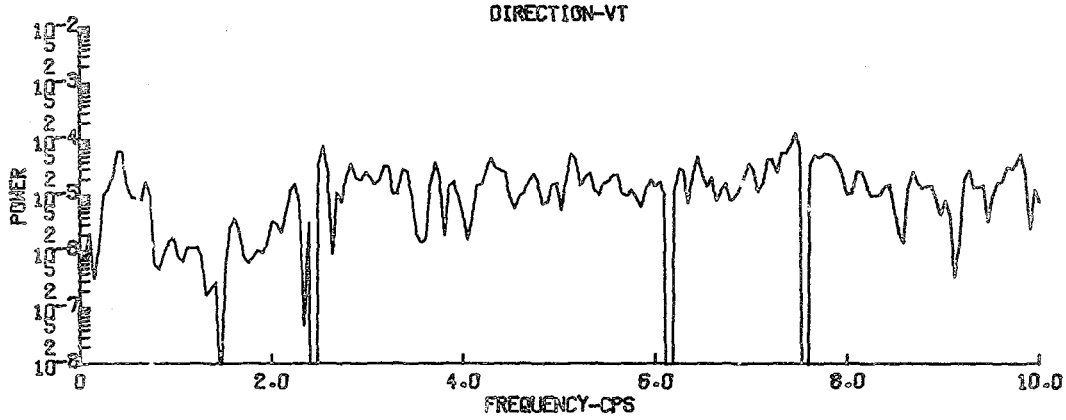

SATSOP 09 - STATION 2 1032 10 SEPT 75
FOURIER POWER SPECTRUM
PORTABLE STATION
DIRECTION-NS

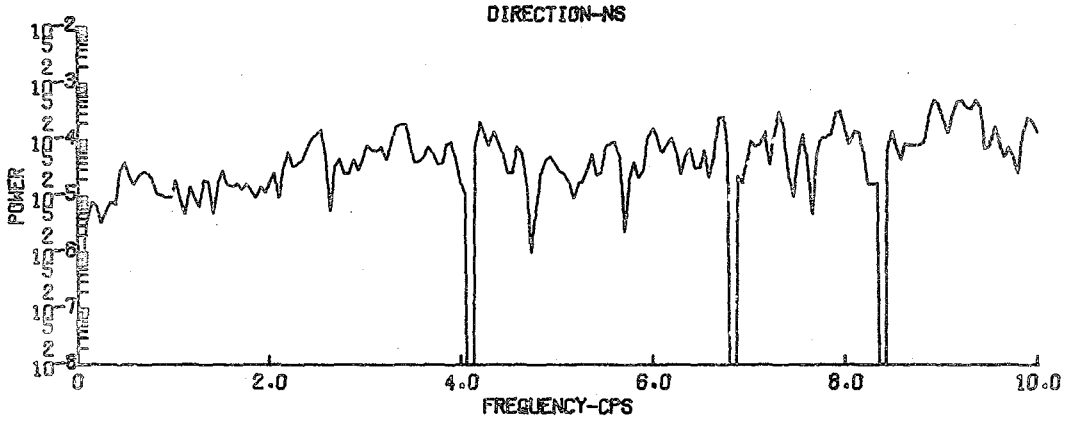

SATSOP 09 - STATION 2 1032 10 SEPT 75
FOURIER POWER SPECTRUM
PORTABLE STATION
DIRECTION-EW

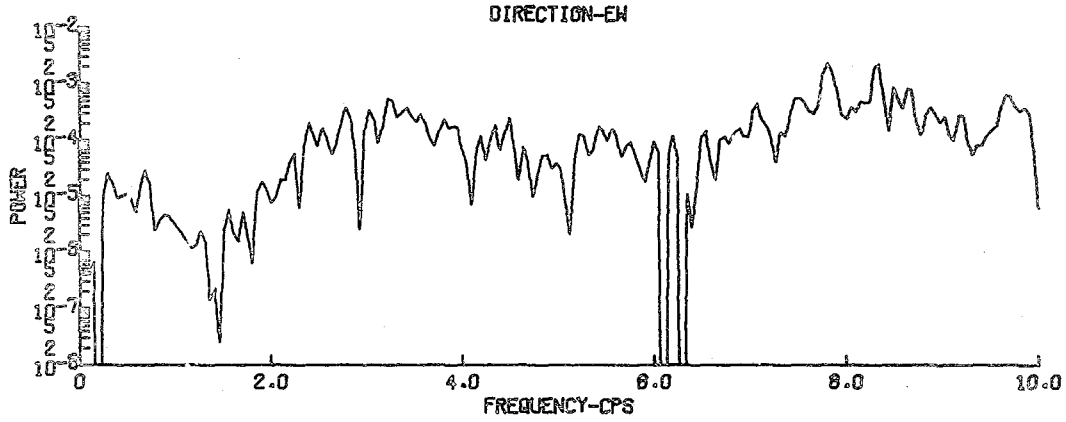

SATSOP 09 - STATION 2 1032 10 SEPT 75
FOURIER POWER SPECTRUM
PORTABLE STATION
DIRECTION-VT

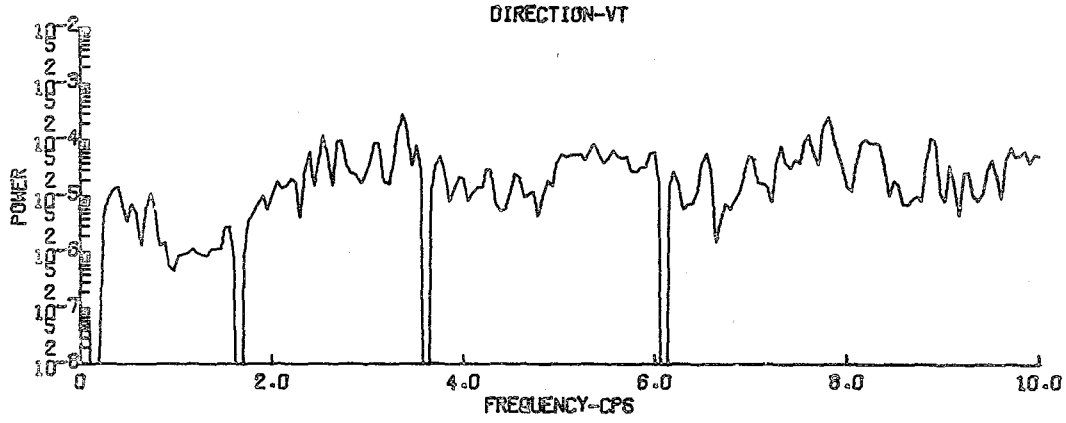

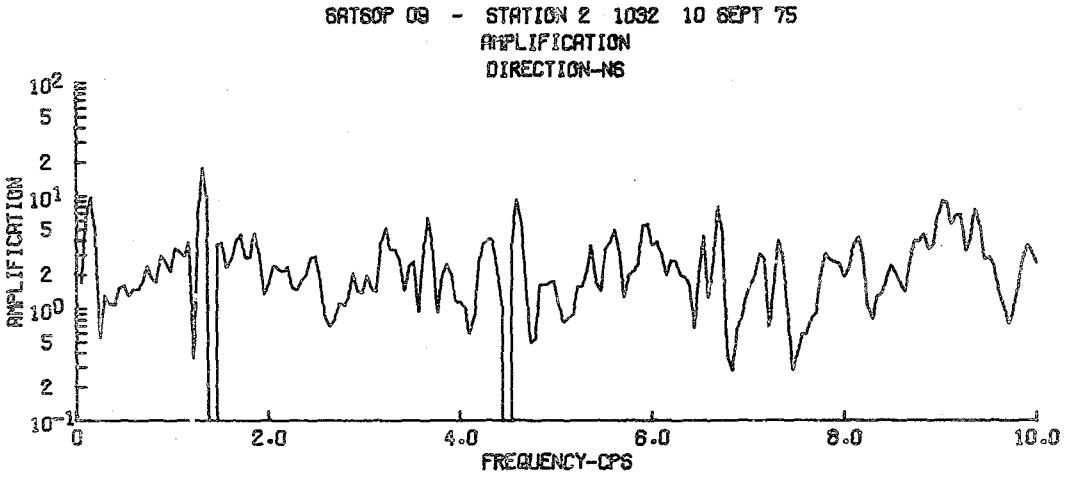
SATSOP 09 - STATION 2 1032 10 SEPT 75
AMPLIFICATION
DIRECTION-NS
AMPLIFICATION
FREQUENCY-CPS
0
2.0
4.0
6.0
8.0
10.0

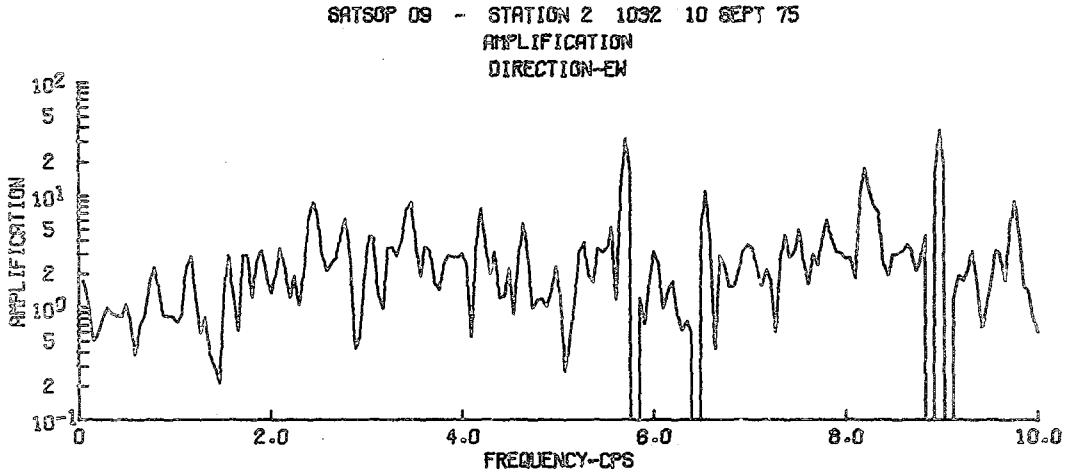
SATSOP 09 - STATION 2 1032 10 SEPT 75
AMPLIFICATION
DIRECTION-EW
AMPLIFICATION
FREQUENCY-CPS
0
2.0
4.0
6.0
8.0
10.0

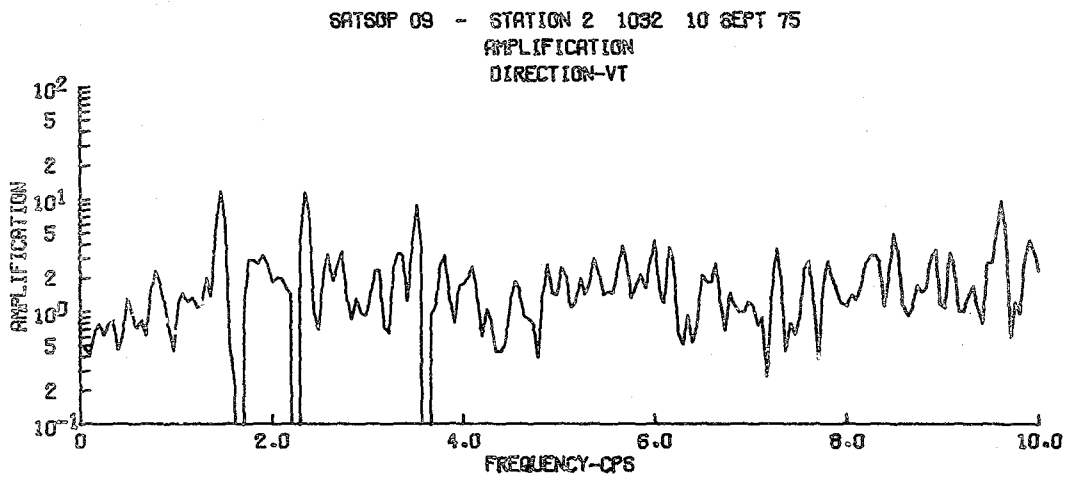
SATSOP 09 - STATION 2 1032 10 SEPT 75
AMPLIFICATION
DIRECTION-VT
AMPLIFICATION
FREQUENCY-CPS
0
2.0
4.0
6.0
8.0
10.0

SATSOP 09 - STATION 2 1032 10 SEPT 75
FOURIER POWER SPECTRUM
BASE STATION
RESULTANT

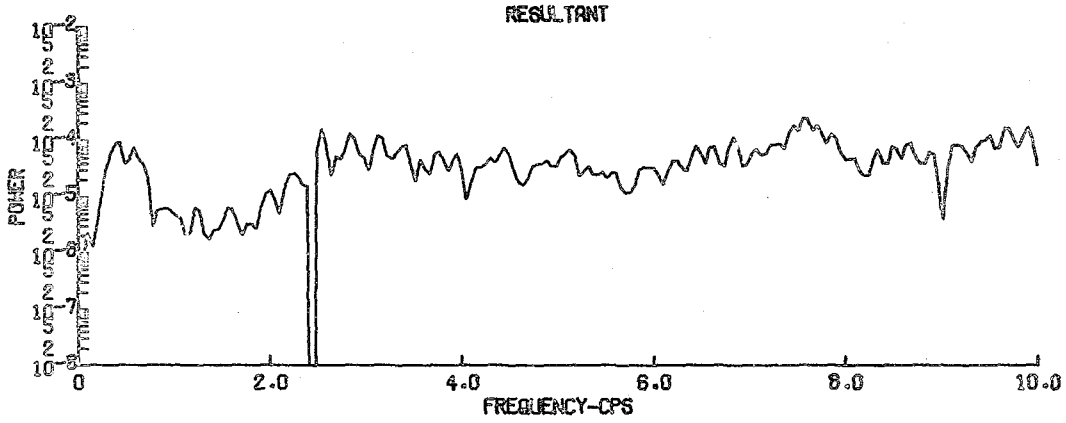

SATSOP 09 - STATION 2 1032 10 SEPT 75
FOURIER POWER SPECTRUM
PORTABLE STATION
RESULTANT

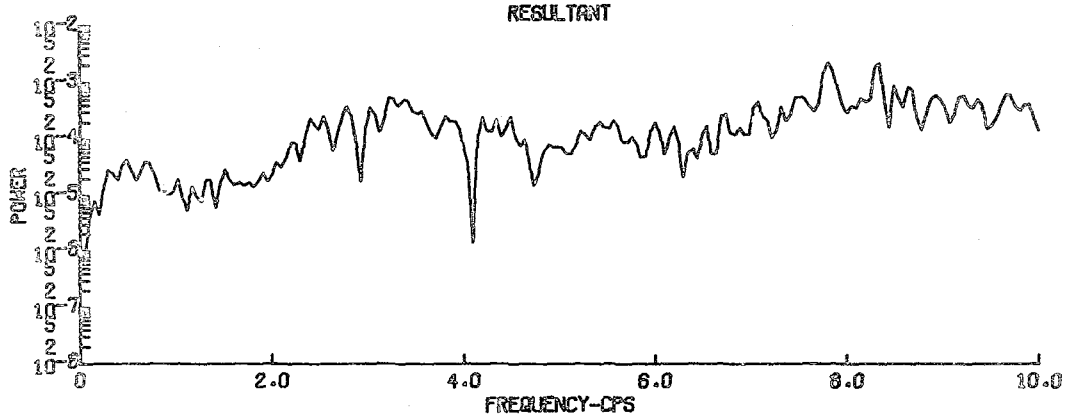

SATSOP 09 - STATION 2 1032 10 SEPT 75
AMPLIFICATION
RESULTANT

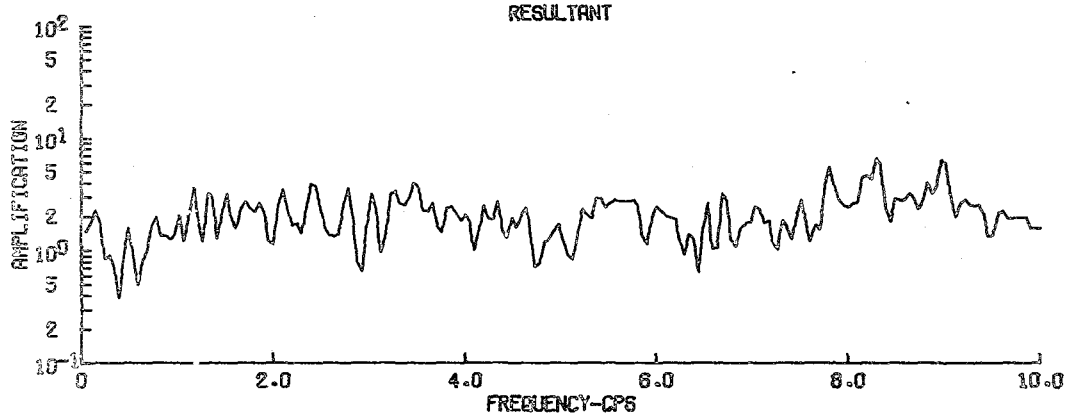

SATSOP 10 - STATION 2 1330 10 SEPT 75
FOURIER POWER SPECTRUM
BASE STATION
DIRECTION-NS

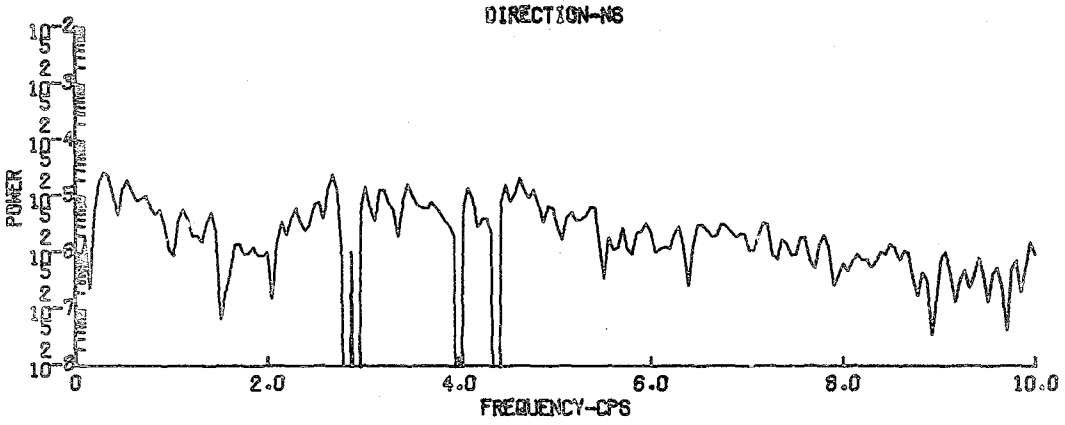

SATSOP 10 - STATION 2 1330 10 SEPT 75
FOURIER POWER SPECTRUM
BASE STATION
DIRECTION-EW

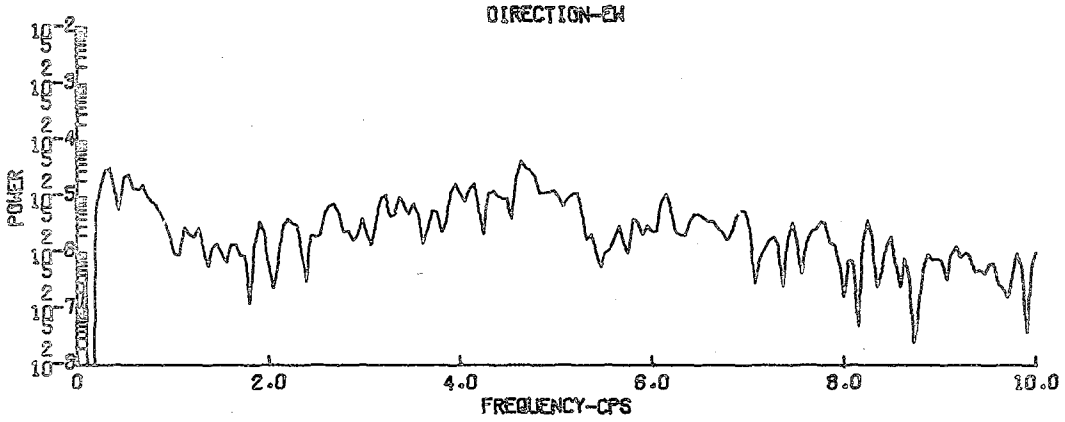

SATSOP 10 - STATION 2 1330 10 SEPT 75
FOURIER POWER SPECTRUM
BASE STATION
DIRECTION-VT

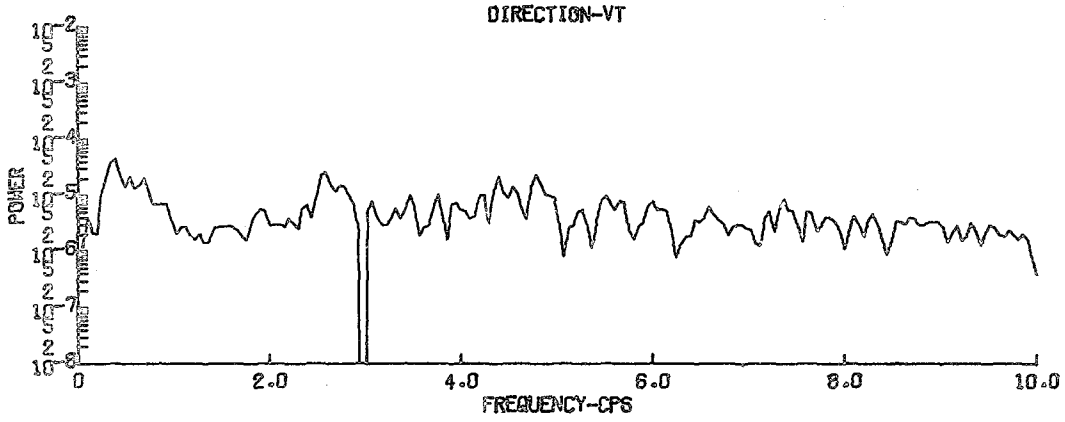

SATSOP 10 - STATION 2 1330 10 SEPT 75
FOURIER POWER SPECTRUM
PORTABLE STATION
DIRECTION-NS

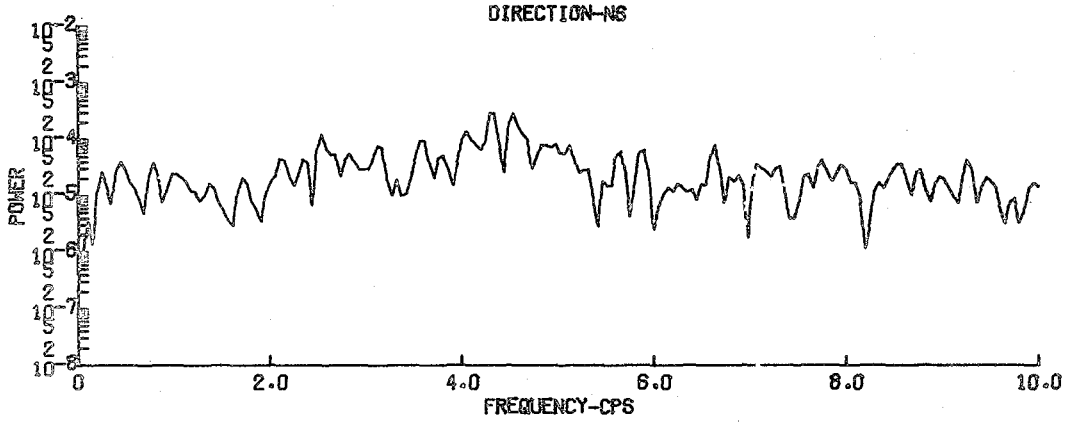

SATSOP 10 - STATION 2 1330 10 SEPT 75
FOURIER POWER SPECTRUM
PORTABLE STATION
DIRECTION-EW

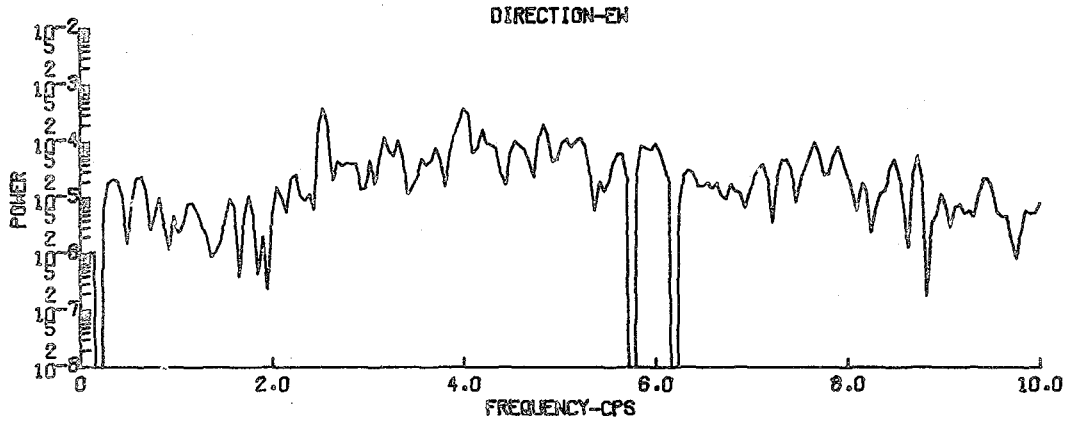

SATSOP 10 - STATION 2 1330 10 SEPT 75
FOURIER POWER SPECTRUM
PORTABLE STATION
DIRECTION-VT

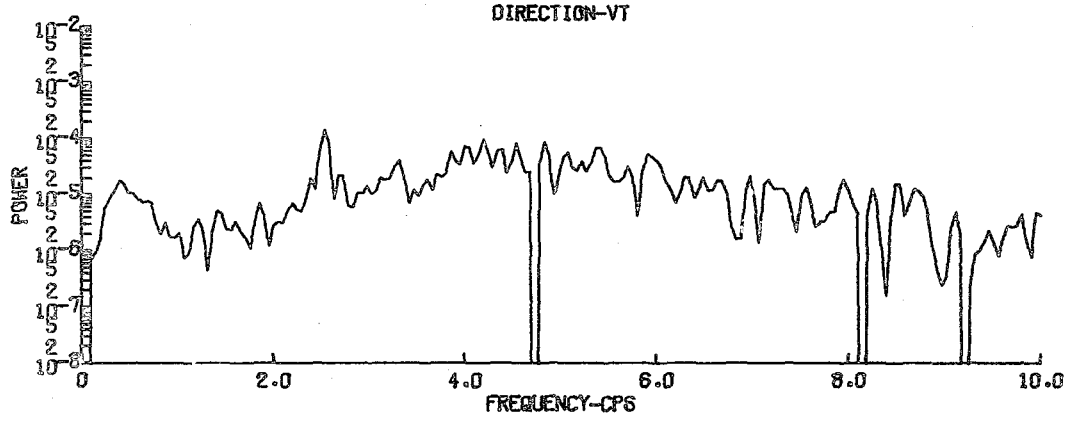

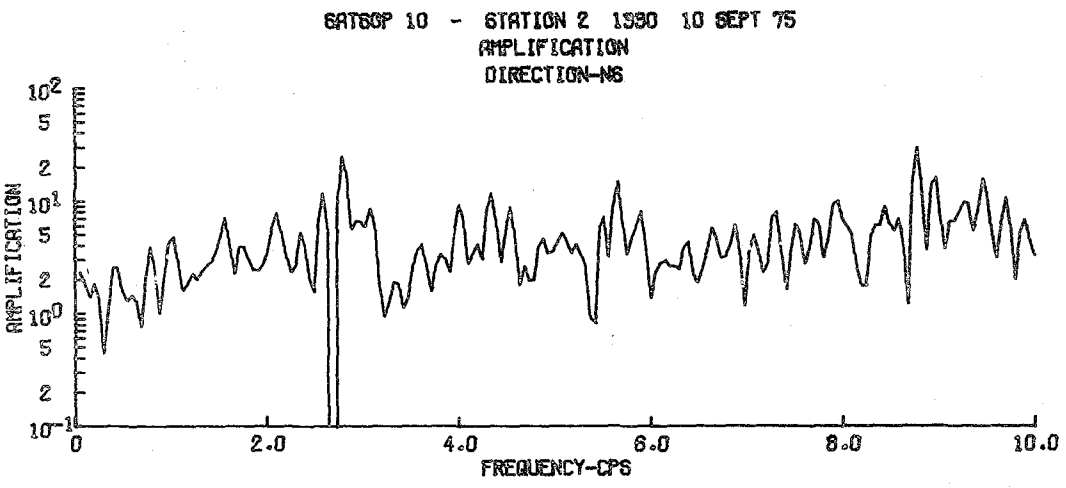
SATSOP 10 - STATION 2 1330 10 SEPT 75
AMPLIFICATION
DIRECTION-NS
AMPLIFICATION
FREQUENCY-CPS
0
2.0
4.0
6.0
8.0
10.0

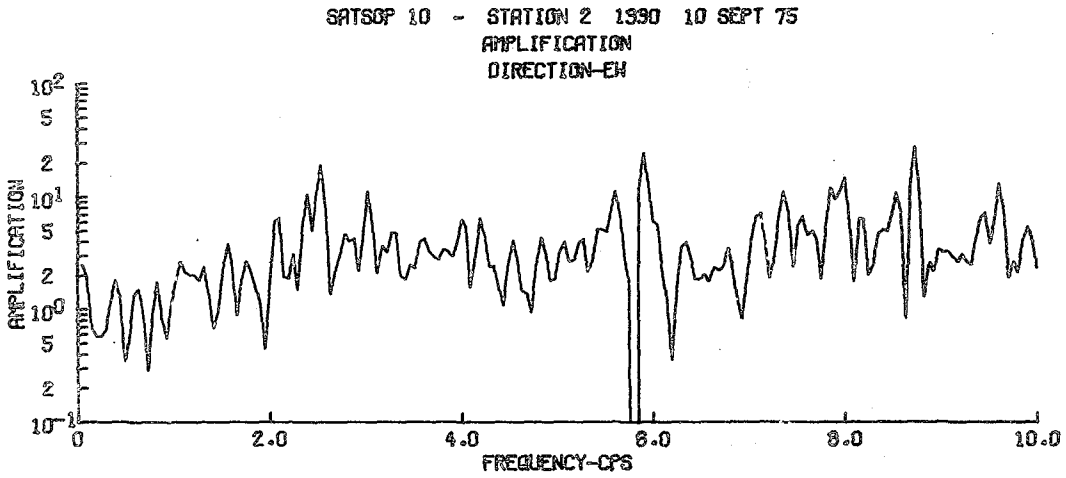
SATSOP 10 - STATION 2 1330 10 SEPT 75
AMPLIFICATION
DIRECTION-EW
AMPLIFICATION
FREQUENCY-CPS
0
2.0
4.0
6.0
8.0
10.0

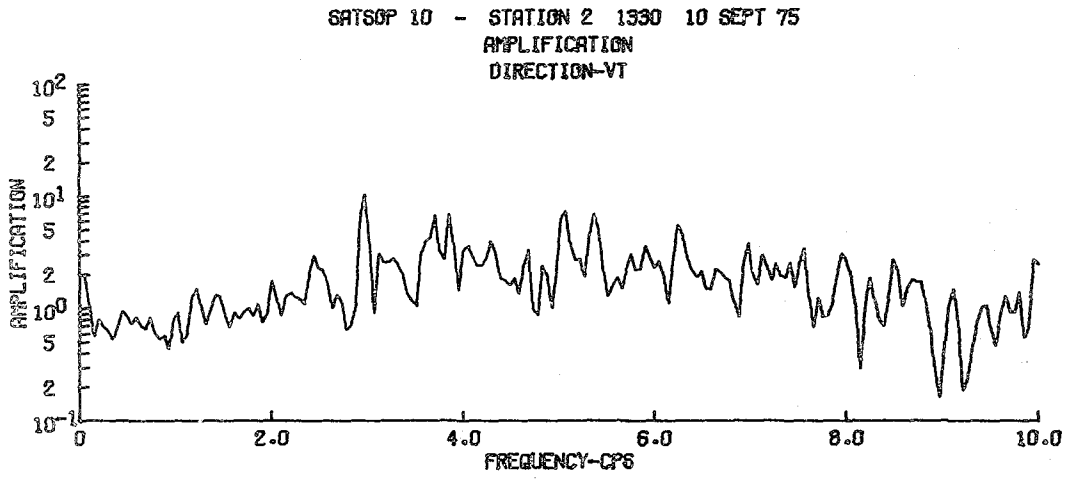
SATSOP 10 - STATION 2 1330 10 SEPT 75
AMPLIFICATION
DIRECTION-VT
AMPLIFICATION
FREQUENCY-CPS
0
2.0
4.0
6.0
8.0
10.0

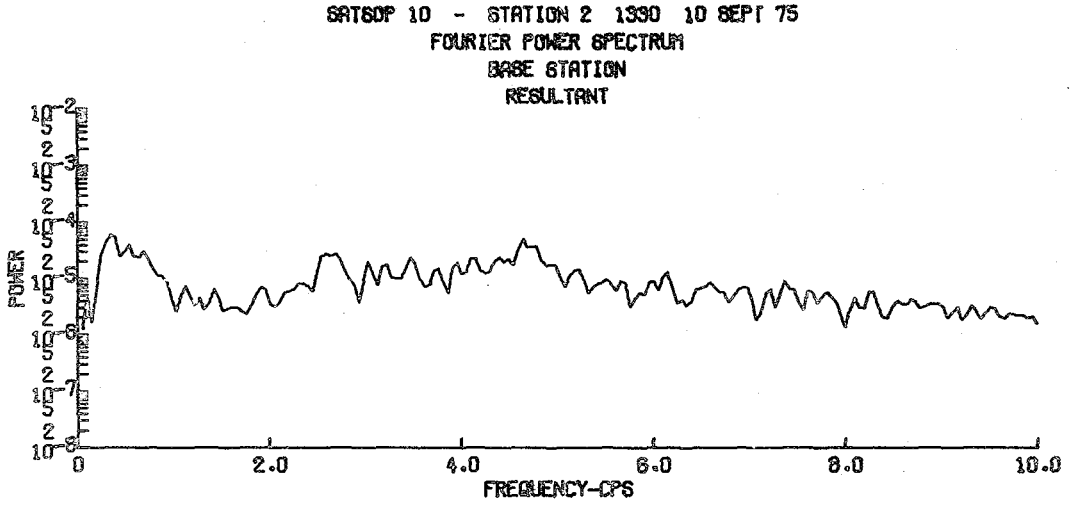
SATSOP 10 - STATION 2 1330 10 SEPT 75
FOURIER POWER SPECTRUM
BASE STATION
RESULTANT
POWER
FREQUENCY-CPS
0
2.0
4.0
6.0
8.0
10.0

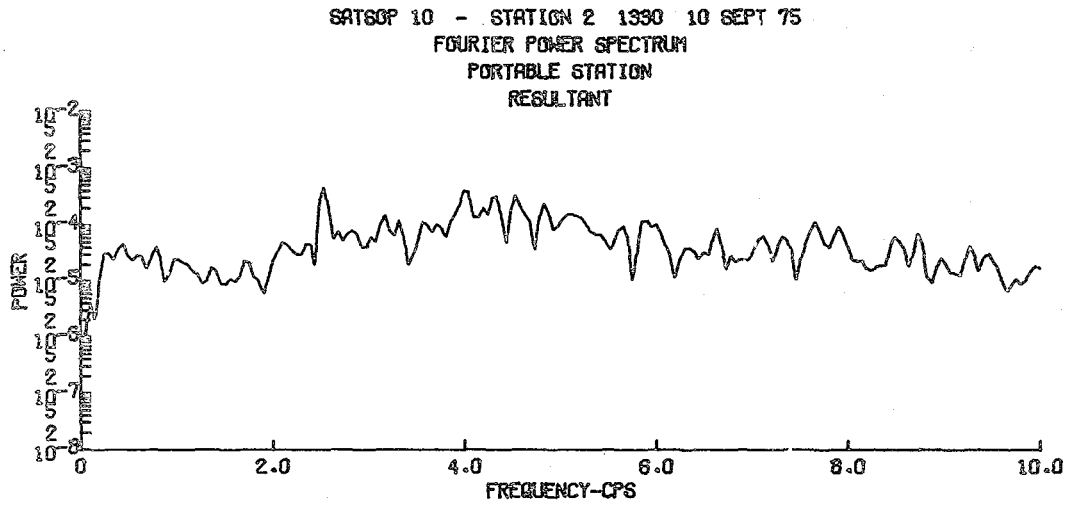
SATSOP 10 - STATION 2 1330 10 SEPT 75
FOURIER POWER SPECTRUM
PORTABLE STATION
RESULTANT
POWER
FREQUENCY-CPS
0
2.0
4.0
6.0
8.0
10.0

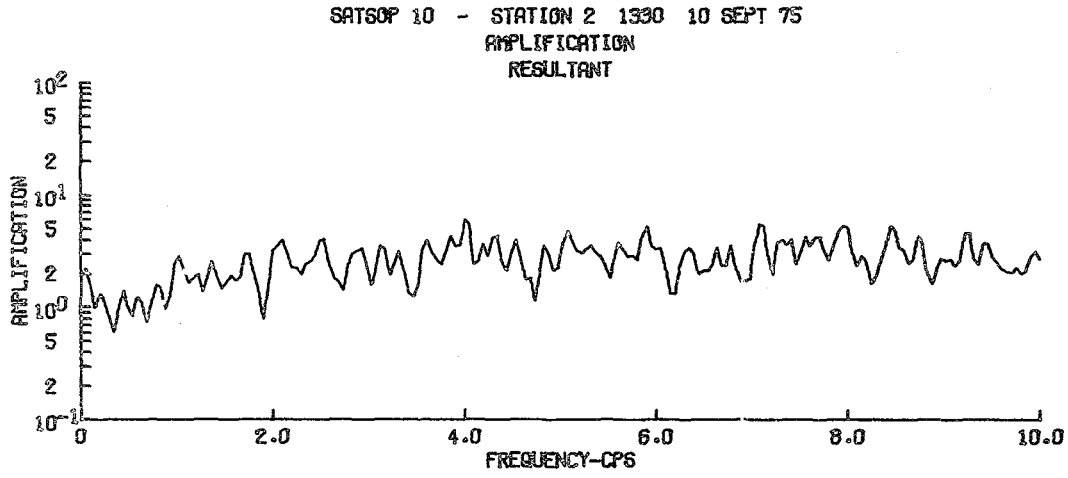
SATSOP 10 - STATION 2 1330 10 SEPT 75
AMPLIFICATION
RESULTANT
AMPLIFICATION
FREQUENCY-CPS
0
2.0
4.0
6.0
8.0
10.0

SATSOP 11 - STATION 3 1205 21 AUG 75
FOURIER POWER SPECTRUM
BASE STATION
DIRECTION-NS

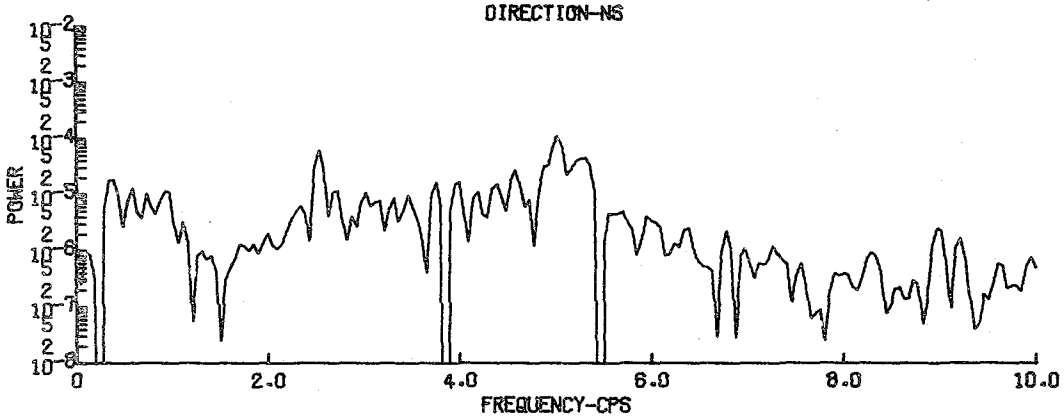

SATSOP 11 - STATION 3 1205 21 AUG 75
FOURIER POWER SPECTRUM
BASE STATION
DIRECTION-EW

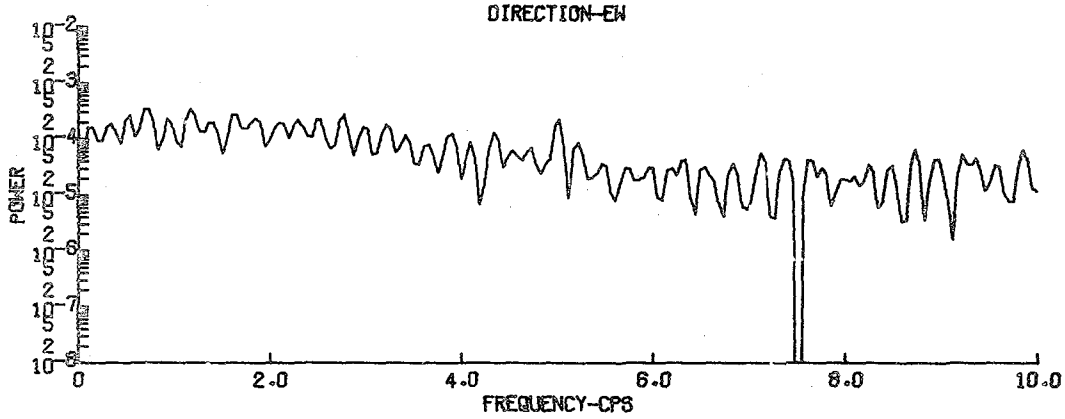

SATSOP 11 - STATION 3 1205 21 AUG 75
FOURIER POWER SPECTRUM
BASE STATION
DIRECTION-VT

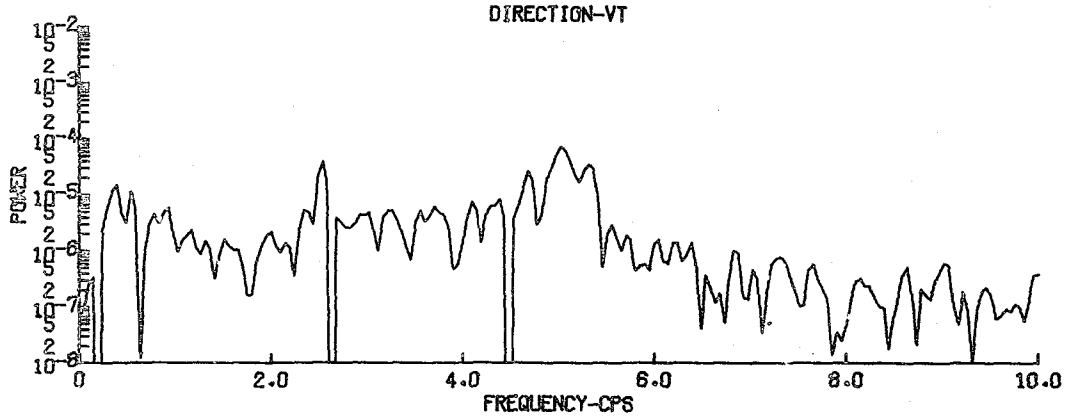

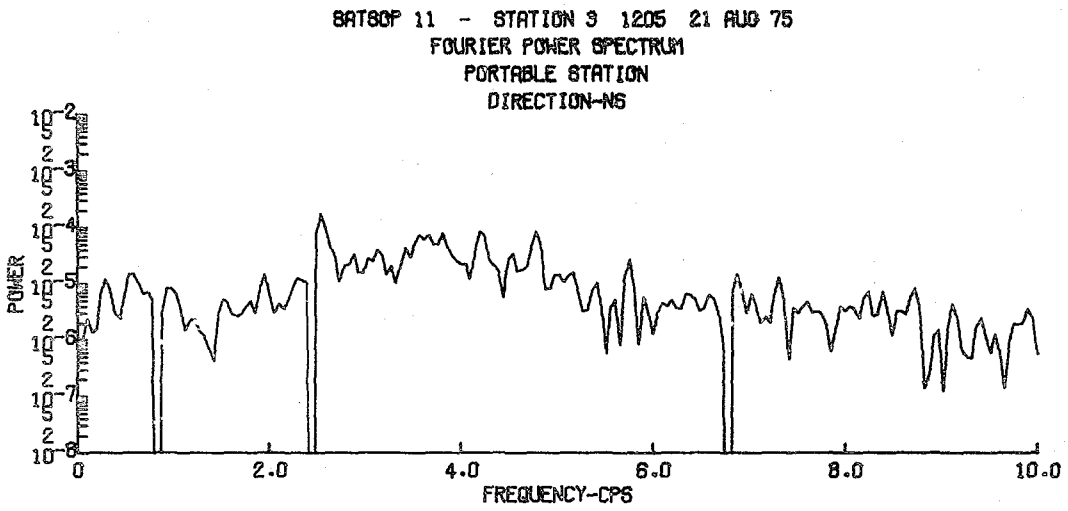
SATSOP 11 - STATION 3 1205 21 AUG 75
FOURIER POWER SPECTRUM
PORTABLE STATION
DIRECTION-NS
POWER
FREQUENCY-CPS
0
2.0
4.0
6.0
8.0
10.0

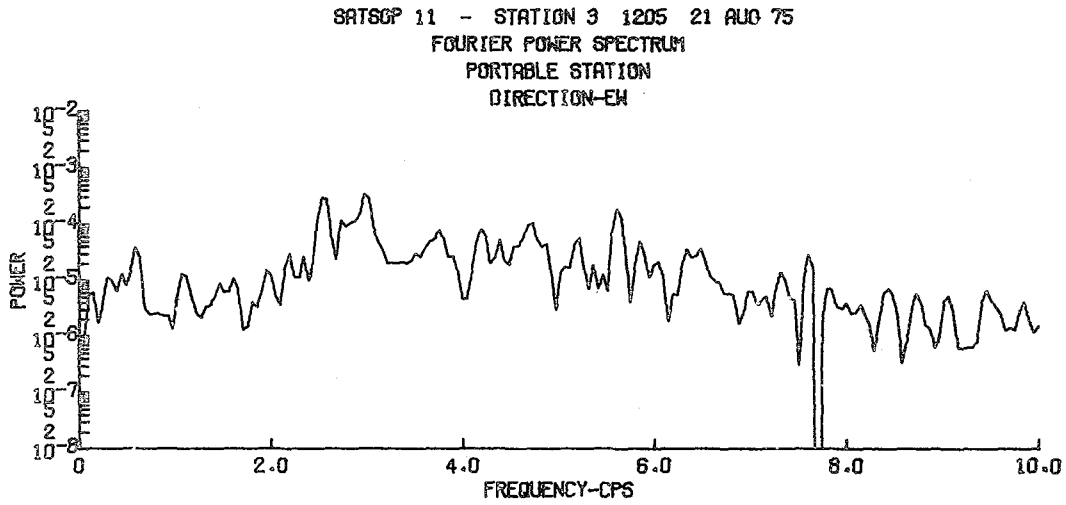
SATSOP 11 - STATION 3 1205 21 AUG 75
FOURIER POWER SPECTRUM
PORTABLE STATION
DIRECTION-EW
POWER
FREQUENCY-CPS
0
2.0
4.0
6.0
8.0
10.0

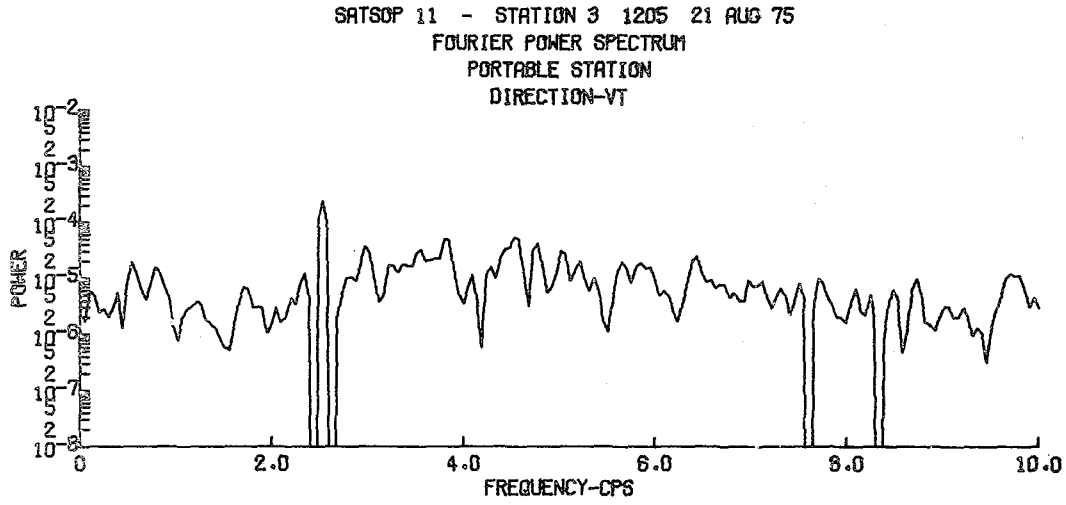
SATSOP 11 - STATION 3 1205 21 AUG 75
FOURIER POWER SPECTRUM
PORTABLE STATION
DIRECTION-VT
POWER
FREQUENCY-CPS
0
2.0
4.0
6.0
8.0
10.0

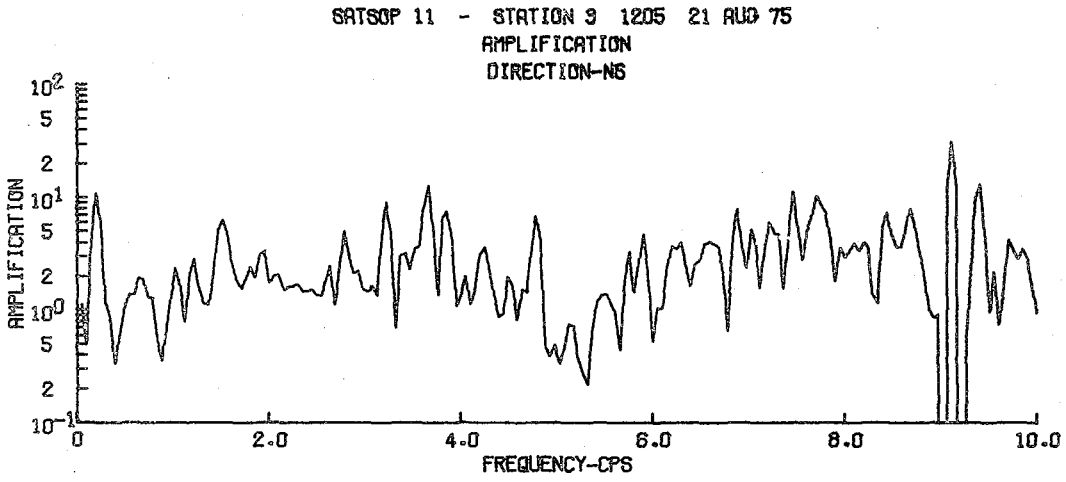
SATSOP 11 - STATION 3 1205 21 AUG 75
AMPLIFICATION
DIRECTION-NS
AMPLIFICATION
FREQUENCY-CPS

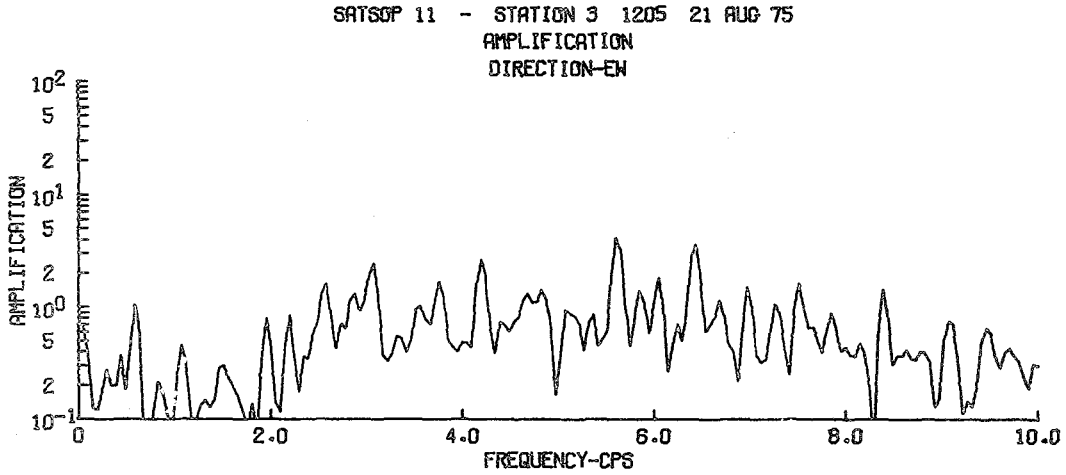
SATSOP 11 - STATION 3 1205 21 AUG 75
AMPLIFICATION
DIRECTION-EW
AMPLIFICATION
FREQUENCY-CPS

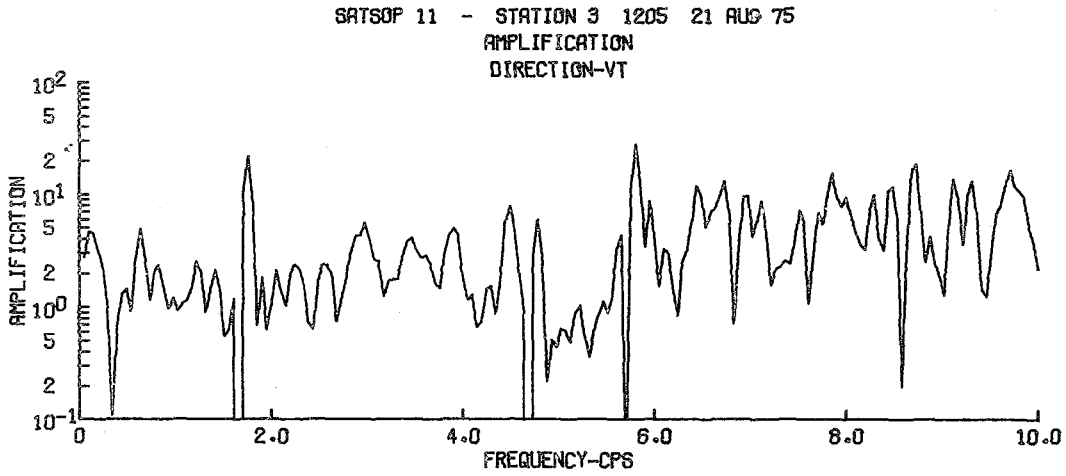
SATSOP 11 - STATION 3 1205 21 AUG 75
AMPLIFICATION
DIRECTION-VT
AMPLIFICATION
FREQUENCY-CPS

SATSOP 11 - STATION 3 1205 21 AUG 75
FOURIER POWER SPECTRUM
BASE STATION
RESULTANT

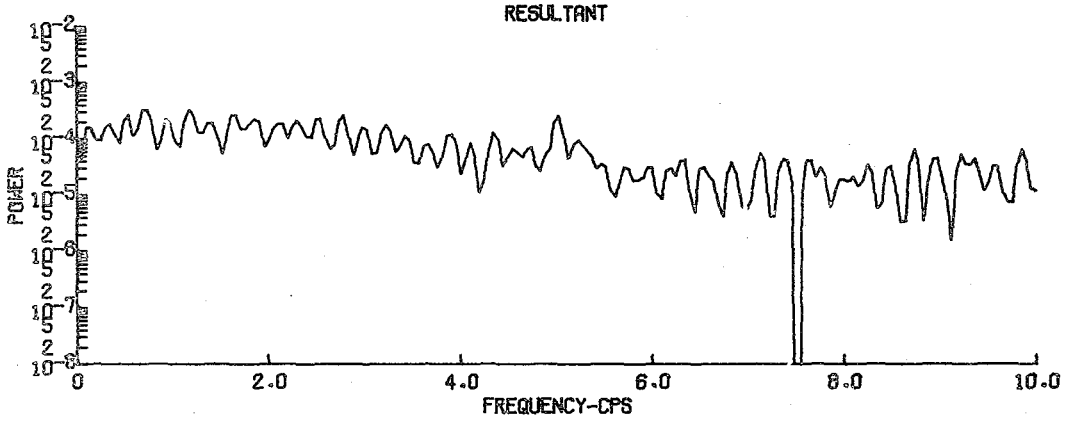

SATSOP 11 - STATION 3 1205 21 AUG 75
FOURIER POWER SPECTRUM
PORTABLE STATION
RESULTANT

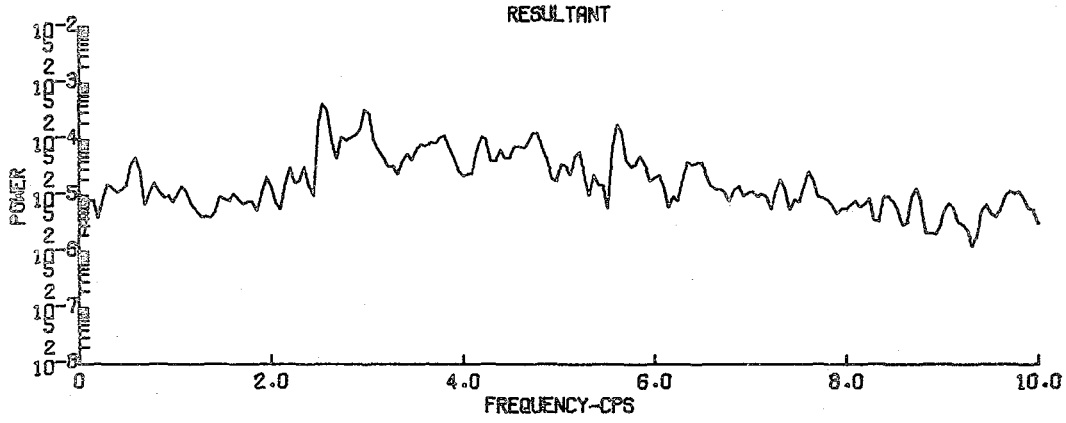

SATSOP 11 - STATION 3 1205 21 AUG 75
AMPLIFICATION
RESULTANT

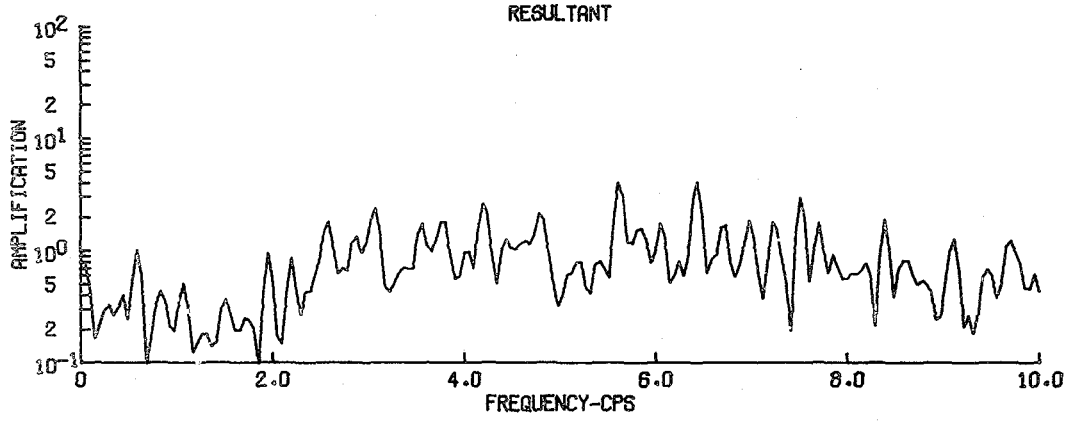

SATSOP 12 - STATION 3 1630 21 AUG 75
FOURIER POWER SPECTRUM
BASE STATION
DIRECTION-NS

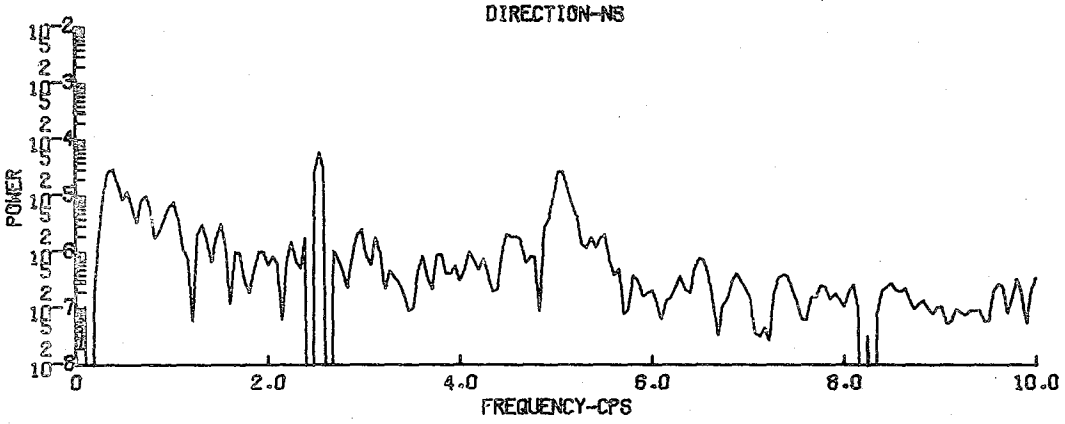

SATSOP 12 - STATION 3 1630 21 AUG 75
FOURIER POWER SPECTRUM
BASE STATION
DIRECTION-EW

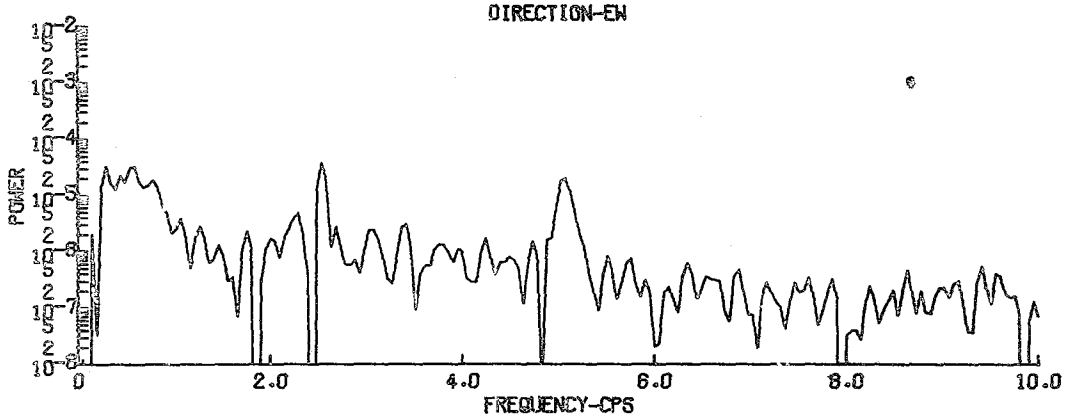

SATSOP 12 - STATION 3 1630 21 AUG 75
FOURIER POWER SPECTRUM
BASE STATION
DIRECTION-VT

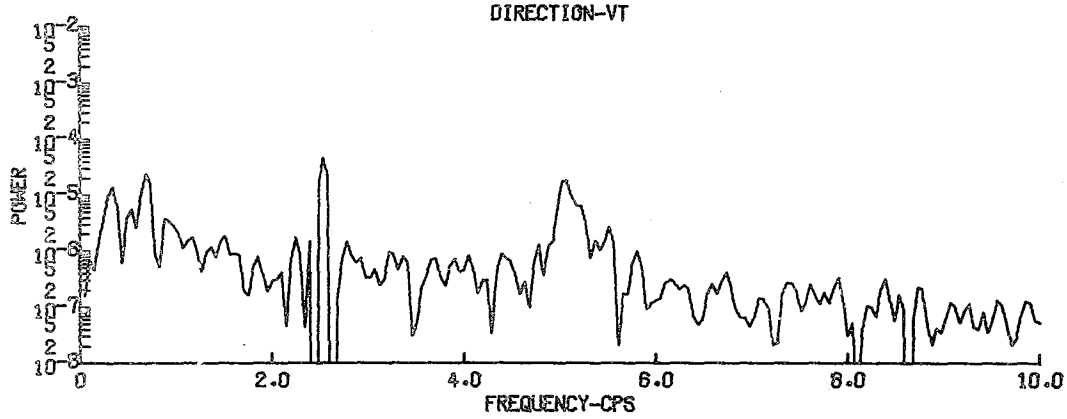

SATSOP 12 - STATION 3 1630 21 AUG 75
FOURIER POWER SPECTRUM
PORTABLE STATION
DIRECTION-NS

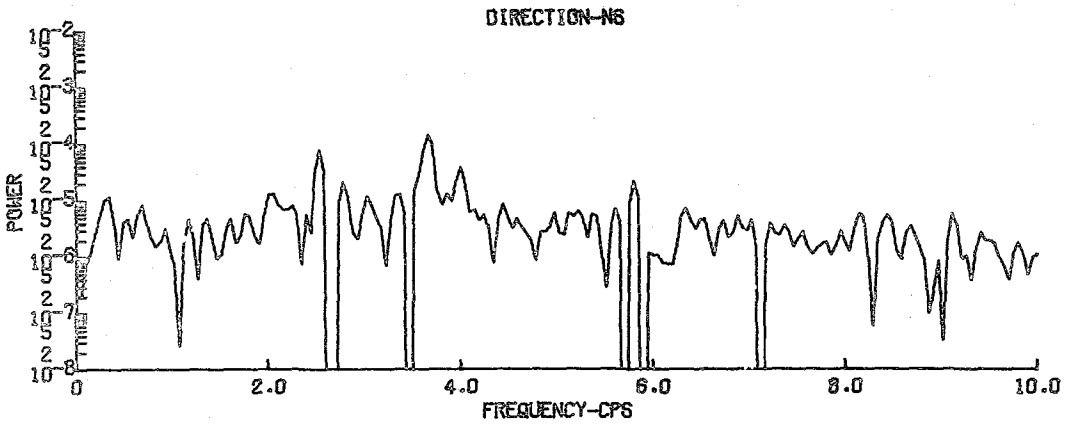

SATSOP 12 - STATION 3 1630 21 AUG 75
FOURIER POWER SPECTRUM
PORTABLE STATION
DIRECTION-EW

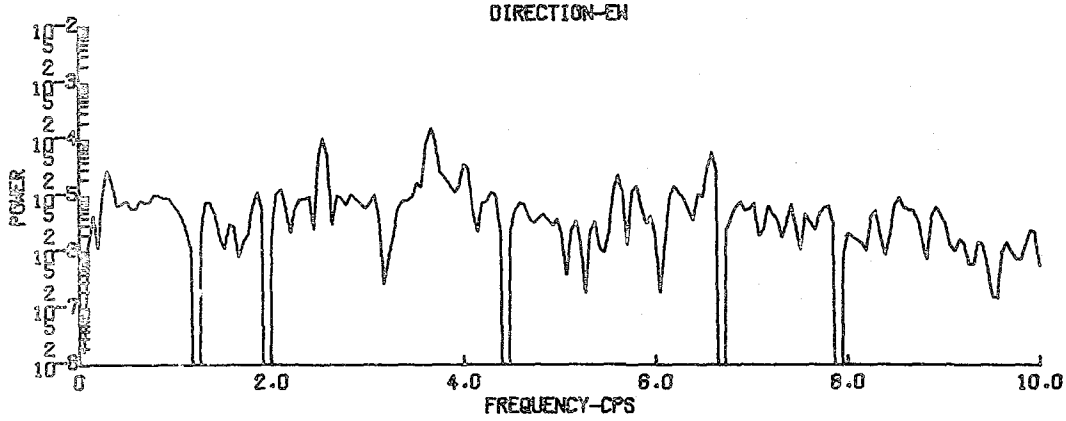

SATSOP 12 - STATION 3 1630 21 AUG 75
FOURIER POWER SPECTRUM
PORTABLE STATION
DIRECTION-VT

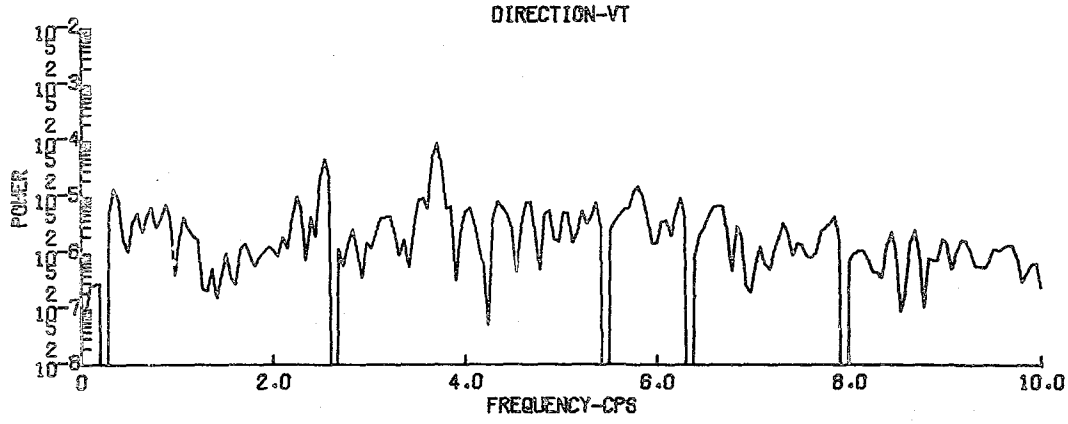

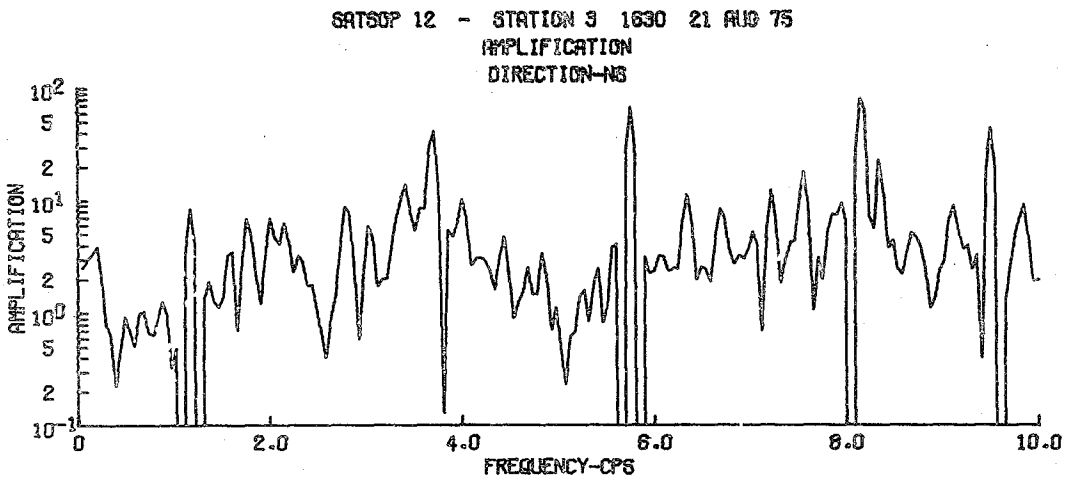
SATSOP 12 - STATION 3 1630 21 AUG 75
AMPLIFICATION
DIRECTION-NS
AMPLIFICATION
FREQUENCY-CPS

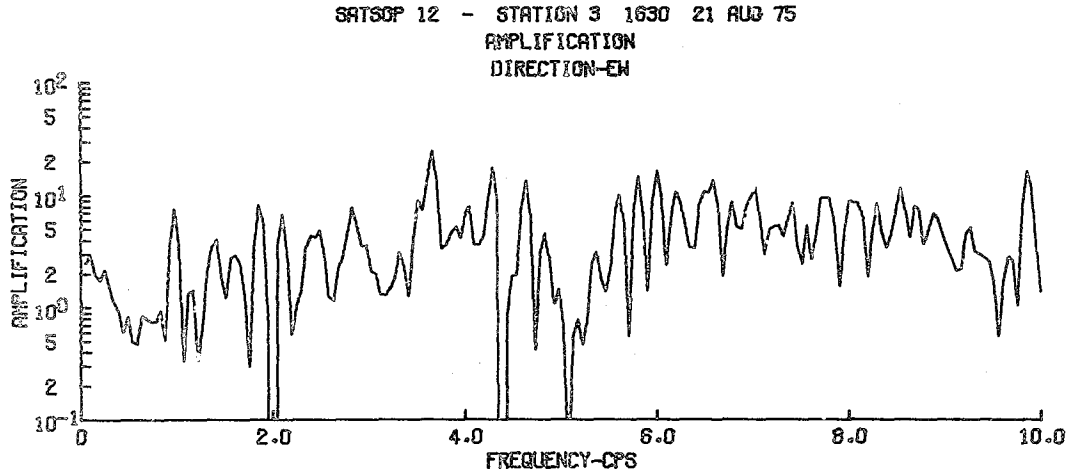
SATSOP 12 - STATION 3 1630 21 AUG 75
AMPLIFICATION
DIRECTION-EW
AMPLIFICATION
FREQUENCY-CPS

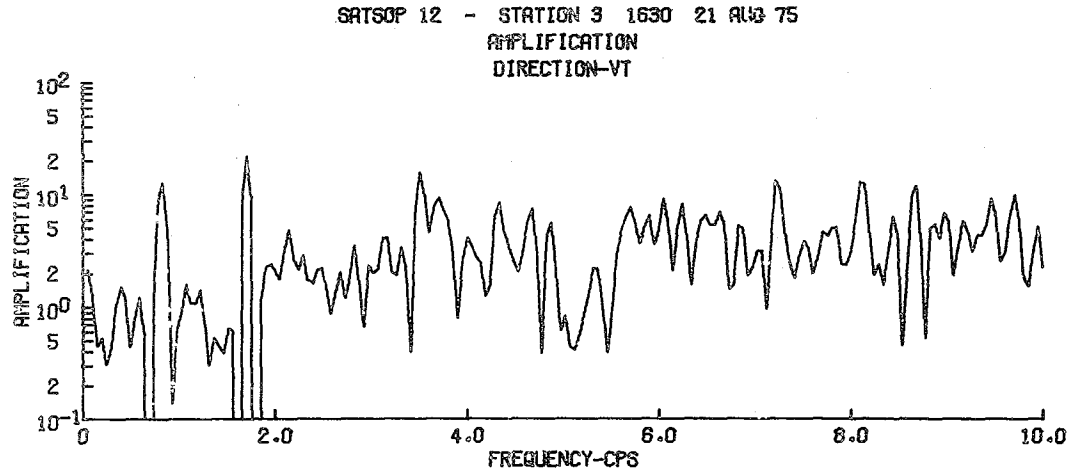
SATSOP 12 - STATION 3 1630 21 AUG 75
AMPLIFICATION
DIRECTION-VT
AMPLIFICATION
FREQUENCY-CPS

SATSOP 12 - STATION 3 1630 21 AUG 75
FOURIER POWER SPECTRUM
BASE STATION
RESULTANT

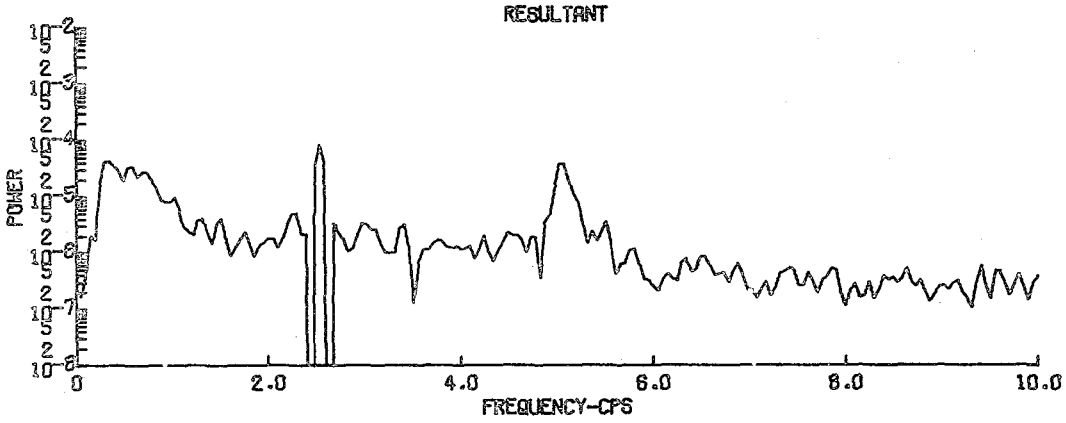

SATSOP 12 - STATION 3 1630 21 AUG 75
FOURIER POWER SPECTRUM
PORTABLE STATION
RESULTANT

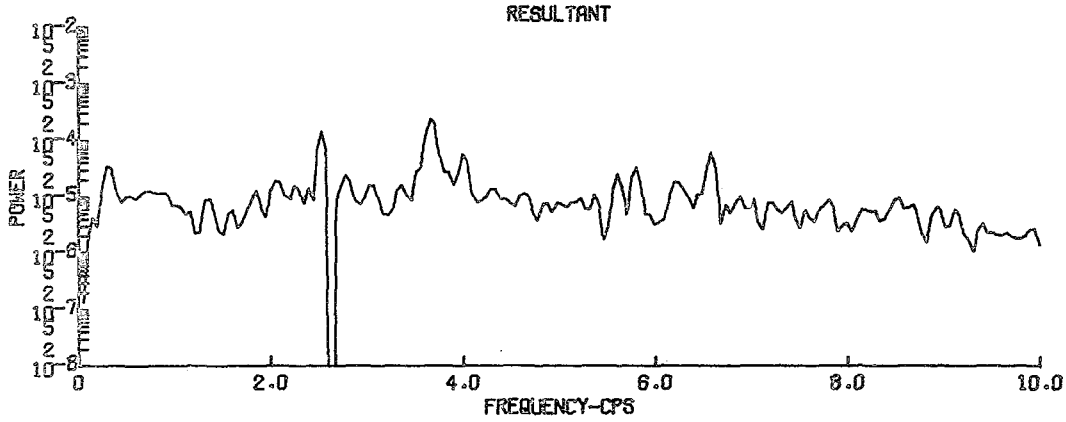

SATSOP 12 - STATION 3 1630 21 AUG 75
AMPLIFICATION
RESULTANT

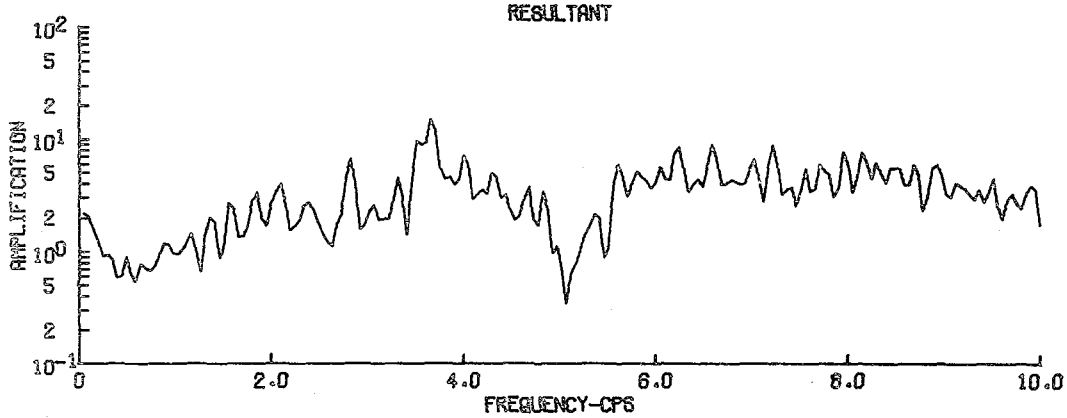

SATSOP 13 - STATION 3 1016 11 SEPT 75
FOURIER POWER SPECTRUM
BASE STATION
DIRECTION-NS

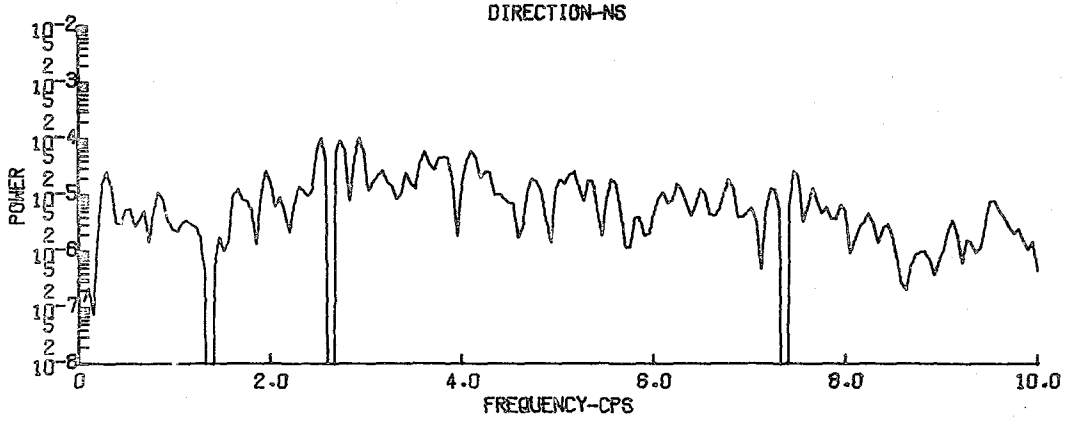

SATSOP 13 - STATION 3 1016 11 SEPT 75
FOURIER POWER SPECTRUM
BASE STATION
DIRECTION-EW

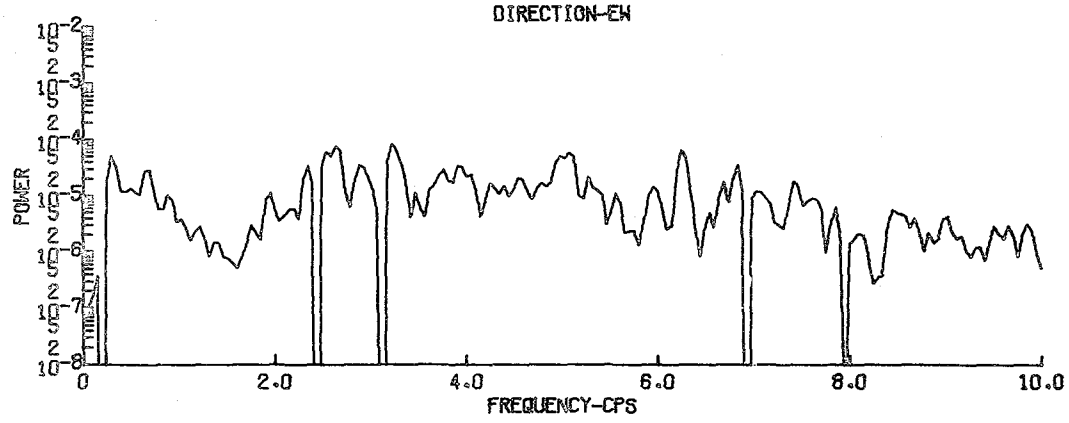

SATSOP 13 - STATION 3 1016 11 SEPT 75
FOURIER POWER SPECTRUM
BASE STATION
DIRECTION-VT

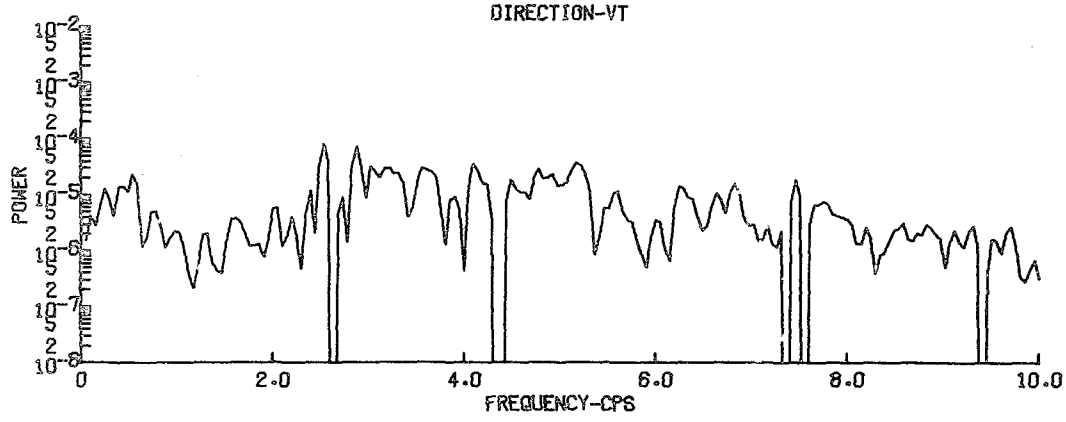

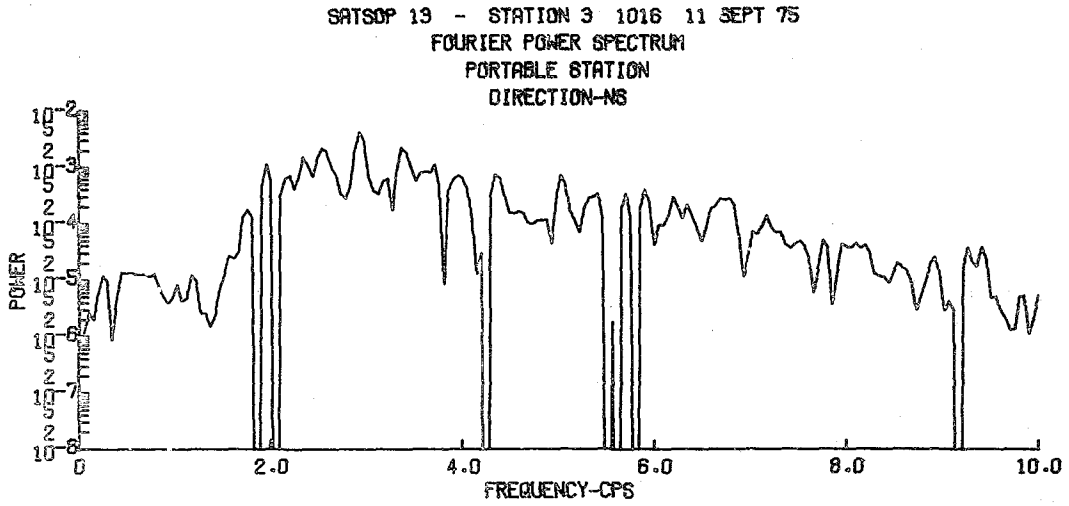
SATSOP 13 - STATION 3 1016 11 SEPT 75
FOURIER POWER SPECTRUM
PORTABLE STATION
DIRECTION-NS
POWER
0
2.0
4.0
6.0
8.0
10.0
FREQUENCY-CPS

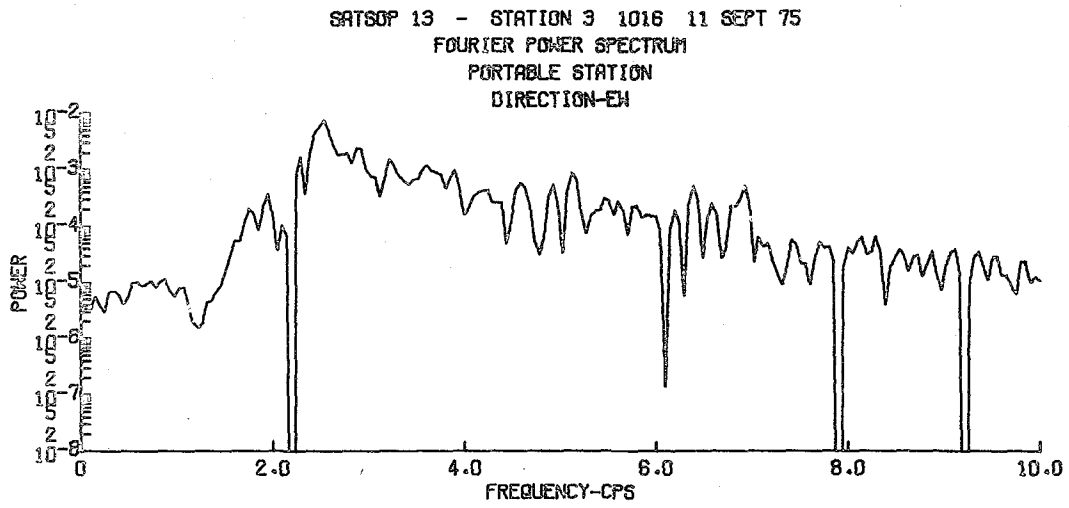
SATSOP 13 - STATION 3 1016 11 SEPT 75
FOURIER POWER SPECTRUM
PORTABLE STATION
DIRECTION-EW
POWER
0
2.0
4.0
6.0
8.0
10.0
FREQUENCY-CPS

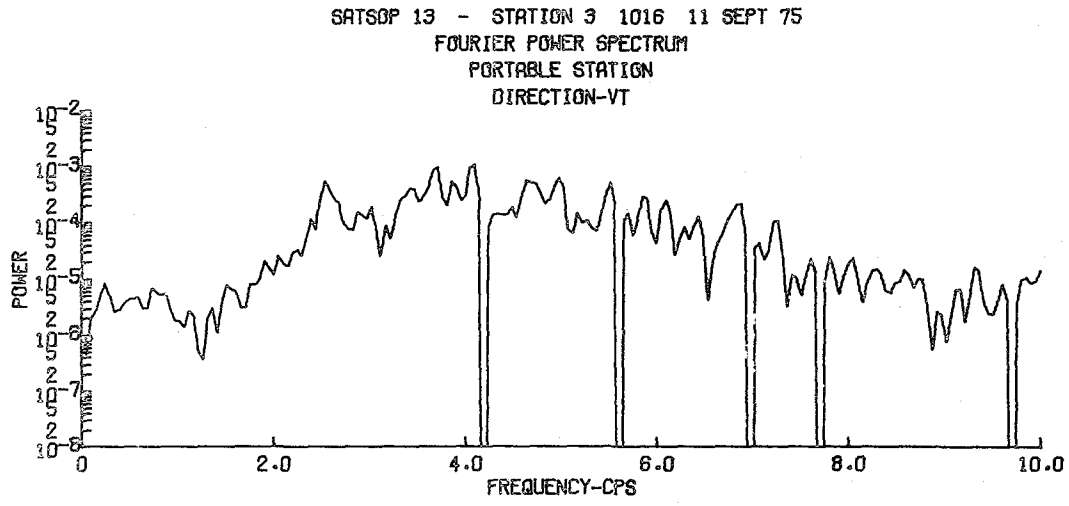
SATSOP 13 - STATION 3 1016 11 SEPT 75
FOURIER POWER SPECTRUM
PORTABLE STATION
DIRECTION-VT
POWER
0
2.0
4.0
6.0
8.0
10.0
FREQUENCY-CPS

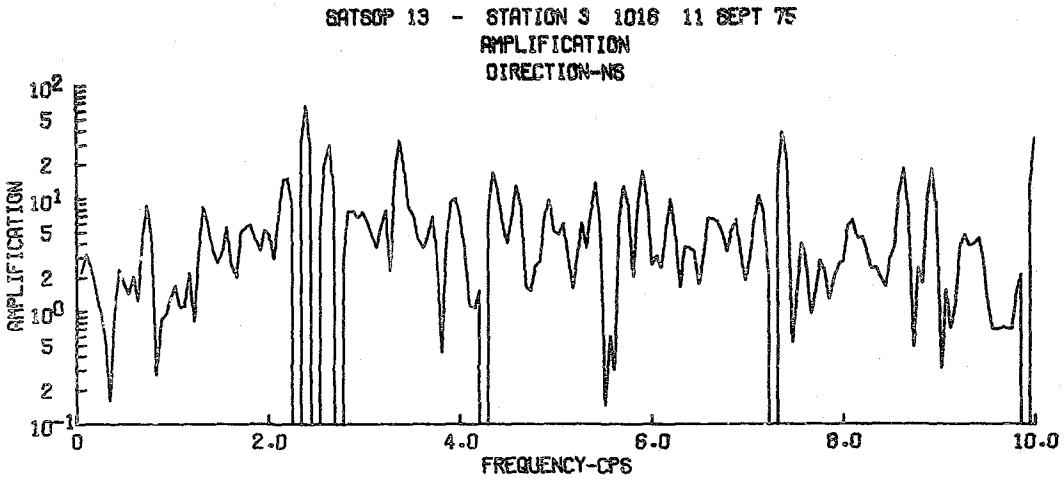
SATSOP 13 - STATION 3 1016 11 SEPT 75
AMPLIFICATION
DIRECTION-NS
AMPLIFICATION
FREQUENCY-CPS

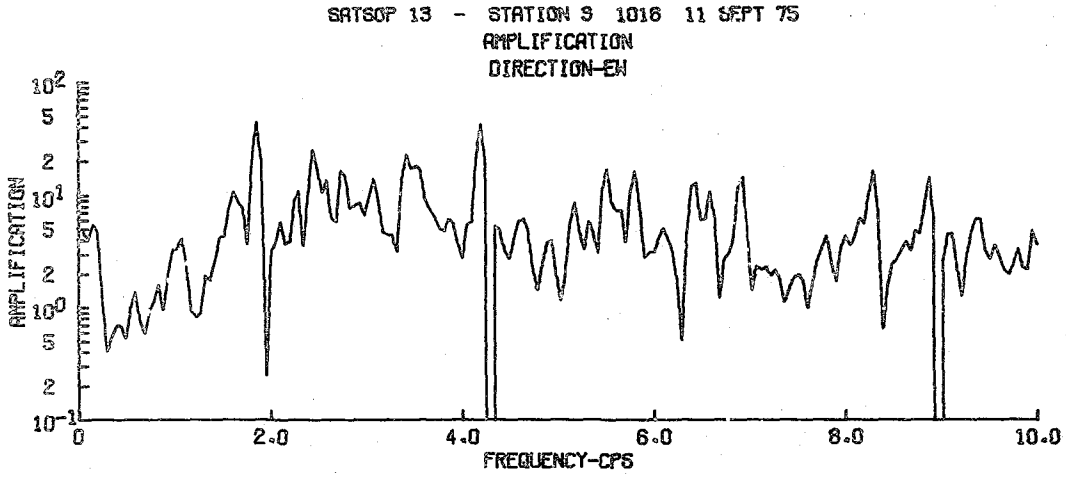
SATSOP 13 - STATION 3 1016 11 SEPT 75
AMPLIFICATION
DIRECTION-EW
AMPLIFICATION
FREQUENCY-CPS

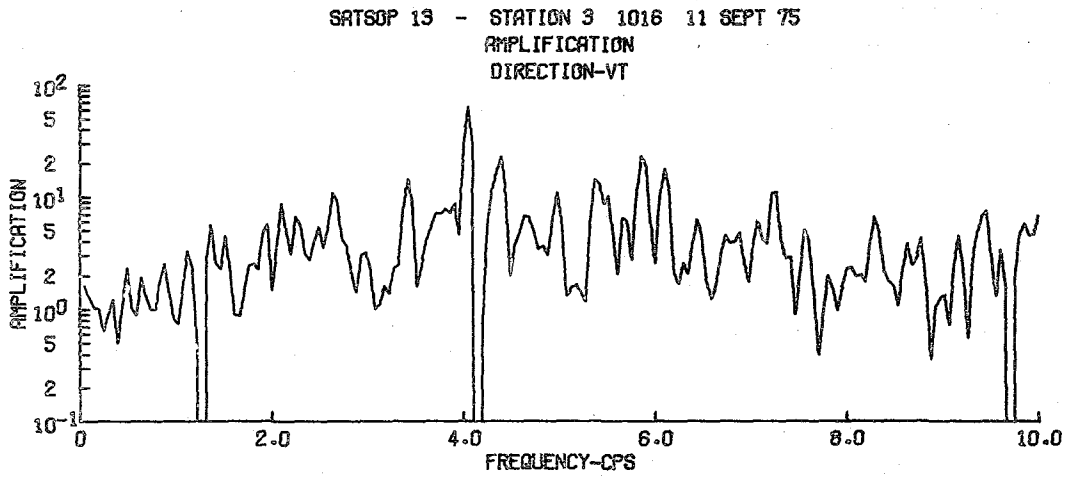
SATSOP 13 - STATION 3 1016 11 SEPT 75
AMPLIFICATION
DIRECTION-VT
AMPLIFICATION
FREQUENCY-CPS

SATSOP 19 - STATION 3 1016 11 SEPT 75
FOURIER POWER SPECTRUM
BASE STATION
RESULTANT

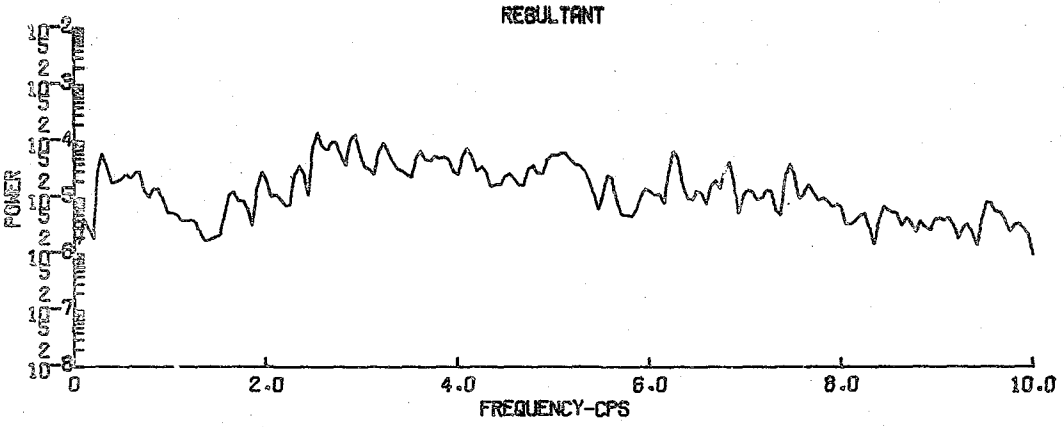

SATSOP 13 - STATION 3 1016 11 SEPT 75
FOURIER POWER SPECTRUM
PORTABLE STATION
RESULTANT

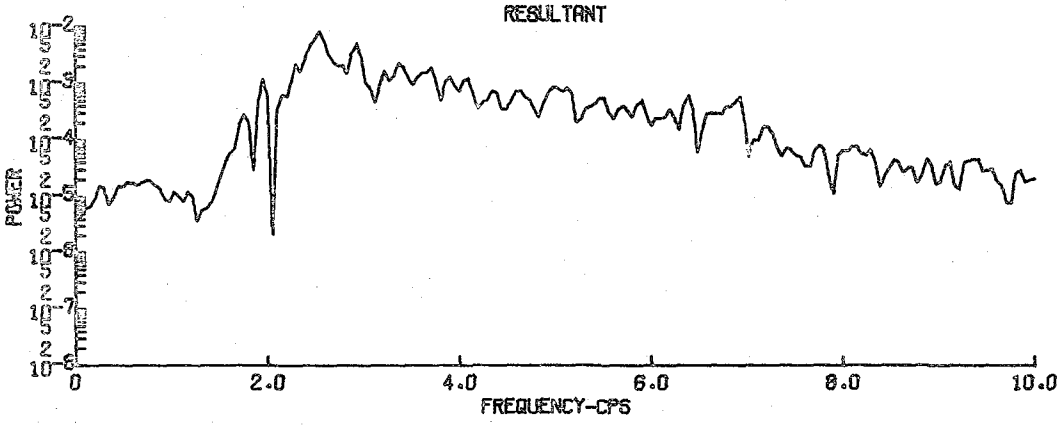

SATSOP 13 - STATION 3 1016 11 SEPT 75
AMPLIFICATION
RESULTANT

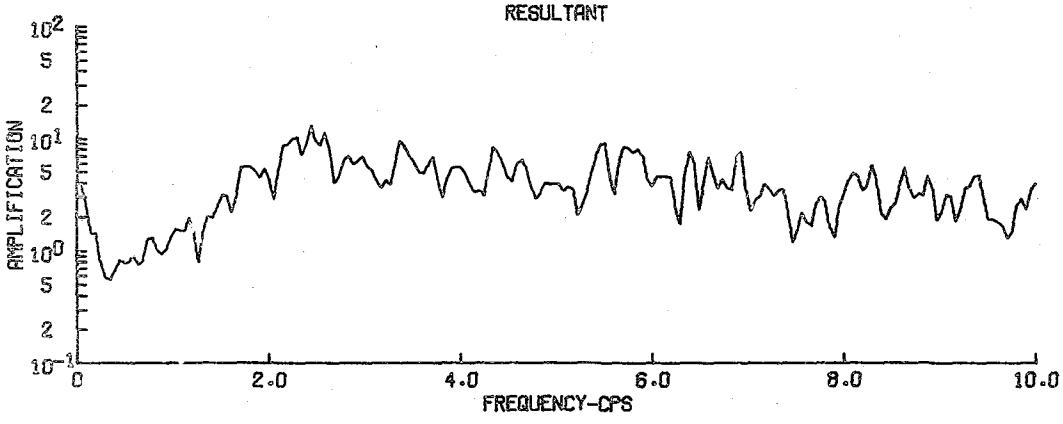

SATSOP 14 - STATION 3 1245 11 SEPT 75
FOURIER POWER SPECTRUM
BASE STATION
DIRECTION-NS

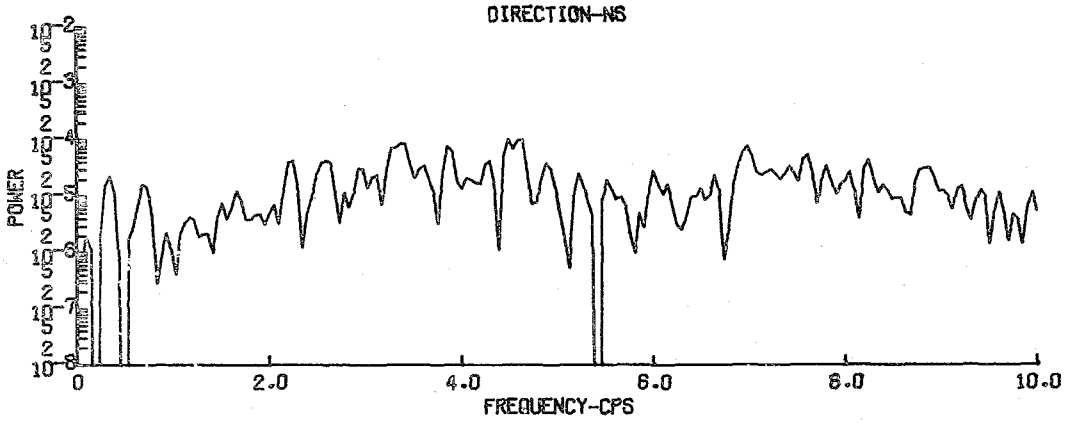

SATSOP 14 - STATION 3 1245 11 SEPT 75
FOURIER POWER SPECTRUM
BASE STATION
DIRECTION-EW

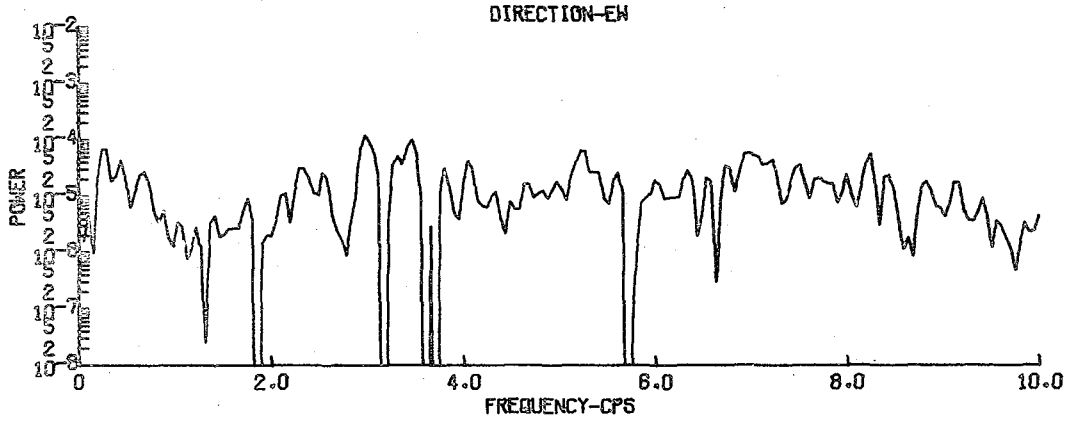

SATSOP 14 - STATION 3 1245 11 SEPT 75
FOURIER POWER SPECTRUM
BASE STATION
DIRECTION-VT

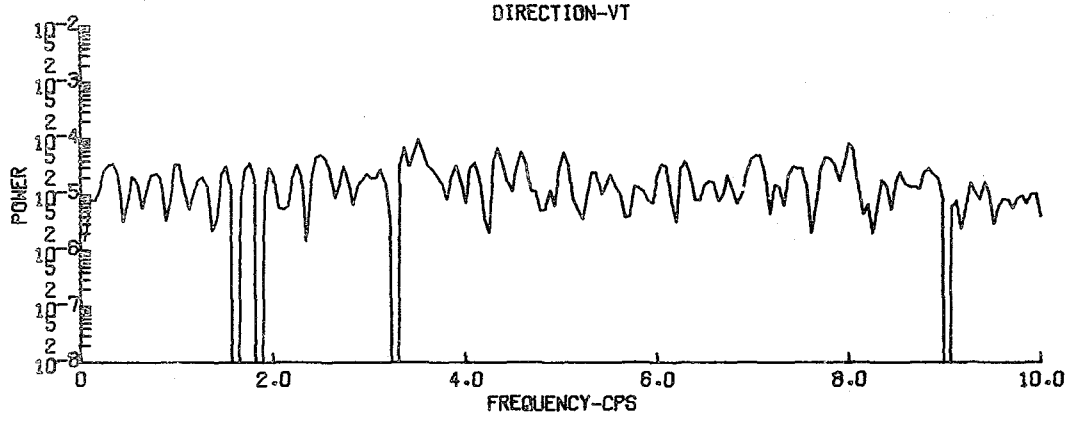

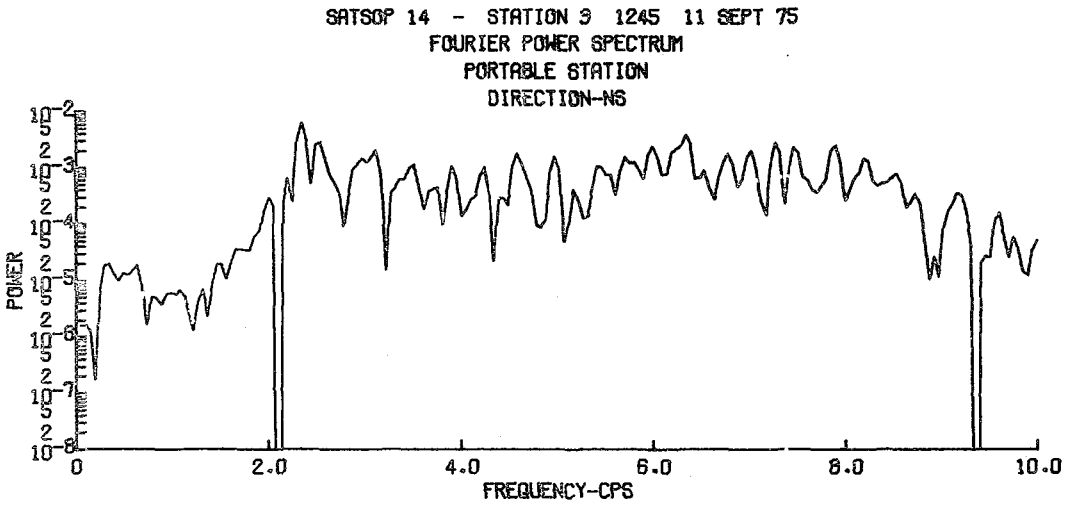
SATSOP 14 - STATION 3 1245 11 SEPT 75
FOURIER POWER SPECTRUM
PORTABLE STATION
DIRECTION-NS
POWER
FREQUENCY-CPS
0
2.0
4.0
6.0
8.0
10.0

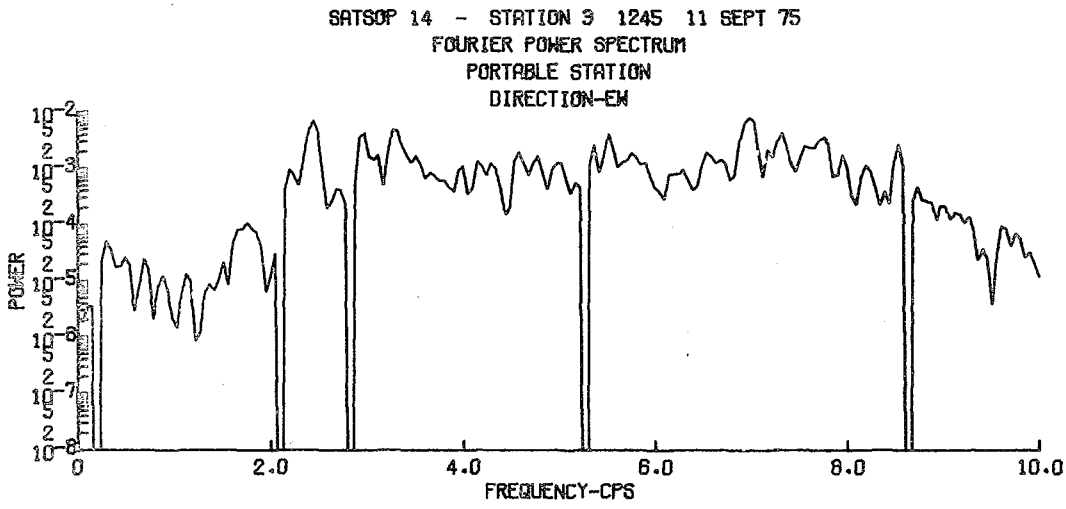
SATSOP 14 - STATION 3 1245 11 SEPT 75
FOURIER POWER SPECTRUM
PORTABLE STATION
DIRECTION-EW
POWER
FREQUENCY-CPS
0
2.0
4.0
6.0
8.0
10.0

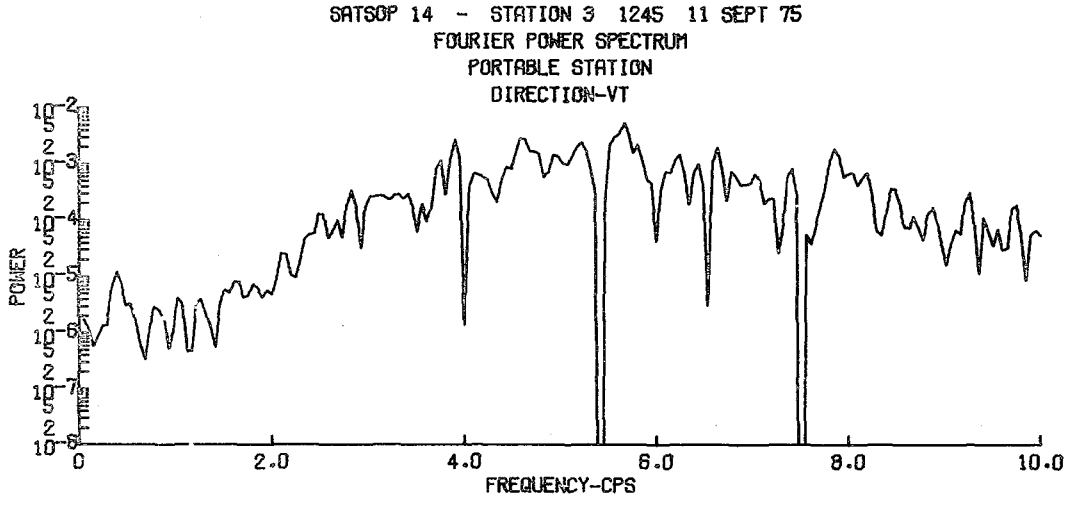
SATSOP 14 - STATION 3 1245 11 SEPT 75
FOURIER POWER SPECTRUM
PORTABLE STATION
DIRECTION-VT
POWER
FREQUENCY-CPS
0
2.0
4.0
6.0
8.0
10.0

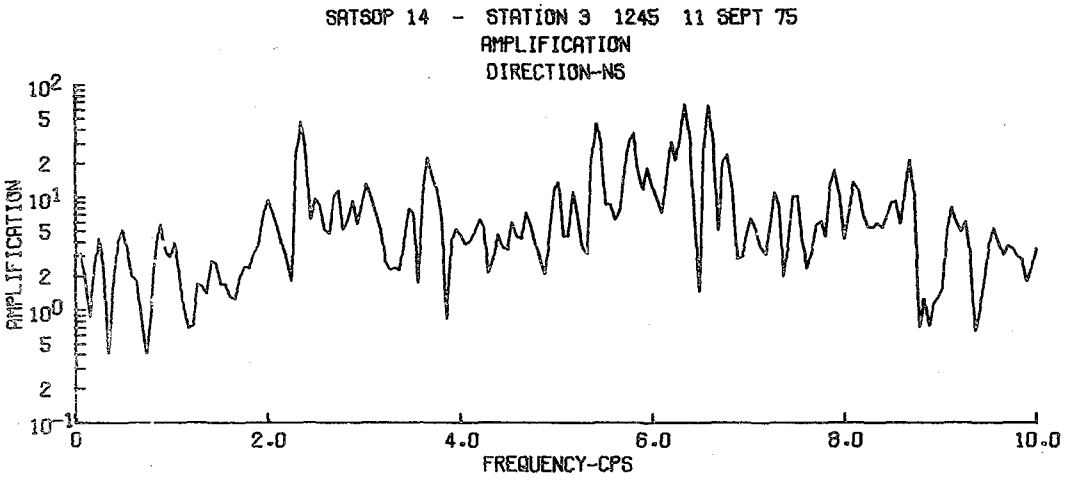
SATSOP 14 - STATION 3 1245 11 SEPT 75
AMPLIFICATION
DIRECTION-NS
AMPLIFICATION
FREQUENCY-CPS
0
2.0
4.0
6.0
8.0
10.0

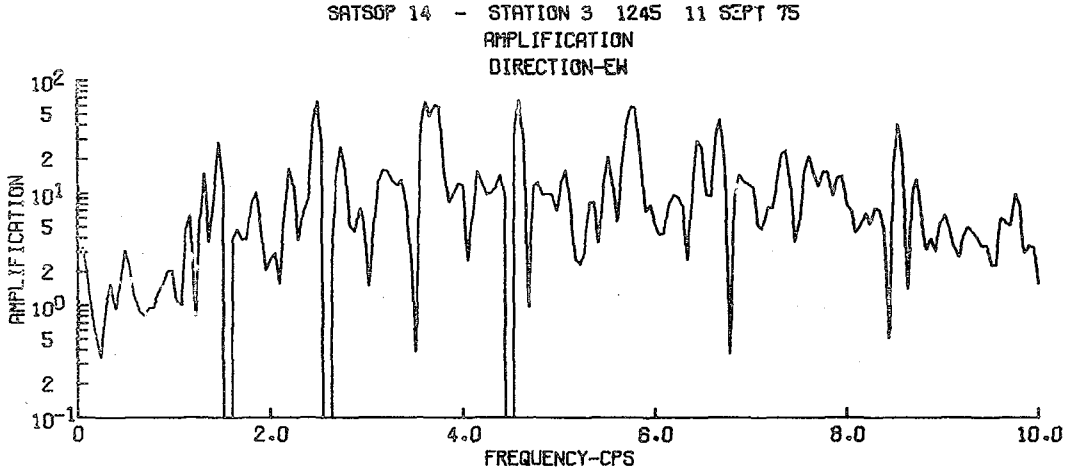
SATSOP 14 - STATION 3 1245 11 SEPT 75
AMPLIFICATION
DIRECTION-EW
AMPLIFICATION
FREQUENCY-CPS
0
2.0
4.0
6.0
8.0
10.0

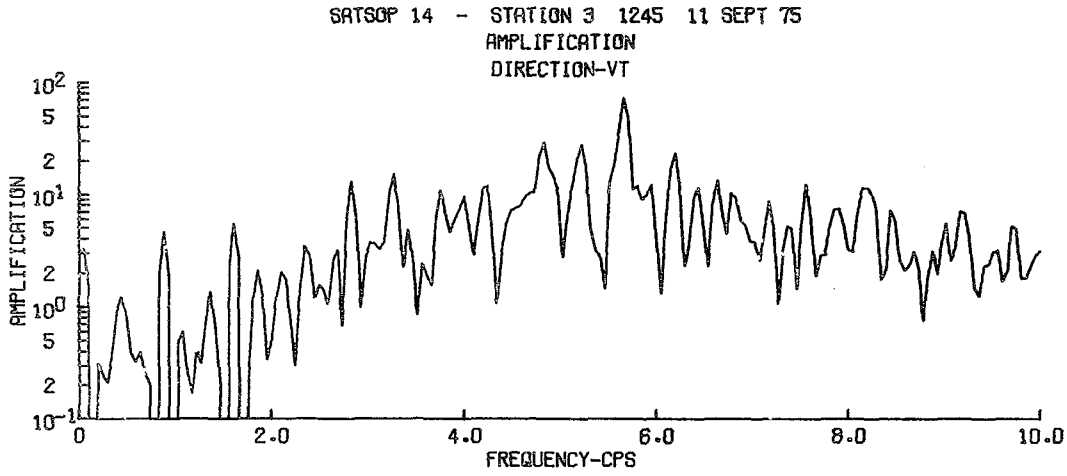
SATSOP 14 - STATION 3 1245 11 SEPT 75
AMPLIFICATION
DIRECTION-VT
AMPLIFICATION
FREQUENCY-CPS
0
2.0
4.0
6.0
8.0
10.0

SATSOP 14 - STATION 3 1245 11 SEPT 75
FOURIER POWER SPECTRUM
BASE STATION
RESULTANT

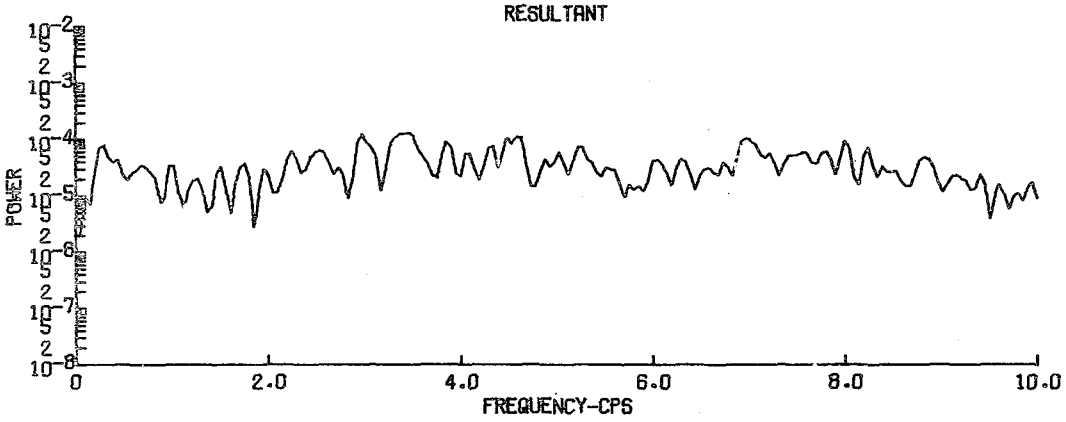

SATSOP 14 - STATION 3 1245 11 SEPT 75
FOURIER POWER SPECTRUM
PORTABLE STATION
RESULTANT

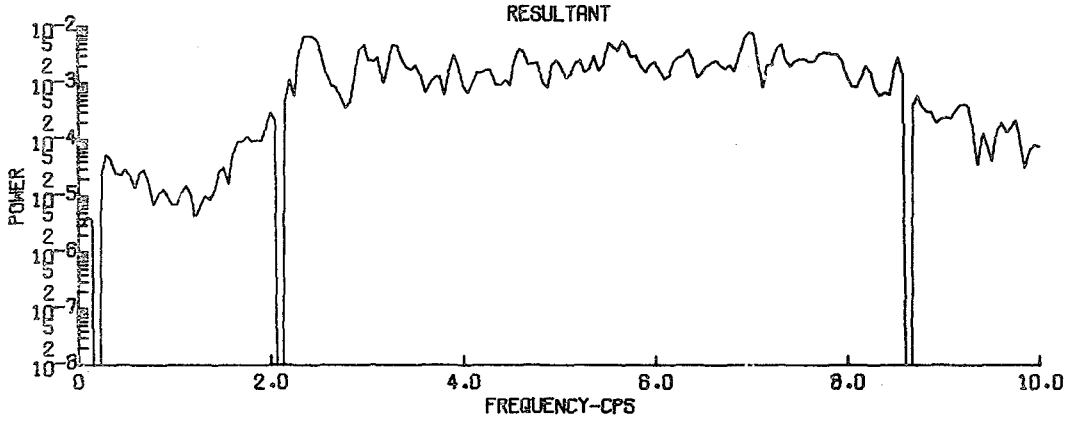

SATSOP 14 - STATION 3 1245 11 SEPT 75
AMPLIFICATION
RESULTANT

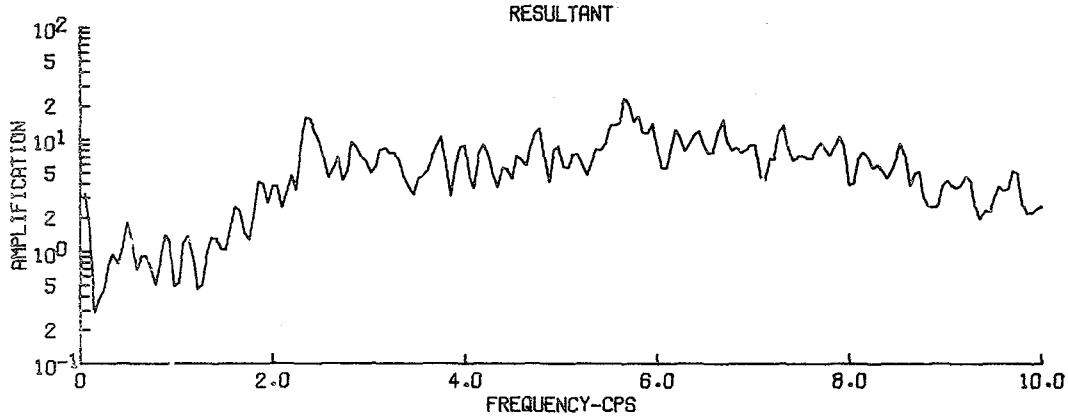

SATSOP 15 - STATION 3 1435 11 SEPT 75
FOURIER POWER SPECTRUM
BASE STATION
DIRECTION-NS

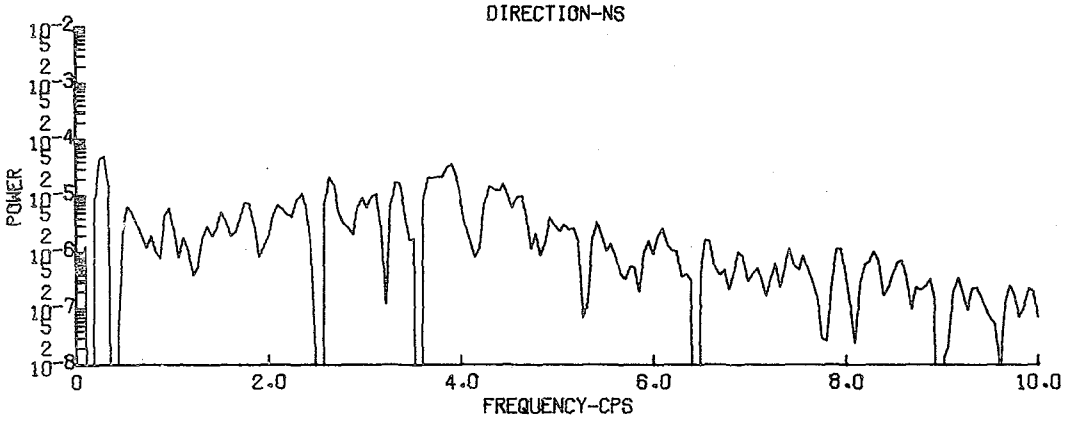

SATSOP 15 - STATION 3 1435 11 SEPT 75
FOURIER POWER SPECTRUM
BASE STATION
DIRECTION-EW

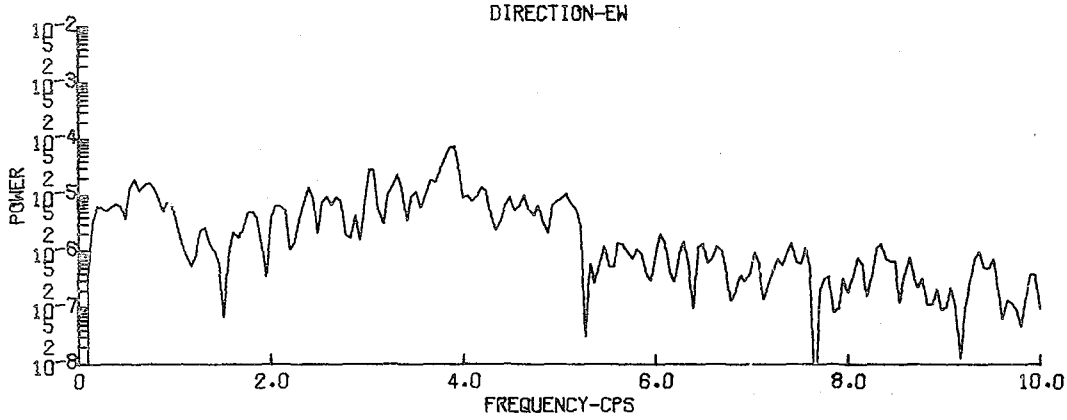

SATSOP 15 - STATION 3 1435 11 SEPT 75
FOURIER POWER SPECTRUM
BASE STATION
DIRECTION-VT

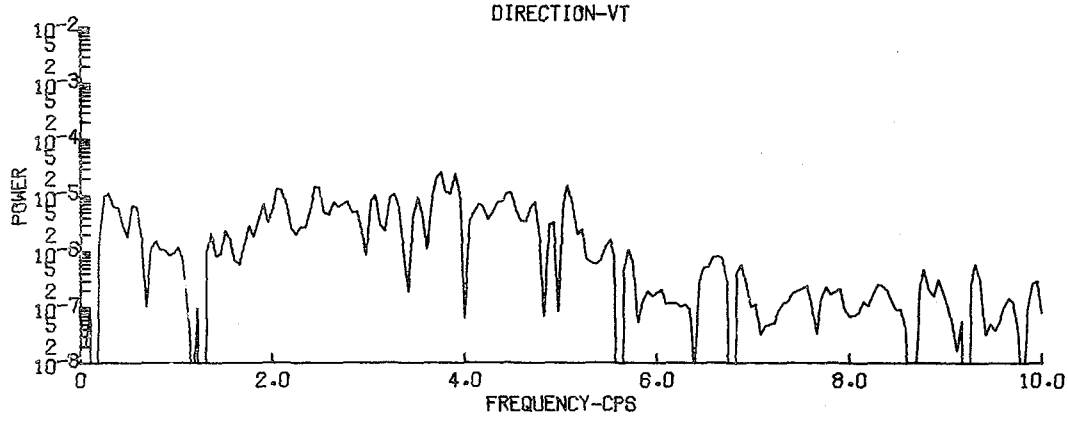

SATSOP 15 - STATION 3 1435 11 SEPT 75
FOURIER POWER SPECTRUM
PORTABLE STATION
DIRECTION-NS

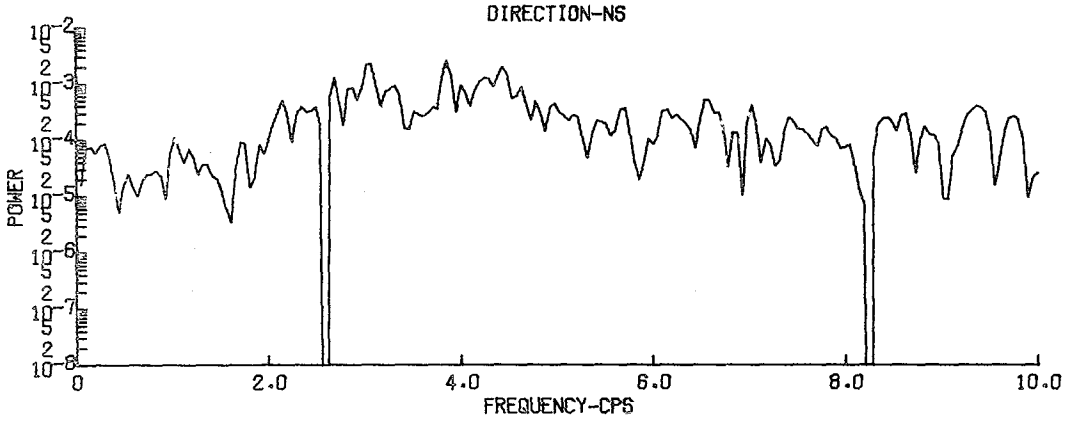

SATSOP 15 - STATION 3 1435 11 SEPT 75
FOURIER POWER SPECTRUM
PORTABLE STATION
DIRECTION-EW

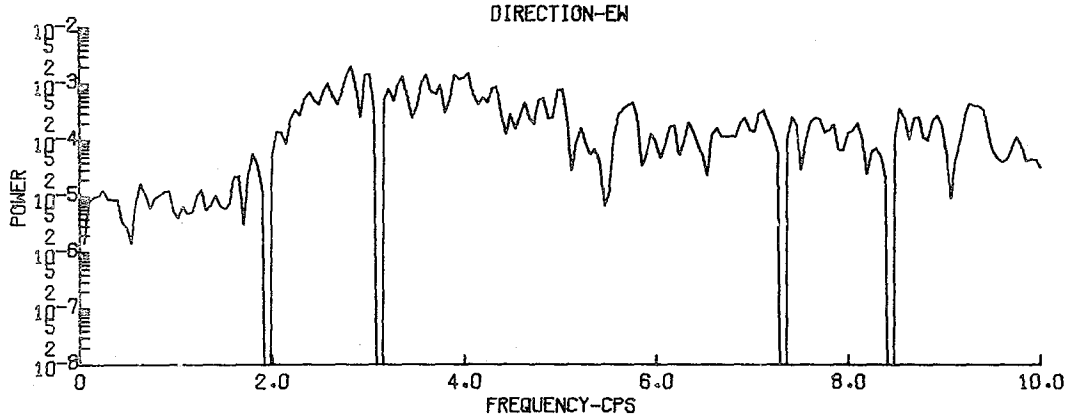

SATSOP 15 - STATION 3 1435 11 SEPT 75
FOURIER POWER SPECTRUM
PORTABLE STATION
DIRECTION-VT

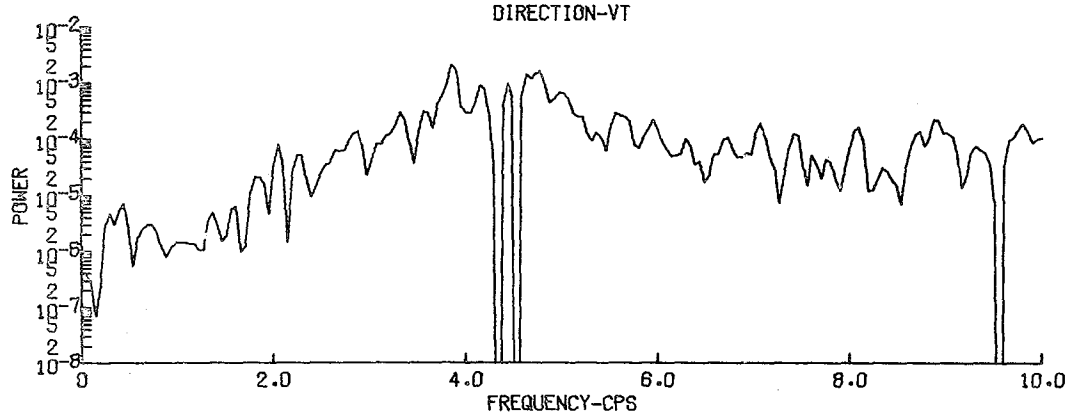

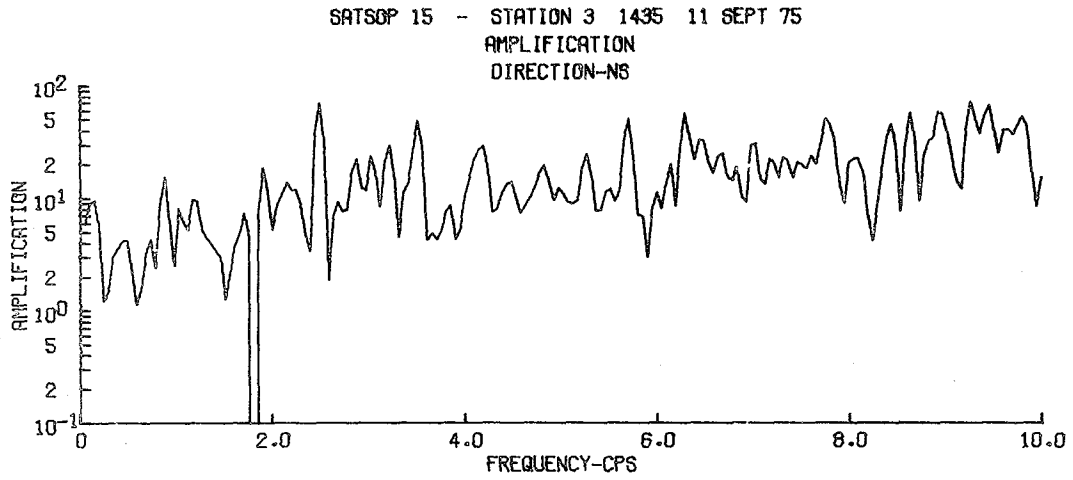
SATSOP 15 - STATION 3 1435 11 SEPT 75
AMPLIFICATION
DIRECTION-NS
AMPLIFICATION
FREQUENCY-CPS
0
2.0
4.0
6.0
8.0
10.0

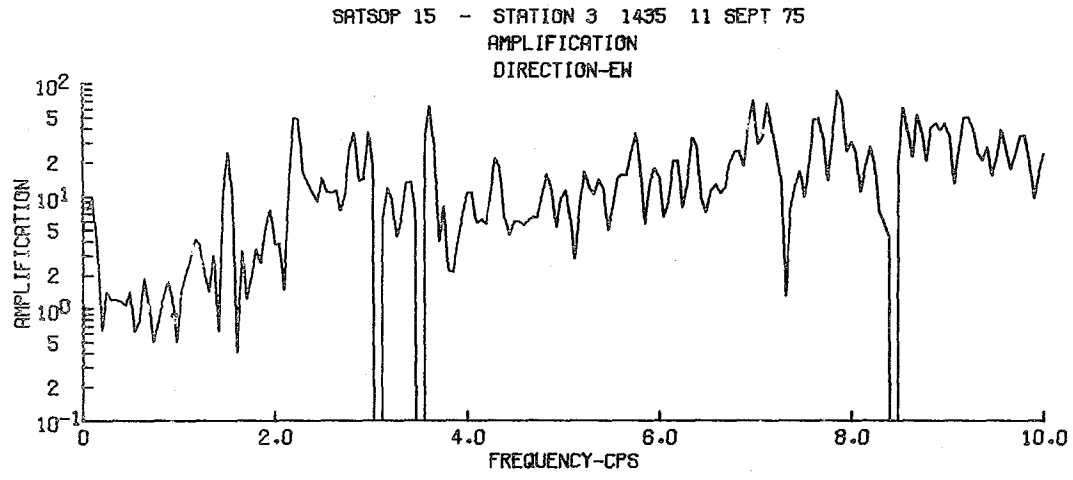
SATSOP 15 - STATION 3 1435 11 SEPT 75
AMPLIFICATION
DIRECTION-EW
AMPLIFICATION
FREQUENCY-CPS
0
2.0
4.0
6.0
8.0
10.0

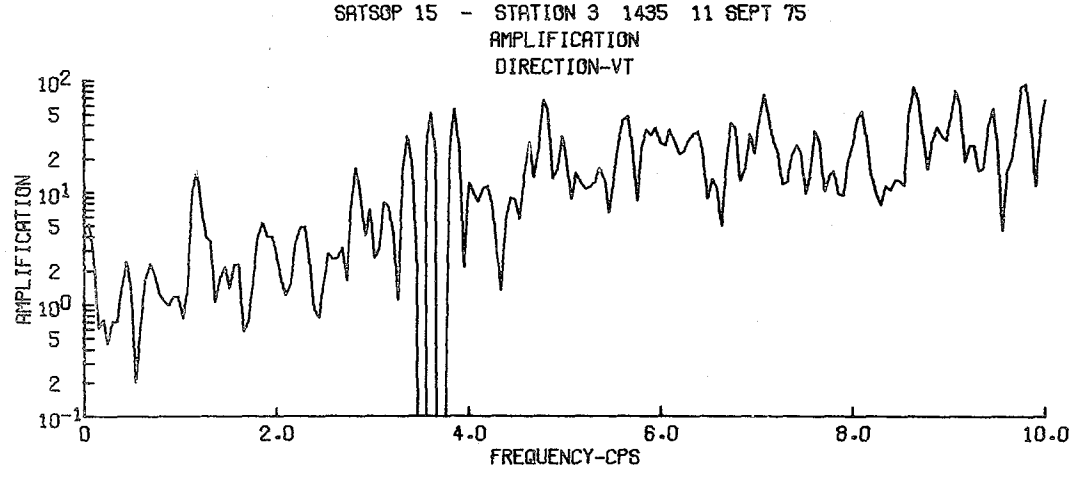
SATSOP 15 - STATION 3 1435 11 SEPT 75
AMPLIFICATION
DIRECTION-VT
AMPLIFICATION
FREQUENCY-CPS
0
2.0
4.0
6.0
8.0
10.0

SATSOP 15 - STATION 3 1435 11 SEPT 75
FOURIER POWER SPECTRUM
BASE STATION
RESULTANT

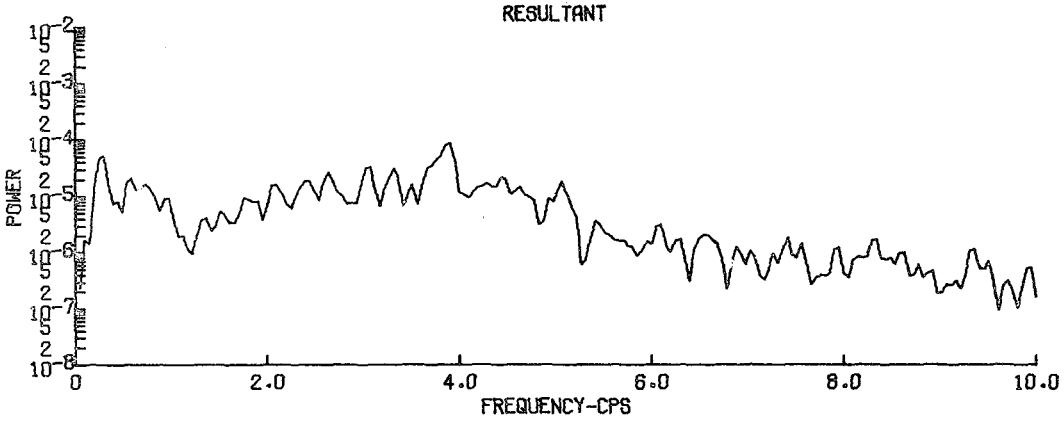

SATSOP 15 - STATION 3 1435 11 SEPT 75
FOURIER POWER SPECTRUM
PORTABLE STATION
RESULTANT

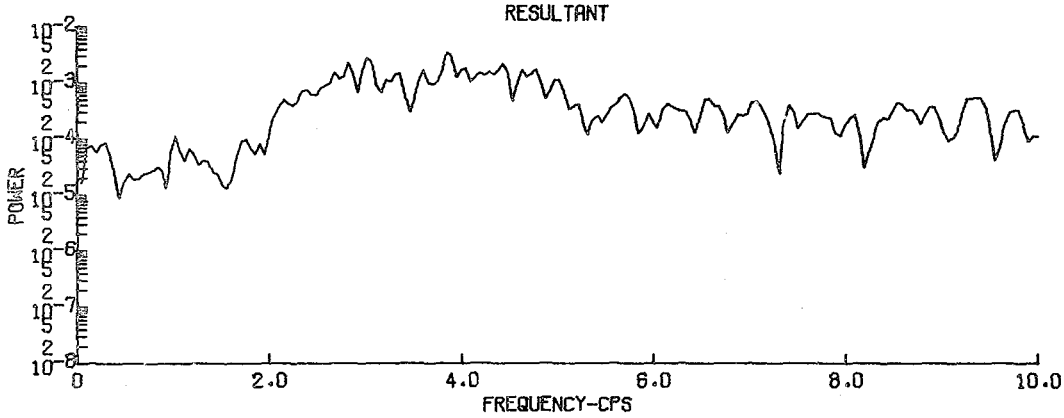

SATSOP 15 - STATION 3 1435 11 SEPT 75
AMPLIFICATION
RESULTANT